

Methodology for analysis and synthesis of inherently force and moment-balanced mechanisms

- theory and applications -

Volkert van der Wijk

METHODOLOGY FOR ANALYSIS AND SYNTHESIS
OF INHERENTLY FORCE AND
MOMENT-BALANCED MECHANISMS

– theory and applications –

2014

Volkert van der Wijk

Thesis committee members:

Prof.dr.G.P.M.R. Dewulf — University of Twente (chairman)
Prof.dr.ir. J.L. Herder — University of Twente (promotor)
Prof.dr.ir. H. van der Kooij — University of Twente
Prof.dr.ir. S. Stramigioli — University of Twente
Prof. V. Parenti-Castelli — Universita di Bologna, Italy
Prof.dr.ir. J. de Schutter — KU Leuven, Belgium
Prof.Dr.-Ing. A. Raatz — Leibniz Universität Hannover, Germany
Dr. B. van der Zon — TNO, Netherlands

Paranimfen:

Wilco Tax
Lianne van der Wijk

This work was performed at the Design of Mechanisms and Robotics group of the Laboratory of Mechanical Automation, Faculty of Engineering Technology, University of Twente, PO Box 217, 7500 AE Enschede, The Netherlands.

ISBN:978-90-365-3630-1

DOI:10.3990/1.9789036536301 (<http://dx.doi.org/10.3990/1.9789036536301>)

Cover design by Volkert van der Wijk, based on *World of Motion* (2001) by Volkert van der Wijk, an action painting on a 4.88 m wide and 1.58 m high canvas created with moving bicycle parts smeared with paint.

Copyright ©2014 Volkert van der Wijk (www.kineticart.nl)

All rights reserved. No part of this book may be reproduced in any form or by any electronic or mechanical means, including information storage and retrieval systems, without written permission from the author, except in the case of a reviewer, who may quote brief passages embodied in critical articles or in a review.

METHODOLOGY FOR ANALYSIS AND SYNTHESIS
OF INHERENTLY FORCE AND
MOMENT-BALANCED MECHANISMS

DISSERTATION

to obtain
the degree of doctor at the University of Twente,
on the authority of the rector magnificus,
prof.dr. H. Brinksma,
on account of the decision of the graduation committee,
to be publicly defended
on Friday the 11th of April 2014 at 14:45

by

Volkert van der Wijk

born on the 22nd of October 1981
in Benschop, The Netherlands

This dissertation has been approved by the promotor:
prof. dr. ir. J.L. Herder

Aan mijn geliefde Silvia

Preface

It's a great pleasure for me to present to you this work, a study and investigation of the motion of masses and inertias relatively to one another and the conditions for dynamic balance. I have tried to observe dynamic balance from a fundamental point of view, to gain the insight and understanding that is needed when synthesizing a mechanism device for a certain purpose, from improving the performance of high-speed machinery to realizing safe and energy efficient large motion of objects. The way masses and inertias move relatively can be regarded a kinematical issue and dynamic balance therefore can be considered as *specific kinematics of masses and inertia*, i.e. the study of mechanism kinematics that are scaled by the mass, the mass distribution, and the mass location of each mechanism element.

My main motivation for this work has been, in addition to pleasing my passion for mechanism motion and manipulating mathematical equations, to find a methodology where dynamic balance is considered in the very beginning of the design process. Commonly the question of dynamic balance is raised not until the design of a machine or device is already completed, or when a machine or device is already operating and it is discovered that its performance is severely limited due to dynamic unbalance. Unfortunately, then it is often too late and hardly possible to apply a dynamic balance solution successfully. This work aims at a paradigm shift in machine design where the importance of dynamic balance is understood and is addressed as a design principle.

I have tried to make this work accessible to a diverse audience by clearly structured explanations that are understandable for anyone with basic mathematical and physical knowledge. I have exerted all effort in illustrations for a realistic impression of the outcomes and possibilities, which allow the designer to start directly without the need of understanding the theory. I have developed prototype mechanisms and provided experimental results to demonstrate the potential of dynamic balance in practice. Unfortunately, or fortunately, this study is far from complete and has led to many new questions. I hope to be able to continue this study on dynamic balance in the years to come, not only on my own but with anyone, either from academia, from industry, or from elsewhere, who becomes enthusiastic about this energizing topic in mechanism design.

I am very thankful to all the people who have been involved in my research in one way or another. In particular I'd like to express my sincere gratitude to my promotor Just Herder for all the years of enjoyable and fruitful cooperation, his endless encouragement, super support, and sharp opinion. I'd like to thank the graduation committee for their willingness to judge and criticize my thesis and the past dean of my faculty Rikus Eising for creating the opportunities for me to realize my ideas, and also for chairing my defence even after his retirement.

I am very thankful to my colleagues of the Laboratory of Mechanical Automation of the University of Twente for the numerous interesting discussions and their support, and also to my colleagues of the TU-Delft where my research was initiated and to my colleagues of LIRMM in Montpellier in France where the experimental part of this work was executed. Especially I'd like to extend my appreciation to François Pierrot and Sébastien Krut for giving me the opportunity and knowledge to design, build, and test a high-speed dynamically balanced manipulator successfully.

I'd like to thank the international IFToMM community, in particular as a member of the technical committees for Computational Kinematics and for Robotics and Mechatronics, for being part of this rich network of expertise and nice people who continuously encourage and enhance mechanism and machine science. I am also very thankful to my industrial partners Stamhuis Lineairtechniek, Control Techniques, Masévon Technology, Ternet, Penta Robotics, Blueprint Automation, Sigma Control, and Hollandia for sharing their practical experience and for supporting the development of dynamic balance demonstrators that have to make the markets ready.

I'd like to thank my family and friends for all good times together. And most of all I'd like to thank my girlfriend Silvia for her immense love and continuous support and for the great times we share.

I wish you a wonderful time with this book, either by reading the words, calculating the equations, or studying the illustrations. Be creative and keep smiling!

Enschede, April 2014

Volkert van der Wijk

Contents

1	Introduction	1
1.1	Principles of shaking force and shaking moment balance	1
1.2	Applications of dynamic balance	4
1.3	Limitations of current balancing methods and balance solutions for multi-degree-of-freedom mechanisms	10
1.4	Focus on inherently balanced mechanism design	12
1.5	Outline	13
2	Inherent force balance of given mechanisms with linear momentum	17
2.1	Open kinematic chains	17
2.2	Closed kinematic chains with open chain method	21
2.2.1	4R four-bar linkage	22
2.2.2	Crank-slider mechanism	23
2.2.3	Delta robot manipulator	24
2.3	Closed kinematic chains including loop-closure relations	26
2.3.1	4R four-bar linkage	27
2.3.2	Parallelogram and pantograph linkage	34
2.3.3	4-RRR parallel manipulator	37
2.3.4	3-RRR parallel manipulator	48
2.3.5	2-RRR parallel manipulator (6R six-bar mechanism and 5R five-bar mechanism)	49
2.4	Discussion and conclusion	51
3	Principal vector linkages for inherent shaking force balance	53
3.1	The 2-DoF pantograph linkage as a principal vector linkage	53
3.2	Principal vector linkage of three principal elements in series	58
3.2.1	Union of pantographs and Fischer's linkage	59
3.2.2	Generalization and calculation of principal dimensions with Equivalent Linear Momentum Systems	61
3.2.3	Method of rotations about the principal joints	72
3.2.4	Kinematic variations of the principal vector linkage	72

3.3	Principal vector linkage of four principal elements in series	77
3.4	Principal vector linkage of four principal elements in parallel	85
3.5	The spatial principal vector linkage.....	96
3.6	Discussion and conclusion	99
4	Closed-chain principal vector linkages	101
4.1	Approaches for synthesis of closed-chain principal vector linkages .	101
4.2	Closed chain of four elements with Open Chain Method	103
4.3	Mass equivalent model of a general element in a closed chain	110
4.4	Mass equivalent principal open chain of three elements	114
4.5	Principal vector linkages of closed chains of n elements	129
4.6	Discussion and conclusion	130
5	Principal vector linkage architecture with similar linkages	135
5.1	Architecture with CoM in invariant point in a similar linkage	135
5.2	Conditions for similarity.....	139
5.3	Force balance conditions from mass equivalent principal chain.....	142
5.4	Discussion and conclusion	155
6	Principal vector linkages for inherent shaking moment balance	161
6.1	Moment balance conditions of open-chain principal vector linkages	161
6.1.1	Moment balance of a 2-DoF pantograph	162
6.1.2	Moment balance of three principal elements in series	165
6.1.3	Moment balance of four principal elements in series	171
6.2	Moment balance conditions of closed-chain principal vector linkages	178
6.3	Discussion and conclusion	179
7	Synthesis of inherently dynamically balanced (IDB) mechanisms	183
7.1	Approach for synthesis of IDB mechanisms	183
7.2	Synthesis of an IDB 2-DoF grasper.....	185
7.3	Synthesis of multi-DoF IDB manipulators	186
7.4	Synthesis of large-size balanced devices	191
7.5	Discussion and conclusion	194
8	Experimental evaluation of a dynamically balanced redundant planar 4-RRR parallel manipulator	197
8.1	Introduction	197
8.2	Approach to the evaluation and comparison of a balanced manipulator	198
8.3	Design of the DUAL-V manipulator	199
8.4	Inverse dynamic model and validation with simulation model.....	201
8.4.1	Inverse dynamic model to derive the actuator torques	201
8.4.2	Simulation and validation of the inverse dynamic model....	206
8.5	Experimental setup	207
8.6	Experiments and experimental results.....	208
8.7	Discussion	212

8.7.1	Shaking forces and shaking moments	212
8.7.2	Sensitivity to balance inaccuracy and payload	216
8.7.3	Actuator torques	217
8.7.4	Bearing forces	218
8.7.5	Evaluation method and experimental setup	218
8.8	Conclusion	219
9	Reflection on the design of inherently balanced mechanisms	221
10	Conclusion	227
A	The work of Otto Fischer and the historical development of his method of principal vectors for mechanism and machine science	229
A.1	Introduction	229
A.2	Otto Fischer and his works	230
A.3	The method of principal vectors	232
A.4	Applications by Otto Fischer	235
A.5	Development and application by other researchers	236
A.6	Conclusion	239
References	241
Summary	247
Samenvatting	249
About the author	251

Chapter 1

Introduction

1.1 Principles of shaking force and shaking moment balance

The problem of action is its reaction. In high-speed machinery such as robotic manipulators (Fig. 1.1), high action forces and moments are generated for fast acceleration of the moving elements. As a reaction, high inertia forces and inertia torques are generated that act on the moving elements and on the base of the machine. While dynamic reactions are required for the dynamics of a machine, when the base is considered they are often a cause of significant undesired vibrations [64, 70, 74]. This is illustrated in Fig. 1.2a and Fig. 1.2b where the dynamic reactions exerted by the manipulator make the base of the machine vibrate.



Fig. 1.1 To mount high-speed robotic manipulators, heavy supports with large footprints are required to resist the high shaking forces and shaking moments in the base. (ABB Flexpicker Delta robot)

Of a machine or mechanism in motion, the resultant inertia force it exerts on its base is named the *shaking force* and the resultant inertia torque it exerts on its base is named the *shaking moment*. It is possible to design a mechanism such that the resultant inertia force on the base is zero for which it is *shaking force balanced* or, in short, *force balanced*. It is also possible to design a mechanism such that the resultant inertia torque on the base is zero for which it is *shaking moment balanced* or, in short, *moment balanced*. A mechanism is named *dynamically balanced* when it is both force and moment balanced.

As opposed to damping, sophisticated control, or increased base mass to reduce the influence of base vibrations, dynamic balancing has the purpose to eliminate the vibrations at its source: by designing the machine such that it does not exert vibrations of the base at all. This is illustrated in Fig. 1.2c where the inertia forces and the inertia torques remain solely inside the mechanism. A dynamically balanced machine then needs minimal support, hypothetically solely a single wire as reaction to gravity as shown in Fig. 1.2d, without losing the ability to operate at high speeds with high accuracies and without affecting the environment such as the floor, other parts of the system mounted on the same base, and other systems.

The principles of dynamic balance are obtained from classical mechanics and can already be found in Newton's corollaries about the state of the common center of mass (center of gravity) and the momentum (quantity of motion) in *The Principia*¹:

The common center of gravity of two or more bodies does not change its state whether of motion or of rest as a result of the actions of the bodies upon one another; and therefore the common center of gravity of all bodies acting upon one another (excluding external actions and impediments) either is at rest or moves uniformly straight forward.

The quantity of motion, which is determined by adding the motions made in one direction and subtracting the motions made in the opposite direction, is not changed by the action of bodies on one another.

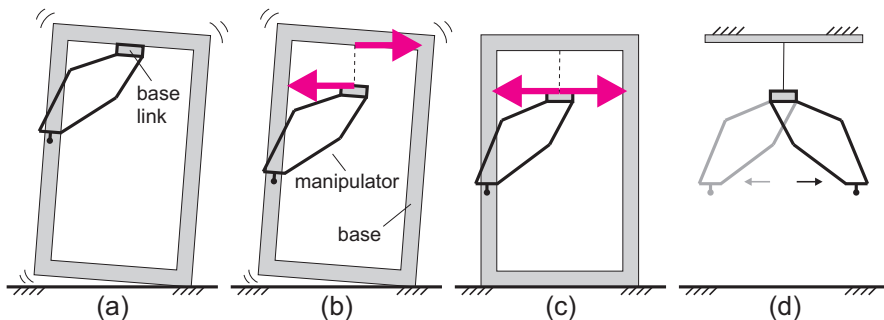


Fig. 1.2 (a) An unbalanced manipulator (b) generates dynamic reactions to the base (c) which are eliminated with dynamic balancing. (d) A balanced manipulator requires minimal support, e.g. by a single wire, while having the ability to operate at high speeds with high accuracies and without affecting the environment, other parts of the system, and other systems.

¹ Isaac Newton - *The Principia*, Cohen and Whitman, 1999, University of California press

With the base considered fixed in the inertial reference frame, the common center of mass (CoM) of a system of moving elements can only accelerate because of forces that interact between the system and the base. This means that when the common CoM is stationary or moves with constant velocity relative to the base, these forces are zero and the system is force balanced. Although a constant velocity of the common CoM of a mechanism is not impossible [96], usually the common CoM of a force-balanced mechanism is stationary with respect to the base.

When there are no forces or moments interacting between a system of moving elements and the base, then the linear momentum and the angular momentum of the system are constant for all relative motion. This is the general characteristic of a dynamically balanced mechanism, it has a constant linear momentum and a constant angular momentum with respect to the base for all motion of the mechanism.

Often the base is part of the mechanism, for instance in Fig. 1.2a where the mechanism element that is rigidly mounted on the base is regarded the base link. Internal forces and internal moments that act among the moving elements and determine the motion of the mechanism therefore also act within the base link. Internal forces and moments include the inertia forces and inertia torques of the individual elements, forces and moments of actuators (driving forces and torques), friction (in linkage or fulcrum), internal collisions (between mechanism links or base link), internal springs (between moving links or base link), and other. Since the momentum of a system of moving elements does not depend on any internal force and moment - their reactions are internal too -, they do not affect the dynamic balance. The sums of all internal forces and moments on the base link therefore are zero.

The methods for deriving the conditions for dynamic balance of a mechanism are based on these principles and are either focussed on (1) calculation of the forces and moments on the base link and the conditions for which their sums are zero [90], (2) determination of the common CoM and the conditions for which it is stationary (for force balance only) [13], and (3) calculation of the linear and angular momentum and the conditions for which they are constant [67].

Because a dynamically balanced mechanism is dynamically decoupled from its base, dynamic behavior of the base does not affect the relative motion of the mechanism. When the base is accelerated linearly or rotationally, e.g. by another device or due to external vibrations, a dynamically balanced mechanism behaves as a single rigid body with the base. This is also the reason that the gravity force does not affect the relative motion of the elements of a force-balanced mechanism. Although the gravity force works on all elements, since the common CoM of the elements is a stationary point within the base, effectively the gravity force only affects the accelerations of the base and the mechanism as a rigid body.

To stress the difference between *shaking force* balance and *static* balance, the latter can be achieved also by maintaining the potential energy of the mechanism constant, for instance by using springs [60]. This means that shaking force balance solutions are a subset of static balance solutions, i.e. shaking-force-balanced mechanisms are statically balanced too. However, since shaking forces are essentially different from static forces, the terms shaking force balance and static balance

should not be confused. Here force balance or shaking force balance will be used, and the term static balance will be reserved for constant potential energy balancing.

1.2 Applications of dynamic balance

There are numerous advantages for which dynamic balance is applied to improve the performance of a machine. For instance, dynamically balanced mechanisms are known to have reduced noise [39] and reduced wear and fatigue [74]. In telescopes dynamic balance is important for moving the mirrors accurately at high frequencies [57]. In robotics, dynamic balance reduces cycle times and improves precision. Because of reduced waiting time for vibrations to die out, the settling time of a dynamically balanced two-degree-of-freedom parallel manipulator was shown to reduce with a factor 16 as compared to the unbalanced case [75, 83]. In this section a range of applications is highlighted with selected examples.

ASML's Twinscan lithographic system, shown in Fig. 1.3, is an example in which dynamic balance is applied for low cycle times with high precision with the aim to lower the costs per product by increasing the output rate [36, 70]. Any vibration of the base is undesired for accurate measurements by sensitive metrology tools that are mounted on the same base and to keep the costs of solutions to damp vibrations low [82]. This machine has moving stages for positioning wafers in the lower part and for positioning reticles in the upper part. The moving stages are accelerated by interaction with a balance mass as illustrated in Fig. 1.4a. Both the stage



Fig. 1.3 AMSL Twinscan XT:1000H, a 248-nm step and scan lithographic system with balanced moving stages for low cycle times and high precision. (www.asml.com, 2014)

and the balance mass float within the horizontal plane with the actuator in between moving them in opposite directions continuously. Then the dynamic forces remain internal and the base does not experience shaking forces. Also the forces from the spring-damper device are internal when compensating the friction forces between the balance mass and the base.

In the upper part of the Twinscan the moving stage is in the same plane as the balance mass as shown in Fig. 1.4b such that full dynamic balance is obtained. Figure 1.4c shows the two stages in the lower part of the machine which float on top of the balance mass. Although they are force balanced, since the stages are in a different plane from the balance mass the dynamic forces still produce shaking moments in the base.

The ABB IRB760 palletizer shown in Fig. 1.5 is a shaking force balanced serial robotic manipulator. It consists of a parallelogram linkage with a balance mass to balance the inertia forces of the motion of both the manipulator and the payload. Since the mass of the payload is not constant, in general the force balance is not perfect. But when the robot is moved quickly, the shaking forces in the base remain relatively small. Because of force balance, it is known that the payload capacity of the manipulator is higher or that it is able to move significantly faster [73], that the actuator torques are lower [30], and that the calibration accuracy is higher [72]. Since actuator torques are internal moments that are not involved with dynamic balance, their reduction is mainly because of static balance. When force balanced, the actuators need not to be active to keep the robot in a certain position. Because of this, a force balanced robot is energy efficient and inherently safe. It remains in any position even in case of power outage or brake failure.

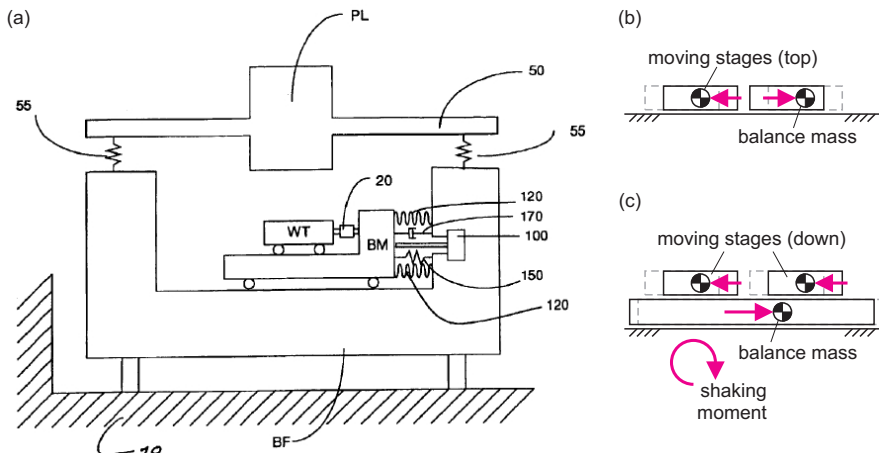


Fig. 1.4 a) Balance principle of the Twinscan system to eliminate base vibrations [36] where b) the stage moves by interaction with a balance mass to have no shaking forces in the base; c) Shaking moments exist when the stages and balance mass are not in the same plane.

For high-speed hand-held tools such as the jig saw in Fig. 1.6, dynamic balance is important for improving the ergonomics. Vibration damping materials, placed for instance in the handles, are not effective here in reducing the vibrations sufficiently. Investigation of a dynamically balanced chain saw showed that risks of injuries such as vascular disease disorders were reduced significantly [64]. Because of reduced vibrations, also the quality of the work is improved.

Figure 1.7 shows an exploded view of part of the jig saw. Part 52 is the crank that is driven by the motor and has a balance mass on opposite side of the pin that drives the saw with which it is force balanced. Part 53 is the balance mass which is driven by a cam transmission from the crank to move in opposite direction of the saw and its connecting parts, among others parts 37 and 38. This means that the common CoM of these parts is in a stationary point in the axis of rotation. Because of the compact assembly of the parts such that they lay almost in the same plane and since the motor speed is constant, the resulting shaking moments are low.

The jig saw is an example of an end-effector that is balanced in order to not perturb its manipulator, the human hand and arm. On the contrary, the Steadicam in Fig. 1.8 is an example of an end-effector that is balanced to not *be* perturbed by the manipulator. To quickly move the camera in any direction while keeping it steady for high quality recordings, the camera system is force balanced with respect to the point where the hand applies for manipulation. Then the common CoM of the camera and the balance mass is in this point.

Figure 1.9 shows the Skycam robotic camera system which can be regarded an advanced and automatized version of the Steadicam [27]. It consists of a dynamically balanced camera system that is applied as an end-effector of a cable-driven parallel manipulator which moves the camera system throughout a large space,



Fig. 1.5 ABB IRB760 palletizer manipulator with balance mass for force balance of manipulator and payload to have low dynamic forces in the base, increased payload capacity, and increased efficiency and safety. (www.ABB.com, 2014)



Fig. 1.6 For high-speed hand-held tools dynamic balance improves ergonomics, reduces the risks of injuries, and improves the quality of the work. (balanced jig saw DW331K, www.dewalt.com, 2014)

spanning for instance a complete sports field. Dynamic balance here is important for proper control of the camera for two reasons. The camera system can easily lose its orientation and start to spin, rotate, and swing (as a pendulum) because of the imposed motion by the manipulator, but also because of motion of the camera system itself since the stiffness of the cable-manipulator is limited. When dynamically balanced, the camera system is dynamically decoupled from the cable-manipulator, vice versa.

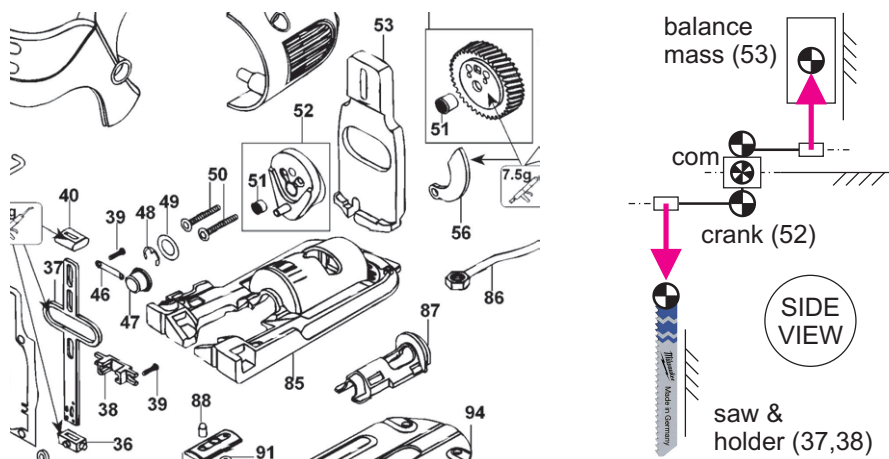


Fig. 1.7 Exploded view and illustration of a jig saw with force-balanced crank (52) and balance mass (53) to balance the reciprocating motion of the saw and connecting parts (a.o. 37 and 38). (www.dewalt.com, 2014)



Fig. 1.8 The Steadicam is force balanced to not be perturbed when manipulated with the hand. ([www.stadicam.com](http://www.steadicam.com), 2014)



Fig. 1.9 The Skycam robotic camera system consists of a cable driven parallel manipulator with a camera system as end-effector that is dynamically balanced for stability. (www.skycam.tv, 2014)

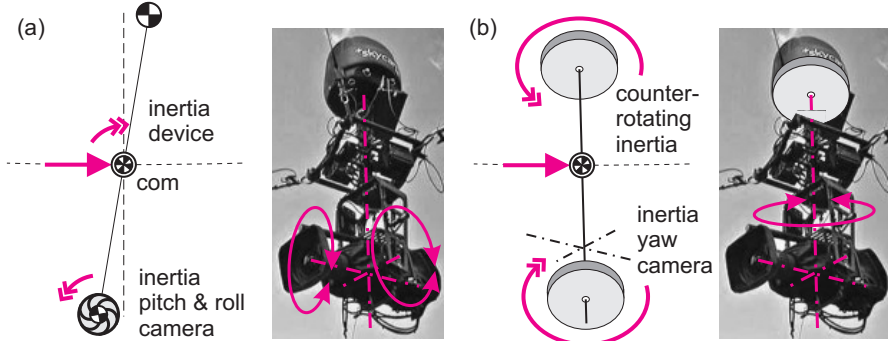


Fig. 1.10 a) The Skycam is force balanced with the CoM of the camera below and the system on top in the point where the cable manipulator applies. Moment balance of the camera's pitching and rolling motions is achieved by counter-rotation of the device about its CoM; b) Moment balance of the yawing motion of the camera is obtained by a counter-rotating inertia on top [27].

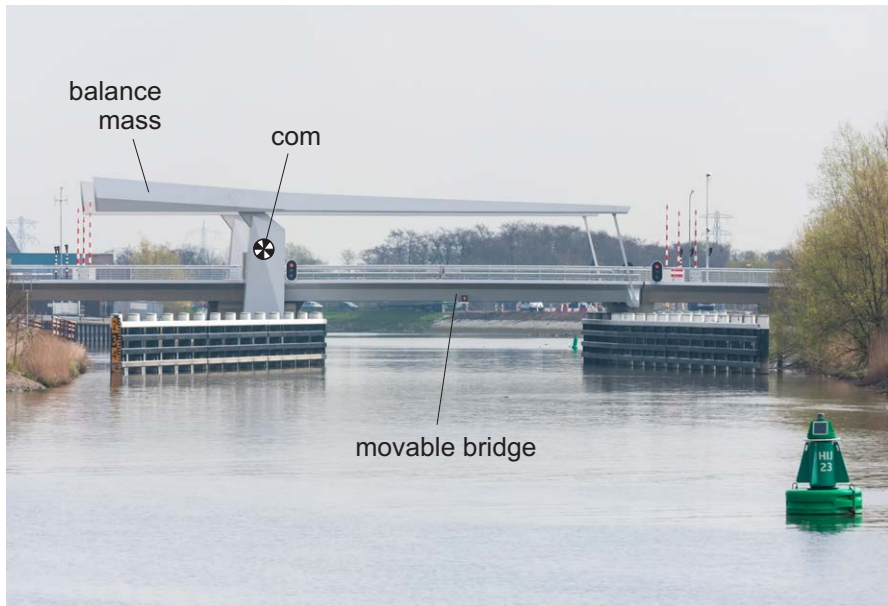


Fig. 1.11 For a bascule bridge force balance reduces the actuation power and the dynamic forces while safety is improved. (Hollandse IJssel near Gouda (NL), constructed in 2012, courtesy of Hollandia)

As illustrated in Fig. 1.10a, the Skycam is force balanced such that the common CoM of the camera below and the electronic system on top is in the point where the cable manipulator applies. The camera can rotate in three directions. The shaking moments of the pitching and rolling motion of the camera are balanced by opposite rotations of the camera support system. These are rotations about the horizontal axes in the plane where the cable manipulator applies. Since the inertia of camera support system is significant larger than the inertia of the camera, these rotations remain relatively small. For the moment balance of the yawing motion of the camera (rotation about vertical axis) a counter-rotating inertia is used that is implemented in top of the camera system as shown in Fig. 1.10b. Since this counter-rotating inertia is both used as force balance mass and as moment balance inertia, it is regarded a counter-rotating countermass which is known to be an advantageous balance solution for low mass and low inertia [102].

The contrary of rapidly moving hand-held mechanisms are slowly moving architectural systems such as the movable bascule bridge in Fig. 1.11. Here a balance mass is used to force balance the bridge while opening and closing. For these type of mechanisms force balance is advantageous for low energy consumption, for low driving forces and torques allowing manual operation, and for safety. During an emergency stop the dynamic forces can become large, but when balanced they remain zero on the base. Also external forces e.g. due earthquakes do not affect the motion of the bridge. Moment balance is partly achieved when the motors and the inertia wheels - that are included in the drive-train of a bridge for the servo-control - rotate in opposite direction of the bridge.

1.3 Limitations of current balancing methods and balance solutions for multi-degree-of-freedom mechanisms

Contrary to the dynamic balancing of one-degree-of-freedom (1-DoF) mechanisms, a topic being investigated for well over a century [7, 8], the dynamic balancing of multi-DoF serial and, in particular, parallel mechanisms, started relatively recently. Force balancing of the serial manipulator PUMA-760 was studied at the end of the 1980's [30, 72, 73] and in 1996 an investigation of the force balancing of a 3-DoF planar parallel manipulator was presented [65]. With the force and moment balancing of a 3-DoF planar parallel manipulator in 2000, dynamic balancing of parallel manipulators was first treated in a systematic way [85].

Although various articles have been published afterwards such as [5, 58, 75, 25, 26], the total volume of related literature still is considerably small. The results also turn out to be technically challenging to apply in practice. In most cases the dynamic balancing of multi-DoF mechanisms is investigated by direct application of known solutions from the dynamic balancing of 1-DoF mechanisms. Therefore two main approaches have evolved, referred to here as the *link-by-link approach* where each link is considered for balance individually and the *leg-by-leg approach* where each leg (connecting the moving platform and the base) of a parallel mechanism is

considered for balance individually [59, 9, 93]. It was shown that these approaches lead to a significant, if not huge, addition of mass and inertia and also to complex designs [94, 102, 98, 97, 93, 92]. An increase of mass and inertia by a factor four as best result showed already to be challenging to obtain. Where low mass is typically important for moving vehicles, space manipulators, and robot end-effectors, low inertia is important for low driving torques and low energy consumption. For high-speed manipulators dynamic balance solutions with low inertia are of specific importance while the mass can be higher since their base, and therefore the mass of the manipulator, remains stationary. Especially balance elements on links that have no pivot with the base are disastrous for the mass and inertia of a mechanisms. Without additional counter-rotations moment balancing is hardly possible [34, 71, 107].

With both the link-by-link approach and the leg-by-leg approach a parallel mechanism is regarded a combination of multiple (serial) mechanisms balanced individually. Closed-loop kinematics then are not considered and therefore the solutions that are obtained are limited. These solutions also risk to have more balance elements than necessary. This is since individually the links and legs have more degrees-of-freedom than the manipulator they are part of.

Another limitation is that the dynamic balancing of multi-DoF mechanisms is considered at the end of the design process in a similar way as the dynamic balancing of 1-DoF mechanisms. The design process is initiated with the kinematic synthesis for a determined motion along a certain trajectory or within a certain workspace as required for the intended task. Various kinematic solutions (i.e. various mechanisms) are found suitable of which one is selected. This solution is optimized for, among others, good force transmissions, low complexity, chosen actuation means, and suitable size. Subsequently the dynamic balancing of the mechanism is considered which then is only possible with additional elements. Therefore the likeliness that the balance solutions are advantageous is particularly small. As a compromise, for 1-DoF mechanisms it was proposed to relax the kinematic requirements in order to improve dynamics [38]. Although for parallel mechanisms this could be advantageous too, this step is still overlooked.

Various solutions exist to reduce shaking forces and shaking moments of manipulators with limited addition of mass and inertia. With motion planning a manipulator is moved along trajectories that cause minimal shaking forces and shaking moments [80]. Partial balancing of the shaking forces and shaking moments, or solely balancing the shaking forces fully or partly can also be useful [25]. For 1-DoF mechanisms, of which the motion trajectory is prescribed, partial balance is often found as best compromise [91]. Another possibility to reduce mass and inertia addition is, instead of balancing each element passively (i.e. by mechanical means), to balance multiple or all elements together with separate actively controlled balance elements on the base [94, 99]. Then less balance effort is required since only the resultant forces and moments are considered. Techniques such as the balancing of specific frequencies in 1-DoF mechanisms or in rotatory machines [112], automatic rotary balancers [28], flywheels [90], and prescribing the input speed for optimal balancing [66] are not applicable for the balancing of multi-DoF robotic manipulators since they require constant repetitive behavior.

Other topics of dynamic balancing include input torque balancing [37], power balancing, pin (bearing) force balancing, and balancing of the internal forces [90, 6, 89], and the dynamic balancing of flexible (compliant) mechanisms [110]. Although they are important and related issues in machine design, their aims are different from the balancing of shaking forces and shaking moments.

1.4 Focus on inherently balanced mechanism design

Because of the additional mass, inertia, and complexity that is needed to balance a mechanism, the current attitude towards dynamic balancing is that "the price paid for shaking force and shaking moment balancing is discouraging" [67]. The question then is *how to design dynamically balanced mechanisms that encourage them to be applied*.

An important difference with 1-DoF mechanisms is that the kinematic design of multi-DoF manipulators is flexible. Especially of parallel mechanisms often a multitude of kinematic solutions are suitable to have the manipulator perform its tasks since motions are determined by the controller. For instance a delta robot as in Fig. 1.1 is able to pick and place from a conveyor belt into a box also when the dimensions of the elements are changed. The selection of the kinematic solution of multi-DoF manipulators however is based on rather intuitive choices. For instance the 'optimal' kinematics of the Adept Quattro - one of the most successful delta robots - were determined by minimizing a cost function of a specific motion along a single specific trajectory, based on minimizing the sum of the link lengths and a specific choice on the condition number [81]. These design criteria can be changed easily. This means that the focus when designing high-speed manipulators can be shifted from kinematic issues to dynamic issues such as dynamic balance.

Mechanism elements that determine the motion of a mechanism can be designed to function for dynamic balance as well, but this has shown to be insufficient for dynamic balance. Additional balance elements however solely function for the dynamic balance while they do not influence the kinematics. They are not involved in determining the motion of the mechanism. This means that there is a possibility to improve the design of balanced mechanisms by involving all elements with the motion as well as with the dynamic balance. A dynamically balanced mechanism where all elements contribute to both the motion and the dynamic balance will be named an *inherently dynamically balanced mechanism*.

To take advantage of the parallel architecture for the purpose of dynamic balance, the common way of designing a balanced mechanism - to first consider solely the kinematics of the manipulator and subsequently its balancing - is not efficient. When, after all the effort to balance a given architecture, the balance solutions are not applicable, the kinematics have to be considered all over again. When, on the contrary, in the conceptual phase of the design it would be possible to consider dynamic balance prior to the kinematic synthesis, then mechanism solutions may be found that are inherently dynamically balanced with advantageous balance charac-

teristics. Dynamic balance then would not be determined by kinematical choices and balance solutions would not be limited beforehand. This may also lead to new kinematic solutions, possibly with fewer elements and with less additional mass, inertia, and complexity. The approach of considering dynamic balance as a design principle in the kinematic synthesis will be referred to as the *inherent dynamic balancing approach of mechanisms*.

The aim of this work is to propose and develop a methodology for analysis and, in particular, synthesis of inherently force and moment-balanced mechanisms and to show the application potential of the results.

1.5 Outline

This work is divided in 10 chapters. In chapter 2 the theory of force balancing is introduced by investigating *how linear momentum equations can be used to find the inherent force balance solutions of given mechanisms and to find advantageous kinematic solutions*. Closed-chain linkages are investigated for force balance by considering the loop closure relations.

From chapter 3 onwards, the theory is approached at a more abstract level. In this chapter it is shown *how mechanism architectures can be designed that are inherently force balanced with solely essential kinematic conditions*. Principal vectors linkages are proposed, developed, and investigated and methods for analysis are found and applied.

Chapter 4 extends the theory by showing *how the loop closure relations of closed kinematic chains can be considered with equivalent masses*. A method is proposed where an element with a general mass distribution is modeled mass equivalently with real and virtual equivalent masses with which closed-chain principal vector linkages are derived.

In chapter 5 various related theories from literature are generalized and combined to investigate *how principal vector linkages can become extended principal vector linkage architectures*. A closed-chain principal vector linkage architecture of two similar linkages with multiple interconnections is created and analyzed.

In chapter 6 moment balancing is considered by showing *how principal vector linkages can be applied for inherent moment balance*. The angular momentum of principal vector linkages is written in a fundamental way from which the moment balance solutions can be derived.

For application of the theory, in chapter 7 it is shown *how inherently balanced mechanism solutions for desired tasks and functions can be synthesized from principal vector linkage architectures*. Concepts of inherently balanced manipulators and end-effectors are derived together with concepts of large moving structures.

In chapter 8 the application of dynamic balance is evaluated with an experimental setup of a high-speed manipulator to show *how an inherently balanced manipulator compares to an unbalanced manipulator and how dynamic balance can be advantageous in practice*. For the first time a high-speed dynamically balanced parallel

manipulator was built and tested. Besides the balance performance also practical aspects as the actuator torques, the bearing forces, and the effect of payload are evaluated.

Chapters 9 and 10 reflect and conclude this work. In the appendix the history of the method of principal vectors and of its founder Otto Fischer are presented.

Part of the content of this work has been published. The content of chapter 2 has been published partly as:

- Van der Wijk, V., Krut, S., Pierrot, F., Herder, J.L.: Generic method for deriving the general shaking force balance conditions of parallel manipulators with application to a redundant planar 4-RRR parallel manipulator. Proceedings of the 13th IFTOMM World Congress on Mechanism and Machine Science, Guanajuato, Mexico (A12-523) (2011)
- Van der Wijk, V., Herder, J. L.: Dynamic balancing of a single crank-double slider mechanism with symmetrically moving couplers. In: Pisla et al. (eds), New Trends in Mechanism Science: Analysis and Design, Proceedings of the IFTOMM 3rd European Conference on Mechanism Science, 413-420, Springer (2010, recipient of the best student paper award)
- Van der Wijk, V., Herder, J.L., Force Balanced Delta Robot, WO2010/128849 (patent, 2010)
- Van der Wijk, V., Herder, J.L.: Dynamic balancing of Clavels delta robot. In: Kecskeméthy and Müller, Computational Kinematics, Proc. of the 5th Int. Workshop on Computational Kinematics, 315322, Springer (2009)

The content of chapter 3 has been published partly as:

- Van der Wijk, V., Herder, J. L.: Synthesis method for linkages with center of mass at invariant link point - pantograph based mechanisms. Mechanism and Machine Theory **24**, 15-28 (2012)
- Van der Wijk, V., Herder, J.L.: On the development of low-mass force balanced manipulators. In: Jadran Lenarčič, Michael M. Stanisic, Advances in Robot Kinematics, Proc. of the IFTOMM 12th Int. Symposium on Advances in Robot Kinematics, 411420, Springer (2010)

The content of chapters 4 and 5 are part of the publication:

- Van der Wijk, V., Herder, J.L.: Inherently balanced 4R four-bar based linkages. In: Lenarčič, J. and Hustý, M. (Eds.), Latest Advances in Robot Kinematics, Proc. of the IFTOMM 13th Int. Symposium on Advances in Robot Kinematics, 309316, Springer (2012)

The content of chapter 6 has been published partly as:

- Van der Wijk, V.: Shaking-moment balancing of mechanisms with principal vectors and momentum". J. of Frontiers of Mechanical Engineering **8**(1), 10-16 (2013)
- Van der Wijk, V., Herder, J. L.: The method of principal vectors for the synthesis of shaking moment balanced linkages. In: Viaderro, F. and Ceccarelli, M. (Eds.), New Trends in Mechanism and Machine Science, MMS 7, Proc. of the

4th IFToMM European Conference on Mechanism Science, 399-407, Springer (2012)

The content of chapter 7 includes parts of various mentioned publications. The content of chapter 8 is part of the publications:

- Van der Wijk, V., Krut, S., Pierrot, F., Herder, J.L.: Design and experimental evaluation of a dynamically balanced redundant planar 4-RRR parallel manipulator. *I.J. of Robotics Research* **32**(6), 744-759 (2013)
- Van der Wijk, V., Krut, S., Pierrot, F., Herder, J.L., Manipulator comprising a fixed base and a movable platform, with four motor-driven chains of articulated links, WO2012-173471A1 (patent, 2012)

The content of the appendix was published as:

- Van der Wijk, V., Herder, J. L.: The work of Otto Fischer and the historical development of his method of principle vectors for mechanism and machine science. In: T. Koetsier, M. Ceccarelli (Eds.), *Explorations in the History of Machines and Mechanisms*, Proc. of the 4th Int. Symp. on the History of Machines and Mechanisms, 521-534, Springer (2012)

Related scientific literature from the author which is not part of this work include:

- Van der Wijk, V., Herder, J.L.: On the addition of degrees of freedom to force-balanced linkages. Proc. of the 19th CISM-IFToMM Symposium on Robot Design, Dynamics, and Control (Romansy), June 12-15, Paris, FR, 2012-025 (2012)
- Van der Wijk, V., Demeulenaere, B., Gosselin, C., Herder, J. L.: Comparative analysis for low-mass and low-inertia dynamic balancing of mechanisms. *ASME Journal of Mechanisms and Robotics*, Vol. 4, Issue 3, 031008 (2012)
- Van der Wijk, V., Herder, J.L.: Active dynamic balancing unit for controlled shaking force and shaking moment balancing. Proc. of IDETC 2010, Vol. 2, Issue PARTS A AND B, 1515-1522, ASME, Montreal, CA, DETC2010 28423 (2010)
- Van der Wijk, V., Herder, J.L.: Force balancing of variable payload by active force-balanced reconfiguration of the mechanism. In: Jian S Dai, Matteo Zoppi and Xianwen Kong, *Reconfigurable Mechanisms and Robotics*, Proceedings of the ASME/IFToMM International Conference on Reconfigurable Mechanisms and Robots, pp. 321-328, KC Edizioni (2009)
- Van der Wijk, V., Herder, J.L.: Guidelines for low mass and low inertia dynamic balancing of mechanisms and robotics. In: Torsten Kröger and Fiedrich M. Wahl, *Advances in Robotics Research*, Proceedings of the German Workshop on Robotics, pp. 21-30, Springer (2009)
- Van der Wijk, V., Herder, J. L., Demeulenaere, B.: Comparison of various dynamic balancing principles regarding additional mass and additional inertia. *ASME Journal of Mechanisms and Robotics*, Vol. 1, Issue 4, 04 1006, pp. 1-9 (2009)
- Van der Wijk, V., Herder, J. L.: Synthesis of dynamically balanced mechanisms by using counter-rotary counter-mass balanced double pendula. *ASME Journal of Mechanical Design*, Vol. 131, Issue 11, 11003 (2009)

- Van der Wijk, V., Herder, J.L.: Dynamic balancing of mechanisms by using an actively driven counter-rotary counter-mass for low mass and low inertia. Proc. of the Second International Workshop on Fundamental Issues and Future Research Directions for Parallel Mechanisms and Manipulators, Montpellier, FR, pp. 241-251 (2008)
- Van der Wijk, V., Herder, J.L.: Double pendulum balanced by counter-rotary counter-masses as useful element for synthesis of dynamically balanced mechanisms. Proceedings of IDETC 2008, Volume 2, Issue PART A, pp. 453-463, ASME, New York, US, DETC2008 49402 (2008)

Chapter 2

Inherent force balance of given mechanisms with linear momentum

Abstract In this chapter it is shown that with linear momentum equations the inherent force balance solutions of given mechanisms can be found in a generic and systematic way. First open kinematic chains are investigated, followed by closed kinematic chains that are composed of open kinematic chains. With the known *open chain method* the loop closure relations of closed kinematic chains are not considered. The *method of linearly independent linear momentum* is proposed as an intuitive and straightforward method to investigate closed kinematic chains by substituting the derivatives of the loop equations in the linear momentum equations. It is shown how the linear momentum equations of a mechanism with multiple closed loops include not only the general force balance conditions, but also a variety of general and specific configurations of force-balanced mechanisms as subsets.

2.1 Open kinematic chains

An open kinematic chain is a chain of multiple connected elements of which only one element has a connection with the base. Generally the force balancing of these chains is investigated by analysis of the location of the common CoM, as for instance with the PUMA 760 serial manipulator of two elements [31, 30, 72, 73]. In this section it is shown how the force balance conditions of open kinematic chains are derived with linear momentum equations. This approach will show its potential when loop equations are considered later on.

Figure 2.1a shows a single rotatable link which is connected to the base with a revolute pair in A_0 . Its orientation is described with angle θ_1 relative to the base. The link has a mass m_1 of which the CoM is defined with parameters e_1 and f_1 as illustrated. The position of the link CoM can be written with respect to the xy -reference frame with origin in A_0 as

$$\bar{r}_1 = \begin{bmatrix} r_{1x} \\ r_{1y} \end{bmatrix} = \bar{A}_0 + \begin{bmatrix} e_1 \cos \theta_1 - f_1 \sin \theta_1 \\ e_1 \sin \theta_1 + f_1 \cos \theta_1 \end{bmatrix} \quad (2.1)$$

The linear momentum \bar{L} of the link then can be written as

$$\bar{L} = m_1 \dot{\bar{r}}_1 = \begin{bmatrix} -m_1 e_1 \sin \theta_1 - m_1 f_1 \cos \theta_1 \\ m_1 e_1 \cos \theta_1 - m_1 f_1 \sin \theta_1 \end{bmatrix} \dot{\theta}_1 = \begin{bmatrix} C_1 \\ C_2 \end{bmatrix} \quad (2.2)$$

with constants C_1 and C_2 . Force balance is obtained for the conditions for which the linear momentum is constant for all motion, which means for any value of the time dependent parameters θ_1 and $\dot{\theta}_1$. In this case a constant linear momentum is only possible for $C_1 = C_2 = 0$ and for the two force balance conditions:

$$m_1 e_1 = 0 \quad m_1 f_1 = 0 \quad (2.3)$$

These conditions mean that the rotatable link is force balanced when the link CoM is located in pivot A_0 as illustrated in Fig. 2.1b.

A planar open chain of two links in series is shown in Fig. 2.2a. Here link 1 has a pivot with the base in A_0 and link 1 and 2 are connected with a revolute pair in A_1 . The distance between A_0 and A_1 is l_1 , which is the length of link 1. The linkage has 2-DoF motion which is described with angles θ_1 and θ_2 . Link 2 has a mass m_2 of which the CoM is defined in link 2 with parameters e_2 and f_2 as illustrated. The position of m_2 with respect to the base can be written as

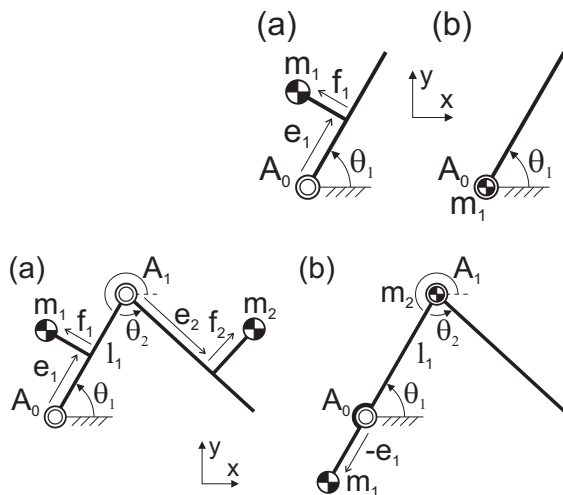
$$\bar{r}_2 = \begin{bmatrix} r_{2x} \\ r_{2y} \end{bmatrix} = \bar{A}_0 + \begin{bmatrix} l_1 \cos \theta_1 + e_2 \cos \theta_2 - f_2 \sin \theta_2 \\ l_1 \sin \theta_1 + e_2 \sin \theta_2 + f_2 \cos \theta_2 \end{bmatrix} \quad (2.4)$$

Together with (2.1), the linear momentum of this linkage can be written as

$$\bar{L} = m_1 \dot{\bar{r}}_1 + m_2 \dot{\bar{r}}_2 = \begin{bmatrix} -(m_1 e_1 + m_2 l_1) \sin \theta_1 - m_1 f_1 \cos \theta_1 \\ (m_1 e_1 + m_2 l_1) \cos \theta_1 - m_1 f_1 \sin \theta_1 \end{bmatrix} \dot{\theta}_1 +$$

Fig. 2.1 a) Single rotatable link with base pivot A_0 and mass m_1 of which the CoM is defined in the link with e_1 and f_1 ; b) Force balance is obtained when the CoM is located in A_0 .

Fig. 2.2 a) 2-DoF open chain of two links with general CoM and with a revolute pair in A_0 and A_1 ; b) For force balance the CoM of the second link is in A_1 while the CoM of link 1 is located at a determined distance from A_0 on the line through A_0 and A_1 .



$$\begin{bmatrix} -m_2 e_2 \sin \theta_2 - m_2 f_2 \cos \theta_2 \\ m_2 e_2 \cos \theta_2 - m_2 f_2 \sin \theta_2 \end{bmatrix} \dot{\theta}_2 = \begin{bmatrix} C_1 \\ C_2 \end{bmatrix} \quad (2.5)$$

The linear momentum equation is constant for all motion (i.e. for any value of the time dependent parameters θ_1 , θ_2 , $\dot{\theta}_1$, and $\dot{\theta}_2$) for $C_1 = C_2 = 0$ and for the four force balance conditions:

$$\begin{aligned} m_1 e_1 + m_2 l_1 &= 0 & m_1 f_1 &= 0 \\ m_2 e_2 &= 0 & m_2 f_2 &= 0 \end{aligned} \quad (2.6)$$

The resulting force balance solution is shown in Fig. 2.2b where the CoM of the second link is in A_1 and the CoM of link 1 is located at a distance $e_1 = -m_2 l_1 / m_1$ from A_0 as illustrated.

Figure 2.3a shows a 3-DoF open chain of three links in series with a revolute pair in A_1 , A_2 , and A_3 . The distance between A_1 and A_2 is l_2 , which is the length of link 2. The motion of the linkage is described with angles θ_1 , θ_2 , and θ_3 . Link 3 has a mass m_3 of which the CoM is defined in link 3 with parameters e_3 and f_3 as illustrated. The position of m_3 with respect to the base can be written as

$$\bar{r}_3 = \begin{bmatrix} r_{3x} \\ r_{3y} \end{bmatrix} = \bar{A}_0 + \begin{bmatrix} l_1 \cos \theta_1 + l_2 \cos \theta_2 + e_3 \cos \theta_3 - f_3 \sin \theta_3 \\ l_1 \sin \theta_1 + l_2 \sin \theta_2 + e_3 \sin \theta_3 + f_3 \cos \theta_3 \end{bmatrix} \quad (2.7)$$

Together with (2.1) and (2.4), the linear momentum of this linkage can be written as

$$\begin{aligned} \bar{L} = m_1 \dot{r}_1 + m_2 \dot{r}_2 + m_3 \dot{r}_3 = & \\ & \left[-(m_1 e_1 + m_2 l_1 + m_3 l_1) \sin \theta_1 - m_1 f_1 \cos \theta_1 \right] \dot{\theta}_1 + \\ & \left[-(m_2 e_2 + m_3 l_2) \sin \theta_2 - m_2 f_2 \cos \theta_2 \right] \dot{\theta}_2 + \\ & \left[(m_2 e_2 + m_3 l_2) \cos \theta_2 - m_2 f_2 \sin \theta_2 \right] \dot{\theta}_3 \end{aligned}$$

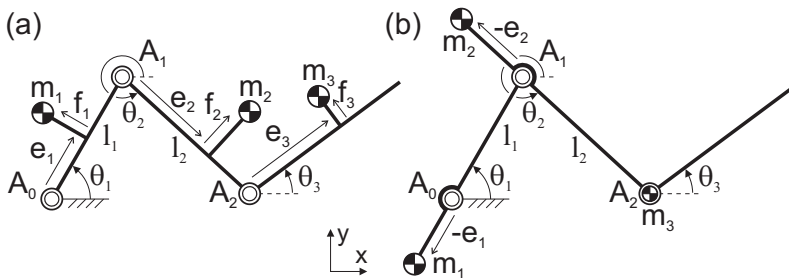


Fig. 2.3 a) 3-DoF open chain of three links with general CoM and with a revolute pair in A_0 , A_1 , and A_2 ; b) For force balance the CoM of the third link is in A_2 and the CoMs of links 1 and 2 are located at determined distances from A_0 on the line through A_0 and A_1 and from A_1 on the line through A_1 and A_2 , respectively.

$$\begin{bmatrix} -m_3 e_3 \sin \theta_3 - m_3 f_3 \cos \theta_3 \\ m_3 e_3 \cos \theta_3 - m_3 f_3 \sin \theta_3 \end{bmatrix} \dot{\theta}_3 = \begin{bmatrix} C_1 \\ C_2 \end{bmatrix} \quad (2.8)$$

The linear momentum equation is constant for all motion (i.e. for any value of the time dependent parameters θ_1 , θ_2 , θ_3 , $\dot{\theta}_1$, $\dot{\theta}_2$, and $\dot{\theta}_3$) for $C_1 = C_2 = 0$ and for the six force balance conditions:

$$\begin{aligned} m_1 e_1 + m_2 l_1 + m_3 l_1 &= 0 & m_1 f_1 &= 0 \\ m_2 e_2 + m_3 l_2 &= 0 & m_2 f_2 &= 0 \\ m_3 e_3 &= 0 & m_3 f_3 &= 0 \end{aligned} \quad (2.9)$$

The resulting force balance solution is illustrated in Fig. 2.3b. From the force balance conditions it is derived that the CoM of the third link is in A_2 , the CoM of link 2 is at a distance $e_2 = -m_3 l_2 / m_2$ from A_1 , and the CoM of link 1 is at a distance $e_1 = -m_2 l_1 / m_1 - m_3 l_1 / m_1$ from A_0 , respectively. This can be explained also as that the combined CoM of m_2 and m_3 is in A_1 and that the combined CoM of $m_2 + m_3$ imagined in A_1 and m_1 is in A_0 .

To compare the approach with linear momentum with the approach of describing the common CoM of the linkage to derive the force balance conditions, with (2.1), (2.4), and (2.7) the position of the common CoM is written as

$$\begin{aligned} \bar{r}_{CoM} &= \frac{1}{m_{tot}} (m_1 r_1 + m_2 r_2 + m_3 r_3) \\ &= \bar{A}_0 + \frac{1}{m_{tot}} \left[(m_1 e_1 + m_2 l_1 + m_3 l_1) \cos \theta_1 - m_1 f_1 \sin \theta_1 \right] + \\ &\quad \frac{1}{m_{tot}} \left[(m_2 e_2 + m_3 l_2) \cos \theta_2 - m_2 f_2 \sin \theta_2 \right] + \\ &\quad \frac{1}{m_{tot}} \left[m_3 e_3 \cos \theta_3 - m_3 f_3 \sin \theta_3 \right] = \begin{bmatrix} C_1 \\ C_2 \end{bmatrix} \end{aligned} \quad (2.10)$$

with $m_{tot} = m_1 + m_2 + m_3$ the total mass of the linkage. Finding the conditions for which \bar{r}_{CoM} is constant for all motion is of similar effort as to finding them from the linear momentum equations.

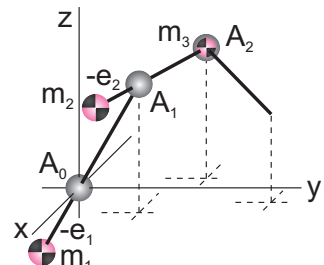


Fig. 2.4 Spatial open chain of three links with spherical joints in A_0 , A_1 , and A_2 which is force balanced with the solution in Fig. 2.3b.

Spatial open chains are force balanced with the same solutions as planar open chains. Figure 2.4 shows a spatial open chain of three links with spherical joints in A_0 , A_1 , and A_2 . This chain is force balanced with the solution in Fig. 2.3b. Since the only connection of the third link is in A_2 , for force balance m_3 is in this point. Subsequently the combined CoM of m_2 and m_3 is in A_1 and the combined CoM of $m_2 + m_3$ imagined in A_1 and m_1 is in A_0 .

2.2 Closed kinematic chains with open chain method

As mentioned with the link-by-link approach and the leg-by-leg approach in section 1.3, these common approaches for the design of balanced closed kinematic chains consist of composing them of balanced open kinematic chains [59, 107, 9, 26]. This is named here the *open chain method* for the design of balanced closed kinematic chains. The loop closure relations then are not considered. The various ways in which a specific balanced closed chain can be composed of balanced open chains determine the obtained force balance solutions. For instance there are multiple ways to model the mass of links around the points where open chains are connected [108]. For comparison with the force balance solutions that are obtained when the loop closure relations are considered, investigated in the next section, here it is shown how application of the open chain method results in conditioned force balance solutions.

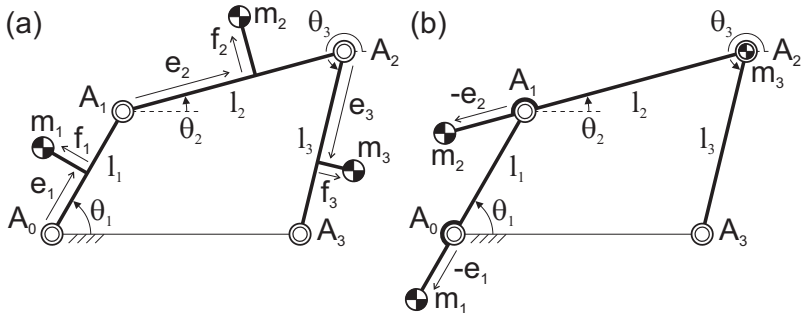


Fig. 2.5 a) When a planar 4R four-bar linkage is regarded an open chain of three links in series of which the first and the third link have pivots with the base then b) it is force balanced with the solution in Fig. 2.3b.

2.2.1 4R four-bar linkage

The planar 4R four-bar linkage in Fig. 2.5a can be regarded composed of the open chain of three links in Fig. 2.3a of which the third link has a pivot with the base in A_3 . Then with the solution in Fig. 2.3b the four-bar linkage is force balanced for the conditions (2.9) as in Fig. 2.5b.

It is also possible to consider a 4R four-bar linkage a combination of the open chain of two links in Fig. 2.2a and the rotatable link in Fig. 2.1a as illustrated in Fig. 2.6a. Both open chains have a pivot with the base and they are connected in A_2 . The force balance solution shown in Fig. 2.6b then is a combination of the solutions in Fig. 2.1b and in Fig. 2.2b. Here the CoM of link 3 is in A_3 and the CoMs of links 1 and 2 are determined with (2.6) where the CoM of link 2 is in A_1 .

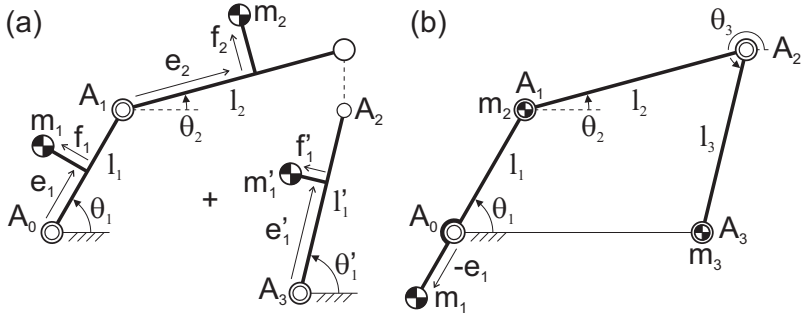


Fig. 2.6 a) When a 4R four-bar linkage is regarded a combination of an open chain of two links in series and a rotatable link then b) it is force balanced with the combination of the solutions in Figs. 2.1b and 2.2b.

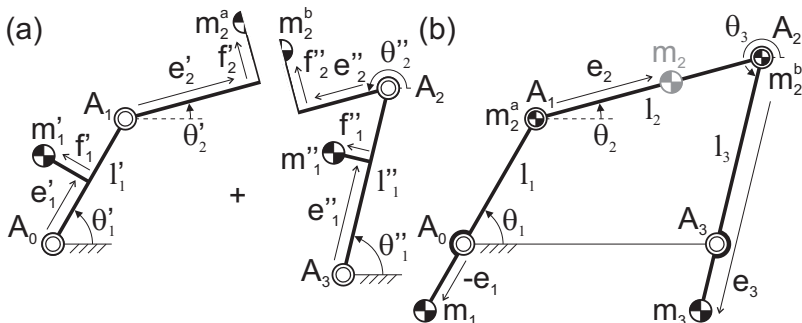


Fig. 2.7 a) When a 4R four-bar linkage is regarded a combination of two open chains of two links in series of which their second links are rigidly connected then b) it is force balanced with the solution in Fig. 2.2b applied to each open chain where m_2 is divided in equivalent masses m_2^a and m_2^b .

Another possibility is to consider a 4R four-bar linkage as a combination of two open chains of two links in series as shown in Fig. 2.7a. Here the second links of each chain are considered rigidly connected. With mass m_2 divided in the two equivalent masses m_2^a and m_2^b such that $m_2^a + m_2^b = m_2$, each chain is force balanced as in Fig. 2.2b where m_2^a is located in A_1 and m_2^b is located in A_2 . With $m_2^a e_2 = m_2^b(l_2 - e_2)$ the CoM of link 2 is located at a distance e_2 from A_1 with $f_2 = 0$ and the equivalent masses are calculated as $m_2^a = m_2(l_2 - e_2)/l_2$ and $m_2^b = m_2 e_2/l_2$.

With different joints such as spherical joints, the force-balanced linkages in Figs. 2.5b, 2.6b, and 2.7b can become spatial force-balanced linkages with equal force balance solutions. The balancing of the spatial 4R four-bar linkage or Bennett linkage, which has only revolute pairs, can also be considered similarly in multiple ways. Figure 2.8 shows the force balance solution when it is considered a combination of two open chains of two links as in Fig. 2.7b. In this case the CoM of link 2 can be located in any point in its link with the equivalent masses m_2^a and m_2^b located on the vertices of a line through the CoM of link 2 with the axes of rotation of joints A_1 and A_2 , of which there is no unique solution [76, 77]. For force balance, the CoMs of link 1 and link 3 can be anywhere on the lines t_1 and t_3 that are parallel to the axes of rotation of joints A_0 and A_3 , respectively.

2.2.2 Crank-slider mechanism

A crank-slider mechanism can be considered composed of an open chain of three links in series as illustrated in Fig. 2.9a where the third link is a slider which does not rotate with respect to the base. With $\dot{\theta}_3 = 0$, the linear momentum equation (2.8) reduces to

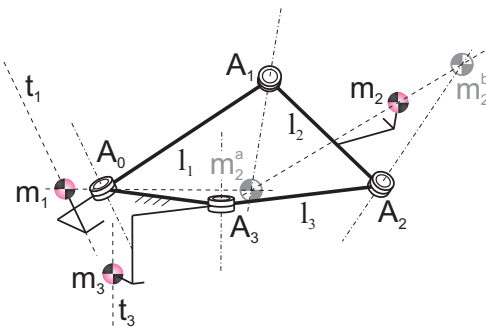


Fig. 2.8 A force-balanced Bennett linkage can be regarded a combination of two balanced open chains of two links with equivalent masses m_2^a and m_2^b on the axes of rotation through A_1 and A_2 , respectively. The CoM of link 2 can be in any point in its link.

$$\begin{aligned} \bar{L} = & \begin{bmatrix} -(m_1 e_1 + m_2 l_1 + m_3 l_1) \sin \theta_1 - m_1 f_1 \cos \theta_1 \\ (m_1 e_1 + m_2 l_1 + m_3 l_1) \cos \theta_1 - m_1 f_1 \sin \theta_1 \end{bmatrix} \dot{\theta}_1 + \\ & \begin{bmatrix} -(m_2 e_2 + m_3 l_2) \sin \theta_2 - m_2 f_2 \cos \theta_2 \\ (m_2 e_2 + m_3 l_2) \cos \theta_2 - m_2 f_2 \sin \theta_2 \end{bmatrix} \dot{\theta}_2 = \begin{bmatrix} C_1 \\ C_2 \end{bmatrix} \quad (2.11) \end{aligned}$$

and the four force balance conditions of the crank-slider mechanism then become:

$$\begin{aligned} m_1 e_1 + m_2 l_1 + m_3 l_1 &= 0 & m_1 f_1 &= 0 \\ m_2 e_2 + m_3 l_2 &= 0 & m_2 f_2 &= 0 \end{aligned} \quad (2.12)$$

These solutions are readily obtained from the linear momentum equation, while if they are obtained from the position of the common CoM (2.10) more effort is required because of handling the constant terms.

The force balance solution is shown in Fig. 2.9b where the CoM of link 3 is not determined and can be located anywhere in the link. The location and the orientation of the slider can be freely chosen without affecting the mass parameters of links 1 and 2. Link 3 can also be a slider in two directions. With spherical joints as in Fig. 2.4, the crank-slider mechanism in Fig. 2.9b becomes a force-balanced spatial crank-slider mechanism. Then it is possible to have link 3 slide in all three directions with any constant orientation without affecting the mass parameters of links 1 and 2.

2.2.3 Delta robot manipulator

Figure 2.10 shows the delta robot manipulator of Fig. 1.1 which is a spatial parallel mechanism of which the moving platform has 3-DoF translational motion [32, 33]. The platform is connected with the base with three arms of which the upper links

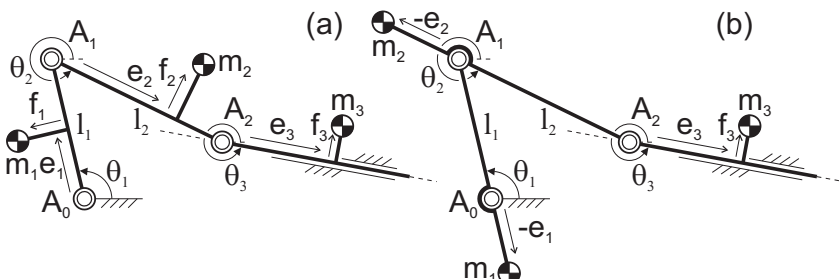


Fig. 2.9 a) A crank-slider mechanism can be regarded an open chain of three links where link 3 solely translates with respect to the base; b) Since link 3 does not rotate, for force balance the CoM of link 3 can be in any point in link 3 while the CoMs of links 1 and 2 are located as if m₃ is in A₂.

have pivots with the base in A_{10} , A_{20} , and A_{30} and the lower links are parallelograms that have spherical joints with the upper links in A_{11} , A_{21} , and A_{31} and spherical joints with the moving platform in A_{12} , A_{22} , and A_{32} .

For force balance each arm can be regarded a spatial open chain of three links, where each parallelogram is considered a single link and the third links of each chain are rigidly connected as the platform. Since the platform is solely translating, the CoM of the mass of the platform and payload m_p can be located in any point in the platform, similarly as with the crank-slider mechanism in Fig. 2.9b. Then with the three equivalent masses m_p^a , m_p^b , and m_p^c in joints A_{12} , A_{22} , and A_{32} , respectively, such that $m_p = m_p^a + m_p^b + m_p^c$, the force-balanced manipulator in Fig. 2.11a is obtained by combination of each force-balanced arm as illustrated in Fig. 2.11b.

The values of the equivalent masses can be chosen freely as long as their sum equals m_p . For instance for $m_p^a = m_p + m_{22}^b + m_{32}^b$, $m_p^b = -m_{22}^b$, and $m_p^c = -m_{32}^b$,

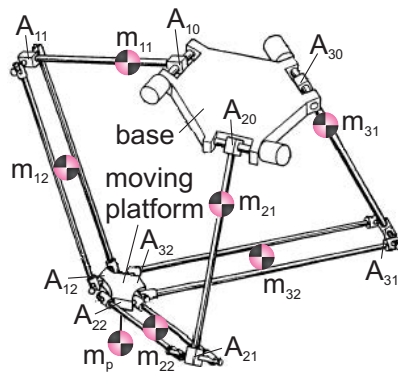


Fig. 2.10 A delta robot is a spatial parallel mechanism of which the moving platform has 3-DoF translational motion.

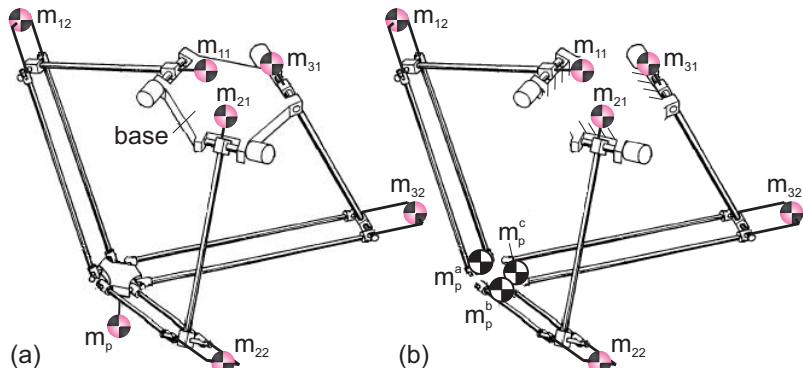


Fig. 2.11 a) Force-balanced delta robot by combination of (b) three individually force-balanced arms. (Patented [100])

where m_{22}^b and m_{32}^b are equivalent masses of the parallelograms of arms 2 and 3, respectively as illustrated in Fig. 2.12b, the force balance solution of the delta robot becomes as shown in Fig. 2.12a. With this solution arms 2 and 3 can be considered force-balanced open chains of two links as in Fig. 2.2 with equivalent masses of the parallelograms m_{22}^a and m_{32}^a .

When a delta robot is equipped with a spindle for an additional rotational DoF of the end-effector, the mass of the spindle can be included too. The spindle is connected to the center of the base and to the center of the platform and by a slider its length is variable. The mass of the spindle can be modeled with two equivalent masses of which one is located in the base and one is located in the platform. The equivalent mass in the platform can be included in m_p while the equivalent mass in the base is not involved since it is stationary.

2.3 Closed kinematic chains including loop-closure relations

The previous section showed that by the open chain method the force balance solutions of closed chains depend on design choices. One way to obtain the general force balance solutions of closed kinematic chains is to consider the loop closure relations. A commonly known method to do this is the method of linearly independent vectors with which the position of the common CoM of a linkage is described [13]. In this section a new method is proposed where the linear momentum of the closed chain linkage is written in a linearly independent form. This is named the *method of linearly independent linear momentum*. This method aims at being more intuitive and straightforward for the synthesis of force balance solutions. The method is first applied to the 4R four-bar linkage and subsequently to a 4-RRR parallel mechanism.

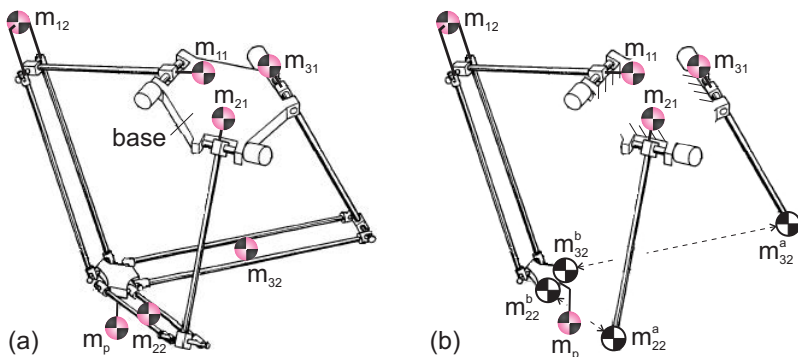


Fig. 2.12 a) Force-balanced delta robot when considered a combination of two open chains of two links and a spatial crank-slider mechanism with platform translating in three directions; b) The mass of two lower links is distributed with equivalent masses to the upper links and to the platform. (Patented [100])

2.3.1 4R four-bar linkage

To derive the general force balance conditions of the 4R four-bar linkage in Fig. 2.13a, the positions of the link CoMs can be written relative to A_0 as

$$\bar{r}_1 = \bar{A}_0 + \begin{bmatrix} e_1 \cos \theta_1 - f_1 \sin \theta_1 \\ e_1 \sin \theta_1 + f_1 \cos \theta_1 \end{bmatrix} \quad (2.13)$$

$$\bar{r}_2 = \bar{A}_0 + \begin{bmatrix} l_1 \cos \theta_1 + e_2 \cos \theta_2 - f_2 \sin \theta_2 \\ l_1 \sin \theta_1 + e_2 \sin \theta_2 + f_2 \cos \theta_2 \end{bmatrix} \quad (2.14)$$

$$\bar{r}_3 = \bar{A}_0 + \begin{bmatrix} l_1 \cos \theta_1 + l_2 \cos \theta_2 + e_3 \cos \theta_3 - f_3 \sin \theta_3 \\ l_1 \sin \theta_1 + l_2 \sin \theta_2 + e_3 \sin \theta_3 + f_3 \cos \theta_3 \end{bmatrix} \quad (2.15)$$

with l_i the length of link i of which each CoM is defined in its link with e_i and f_i , as illustrated. The linear momentum is then written as

$$\begin{aligned} \bar{L} &= m_1 \dot{\bar{r}}_1 + m_2 \dot{\bar{r}}_2 + m_3 \dot{\bar{r}}_3 \\ &= \left[\begin{array}{c} -(m_1 e_1 + m_2 l_1 + m_3 l_1) \sin \theta_1 - m_1 f_1 \cos \theta_1 \\ (m_1 e_1 + m_2 l_1 + m_3 l_1) \cos \theta_1 - m_1 f_1 \sin \theta_1 \end{array} \right] \dot{\theta}_1 + \\ &\quad \left[\begin{array}{c} -(m_2 e_2 + m_3 l_2) \sin \theta_2 - m_2 f_2 \cos \theta_2 \\ (m_2 e_2 + m_3 l_2) \cos \theta_2 - m_2 f_2 \sin \theta_2 \end{array} \right] \dot{\theta}_2 + \\ &\quad \left[\begin{array}{c} -m_3 e_3 \sin \theta_3 - m_3 f_3 \cos \theta_3 \\ m_3 e_3 \cos \theta_3 - m_3 f_3 \sin \theta_3 \end{array} \right] \dot{\theta}_3 \end{aligned} \quad (2.16)$$

The loop equations can be formulated as

$$\begin{aligned} l_1 \cos \theta_1 + l_2 \cos \theta_2 + l_3 \cos \theta_3 - l_4 \cos \theta_4 &= 0 \\ l_1 \sin \theta_1 + l_2 \sin \theta_2 + l_3 \sin \theta_3 - l_4 \sin \theta_4 &= 0 \end{aligned} \quad (2.17)$$

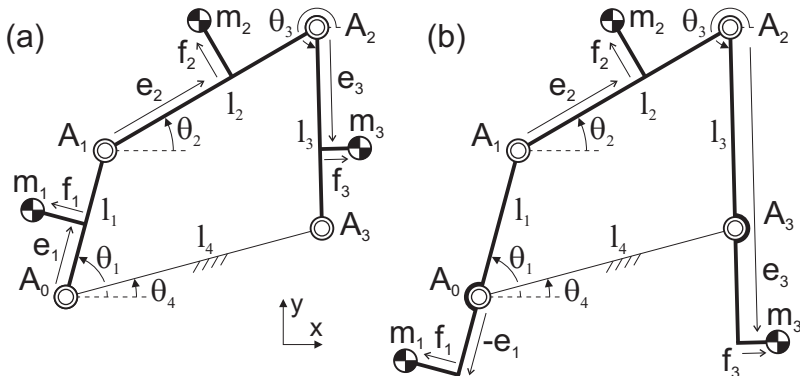


Fig. 2.13 a) A general 4R four-bar linkage and b) the force balance configuration where the link CoM of link 2 is freely selected.

To include the loop equations in the linear momentum equations, their time derivatives need to be substituted which are obtained as

$$\begin{aligned} -l_1 \sin \theta_1 \dot{\theta}_1 - l_2 \sin \theta_2 \dot{\theta}_2 - l_3 \sin \theta_3 \dot{\theta}_3 &= 0 \\ l_1 \cos \theta_1 \dot{\theta}_1 + l_2 \cos \theta_2 \dot{\theta}_2 + l_3 \cos \theta_3 \dot{\theta}_3 &= 0 \end{aligned} \quad (2.18)$$

and can be rearranged as

$$\begin{aligned} \sin \theta_2 \dot{\theta}_2 &= -\frac{l_1}{l_2} \sin \theta_1 \dot{\theta}_1 - \frac{l_3}{l_2} \sin \theta_3 \dot{\theta}_3 \\ \cos \theta_2 \dot{\theta}_2 &= -\frac{l_1}{l_2} \cos \theta_1 \dot{\theta}_1 - \frac{l_3}{l_2} \cos \theta_3 \dot{\theta}_3 \end{aligned} \quad (2.19)$$

Substituting these equations for $\sin \theta_2 \dot{\theta}_2$ and $\cos \theta_2 \dot{\theta}_2$ in (2.16) results in

$$\bar{L} = \left[\begin{array}{l} -(m_1 e_1 + m_2(1 - \frac{e_2}{l_2})l_1) \sin \theta_1 - (m_1 f_1 - m_2 \frac{f_2}{l_2} l_1) \cos \theta_1 \\ (m_1 e_1 + m_2(1 - \frac{e_2}{l_2})l_1) \cos \theta_1 - (m_1 f_1 - m_2 \frac{f_2}{l_2} l_1) \sin \theta_1 \\ (m_3(l_3 - e_3) + m_2 \frac{e_2}{l_2} l_3) \sin \theta_3 - (m_3 f_3 - m_2 \frac{f_2}{l_2} l_3) \cos \theta_3 \\ -(m_3(l_3 - e_3) + m_2 \frac{e_2}{l_2} l_3) \cos \theta_3 - (m_3 f_3 - m_2 \frac{f_2}{l_2} l_3) \sin \theta_3 \end{array} \right] \dot{\theta}_1 + \left[\begin{array}{l} (m_3(l_3 - e_3) + m_2 \frac{e_2}{l_2} l_3) \sin \theta_3 - (m_3 f_3 - m_2 \frac{f_2}{l_2} l_3) \cos \theta_3 \\ -(m_3(l_3 - e_3) + m_2 \frac{e_2}{l_2} l_3) \cos \theta_3 - (m_3 f_3 - m_2 \frac{f_2}{l_2} l_3) \sin \theta_3 \end{array} \right] \dot{\theta}_3 \quad (2.20)$$

The force balance conditions for which the linear momentum is constant for all motion are readily obtained as:

$$\begin{aligned} m_1 e_1 + m_2(1 - \frac{e_2}{l_2})l_1 &= 0 & m_1 f_1 - m_2 \frac{f_2}{l_2} l_1 &= 0 \\ m_3(l_3 - e_3) + m_2 \frac{e_2}{l_2} l_3 &= 0 & m_3 f_3 - m_2 \frac{f_2}{l_2} l_3 &= 0 \end{aligned} \quad (2.21)$$

These results are equal to the results found with the method of linearly independent vectors in [13]. Different from that method however is that no parameters related to the location of the common CoM are involved. The linear momentum equations only include parameters of the moving elements. By including the loop equations, the linear momentum of link 2 is written in linear terms of the motion of links 1 and 3. When the non-linear relation between the motion of links 1 and 3 is included, and the linear momentum is written depending on the motion of one of them, this does not result in different or more general force balance conditions.

Figure 2.13b shows a resulting force balance configuration where the CoM of link 2 is freely selected, and from (2.21) the locations of the CoMs of links 1 and 3 are calculated with

$$\begin{aligned} e_1 &= -m_2(1 - \frac{e_2}{l_2}) \frac{l_1}{m_1} & f_1 &= \frac{m_2 f_2}{l_2} \frac{l_1}{m_1} \\ e_3 &= m_2 \frac{e_2}{l_2} \frac{l_3}{m_3} + l_3 & f_3 &= \frac{m_2 f_2}{l_2} \frac{l_3}{m_3} \end{aligned} \quad (2.22)$$

For the synthesis of balanced mechanisms it can be useful to consider a force-balanced mechanism as a mechanism of which the common CoM of all elements is in an invariant point in one of the links. The mechanism then is force balanced about this invariant point. For instance for a four-bar mechanism this means that the mass of all four links is taken into account. The importance of considering the mass

of all elements depends on the application. For floating mechanisms such as robot end-effectors this can be required.

In Fig. 2.14a the 4R four-bar linkage is shown with a general CoM in each of the four elements, with m_4 the mass of link 4. The position of the CoM of link 4 can be written relative to A_0 as

$$\bar{r}_4 = \bar{A}_0 + \begin{bmatrix} (l_4 - e_4) \cos \theta_4 + f_4 \sin \theta_4 \\ (l_4 - e_4) \sin \theta_4 - f_4 \cos \theta_4 \end{bmatrix} \quad (2.23)$$

An invariant point S in link 4 is defined with o_1 and o_2 relative to A_3 . The position of S relative to A_0 can be written as

$$\bar{r}_S = \bar{A}_0 + \begin{bmatrix} (l_4 - o_1) \cos \theta_4 + o_2 \sin \theta_4 \\ (l_4 - o_1) \sin \theta_4 - o_2 \cos \theta_4 \end{bmatrix} \quad (2.24)$$

To find the force balance conditions for which S is the common CoM of the four links, the linear momentum of the linkage about S can be written as

$$\begin{aligned} \bar{L}_S &= m_1 \dot{\bar{r}}_1 + m_2 \dot{\bar{r}}_2 + m_3 \dot{\bar{r}}_3 + m_4 \dot{\bar{r}}_4 - m_{tot} \dot{\bar{r}}_S \\ &= \left[\begin{array}{c} -(m_1 e_1 + m_2 l_1 + m_3 l_1) \sin \theta_1 - m_1 f_1 \cos \theta_1 \\ (m_1 e_1 + m_2 l_1 + m_3 l_1) \cos \theta_1 - m_1 f_1 \sin \theta_1 \end{array} \right] \dot{\theta}_1 + \\ &\quad \left[\begin{array}{c} -(m_2 e_2 + m_3 l_2) \sin \theta_2 - m_2 f_2 \cos \theta_2 \\ (m_2 e_2 + m_3 l_2) \cos \theta_2 - m_2 f_2 \sin \theta_2 \end{array} \right] \dot{\theta}_2 + \\ &\quad \left[\begin{array}{c} -m_3 e_3 \sin \theta_3 - m_3 f_3 \cos \theta_3 \\ m_3 e_3 \cos \theta_3 - m_3 f_3 \sin \theta_3 \end{array} \right] \dot{\theta}_3 + \\ &\quad \left[\begin{array}{c} -m_4 (l_4 - e_4) \sin \theta_4 + m_4 f_4 \cos \theta_4 \\ m_4 (l_4 - e_4) \cos \theta_4 + m_4 f_4 \sin \theta_4 \end{array} \right] \dot{\theta}_4 - \end{aligned} \quad (2.25)$$

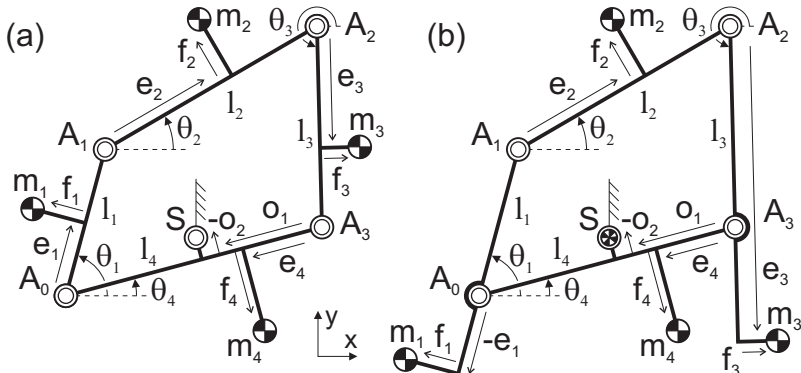


Fig. 2.14 a) Of a four-bar linkage where the mass of all four links is considered, b) force balance relative to link 4 is obtained when the common CoM is in an invariant point S in link 4.

$$\begin{bmatrix} -m_{tot}(l_4 - o_1) \sin \theta_4 + m_{tot}o_2 \cos \theta_4 \\ m_{tot}(l_4 - o_1) \cos \theta_4 + m_{tot}o_2 \sin \theta_4 \end{bmatrix} \dot{\theta}_4$$

with $m_{tot} = m_1 + m_2 + m_3 + m_4$ the total mass of the linkage. Since here θ_4 is a time dependent parameter, the derivatives of the loop equations (2.17) write

$$\begin{aligned} -l_1 \sin \theta_1 \dot{\theta}_1 - l_2 \sin \theta_2 \dot{\theta}_2 - l_3 \sin \theta_3 \dot{\theta}_3 + l_4 \sin \theta_4 \dot{\theta}_4 &= 0 \\ l_1 \cos \theta_1 \dot{\theta}_1 + l_2 \cos \theta_2 \dot{\theta}_2 + l_3 \cos \theta_3 \dot{\theta}_3 - l_4 \cos \theta_4 \dot{\theta}_4 &= 0 \end{aligned} \quad (2.26)$$

which can be rearranged as

$$\begin{aligned} \sin \theta_2 \dot{\theta}_2 &= -\frac{l_1}{l_2} \sin \theta_1 \dot{\theta}_1 - \frac{l_3}{l_2} \sin \theta_3 \dot{\theta}_3 + \frac{l_4}{l_2} \sin \theta_4 \dot{\theta}_4 \\ \cos \theta_2 \dot{\theta}_2 &= -\frac{l_1}{l_2} \cos \theta_1 \dot{\theta}_1 - \frac{l_3}{l_2} \cos \theta_3 \dot{\theta}_3 + \frac{l_4}{l_2} \cos \theta_4 \dot{\theta}_4 \end{aligned} \quad (2.27)$$

After substitution for $\sin \theta_2 \dot{\theta}_2$ and $\cos \theta_2 \dot{\theta}_2$ the linear momentum can be written as

$$\bar{L}_S = \begin{bmatrix} -(m_1 e_1 + m_2(1 - \frac{e_2}{l_2})l_1) \sin \theta_1 - (m_1 f_1 - m_2 \frac{f_2}{l_2}l_1) \cos \theta_1 \\ (m_1 e_1 + m_2(1 - \frac{e_2}{l_2})l_1) \cos \theta_1 - (m_1 f_1 - m_2 \frac{f_2}{l_2}l_1) \sin \theta_1 \end{bmatrix} \dot{\theta}_1 + \begin{bmatrix} (m_3(l_3 - e_3) + m_2 \frac{e_2}{l_2}l_3) \sin \theta_3 - (m_3 f_3 - m_2 \frac{f_2}{l_2}l_3) \cos \theta_3 \\ -(m_3(l_3 - e_3) + m_2 \frac{e_2}{l_2}l_3) \cos \theta_3 - (m_3 f_3 - m_2 \frac{f_2}{l_2}l_3) \sin \theta_3 \end{bmatrix} \dot{\theta}_3 - \begin{bmatrix} -(m_{tot}(l_4 - o_1) - m_2 \frac{e_2}{l_2}l_4 - m_3 l_4 - m_4(l_4 - e_4)) \sin \theta_4 + \\ (m_{tot}o_2 + m_2 \frac{f_2}{l_2}l_4 - m_4 f_4) \cos \theta_4 \\ (m_{tot}(l_4 - o_1) - m_2 \frac{e_2}{l_2}l_4 - m_3 l_4 - m_4(l_4 - e_4)) \cos \theta_4 + \\ (m_{tot}o_2 + m_2 \frac{f_2}{l_2}l_4 - m_4 f_4) \sin \theta_4 \end{bmatrix} \dot{\theta}_4 \quad (2.28)$$

The conditions for which S is the common CoM for all motion, i.e. for which the linear momentum is constant for all motion, are the general force balance conditions of the 4R four-bar linkage:

$m_1 e_1 + m_2(1 - \frac{e_2}{l_2})l_1 = 0$	$m_1 f_1 - m_2 \frac{f_2}{l_2}l_1 = 0$
$m_3(l_3 - e_3) + m_2 \frac{e_2}{l_2}l_3 = 0$	$m_3 f_3 - m_2 \frac{f_2}{l_2}l_3 = 0$
$m_{tot}(l_4 - o_1) - m_2 \frac{e_2}{l_2}l_4 - m_3 l_4 - m_4(l_4 - e_4) = 0$	$m_{tot}o_2 + m_2 \frac{f_2}{l_2}l_4 - m_4 f_4 = 0$

(2.29)

Four of the force balance conditions are equal to (2.21). The other two determine the locations of S and m_4 in link 4. With the CoMs of link 2 and link 4 freely selected as in the resulting force balance configuration in Fig. 2.14b, from the force balance conditions the locations of the CoMs of link 1 and link 3 and of S are calculated as

$$\begin{aligned} e_1 &= -\frac{m_2}{m_1}(1 - \frac{e_2}{l_2})l_1 & f_1 &= \frac{l_1}{m_1} \frac{m_2 f_2}{l_2} & o_1 &= \frac{l_4}{m_{tot}}(m_1 + m_2(1 - \frac{e_2}{l_2}) + m_4 \frac{e_4}{l_4}) \\ e_3 &= \frac{m_2}{m_3} \frac{e_2}{l_2}l_3 + l_3 & f_3 &= \frac{l_3}{m_3} \frac{m_2 f_2}{l_2} & o_2 &= -\frac{l_4}{m_{tot}}(m_2 \frac{f_2}{l_2} - m_4 \frac{f_4}{l_4}) \end{aligned} \quad (2.30)$$

If the location of S in link 4 is freely selected, the location of the CoM of link 4 is derived as

$$e_4 = \frac{m_{tot}}{m_4} o_1 - \frac{l_4}{m_4} (m_1 + m_2 (1 - \frac{e_2}{l_2})) \quad f_4 = \frac{m_{tot}}{m_4} o_2 + \frac{l_4}{m_4} \frac{m_2 f_2}{l_2} \quad (2.31)$$

From the force balance conditions (2.29) a variety of force balance configurations can be found. With $m_4 = 0$ the solution in Fig. 2.13b is obtained and with $m_4 = 0$ and $f_1 = f_2 = f_3 = 0$ the force balance solutions in Figs. 2.5b, 2.6b, and 2.7b are obtained. Figure 2.15 shows force balance configurations where m_3 is freely selected. It is shown how the locations of m_1 and m_2 depend on the location of m_3 where parameters f_1 , f_2 , and f_3 keep the same sign. Dependent on the location of m_4 , the location of S can also change of side. Figure 2.16a shows a force balance configuration where all link CoMs are located in points extended from their links, and in the configuration in Fig. 2.16b S coincides with A_0 , $e_2 = 0$, and $e_3 = l_3$.

Figure 2.17 shows a physical model in two poses of the force-balanced mechanism in Fig. 2.14b with $f_i = 0$. The links are made of $\varnothing 4$ mm welding rod with shiny copper-brown appearance while the joint axles are made of $\varnothing 2$ mm welding rod. To limit the lengths of links 1 and 3, each has a counter-mass of steel. Figure 2.18 shows a physical model in two poses of the force-balanced mechanism in Fig. 2.15a with $f_i = 0$. Also this model is made of $\varnothing 4$ mm and $\varnothing 2$ mm welding rod.

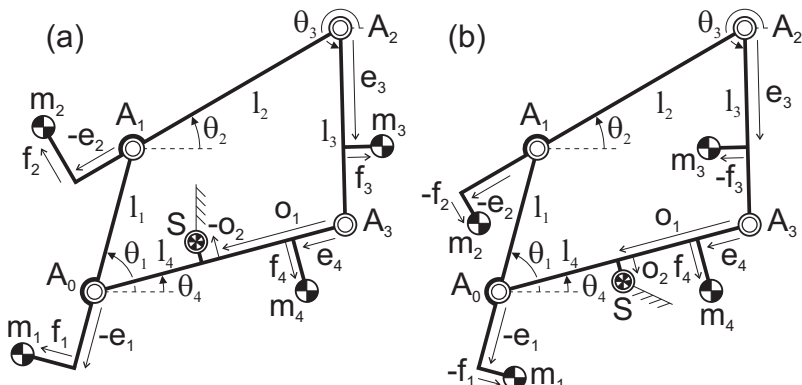


Fig. 2.15 Force balance configurations for freely selected CoM of link 3 when defined with (a) positive f_3 and (b) negative f_3 .

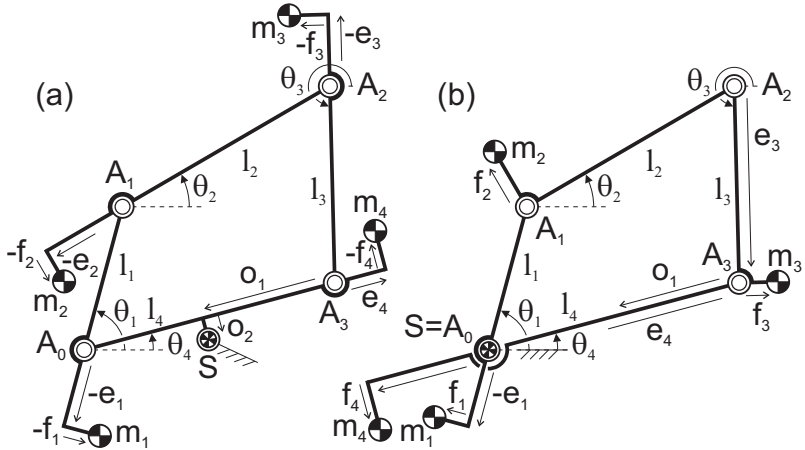


Fig. 2.16 a) Force balance configuration with all link CoMs in points extended from their links; b) Force-balance configuration with S and A_0 coinciding and where m_2 and m_3 are located on the lines through A_1 and A_3 perpendicular to their links, respectively.

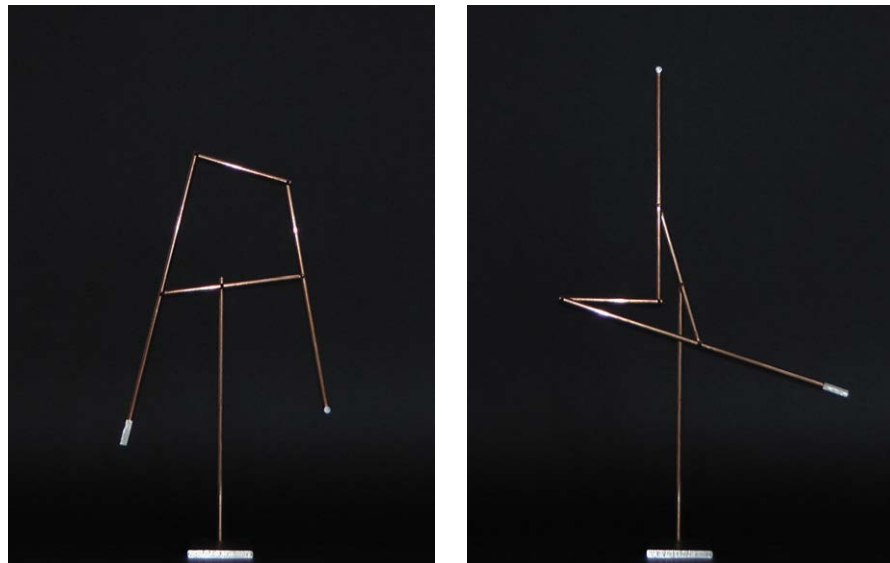


Fig. 2.17 Physical model in two poses of the force-balanced four-bar linkage in Fig. 2.14b when $f_i = 0$. (see model in motion at: www.kineticart.nl)



Fig. 2.18 Physical model in two poses of the force-balanced four-bar linkage in Fig. 2.15 when $f_i = 0$. (see model in motion at: www.kineticart.nl)

2.3.2 Parallelogram and pantograph linkage

The linear momentum (2.28) of the general 4R four-bar linkage consists of three non-linearly dependent terms. When specific kinematic conditions are found for which some of these terms become linearly dependent, then they can be summed and reduced force balance conditions can be obtained. For instance for the specific kinematic conditions that $\theta_3 = \theta_1 + \pi$ and $\theta_4 = \theta_2$ ($\dot{\theta}_3 = \dot{\theta}_1$ and $\dot{\theta}_4 = \dot{\theta}_2$), which is for the geometrical conditions $l_1 = l_3 = a_1$ and $l_2 = l_4 = a_2$, the linear momentum in (2.28) can be written as

$$\bar{L}_S = \begin{bmatrix} -(m_1 e_1 + m_2 a_1 + m_3(a_1 - e_3)) \sin \theta_1 - (m_1 f_1 - m_3 f_3) \cos \theta_1 \\ (m_1 e_1 + m_2 a_1 + m_3(a_1 - e_3)) \cos \theta_1 - (m_1 f_1 - m_3 f_3) \sin \theta_1 \end{bmatrix} \dot{\theta}_1 - \begin{bmatrix} -(m_{tot}(a_2 - o_1) - m_2 e_2 - m_3 a_2 - m_4(a_2 - e_4)) \sin \theta_2 + \\ (m_{tot} o_2 + m_2 f_2 - m_4 f_4) \cos \theta_2 \\ (m_{tot}(a_2 - o_1) - m_2 e_2 - m_3 a_2 - m_4(a_2 - e_4)) \cos \theta_2 + \\ (m_{tot} o_2 + m_2 f_2 - m_4 f_4) \sin \theta_2 \end{bmatrix} \dot{\theta}_2 \quad (2.32)$$

The linear momentum is constant for all motion for the force balance conditions:

$$\begin{aligned} m_1 e_1 + m_2 a_1 + m_3(a_1 - e_3) &= 0 & m_1 f_1 - m_3 f_3 &= 0 \\ m_{tot}(a_2 - o_1) - m_2 e_2 - m_3 a_2 - m_4(a_2 - e_4) &= 0 & m_{tot} o_2 + m_2 f_2 - m_4 f_4 &= 0 \end{aligned} \quad (2.33)$$

Figure 2.19a illustrates the obtained mechanism which is a parallelogram linkage. As compared to the general four-bar linkage which has six force balance conditions, with four force balance conditions one additional link CoM can be freely selected, which is shown here for m_3 . This means that the mechanism has more

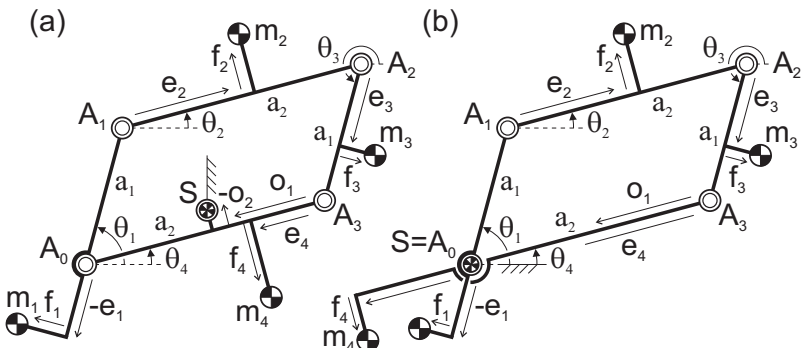


Fig. 2.19 a) Force-balanced parallelogram linkage where the CoMs of links 2 and 3 are freely selected; b) Force balance configuration with S and A_0 coinciding where the CoMs of links 2 and 3 are freely selected.

freedom for balanced design. For instance in the solution shown in Fig. 2.19b the locations of the CoMs of links 2 and 3 are not limited as in Fig. 2.16b.

Alternative force balance configurations are shown in Fig. 2.20 where S and A_3 coincide. The mechanism in Fig. 2.20b is also known as a pantograph linkage. It can be considered a specific version of Sylvester's pantograph or a modified version of Scheiner's pantograph [11]. The pantograph linkage is known for balancing because of its properties of similarity [61, 7, 107, 25]. In the next chapters it will be shown how the pantograph is a fundamental mechanism for the synthesis of inherently dynamically balanced linkages.

A physical model of a force-balanced pantograph linkage is shown in various poses in Fig. 2.21. All elements were made of steel and all joint axles were made of Ø 2mm welding rod. The diagonally oriented elements in the left picture are double layered, while the horizontally orientated elements are single layered and positioned in between.

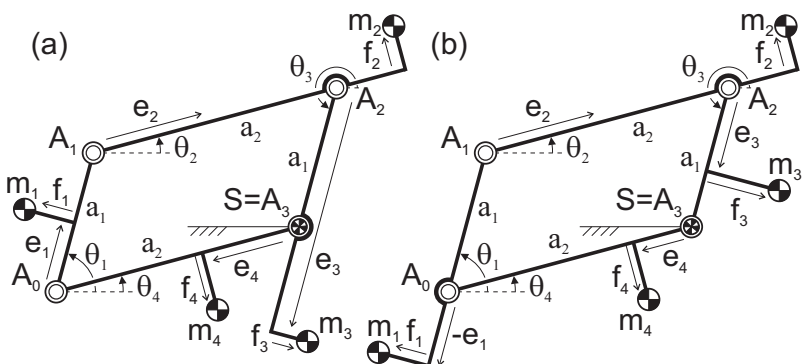


Fig. 2.20 Specific force balance configurations where S and A_3 coincide. The configuration in (b) is known as a balanced pantograph linkage.



Fig. 2.21 Physical model of the force-balanced pantograph linkage in Fig. 2.20b in various poses.
(see model in motion at: www.kineticart.nl)

2.3.3 4-RRR parallel manipulator

In this section it is shown how the method of linearly independent linear momentum is applied to find the inherent force balance conditions of mechanisms with multiple closed loops. Therefore a planar 4-RRR parallel manipulator is investigated. It is also shown how for specific kinematic conditions specific force balance configurations are obtained.

The general configuration of a 3-DoF planar 4-RRR parallel manipulator is shown in Fig. 2.22. It has four arms i consisting each of two links j with lengths l_{ij} which are connected with revolute pairs in B_i . The orientation of each link is described with θ_{ij} with respect to the x -axis of the reference frame. Each arm is connected to the base with pivots in A_i and to the moving platform with revolute pairs in C_i . The moving platform has a width c_5 , a height d_5 , and an orientation θ_5 . The CoM of mass m_{ij} in each link is defined with e_{ij} and f_{ij} as illustrated. The platform has a mass m_5 of which the CoM is defined with e_5 and f_5 with respect to its center.

The positions of the link CoMs can be written in various ways. The shortest way is to write the link CoMs of each arm with respect to its base pivot as

$$\begin{aligned}\bar{r}_{i1} &= \bar{A}_i + \begin{bmatrix} e_{i1} \cos \theta_{i1} - f_{i1} \sin \theta_{i1} \\ e_{i1} \sin \theta_{i1} + f_{i1} \cos \theta_{i1} \end{bmatrix} \\ \bar{r}_{i2} &= \bar{A}_i + \begin{bmatrix} l_{i1} \cos \theta_{i1} + e_{i2} \cos \theta_{i2} - f_{i2} \sin \theta_{i2} \\ l_{i1} \sin \theta_{i1} + e_{i2} \sin \theta_{i2} + f_{i2} \cos \theta_{i2} \end{bmatrix}\end{aligned}\quad (2.24)$$

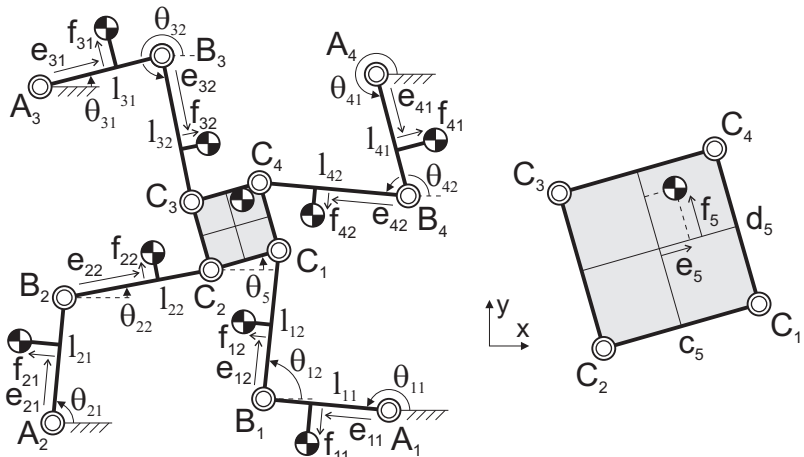


Fig. 2.22 General configuration of a planar 3-DoF 4-RRR parallel manipulator. Four arms of two links connect the moving platform $C_1C_2C_3C_4$ to the base in pivots A_1, A_2, A_3 , and A_4 .

The position of the CoM of the platform can also be written in various ways, for instance with respect to one of the pivots A_i . A shorter solution is to divide the mass of the platform in four equivalent masses μ_{5i} that are located in joints C_i , of which the positions are written as

$$\bar{r}_{5i} = \bar{A}_i + \begin{bmatrix} l_{i1} \cos \theta_{i1} + l_{i2} \cos \theta_{i2} \\ l_{i1} \sin \theta_{i1} + l_{i2} \sin \theta_{i2} \end{bmatrix} \quad (2.35)$$

In this case parameter θ_5 is omitted. The equivalent masses are related to the mass and the CoM of the platform as

$$\mu_{51} + \mu_{52} + \mu_{53} + \mu_{54} = m_5 \quad (2.36)$$

$$\mu_{51} - \mu_{52} - \mu_{53} + \mu_{54} = \frac{m_5 e_5}{c_5} \quad (2.37)$$

$$-\mu_{51} - \mu_{52} + \mu_{53} + \mu_{54} = \frac{m_5 f_5}{d_5} \quad (2.38)$$

This equivalent mass model is illustrated in Fig. 2.23. With three equations, one of the four equivalent masses is independent. The linear momentum of the manipulator can be written with the derivatives of the position vectors as

$$\begin{aligned} \bar{L} &= \sum_{i=1}^4 (m_{i1} \dot{r}_{i1} + m_{i2} \dot{r}_{i2} + \mu_{5i} \dot{r}_{5i}) \\ &= \begin{bmatrix} -\lambda_{111} \sin \theta_{11} - \lambda_{112} \cos \theta_{11} \\ \lambda_{111} \cos \theta_{11} - \lambda_{112} \sin \theta_{11} \end{bmatrix} \dot{\theta}_{11} + \begin{bmatrix} -\lambda_{211} \sin \theta_{21} - \lambda_{212} \cos \theta_{21} \\ \lambda_{211} \cos \theta_{21} - \lambda_{212} \sin \theta_{21} \end{bmatrix} \dot{\theta}_{21} + \\ &\quad \begin{bmatrix} -\lambda_{311} \sin \theta_{31} - \lambda_{312} \cos \theta_{31} \\ \lambda_{311} \cos \theta_{31} - \lambda_{312} \sin \theta_{31} \end{bmatrix} \dot{\theta}_{31} + \begin{bmatrix} -\lambda_{411} \sin \theta_{41} - \lambda_{412} \cos \theta_{41} \\ \lambda_{411} \cos \theta_{41} - \lambda_{412} \sin \theta_{41} \end{bmatrix} \dot{\theta}_{41} + \\ &\quad \begin{bmatrix} -\lambda_{121} \sin \theta_{12} - \lambda_{122} \cos \theta_{12} \\ \lambda_{121} \cos \theta_{12} - \lambda_{122} \sin \theta_{12} \end{bmatrix} \dot{\theta}_{12} + \begin{bmatrix} -\lambda_{221} \sin \theta_{22} - \lambda_{222} \cos \theta_{22} \\ \lambda_{221} \cos \theta_{22} - \lambda_{222} \sin \theta_{22} \end{bmatrix} \dot{\theta}_{22} + \\ &\quad \begin{bmatrix} -\lambda_{321} \sin \theta_{32} - \lambda_{322} \cos \theta_{32} \\ \lambda_{321} \cos \theta_{32} - \lambda_{322} \sin \theta_{32} \end{bmatrix} \dot{\theta}_{32} + \begin{bmatrix} -\lambda_{421} \sin \theta_{42} - \lambda_{422} \cos \theta_{42} \\ \lambda_{421} \cos \theta_{42} - \lambda_{422} \sin \theta_{42} \end{bmatrix} \dot{\theta}_{42} \end{aligned} \quad (2.39)$$

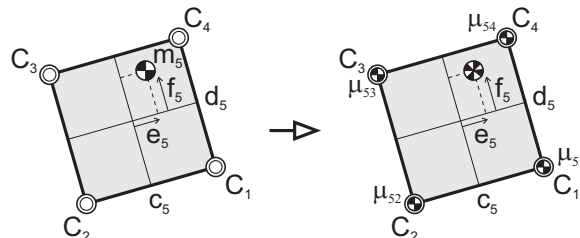


Fig. 2.23 For the shortest description of the position of the platform CoM, its mass m_5 is modeled with four equivalent masses μ_{5i} in the joints C_i .

with

$$\begin{aligned}\lambda_{i11} &= m_{i1}e_{i1} + m_{i2}l_{i1} + \mu_{5i}l_{i1} & \lambda_{i12} &= m_{i1}f_{i1} \\ \lambda_{i21} &= m_{i2}e_{i2} + \mu_{5i}l_{i2} & \lambda_{i22} &= m_{i2}f_{i2}\end{aligned}\quad (2.40)$$

Since the linear momentum is zero for all motion when $\lambda_{ijk} = 0$, already various force balance solutions are obtained. For instance the force balance configuration in Fig. 2.24a where one μ_{5i} is freely selected and each arm is force balanced individually as with the open chain method. Figure 2.24b shows a force balance configuration where e_{22} and e_{42} are freely selected and μ_{52} and μ_{54} are obtained from (2.40) as

$$\mu_{52} = \frac{-e_{22}m_{22}}{l_{22}}, \quad \mu_{54} = \frac{-e_{42}m_{42}}{l_{42}}$$

Characteristic of these force balance solutions is that $f_{ij} = 0$.

The 4-RRR manipulator has three independent closed loops of which the relations can be written as

$$\begin{aligned}\bar{r}_{51} &= \overline{A_1 A_2} + \bar{r}_{52} + c_5 \begin{bmatrix} c\theta_5 \\ s\theta_5 \end{bmatrix} \\ \bar{r}_{51} &= \overline{A_1 A_3} + \bar{r}_{53} + c_5 \begin{bmatrix} c\theta_5 \\ s\theta_5 \end{bmatrix} + d_5 \begin{bmatrix} s\theta_5 \\ -c\theta_5 \end{bmatrix} \\ \bar{r}_{51} &= \overline{A_1 A_4} + \bar{r}_{54} + d_5 \begin{bmatrix} s\theta_5 \\ -c\theta_5 \end{bmatrix}\end{aligned}\quad (2.41)$$

with $c()$ and $s()$ as shorthand for $\cos()$ and $\sin()$, respectively. The time derivatives of the loop equations can be derived as

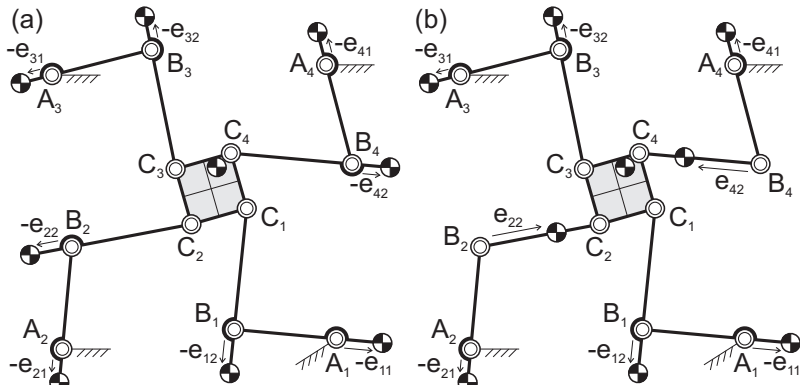


Fig. 2.24 Force balance configurations without considering the loop-closure relations where (a) one μ_{5i} is freely selected and (b) the CoMs of links 22 and 42 are freely selected.

$$l_{11} \begin{bmatrix} -s\theta_{11} \\ c\theta_{11} \end{bmatrix} \dot{\theta}_{11} + l_{12} \begin{bmatrix} -s\theta_{12} \\ c\theta_{12} \end{bmatrix} \dot{\theta}_{12} = l_{21} \begin{bmatrix} -s\theta_{21} \\ c\theta_{21} \end{bmatrix} \dot{\theta}_{21} + \\ l_{22} \begin{bmatrix} -s\theta_{22} \\ c\theta_{22} \end{bmatrix} \dot{\theta}_{22} + c_5 \begin{bmatrix} -s\theta_5 \\ c\theta_5 \end{bmatrix} \dot{\theta}_5 \quad (2.42)$$

$$l_{11} \begin{bmatrix} -s\theta_{11} \\ c\theta_{11} \end{bmatrix} \dot{\theta}_{11} + l_{12} \begin{bmatrix} -s\theta_{12} \\ c\theta_{12} \end{bmatrix} \dot{\theta}_{12} = l_{31} \begin{bmatrix} -s\theta_{31} \\ c\theta_{31} \end{bmatrix} \dot{\theta}_{31} + \\ l_{32} \begin{bmatrix} -s\theta_{32} \\ c\theta_{32} \end{bmatrix} \dot{\theta}_{32} + c_5 \begin{bmatrix} -s\theta_5 \\ c\theta_5 \end{bmatrix} \dot{\theta}_5 + d_5 \begin{bmatrix} c\theta_5 \\ s\theta_5 \end{bmatrix} \dot{\theta}_5 \quad (2.43)$$

$$l_{11} \begin{bmatrix} -s\theta_{11} \\ c\theta_{11} \end{bmatrix} \dot{\theta}_{11} + l_{12} \begin{bmatrix} -s\theta_{12} \\ c\theta_{12} \end{bmatrix} \dot{\theta}_{12} = l_{41} \begin{bmatrix} -s\theta_{41} \\ c\theta_{41} \end{bmatrix} \dot{\theta}_{41} + \\ l_{42} \begin{bmatrix} -s\theta_{42} \\ c\theta_{42} \end{bmatrix} \dot{\theta}_{42} + d_5 \begin{bmatrix} c\theta_5 \\ s\theta_5 \end{bmatrix} \dot{\theta}_5 \quad (2.44)$$

Since vectors $\overline{A_1A_2}$, $\overline{A_1A_3}$, and $\overline{A_1A_4}$ are constant, they do not appear in the time derivatives. It is possible to reduce these 6 equations to 4 equations by eliminating θ_5 and $\dot{\theta}_5$. Rearranging the resulting equations for θ_{12} and θ_{32} then results in

$$\begin{bmatrix} s\theta_{12} \\ c\theta_{12} \end{bmatrix} \dot{\theta}_{12} = -\frac{l_{11}}{l_{12}} \begin{bmatrix} s\theta_{11} \\ c\theta_{11} \end{bmatrix} \dot{\theta}_{11} + \frac{l_{21}}{Ul_{12}} \begin{bmatrix} c\theta_{21} \\ -s\theta_{21} \end{bmatrix} \dot{\theta}_{21} + \frac{l_{22}}{Ul_{12}} \begin{bmatrix} c\theta_{22} \\ -s\theta_{22} \end{bmatrix} \dot{\theta}_{22} + \\ \frac{l_{41}}{Ul_{12}} \begin{bmatrix} -c\theta_{41} \\ s\theta_{41} \end{bmatrix} \dot{\theta}_{41} + \frac{l_{42}}{Ul_{12}} \begin{bmatrix} -c\theta_{42} \\ s\theta_{42} \end{bmatrix} \dot{\theta}_{42} + \frac{d_5 l_{21}}{c_5 Ul_{12}} \begin{bmatrix} s\theta_{21} \\ c\theta_{21} \end{bmatrix} \dot{\theta}_{21} + \\ \frac{d_5 l_{22}}{c_5 Ul_{12}} \begin{bmatrix} s\theta_{22} \\ c\theta_{22} \end{bmatrix} \dot{\theta}_{22} + \frac{c_5 l_{41}}{d_5 Ul_{12}} \begin{bmatrix} s\theta_{41} \\ c\theta_{41} \end{bmatrix} \dot{\theta}_{41} + \frac{c_5 l_{42}}{d_5 Ul_{12}} \begin{bmatrix} s\theta_{42} \\ c\theta_{42} \end{bmatrix} \dot{\theta}_{42} \quad (2.45)$$

$$\begin{bmatrix} s\theta_{32} \\ c\theta_{32} \end{bmatrix} \dot{\theta}_{32} = -\frac{l_{31}}{l_{32}} \begin{bmatrix} s\theta_{31} \\ c\theta_{31} \end{bmatrix} \dot{\theta}_{31} + \frac{l_{21}}{l_{32}} \begin{bmatrix} s\theta_{21} \\ c\theta_{21} \end{bmatrix} \dot{\theta}_{21} + \frac{l_{22}}{l_{32}} \begin{bmatrix} s\theta_{22} \\ c\theta_{22} \end{bmatrix} \dot{\theta}_{22} + \frac{l_{41}}{l_{32}} \begin{bmatrix} s\theta_{41} \\ c\theta_{41} \end{bmatrix} \dot{\theta}_{41} + \\ \frac{l_{42}}{l_{32}} \begin{bmatrix} s\theta_{42} \\ c\theta_{42} \end{bmatrix} \dot{\theta}_{42} + \frac{l_{21}}{Ul_{32}} \begin{bmatrix} -c\theta_{21} \\ c\theta_{21} \end{bmatrix} \dot{\theta}_{21} + \frac{l_{22}}{Ul_{32}} \begin{bmatrix} -c\theta_{22} \\ c\theta_{22} \end{bmatrix} \dot{\theta}_{22} + \\ \frac{l_{41}}{Ul_{32}} \begin{bmatrix} c\theta_{41} \\ -s\theta_{41} \end{bmatrix} \dot{\theta}_{41} + \frac{l_{42}}{Ul_{32}} \begin{bmatrix} c\theta_{42} \\ -s\theta_{42} \end{bmatrix} \dot{\theta}_{42} - \frac{d_5 l_{21}}{c_5 Ul_{32}} \begin{bmatrix} s\theta_{21} \\ c\theta_{21} \end{bmatrix} \dot{\theta}_{21} - \\ \frac{d_5 l_{22}}{c_5 Ul_{32}} \begin{bmatrix} s\theta_{22} \\ c\theta_{22} \end{bmatrix} \dot{\theta}_{22} - \frac{c_5 l_{41}}{d_5 Ul_{32}} \begin{bmatrix} s\theta_{41} \\ c\theta_{41} \end{bmatrix} \dot{\theta}_{41} - \frac{c_5 l_{42}}{d_5 Ul_{32}} \begin{bmatrix} s\theta_{42} \\ c\theta_{42} \end{bmatrix} \dot{\theta}_{42} \quad (2.46)$$

with $U = \frac{c_5}{d_5} + \frac{d_5}{c_5}$. When these equations are substituted for $s\theta_{12}\dot{\theta}_{12}$, $c\theta_{12}\dot{\theta}_{12}$, $s\theta_{32}\dot{\theta}_{32}$, and $c\theta_{32}\dot{\theta}_{32}$ in (2.39), the linear momentum equations become

$$\bar{L} = \begin{bmatrix} (-\lambda_{111} + \frac{l_{11}}{l_{12}} \lambda_{121})s\theta_{11} + (-\lambda_{112} + \frac{l_{11}}{l_{12}} \lambda_{122})c\theta_{11} \\ (\lambda_{111} - \frac{l_{11}}{l_{12}} \lambda_{121})c\theta_{11} + (-\lambda_{112} + \frac{l_{11}}{l_{12}} \lambda_{122})s\theta_{11} \end{bmatrix} \dot{\theta}_{11} + \quad (2.47)$$

$$\begin{bmatrix} (-\lambda_{211} + \frac{l_{21}}{U l_{12}} \lambda_{122} - \frac{d_5 l_{21}}{c_5 U l_{12}} \lambda_{121} - \frac{l_{21}}{l_{32}} \lambda_{321} - \frac{l_{21}}{U l_{32}} \lambda_{322} + \frac{d_5 l_{21}}{c_5 U l_{32}} \lambda_{321})s\theta_{21} + \\ (-\lambda_{212} - \frac{l_{21}}{U l_{12}} \lambda_{121} - \frac{d_5 l_{21}}{c_5 U l_{12}} \lambda_{122} - \frac{l_{21}}{l_{32}} \lambda_{322} + \frac{l_{21}}{U l_{32}} \lambda_{321} + \frac{d_5 l_{21}}{c_5 U l_{32}} \lambda_{322})c\theta_{21} \\ (\lambda_{211} - \frac{l_{21}}{U l_{12}} \lambda_{122} + \frac{d_5 l_{21}}{c_5 U l_{12}} \lambda_{121} + \frac{l_{21}}{l_{32}} \lambda_{321} + \frac{l_{21}}{U l_{32}} \lambda_{322} - \frac{d_5 l_{21}}{c_5 U l_{32}} \lambda_{321})c\theta_{21} + \\ (-\lambda_{212} - \frac{l_{21}}{U l_{12}} \lambda_{121} - \frac{d_5 l_{21}}{c_5 U l_{12}} \lambda_{122} - \frac{l_{21}}{l_{32}} \lambda_{322} + \frac{l_{21}}{U l_{32}} \lambda_{321} + \frac{d_5 l_{21}}{c_5 U l_{32}} \lambda_{322})s\theta_{21} \end{bmatrix} \dot{\theta}_{21} +$$

$$\begin{bmatrix} (-\lambda_{311} + \frac{l_{31}}{l_{32}} \lambda_{321})s\theta_{31} + (-\lambda_{312} + \frac{l_{31}}{l_{32}} \lambda_{322})c\theta_{31} \\ (\lambda_{311} - \frac{l_{31}}{l_{32}} \lambda_{321})c\theta_{31} + (-\lambda_{312} + \frac{l_{31}}{l_{32}} \lambda_{322})s\theta_{31} \end{bmatrix} \dot{\theta}_{31} +$$

$$\begin{bmatrix} (-\lambda_{411} - \frac{l_{41}}{U l_{12}} \lambda_{122} - \frac{c_5 l_{41}}{d_5 U l_{12}} \lambda_{121} - \frac{l_{41}}{l_{32}} \lambda_{321} + \frac{l_{41}}{U l_{32}} \lambda_{322} + \frac{c_5 l_{41}}{d_5 U l_{32}} \lambda_{321})s\theta_{41} + \\ (-\lambda_{412} + \frac{l_{41}}{U l_{12}} \lambda_{121} - \frac{c_5 l_{41}}{d_5 U l_{12}} \lambda_{122} - \frac{l_{41}}{l_{32}} \lambda_{322} - \frac{l_{41}}{U l_{32}} \lambda_{321} + \frac{c_5 l_{41}}{d_5 U l_{32}} \lambda_{322})c\theta_{41} \\ (\lambda_{411} + \frac{l_{41}}{U l_{12}} \lambda_{122} + \frac{c_5 l_{41}}{d_5 U l_{12}} \lambda_{121} + \frac{l_{41}}{l_{32}} \lambda_{321} - \frac{l_{41}}{U l_{32}} \lambda_{322} - \frac{c_5 l_{41}}{d_5 U l_{32}} \lambda_{321})c\theta_{41} + \\ (-\lambda_{412} + \frac{l_{41}}{U l_{12}} \lambda_{121} - \frac{c_5 l_{41}}{d_5 U l_{12}} \lambda_{122} - \frac{l_{41}}{l_{32}} \lambda_{322} - \frac{l_{41}}{U l_{32}} \lambda_{321} + \frac{c_5 l_{41}}{d_5 U l_{32}} \lambda_{322})s\theta_{41} \end{bmatrix} \dot{\theta}_{41} +$$

$$\begin{bmatrix} (-\lambda_{221} + \frac{l_{22}}{U l_{12}} \lambda_{122} - \frac{d_5 l_{22}}{c_5 U l_{12}} \lambda_{121} - \frac{l_{22}}{l_{32}} \lambda_{321} - \frac{l_{22}}{U l_{32}} \lambda_{322} + \frac{d_5 l_{22}}{c_5 U l_{32}} \lambda_{321})s\theta_{22} + \\ (-\lambda_{222} - \frac{l_{22}}{U l_{12}} \lambda_{121} - \frac{d_5 l_{22}}{c_5 U l_{12}} \lambda_{122} - \frac{l_{22}}{l_{32}} \lambda_{322} + \frac{l_{22}}{U l_{32}} \lambda_{321} + \frac{d_5 l_{22}}{c_5 U l_{32}} \lambda_{322})c\theta_{22} \\ (\lambda_{221} - \frac{l_{22}}{U l_{12}} \lambda_{122} + \frac{d_5 l_{22}}{c_5 U l_{12}} \lambda_{121} + \frac{l_{22}}{l_{32}} \lambda_{321} + \frac{l_{22}}{U l_{32}} \lambda_{322} - \frac{d_5 l_{22}}{c_5 U l_{32}} \lambda_{321})c\theta_{22} + \\ (-\lambda_{222} - \frac{l_{22}}{U l_{12}} \lambda_{121} - \frac{d_5 l_{22}}{c_5 U l_{12}} \lambda_{122} - \frac{l_{22}}{l_{32}} \lambda_{322} + \frac{l_{22}}{U l_{32}} \lambda_{321} + \frac{d_5 l_{22}}{c_5 U l_{32}} \lambda_{322})s\theta_{22} \end{bmatrix} \dot{\theta}_{22} +$$

$$\begin{bmatrix} (-\lambda_{421} - \frac{l_{42}}{U l_{12}} \lambda_{122} - \frac{c_5 l_{42}}{d_5 U l_{12}} \lambda_{121} - \frac{l_{42}}{l_{32}} \lambda_{321} + \frac{l_{42}}{U l_{32}} \lambda_{322} + \frac{c_5 l_{42}}{d_5 U l_{32}} \lambda_{321})s\theta_{42} + \\ (-\lambda_{422} + \frac{l_{42}}{U l_{12}} \lambda_{121} - \frac{c_5 l_{42}}{d_5 U l_{12}} \lambda_{122} - \frac{l_{42}}{l_{32}} \lambda_{322} - \frac{l_{42}}{U l_{32}} \lambda_{321} + \frac{c_5 l_{42}}{d_5 U l_{32}} \lambda_{322})c\theta_{42} \\ (\lambda_{421} + \frac{l_{42}}{U l_{12}} \lambda_{122} + \frac{c_5 l_{42}}{d_5 U l_{12}} \lambda_{121} + \frac{l_{42}}{l_{32}} \lambda_{321} - \frac{l_{42}}{U l_{32}} \lambda_{322} - \frac{c_5 l_{42}}{d_5 U l_{32}} \lambda_{321})c\theta_{42} + \\ (-\lambda_{422} + \frac{l_{42}}{U l_{12}} \lambda_{121} - \frac{c_5 l_{42}}{d_5 U l_{12}} \lambda_{122} - \frac{l_{42}}{l_{32}} \lambda_{322} - \frac{l_{42}}{U l_{32}} \lambda_{321} + \frac{c_5 l_{42}}{d_5 U l_{32}} \lambda_{322})s\theta_{42} \end{bmatrix} \dot{\theta}_{42}$$

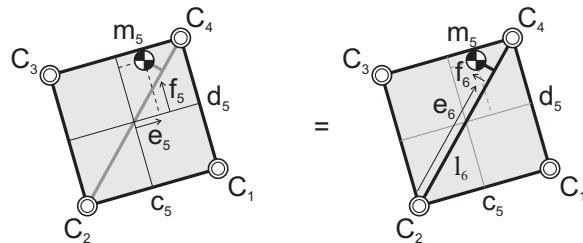


Fig. 2.25 Description of the platform CoM with parameters e_6 and f_6 along line C_2C_4 with length l_6 .

For force balance the linear momentum has to be constant for all motion, i.e. for all values of the time dependent parameters. This means that the 12 different coefficients in the linear momentum equations have to be zero. After substituting λ_{ijk} , μ_{5i} , and U , the twelve general force balance conditions of the planar 4-RRA parallel manipulator are derived as:

$$\begin{aligned}
m_{11}e_{11} + m_{12}l_{11}\left(1 - \frac{e_{12}}{l_{12}}\right) &= 0 \\
m_{31}e_{31} + m_{32}l_{31}\left(1 - \frac{e_{32}}{l_{32}}\right) &= 0 \\
m_{11}f_{11} - m_{12}l_{11}\frac{f_{12}}{l_{12}} &= 0 \\
m_{31}f_{31} - m_{32}l_{31}\frac{f_{32}}{l_{32}} &= 0 \\
m_{21}e_{21} + m_{22}l_{21} + m_{12}l_{21}\left(\frac{d_5^2}{l_6^2}\frac{e_{12}}{l_{12}} - \frac{c_5d_5}{l_6^2}\frac{f_{12}}{l_{12}}\right) + m_{32}l_{21}\left(\frac{c_5^2}{l_6^2}\frac{e_{32}}{l_{32}} + \frac{c_5d_5}{l_6^2}\frac{f_{32}}{l_{32}}\right) + \\
m_5l_{21}\frac{l_6 - e_6}{l_6} &= 0 \\
m_{41}e_{41} + m_{42}l_{41} + m_{12}l_{41}\left(\frac{c_5^2}{l_6^2}\frac{e_{12}}{l_{12}} + \frac{c_5d_5}{l_6^2}\frac{f_{12}}{l_{12}}\right) + m_{32}l_{41}\left(\frac{d_5^2}{l_6^2}\frac{e_{32}}{l_{32}} - \frac{c_5d_5}{l_6^2}\frac{f_{32}}{l_{32}}\right) + \\
m_5l_{41}\frac{e_6}{l_6} &= 0 \\
m_{22}e_{22} + m_{12}l_{22}\left(\frac{d_5^2}{l_6^2}\frac{e_{12}}{l_{12}} - \frac{c_5d_5}{l_6^2}\frac{f_{12}}{l_{12}}\right) + m_{32}l_{22}\left(\frac{c_5^2}{l_6^2}\frac{e_{32}}{l_{32}} + \frac{c_5d_5}{l_6^2}\frac{f_{32}}{l_{32}}\right) + \\
m_5l_{22}\frac{l_6 - e_6}{l_6} &= 0 \\
m_{42}e_{42} + m_{12}l_{42}\left(\frac{c_5^2}{l_6^2}\frac{e_{12}}{l_{12}} + \frac{c_5d_5}{l_6^2}\frac{f_{12}}{l_{12}}\right) + m_{32}l_{42}\left(\frac{d_5^2}{l_6^2}\frac{e_{32}}{l_{32}} - \frac{c_5d_5}{l_6^2}\frac{f_{32}}{l_{32}}\right) + \\
m_5l_{42}\frac{e_6}{l_6} &= 0 \\
m_{21}f_{21} + m_{12}l_{21}\left(\frac{c_5d_5}{l_6^2}\frac{e_{12}}{l_{12}} + \frac{d_5^2}{l_6^2}\frac{f_{12}}{l_{12}}\right) + m_{32}l_{21}\left(-\frac{c_5d_5}{l_6^2}\frac{e_{32}}{l_{32}} + \frac{c_5^2}{l_6^2}\frac{f_{32}}{l_{32}}\right) - \\
m_5l_{21}\frac{f_6}{l_6} &= 0 \\
m_{41}f_{41} + m_{12}l_{41}\left(-\frac{c_5d_5}{l_6^2}\frac{e_{12}}{l_{12}} + \frac{c_5^2}{l_6^2}\frac{f_{12}}{l_{12}}\right) + m_{32}l_{41}\left(\frac{c_5d_5}{l_6^2}\frac{e_{32}}{l_{32}} + \frac{d_5^2}{l_6^2}\frac{f_{32}}{l_{32}}\right) + \\
m_5l_{41}\frac{f_6}{l_6} &= 0 \\
m_{22}f_{22} + m_{12}l_{22}\left(\frac{c_5d_5}{l_6^2}\frac{e_{12}}{l_{12}} + \frac{d_5^2}{l_6^2}\frac{f_{12}}{l_{12}}\right) + m_{32}l_{22}\left(-\frac{c_5d_5}{l_6^2}\frac{e_{32}}{l_{32}} + \frac{c_5^2}{l_6^2}\frac{f_{32}}{l_{32}}\right) - \\
m_5l_{22}\frac{f_6}{l_6} &= 0 \\
m_{42}f_{42} + m_{12}l_{42}\left(-\frac{c_5d_5}{l_6^2}\frac{e_{12}}{l_{12}} + \frac{c_5^2}{l_6^2}\frac{f_{12}}{l_{12}}\right) + m_{32}l_{42}\left(\frac{c_5d_5}{l_6^2}\frac{e_{32}}{l_{32}} + \frac{d_5^2}{l_6^2}\frac{f_{32}}{l_{32}}\right) + \\
m_5l_{42}\frac{f_6}{l_6} &= 0
\end{aligned} \tag{2.48}$$

with

$$l_6 = \sqrt{c_5^2 + d_5^2} \quad e_6 = \frac{l_6}{2} + \frac{c_5e_5 + d_5f_5}{l_6} \quad f_6 = \frac{c_5f_5 - d_5e_5}{l_6} \tag{2.49}$$

where parameters e_6 and f_6 describe the CoM of the platform along the diagonal line C_2C_4 , which has a length l_6 as illustrated in Fig. 2.25.

In Figs. 2.26 and 2.27 four force balance configurations are presented that can be derived from these general force balance conditions. Different from the configura-

tions in Fig. 2.24 the parameters f_{ij} are not required to be zero. In the configuration in Fig. 2.26a the CoMs of the platform and of links 12 and 32 are freely selected and in the configuration in Fig. 2.26b the CoMs of the platform and of links 22 and 32 are freely selected. In the configuration in Fig. 2.27a the CoMs of the platform and of links 21 and 31 are freely selected and Figure 2.27b show a generalized version of the configuration in Fig. 2.24a. It is observed that in each configuration in total 3 link CoMs can be freely selected. This number is equal to the number of independent closed loops. Since each link CoM is defined with two parameters, in total 6 mass parameters can be defined by the designer.

Force balance solutions for specific kinematic conditions

The linear momentum (2.47) of the general 4-RRR parallel manipulator consists of six non-linearly dependent terms. Reduced force balance configurations can be obtained for specific kinematic conditions for which some of these terms become linearly dependent. For instance when $\theta_{11} = \theta_{42}$ and $\theta_{22} = \theta_{31}$ ($\dot{\theta}_{11} = \dot{\theta}_{42}$ and $\dot{\theta}_{22} = \dot{\theta}_{31}$) the first and sixth and the third and fifth term in (2.47) are linearly dependent, respectively. The linear momentum equations then reduce to

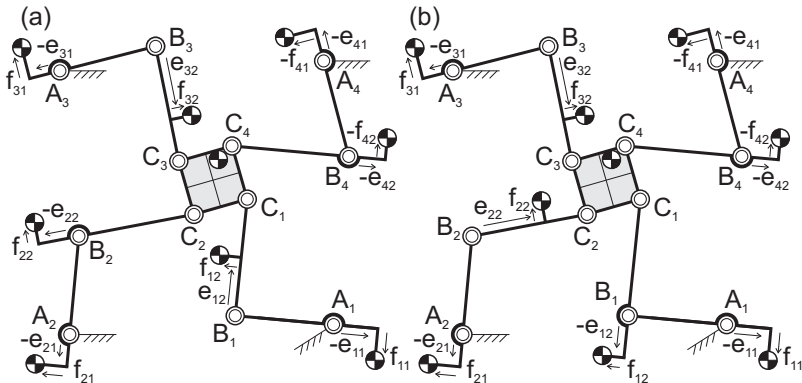


Fig. 2.26 Force balance configurations from general force balance conditions with (a) CoMs of platform and of links 12 and 32 freely selected and (b) CoMs of platform and of links 22 and 32 freely selected.

$$\bar{L} = \begin{bmatrix} \left[\begin{array}{l} (-\lambda_{111} + \frac{l_{11}}{l_{12}}\lambda_{121} - \lambda_{421} - \frac{l_{42}}{Ul_{12}}\lambda_{122} - \frac{c_5l_{42}}{d_5Ul_{12}}\lambda_{121} - \frac{l_{42}}{l_{32}}\lambda_{321} + \\ \frac{l_{42}}{Ul_{32}}\lambda_{322} + \frac{c_5l_{42}}{d_5Ul_{32}}\lambda_{321})s\theta_{11} + (-\lambda_{112} + \frac{l_{11}}{l_{12}}\lambda_{122} - \lambda_{422} + \\ \frac{l_{42}}{Ul_{12}}\lambda_{121} - \frac{c_5l_{42}}{d_5Ul_{12}}\lambda_{122} - \frac{l_{42}}{l_{32}}\lambda_{322} - \frac{l_{42}}{Ul_{32}}\lambda_{321} + \frac{c_5l_{42}}{d_5Ul_{32}}\lambda_{322})c\theta_{11} \\ (\lambda_{111} - \frac{l_{11}}{l_{12}}\lambda_{121} + \lambda_{421} + \frac{l_{42}}{Ul_{12}}\lambda_{122} + \frac{c_5l_{42}}{d_5Ul_{12}}\lambda_{121} + \frac{l_{42}}{l_{32}}\lambda_{321} - \\ \frac{l_{42}}{Ul_{32}}\lambda_{322} - \frac{c_5l_{42}}{d_5Ul_{32}}\lambda_{321})c\theta_{11} + (-\lambda_{112} + \frac{l_{11}}{l_{12}}\lambda_{122} - \lambda_{422} + \\ \frac{l_{42}}{Ul_{12}}\lambda_{121} - \frac{c_5l_{42}}{d_5Ul_{12}}\lambda_{122} - \frac{l_{42}}{l_{32}}\lambda_{322} - \frac{l_{42}}{Ul_{32}}\lambda_{321} + \frac{c_5l_{42}}{d_5Ul_{32}}\lambda_{322})s\theta_{11} \end{array} \right] \dot{\theta}_{11} + \quad (2.50) \\ \left[\begin{array}{l} (-\lambda_{211} + \frac{l_{21}}{Ul_{12}}\lambda_{122} - \frac{d_5l_{21}}{c_5Ul_{12}}\lambda_{121} - \frac{l_{21}}{l_{32}}\lambda_{321} - \frac{l_{21}}{Ul_{32}}\lambda_{322} + \frac{d_5l_{21}}{c_5Ul_{32}}\lambda_{321})s\theta_{21} + \\ (-\lambda_{212} - \frac{l_{21}}{Ul_{12}}\lambda_{121} - \frac{d_5l_{21}}{c_5Ul_{12}}\lambda_{122} - \frac{l_{21}}{l_{32}}\lambda_{322} + \frac{l_{21}}{Ul_{32}}\lambda_{321} + \frac{d_5l_{21}}{c_5Ul_{32}}\lambda_{322})c\theta_{21} \\ (\lambda_{211} - \frac{l_{21}}{Ul_{12}}\lambda_{122} + \frac{d_5l_{21}}{c_5Ul_{12}}\lambda_{121} + \frac{l_{21}}{l_{32}}\lambda_{321} + \frac{l_{21}}{Ul_{32}}\lambda_{322} - \frac{d_5l_{21}}{c_5Ul_{32}}\lambda_{321})c\theta_{21} + \\ (-\lambda_{212} - \frac{l_{21}}{Ul_{12}}\lambda_{121} - \frac{d_5l_{21}}{c_5Ul_{12}}\lambda_{122} - \frac{l_{21}}{l_{32}}\lambda_{322} + \frac{l_{21}}{Ul_{32}}\lambda_{321} + \frac{d_5l_{21}}{c_5Ul_{32}}\lambda_{322})s\theta_{21} \end{array} \right] \dot{\theta}_{21} + \\ \left[\begin{array}{l} (-\lambda_{311} + \frac{l_{31}}{l_{32}}\lambda_{321} - \lambda_{221} + \frac{l_{22}}{Ul_{12}}\lambda_{122} - \frac{d_5l_{22}}{c_5Ul_{12}}\lambda_{121} - \frac{l_{22}}{l_{32}}\lambda_{321} - \frac{l_{22}}{Ul_{32}}\lambda_{322} + \\ \frac{d_5l_{22}}{c_5Ul_{32}}\lambda_{321})s\theta_{31} + (-\lambda_{312} + \frac{l_{31}}{l_{32}}\lambda_{322} - \lambda_{222} - \frac{l_{22}}{Ul_{12}}\lambda_{121} - \frac{d_5l_{22}}{c_5Ul_{12}}\lambda_{122} - \\ \frac{l_{22}}{l_{32}}\lambda_{322} + \frac{l_{22}}{Ul_{32}}\lambda_{321} + \frac{d_5l_{22}}{c_5Ul_{32}}\lambda_{322})c\theta_{31} \\ (\lambda_{311} - \frac{l_{31}}{l_{32}}\lambda_{321} + \lambda_{221} - \frac{l_{22}}{Ul_{12}}\lambda_{122} + \frac{d_5l_{22}}{c_5Ul_{12}}\lambda_{121} + \frac{l_{22}}{l_{32}}\lambda_{321} + \frac{l_{22}}{Ul_{32}}\lambda_{322} - \\ \frac{d_5l_{22}}{c_5Ul_{32}}\lambda_{321})c\theta_{31} + (-\lambda_{312} + \frac{l_{31}}{l_{32}}\lambda_{322} - \lambda_{222} - \frac{l_{22}}{Ul_{12}}\lambda_{121} - \frac{d_5l_{22}}{c_5Ul_{12}}\lambda_{122} - \\ \frac{l_{22}}{l_{32}}\lambda_{322} + \frac{l_{22}}{Ul_{32}}\lambda_{321} + \frac{d_5l_{22}}{c_5Ul_{32}}\lambda_{322})s\theta_{31} \end{array} \right] \dot{\theta}_{31} + \\ \left[\begin{array}{l} (-\lambda_{411} - \frac{l_{41}}{Ul_{12}}\lambda_{122} - \frac{c_5l_{41}}{d_5Ul_{12}}\lambda_{121} - \frac{l_{41}}{l_{32}}\lambda_{321} + \frac{l_{41}}{Ul_{32}}\lambda_{322} + \frac{c_5l_{41}}{d_5Ul_{32}}\lambda_{321})s\theta_{41} + \\ (-\lambda_{412} + \frac{l_{41}}{Ul_{12}}\lambda_{121} - \frac{c_5l_{41}}{d_5Ul_{12}}\lambda_{122} - \frac{l_{41}}{l_{32}}\lambda_{322} - \frac{l_{41}}{Ul_{32}}\lambda_{321} + \frac{c_5l_{41}}{d_5Ul_{32}}\lambda_{322})c\theta_{41} \\ (\lambda_{411} + \frac{l_{41}}{Ul_{12}}\lambda_{122} + \frac{c_5l_{41}}{d_5Ul_{12}}\lambda_{121} + \frac{l_{41}}{l_{32}}\lambda_{321} - \frac{l_{41}}{Ul_{32}}\lambda_{322} - \frac{c_5l_{41}}{d_5Ul_{32}}\lambda_{321})c\theta_{41} + \\ (-\lambda_{412} + \frac{l_{41}}{Ul_{12}}\lambda_{121} - \frac{c_5l_{41}}{d_5Ul_{12}}\lambda_{122} - \frac{l_{41}}{l_{32}}\lambda_{322} - \frac{l_{41}}{Ul_{32}}\lambda_{321} + \frac{c_5l_{41}}{d_5Ul_{32}}\lambda_{322})s\theta_{41} \end{array} \right] \dot{\theta}_{41} \end{bmatrix}$$

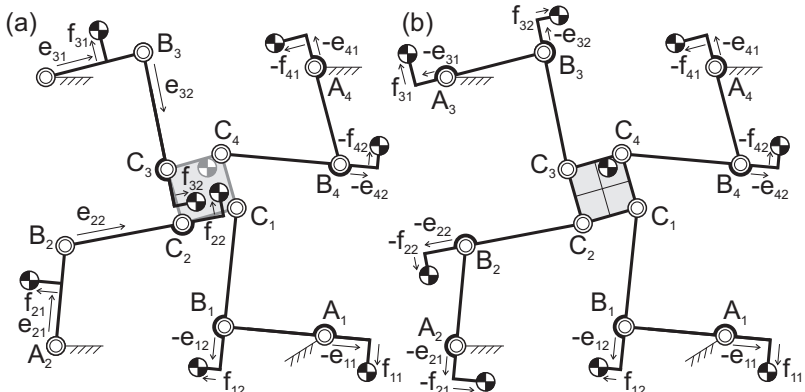


Fig. 2.27 Force balance configurations from general force balance conditions with (a) CoMs of platform and of links 21 and 31 freely selected and (b) as generalized version of the configuration in Fig. 2.24a.

With λ_{ijk} , μ_{5i} , and U substituted, from these linear momentum equations eight force balance conditions are obtained as:

$$\begin{aligned}
& m_{11}e_{11} + m_{12}l_{11}(1 - \frac{e_{12}}{l_{12}}) + m_{42}e_{42} + m_{12}l_{42}(\frac{c_5^2}{l_6^2} \frac{e_{12}}{l_{12}} + \frac{c_5 d_5}{l_6^2} \frac{f_{12}}{l_{12}}) + \\
& m_{32}l_{42}(\frac{d_5^2}{l_6^2} \frac{e_{32}}{l_{32}} - \frac{c_5 d_5}{l_6^2} \frac{f_{32}}{l_{32}}) + m_5 l_{42} \frac{e_6}{l_6} = 0 \\
& m_{31}e_{31} + m_{32}l_{31}(1 - \frac{e_{32}}{l_{32}}) + m_{22}e_{22} + m_{12}l_{22}(\frac{d_5^2}{l_6^2} \frac{e_{12}}{l_{12}} - \frac{c_5 d_5}{l_6^2} \frac{f_{12}}{l_{12}}) + \\
& m_{32}l_{22}(\frac{c_5^2}{l_6^2} \frac{e_{32}}{l_{32}} + \frac{c_5 d_5}{l_6^2} \frac{f_{32}}{l_{32}}) + m_5 l_{22} \frac{l_6 - e_6}{l_6} = 0 \\
& m_{11}f_{11} - m_{12}l_{11} \frac{f_{12}}{l_{12}} + m_{42}f_{42} + m_{12}l_{42}(-\frac{c_5 d_5}{l_6^2} \frac{e_{12}}{l_{12}} + \frac{c_5^2}{l_6^2} \frac{f_{12}}{l_{12}}) + \\
& m_{32}l_{42}(\frac{c_5 d_5}{l_6^2} \frac{e_{32}}{l_{32}} + \frac{d_5^2}{l_6^2} \frac{f_{32}}{l_{32}}) + m_5 l_{42} \frac{f_6}{l_6} = 0 \\
& m_{31}f_{31} - m_{32}l_{31} \frac{f_{32}}{l_{32}} + m_{22}f_{22} + m_{12}l_{22}(\frac{c_5 d_5}{l_6^2} \frac{e_{12}}{l_{12}} + \frac{d_5^2}{l_6^2} \frac{f_{12}}{l_{12}}) + \\
& m_{32}l_{22}(-\frac{c_5 d_5}{l_6^2} \frac{e_{32}}{l_{32}} + \frac{c_5^2}{l_6^2} \frac{f_{32}}{l_{32}}) - m_5 l_{22} \frac{f_6}{l_6} = 0 \quad (2.51) \\
& m_{21}e_{21} + m_{22}l_{21} + m_{12}l_{21}(\frac{d_5^2}{l_6^2} \frac{e_{12}}{l_{12}} - \frac{c_5 d_5}{l_6^2} \frac{f_{12}}{l_{12}}) + \\
& m_{32}l_{21}(\frac{c_5^2}{l_6^2} \frac{e_{32}}{l_{32}} + \frac{c_5 d_5}{l_6^2} \frac{f_{32}}{l_{32}}) + m_5 l_{21} \frac{l_6 - e_6}{l_6} = 0 \\
& m_{41}e_{41} + m_{42}l_{41} + m_{12}l_{41}(\frac{c_5^2}{l_6^2} \frac{e_{12}}{l_{12}} + \frac{c_5 d_5}{l_6^2} \frac{f_{12}}{l_{12}}) + \\
& m_{32}l_{41}(\frac{d_5^2}{l_6^2} \frac{e_{32}}{l_{32}} - \frac{c_5 d_5}{l_6^2} \frac{f_{32}}{l_{32}}) + m_5 l_{41} \frac{e_6}{l_6} = 0 \\
& m_{21}f_{21} + m_{12}l_{21}(\frac{c_5 d_5}{l_6^2} \frac{e_{12}}{l_{12}} + \frac{d_5^2}{l_6^2} \frac{f_{12}}{l_{12}}) + \\
& m_{32}l_{21}(-\frac{c_5 d_5}{l_6^2} \frac{e_{32}}{l_{32}} + \frac{c_5^2}{l_6^2} \frac{f_{32}}{l_{32}}) - m_5 l_{21} \frac{f_6}{l_6} = 0 \\
& m_{41}f_{41} + m_{12}l_{41}(-\frac{c_5 d_5}{l_6^2} \frac{e_{12}}{l_{12}} + \frac{c_5^2}{l_6^2} \frac{f_{12}}{l_{12}}) + \\
& m_{32}l_{41}(\frac{c_5 d_5}{l_6^2} \frac{e_{32}}{l_{32}} + \frac{d_5^2}{l_6^2} \frac{f_{32}}{l_{32}}) + m_5 l_{41} \frac{f_6}{l_6} = 0
\end{aligned}$$

These force balance conditions are a combination of the twelve force balance conditions in (2.48). For the specific kinematic conditions Fig. 2.28a shows a possible configuration of the 4-RRR manipulator that has also the kinematic conditions $\theta_{21} = \theta_{32}$, $\theta_{12} = \theta_{41}$, and $\theta_5 = 0$ ($\dot{\theta}_{21} = \dot{\theta}_{32}$, $\dot{\theta}_{12} = \dot{\theta}_{41}$, and $\dot{\theta}_5 = 0$) and the geometric conditions $l_{11} = l_{42}$, $l_{12} = l_{41}$, $l_{21} = l_{32}$, and $l_{22} = l_{31}$. Then $l_{11} \parallel l_{42}$, $l_{12} \parallel l_{41}$, $l_{21} \parallel l_{32}$, $l_{22} \parallel l_{31}$, $A_1A_4 \parallel C_1C_4$, and $A_2A_3 \parallel C_2C_3$ for all motion of the manipulator with non-rotating but solely translating platform.

A possible force balance configuration is shown in Fig. 2.29a where the CoMs of the platform and of links $i2$ are freely selected. Then the CoMs of links $i1$ are determined for balance. In practice this is an advantageous force balance configuration for low mass and low inertia, since it can be achieved with counter-masses that are mounted solely about pivots with the base [97].

Other specific kinematic conditions for which terms of the linear momentum become linearly dependent are $\theta_{11} = \theta_{41}$ and $\theta_{21} = \theta_{31}$ ($\dot{\theta}_{11} = \dot{\theta}_{41}$ and $\dot{\theta}_{21} = \dot{\theta}_{31}$).

When substituted in the linear momentum (2.47), eight force balance conditions are obtained as

$$\begin{aligned}
 & m_{11}e_{11} + m_{12}l_{11}(1 - \frac{e_{12}}{l_{12}}) + m_{41}e_{41} + m_{42}l_{41} + \\
 & m_{12}l_{41}(\frac{c_5^2}{l_6^2} \frac{e_{12}}{l_{12}} + \frac{c_5d_5}{l_6^2} \frac{f_{12}}{l_{12}}) + m_{32}l_{41}(\frac{d_5^2}{l_6^2} \frac{e_{32}}{l_{32}} - \frac{c_5d_5}{l_6^2} \frac{f_{32}}{l_{32}}) + m_5l_{41}\frac{e_6}{l_6} = 0 \\
 & m_{31}e_{31} + m_{32}l_{31}(1 - \frac{e_{32}}{l_{32}}) + m_{21}e_{21} + m_{22}l_{21} + \\
 & m_{12}l_{21}(\frac{d_5^2}{l_6^2} \frac{e_{12}}{l_{12}} - \frac{c_5d_5}{l_6^2} \frac{f_{12}}{l_{12}}) + m_{32}l_{21}(\frac{c_5^2}{l_6^2} \frac{e_{32}}{l_{32}} + \frac{c_5d_5}{l_6^2} \frac{f_{32}}{l_{32}}) + m_5l_{21}\frac{l_6 - e_6}{l_6} = 0 \\
 & m_{11}f_{11} - m_{12}l_{11}\frac{f_{12}}{l_{12}} + m_{41}f_{41} + m_{12}l_{41}(-\frac{c_5d_5}{l_6^2} \frac{e_{12}}{l_{12}} + \frac{c_5^2}{l_6^2} \frac{f_{12}}{l_{12}}) + \\
 & m_{32}l_{41}(\frac{c_5d_5}{l_6^2} \frac{e_{32}}{l_{32}} + \frac{d_5^2}{l_6^2} \frac{f_{32}}{l_{32}}) + m_5l_{41}\frac{f_6}{l_6} = 0 \\
 & m_{31}f_{31} - m_{32}l_{31}\frac{f_{32}}{l_{32}} + m_{21}f_{21} + m_{12}l_{21}(\frac{c_5d_5}{l_6^2} \frac{e_{12}}{l_{12}} + \frac{d_5^2}{l_6^2} \frac{f_{12}}{l_{12}}) + \\
 & m_{32}l_{21}(-\frac{c_5d_5}{l_6^2} \frac{e_{32}}{l_{32}} + \frac{c_5^2}{l_6^2} \frac{f_{32}}{l_{32}}) - m_5l_{21}\frac{f_6}{l_6} = 0 \\
 & m_{22}e_{22} + m_{12}l_{22}(\frac{d_5^2}{l_6^2} \frac{e_{12}}{l_{12}} - \frac{c_5d_5}{l_6^2} \frac{f_{12}}{l_{12}}) + m_{32}l_{22}(\frac{c_5^2}{l_6^2} \frac{e_{32}}{l_{32}} + \frac{c_5d_5}{l_6^2} \frac{f_{32}}{l_{32}}) + \\
 & m_5l_{22}\frac{l_6 - e_6}{l_6} = 0 \\
 & m_{42}e_{42} + m_{12}l_{42}(\frac{c_5^2}{l_6^2} \frac{e_{12}}{l_{12}} + \frac{c_5d_5}{l_6^2} \frac{f_{12}}{l_{12}}) + m_{32}l_{42}(\frac{d_5^2}{l_6^2} \frac{e_{32}}{l_{32}} - \frac{c_5d_5}{l_6^2} \frac{f_{32}}{l_{32}}) + \\
 & m_5l_{42}\frac{e_6}{l_6} = 0 \\
 & m_{22}f_{22} + m_{12}l_{22}(\frac{c_5d_5}{l_6^2} \frac{e_{12}}{l_{12}} + \frac{d_5^2}{l_6^2} \frac{f_{12}}{l_{12}}) + m_{32}l_{22}(-\frac{c_5d_5}{l_6^2} \frac{e_{32}}{l_{32}} + \frac{c_5^2}{l_6^2} \frac{f_{32}}{l_{32}}) - \\
 & m_5l_{22}\frac{f_6}{l_6} = 0 \\
 & m_{42}f_{42} + m_{12}l_{42}(-\frac{c_5d_5}{l_6^2} \frac{e_{12}}{l_{12}} + \frac{c_5^2}{l_6^2} \frac{f_{12}}{l_{12}}) + m_{32}l_{42}(\frac{c_5d_5}{l_6^2} \frac{e_{32}}{l_{32}} + \frac{d_5^2}{l_6^2} \frac{f_{32}}{l_{32}}) + \\
 & m_5l_{42}\frac{f_6}{l_6} = 0
 \end{aligned} \tag{2.52}$$

These force balance conditions are also a combination of the twelve general force balance conditions in (2.48). For these specific kinematic conditions Fig. 2.28b

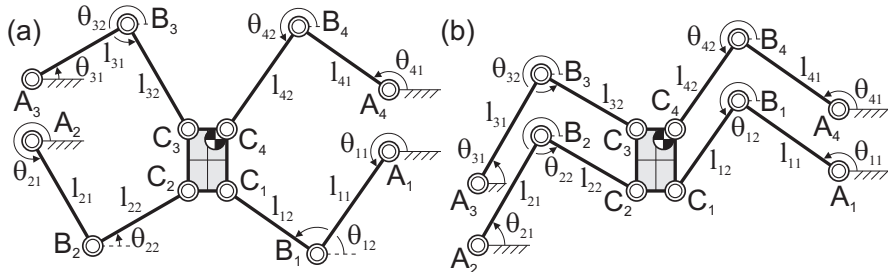


Fig. 2.28 Configurations of the 4-RRR parallel manipulator for the specific kinematic conditions that (a) the platform does not rotate, $\theta_{11} = \theta_{42}$, and $\theta_{22} = \theta_{31}$ and (b) the platform does not rotate, $\theta_{11} = \theta_{41}$, and $\theta_{21} = \theta_{31}$.

shows a possible configuration of the 4-RRR parallel manipulator that has also the kinematic conditions $\theta_{12} = \theta_{42}$, $\theta_{22} = \theta_{32}$, and $\theta_5 = 0$ ($\dot{\theta}_{12} = \dot{\theta}_{42}$, $\dot{\theta}_{22} = \dot{\theta}_{32}$, $\dot{\theta}_5 = 0$) and the geometric conditions $l_{11} = l_{41}$, $l_{12} = l_{42}$, $l_{21} = l_{31}$, and $l_{22} = l_{32}$. Then $l_{11} \parallel l_{41}$, $l_{12} \parallel l_{42}$, $l_{21} \parallel l_{31}$, $l_{22} \parallel l_{32}$, $A_1A_4 \parallel C_1C_4$, and $A_2A_3 \parallel C_2C_3$ for all motion of the manipulator with non-rotating but solely translating platform.

Figure 2.29b shows a possible force balance configuration where the CoMs of the platform and of links 12, 22, 31, and 41 are freely selected and the CoMs of link 11, 21, 32, and 42 are determined for force balance. In practice, solutions with determined CoMs of floating links lead to significant mass and inertia of the mechanism [97].

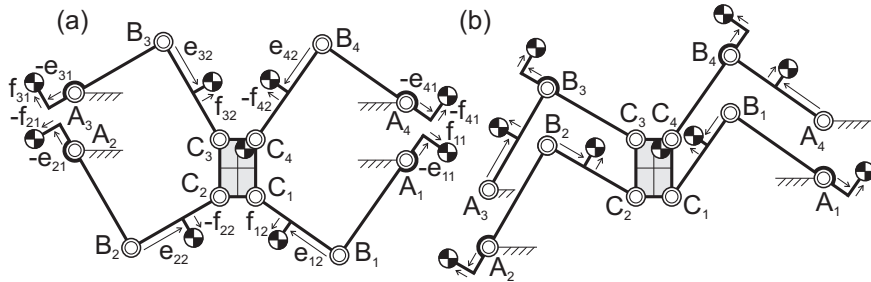


Fig. 2.29 Force balance configurations for (a) the kinematic conditions in Fig. 2.28a; (b) the kinematic conditions in Fig. 2.28b.

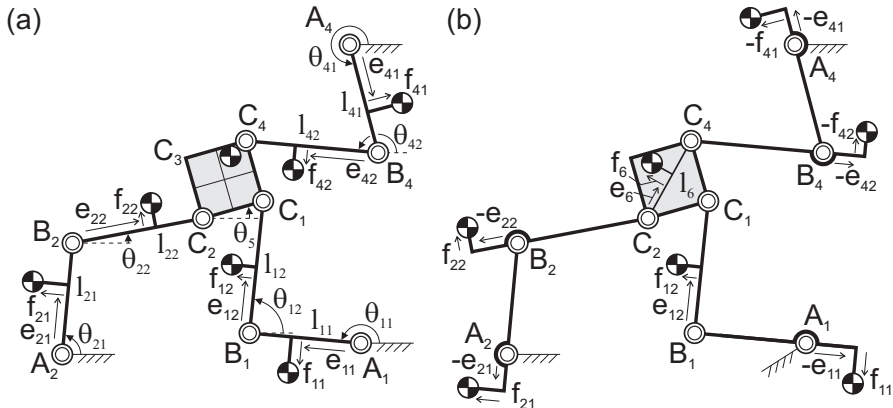


Fig. 2.30 a) Planar 3-RRR parallel manipulator derived from Fig. 2.22 by elimination of arm 3; b) Force balance configuration where CoMs of the platform and of link 12 are freely selected.

2.3.4 3-RRR parallel manipulator

To find the general force balance conditions of the planar 3-RRR parallel manipulator in Fig. 2.30a it is possible to apply the method of linearly dependent linear momentum from the beginning. It is also possible to obtain them as a subset of the force balance conditions of the 4-RRR parallel manipulator. For instance when links 31 and 32 in the configuration in Fig. 2.22 are eliminated, the general force balance conditions of the 3-RRR parallel manipulator are obtained by substituting $m_{31} = m_{32} = 0$ in (2.48) which results in the ten force balance conditions:

$$\begin{aligned}
 m_{11}e_{11} + m_{12}l_{11}\left(1 - \frac{e_{12}}{l_{12}}\right) &= 0 \\
 m_{11}f_{11} - m_{12}l_{11}\frac{f_{12}}{l_{12}} &= 0 \\
 m_{21}e_{21} + m_{22}l_{21} + m_{12}l_{21}\left(\frac{d_5^2}{l_6^2}\frac{e_{12}}{l_{12}} - \frac{c_5d_5}{l_6^2}\frac{f_{12}}{l_{12}}\right) + m_5l_{21}\frac{l_6 - e_6}{l_6} &= 0 \\
 m_{41}e_{41} + m_{42}l_{41} + m_{12}l_{41}\left(\frac{c_5}{l_6^2}\frac{e_{12}}{l_{12}} + \frac{c_5d_5}{l_6^2}\frac{f_{12}}{l_{12}}\right) + m_5l_{41}\frac{e_6}{l_6} &= 0 \\
 m_{22}e_{22} + m_{12}l_{22}\left(\frac{d_5^2}{l_6^2}\frac{e_{12}}{l_{12}} - \frac{c_5d_5}{l_6^2}\frac{f_{12}}{l_{12}}\right) + m_5l_{22}\frac{l_6 - e_6}{l_6} &= 0 \\
 m_{42}e_{42} + m_{12}l_{42}\left(\frac{c_5}{l_6^2}\frac{e_{12}}{l_{12}} + \frac{c_5d_5}{l_6^2}\frac{f_{12}}{l_{12}}\right) + m_5l_{42}\frac{e_6}{l_6} &= 0 \quad (2.53) \\
 m_{21}f_{21} + m_{12}l_{21}\left(\frac{c_5d_5}{l_6^2}\frac{e_{12}}{l_{12}} + \frac{d_5^2}{l_6^2}\frac{f_{12}}{l_{12}}\right) - m_5l_{21}\frac{f_6}{l_6} &= 0 \\
 m_{41}f_{41} + m_{12}l_{41}\left(-\frac{c_5d_5}{l_6^2}\frac{e_{12}}{l_{12}} + \frac{c_5^2}{l_6^2}\frac{f_{12}}{l_{12}}\right) + m_5l_{41}\frac{f_6}{l_6} &= 0 \\
 m_{22}f_{22} + m_{12}l_{22}\left(\frac{c_5d_5}{l_6^2}\frac{e_{12}}{l_{12}} + \frac{d_5^2}{l_6^2}\frac{f_{12}}{l_{12}}\right) - m_5l_{22}\frac{f_6}{l_6} &= 0 \\
 m_{42}f_{42} + m_{12}l_{42}\left(-\frac{c_5d_5}{l_6^2}\frac{e_{12}}{l_{12}} + \frac{c_5^2}{l_6^2}\frac{f_{12}}{l_{12}}\right) + m_5l_{42}\frac{f_6}{l_6} &= 0
 \end{aligned}$$

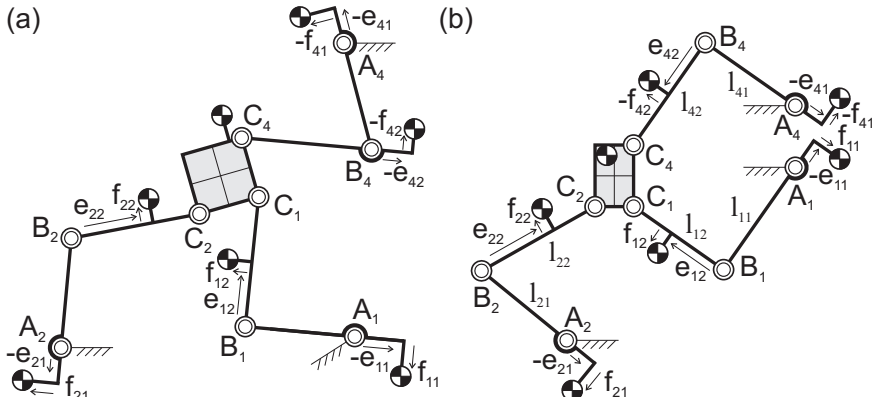


Fig. 2.31 a) Force balance configuration where the CoMs of links 12 and 22 are freely selected;
b) Force balance configuration for specific kinematic conditions where the CoMs of the platform
and of links 12, 22, and 42 are freely selected.

Figure 2.30b shows a force balance configuration where the CoMs of the platform and of link 12 are freely selected. It is also possible to obtain a force balance configuration where the CoMs of links 12 and 22 are freely selected as illustrated in Fig. 2.31a. Figure 2.31b shows a force balance configuration for the specific kinematics conditions $\theta_{11} = \theta_{42}$ and $\theta_5 = 0$ ($\dot{\theta}_{11} = \dot{\theta}_{42}$ and $\dot{\theta}_5 = 0$) where the CoMs of the platform and of links 12, 22, and 42 are freely selected.

2.3.5 2-RRR parallel manipulator (6R six-bar mechanism and 5R five-bar mechanism)

Also the general force balance conditions of the planar 2-RRR parallel manipulator (or 6R six-bar mechanism) in Fig. 2.32a can be obtained as a subset of the force balance conditions of the 4-RRR manipulator. For instance when links 11, 12, 31, and 32 in the configuration in Fig. 2.22 are eliminated, they are obtained by substituting $m_{11} = m_{12} = m_{31} = m_{32} = 0$ in (2.48) which results in the eight force balance conditions:

$$\begin{aligned} m_{21}e_{21} + m_{22}l_{21} + m_5l_{21} \frac{l_6 - e_6}{l_6} &= 0 & m_{21}f_{21} - m_5l_{21} \frac{f_6}{l_6} &= 0 \\ m_{41}e_{41} + m_{42}l_{41} + m_5l_{41} \frac{e_6}{l_6} &= 0 & m_{41}f_{41} + m_5l_{41} \frac{f_6}{l_6} &= 0 \\ m_{22}e_{22} + m_5l_{22} \frac{l_6 - e_6}{l_6} &= 0 & m_{22}f_{22} - m_5l_{22} \frac{f_6}{l_6} &= 0 \\ m_{42}e_{42} + m_5l_{42} \frac{e_6}{l_6} &= 0 & m_{42}f_{42} + m_5l_{42} \frac{f_6}{l_6} &= 0 \end{aligned} \quad (2.54)$$

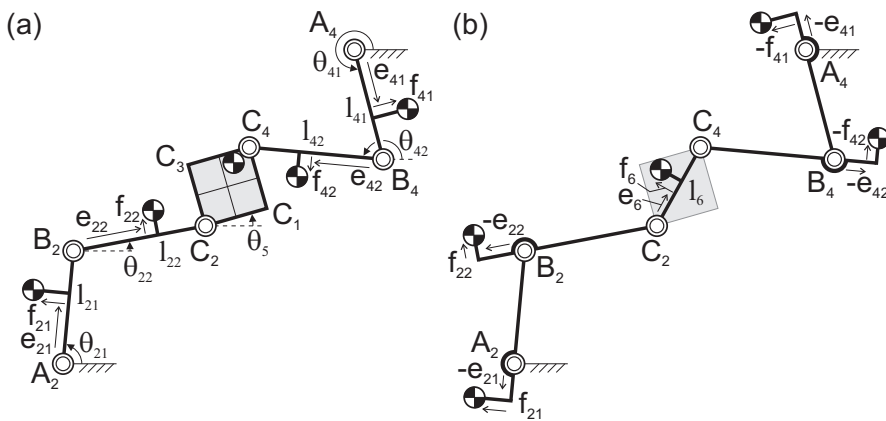


Fig. 2.32 a) Planar 2-RRR parallel manipulator (or 6R six-bar linkage) derived from Fig. 2.22 by eliminating arms 1 and 3; b) Force balance configuration when CoM of the platform is freely selected.

A force balance configuration is shown in Fig. 2.32b where the CoM of the platform, which has reduced to a link, is freely selected. Figure 2.33a shows a force balance configuration where the CoM of link 22 is freely selected. Figures 2.33b and 2.33c show two force balance configurations for the specific kinematic conditions that $\theta_{11} = \theta_{42}$ and $\dot{\theta}_5 = 0$ ($\dot{\theta}_{11} = \dot{\theta}_{42}$ and $\dot{\theta}_5 = 0$) where the CoMs of the platform and of links 22, and 42 are freely selected.

The general force balance conditions of a 5R five-bar mechanism can be derived from the force balance conditions of the 2-RRR parallel manipulator by, for instance, reducing link 22 such that it disappears as shown in Fig. 2.34a. Then joints B_2 and C_2 coincide. The force balance conditions of the 5R five-bar mechanism then are obtained by substituting $m_{22} = 0$ and $l_{22} = 0$ in (2.54) which results in the six force balance conditions:

$$\begin{aligned} m_{21}e_{21} + m_5l_{21}\frac{l_6 - e_6}{l_6} &= 0 & m_{21}f_{21} - m_5l_{21}\frac{f_6}{l_6} &= 0 \\ m_{41}e_{41} + m_{42}l_{41} + m_5l_{41}\frac{e_6}{l_6} &= 0 & m_{41}f_{41} + m_5l_{41}\frac{f_6}{l_6} &= 0 \\ m_{42}e_{42} + m_5l_{42}\frac{e_6}{l_6} &= 0 & m_{42}f_{42} + m_5l_{42}\frac{f_6}{l_6} &= 0 \end{aligned} \quad (2.55)$$

A force balance configuration is shown in Fig. 2.34b in which the CoM of the platform link is freely selected. When subsequently the force-balanced 5R five-bar mechanism is reduced, for instance such that link 42 disappears and joints B_4 and C_4 coincide, then the force-balanced 4R four-bar linkage in Fig. 2.13b is obtained.

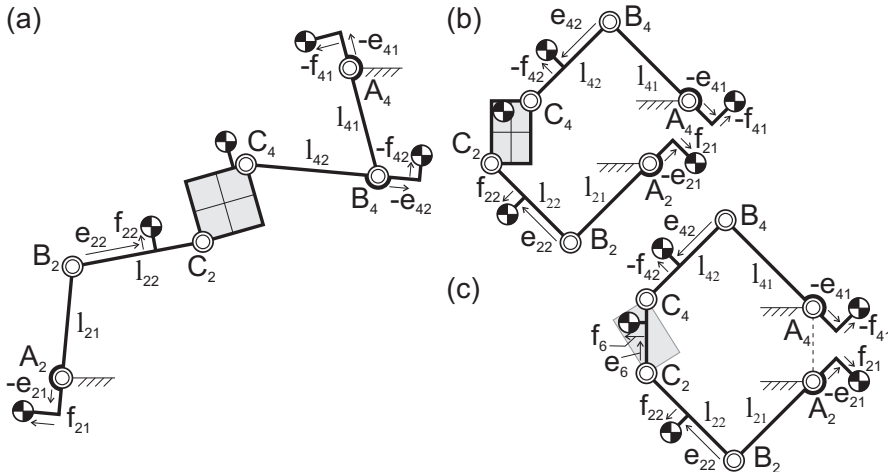


Fig. 2.33 a) Force balance configuration when CoM of link 22 is freely selected; b-c) Force balance configurations for specific kinematic conditions where the CoMs of the platform and of links 22, and 42 are freely selected.

2.4 Discussion and conclusion

In this chapter it was shown that the inherent force balance solutions of given mechanisms can be found with linear momentum equations in a generic and systematic way. With the open chain method it was shown that force-balanced closed-chain mechanisms can be derived quickly, but that the results are limited and dependent on design choices. This is because the interaction among the open chains is not considered. The force balance configuration of the delta robot in Fig. 2.12 has one determined mass on a floating link, likely achieved with a counter-mass. Since in practice often one of the arms of a delta robot exhibits relatively little motion when its orientation is perpendicular to the main direction of the pick and place motion, advantage is taken when this arm is the arm with the counter-mass on a floating link.

The method of linearly independent linear momentum was proposed for deriving the general force balance conditions of closed-chain mechanisms of which the results are not limited and dependent on design choices. This was achieved by substituting the derivatives of the loop equations in the linear momentum equations of the mechanism from which the force balance conditions are readily obtained. Application of the method was illustrated for a 4R four-bar linkage with one closed loop and a 4-RRR parallel mechanism with three closed loops. From the general force balance conditions various force balance configurations are obtained by selecting link CoM locations. It was shown that for each independent closed loop 1 link CoM can be freely selected.

The linear momentum equations are suitable for an intuitive search for specific kinematic conditions for which specific force balance configurations are obtained. Specific kinematic conditions then are found which reduce the number of terms in the linear momentum equations. From these specific kinematic conditions geometric conditions of the mechanism configuration are derived. For the 4-RRR paral-

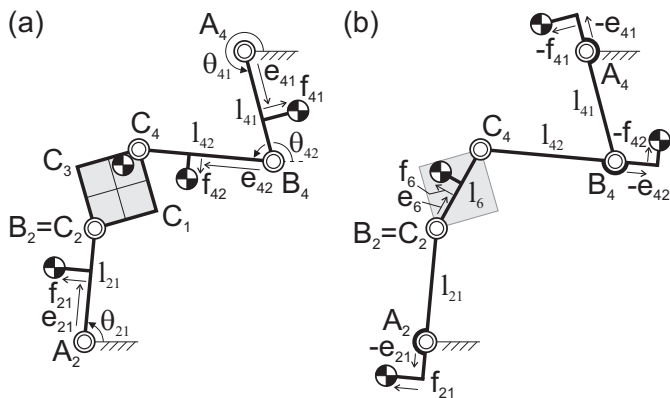


Fig. 2.34 a) 5R five-bar linkage derived from a 2-RRR parallel manipulator by reducing link 22 such that B_2 and C_2 coincide; b) Force balance configuration with CoM of platform link freely selected.

lel manipulator an advantageous force balance configuration was found with solely counter-masses about the pivots with the base. Since this configuration is only perfectly force balanced for a non-rotating platform, while the manipulator still has this DoF, this method is also suitable for deriving near-to-perfect force balance configurations. In addition, it was also shown how various generally and specifically reduced force-balanced mechanism configurations can be obtained as subsets.

As compared with the linearly independent vector method in [13], the method of linearly independent linear momentum is simpler, especially for mechanisms with multiple closed loops. This is because parameters related to the base and base pivots are not considered with linear momentum where only parameters of moving elements are involved. The substitution of the derivatives of the loop equations in the linear momentum requires significant effort, especially for multiple closed loops. Since the method is straightforward and systematic, it is suitable for automation by computer software.

The loop equations (2.42-2.44) were substituted in the linear momentum (2.39) for $s\theta_{12}\dot{\theta}_{12}$, $c\theta_{12}\dot{\theta}_{12}$, $s\theta_{32}\dot{\theta}_{32}$, and $c\theta_{32}\dot{\theta}_{32}$. When they are substituted for $s\theta_{12}\dot{\theta}_{12}$, $c\theta_{12}\dot{\theta}_{12}$, $s\theta_{42}\dot{\theta}_{42}$, and $c\theta_{42}\dot{\theta}_{42}$ the resulting linear momentum equations become simpler than in (2.47). This is because of decoupling of parameters c_5 and d_5 for which a general description of the platform joints is lost. The force balance configurations that then are obtained are limited.

Extending the method of linearly independent linear momentum to spatial mechanisms can be challenging because of the products of $\sin()$ and $\cos()$ terms that are difficult to handle. This however is a topic of further investigation.

Chapter 3

Principal vector linkages for inherent shaking force balance

Abstract The *method of principal vectors* is investigated in this chapter for the development of *principal vector linkages*. These linkages have the common center-of-mass of all elements in an invariant point in at least one of the elements. When pivoted about this point, the resulting linkages are force balanced for all motion and can be applied for the synthesis of inherently force-balanced mechanism solutions. It is shown that multi-DoF principal vector linkages, both planar and spatial, consist of unions of pantograph mechanisms. With linear momentum equations and *equivalent linear momentum systems* as a proposed method to represent the linear momentum, their principal dimensions are calculated. It is shown that then each degree-of-freedom is considered individually.

3.1 The 2-DoF pantograph linkage as a principal vector linkage

In this section it is shown how the 2-DoF pantograph linkage is considered a principal vector linkage. An approach with linear momentum equations is proposed to determine the principal dimensions of this force-balanced linkage from each DoF individually.

Figure 3.1a depicts the pantograph mechanism of Fig. 2.20b with massless links and two lumped masses m_A and m_B in points Q and R , respectively. About an arbitrary invariant point in one of the elements this parallelogram mechanism has 2-DoF planar motion, defined with angular rotations θ_1 and θ_2 . Joint S is an invariant link point in both links SP_1 and SP_2 and is the common CoM of the linkage for all motion if $m_Aa''_1 = m_Ba''_2$, where a''_1 and a''_2 are the distances SQ and SR , respectively. From the similarity $\triangle P_1SQ \sim \triangle P_2RS$ it follows that $a''_1/a''_2 = a'_1/a_1 = a_2/a'_2 = k$ with constant k representing the scaling factor of the pantograph and with a_1, a_2, a'_1 , and a'_2 the distances P_1A, P_2A, P_1Q , and P_2R , respectively. This leads to the conditions $m_Aa'_1 = m_Ba_1$ and $m_Aa_2 = m_Ba'_2$ for which joint S is the common CoM for all motion.

Points P_1 , P_2 , Q , and R can be described with respect to the common CoM in S with vectors \bar{a}_1 , \bar{a}_2 , \bar{a}'_1 , and \bar{a}'_2 as illustrated in Fig. 3.1b. These vectors are named the *principal vectors* with which the *principal vector linkage* in Fig. 3.1a is defined. The norms of these vectors a_1 , a_2 , a'_1 , and a'_2 are the *principal dimensions* and P_1 and P_2 are the *principal points* in the *principal elements* P_1A and P_2A where A is the *principal joint*. Links SP_1 and SP_2 will be referred to as the *principal vector links*. The principal vector linkage is force-balanced about an invariant link point for all motion. This link point is characterized as the common CoM and when made stationary with respect to the base, for instance with a pivot in this point, a force-balanced mechanism is obtained.

When the mass of all links is considered with a general CoM in each link, the principal vector linkage in Fig. 3.2 is obtained. The CoM in each link is defined with parameters p_i and q_i relative to the principal vectors as illustrated. A common approach to determine the conditions for which S is the common CoM of the complete linkage is to develop the equations of the position of the CoM. It is also possible to develop the linear momentum equations per DoF with which the motion of the common CoM is described. These two approaches will be compared.

With S as origin of the xy -reference frame, the position of the common CoM of the linkage in Fig. 3.2 can be written as

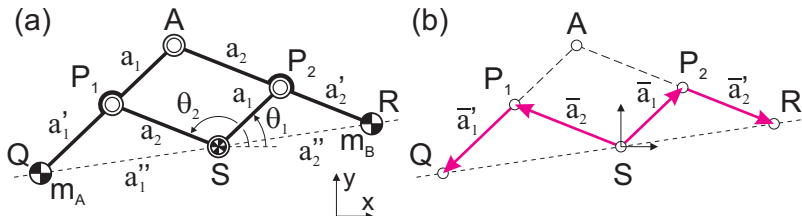


Fig. 3.1 (a) 2-DoF principal vector linkage with principal dimensions a_1 and a_2 of which the common CoM of masses m_A and m_B is in S , which is an invariant point in both links SP_1 and SP_2 ; (b) Principal vectors \bar{a}_1 and \bar{a}_2 describe the positions of the principal points P_1 and P_2 with respect to S while vectors \bar{a}'_1 and \bar{a}'_2 describe the positions of Q and R relative to the principal points.

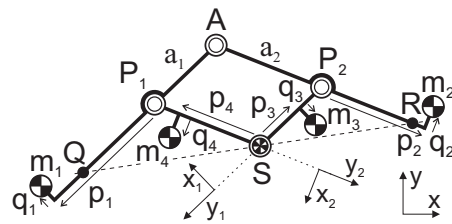


Fig. 3.2 General 2-DoF principal vector linkage with the common CoM of link masses m_1 , m_2 , m_3 , and m_4 in S for all motion. P_1 and P_2 are the principal points of the linkage and Q and R are a set of similarity points.

$$\begin{aligned}\bar{r}_{CoM} = \bar{S} + m_1 & \left[\begin{matrix} a_2 c \theta_2 - p_1 c \theta_1 - q_1 s \theta_1 \\ a_2 s \theta_2 - p_1 s \theta_1 + q_1 c \theta_1 \end{matrix} \right] + m_2 \left[\begin{matrix} a_1 c \theta_1 - p_2 c \theta_2 + q_2 s \theta_2 \\ a_1 s \theta_1 - p_2 s \theta_2 - q_2 c \theta_2 \end{matrix} \right] + \\ m_3 & \left[\begin{matrix} p_3 c \theta_1 + q_3 s \theta_1 \\ p_3 s \theta_1 - q_3 c \theta_1 \end{matrix} \right] + m_4 \left[\begin{matrix} p_4 c \theta_2 - q_4 s \theta_2 \\ p_4 s \theta_2 + q_4 c \theta_2 \end{matrix} \right]\end{aligned}\quad (3.1)$$

with $s()$ and $c()$ as shorthand for $\sin()$ and $\cos()$, respectively. For all values of the time dependent parameters the equations have to be constant to have the common CoM in S for all motion. After rearrangement of the equations by rewriting them in terms of the four time dependent parameters, the four force balance conditions are found as:

$$\begin{aligned}m_1 p_1 &= m_2 a_1 + m_3 p_3 \\ m_1 q_1 &= m_3 q_3 \\ m_2 p_2 &= m_1 a_2 + m_4 p_4 \\ m_2 q_2 &= m_4 q_4\end{aligned}\quad (3.2)$$

This procedure for this relatively simple linkage requires already a considerable effort, especially for the rearrangement of the equations. With linear momentum equations these conditions can be found more conveniently per DoF individually. Figure 3.3a illustrates the relative motion of DoF 1 of the linkage for which $\dot{\theta}_2 = 0$. This can be regarded as link SP_1 being fixed with link P_1A solely rotating and link P_2A solely translating. The linear momentum \bar{L}_1 of this motion can be written with respect to reference frame x_1y_1 which has the y_1 -axis aligned with the principal vector \bar{a}_1 as illustrated. This results in

$$\bar{L}_1 = \begin{bmatrix} -m_1 p_1 + m_2 a_1 + m_3 p_3 \\ m_1 q_1 - m_3 q_3 \end{bmatrix} \dot{\theta}_1 = \begin{bmatrix} 0 \\ 0 \end{bmatrix}\quad (3.3)$$

Similarly, the linear momentum \bar{L}_2 of the relative motion of DoF 2 with $\dot{\theta}_1 = 0$, which is illustrated in Fig. 3.3b, can be written with respect to reference frame x_2y_2 with the y_2 -axis aligned with principal vector \bar{a}_2 as illustrated. This results in

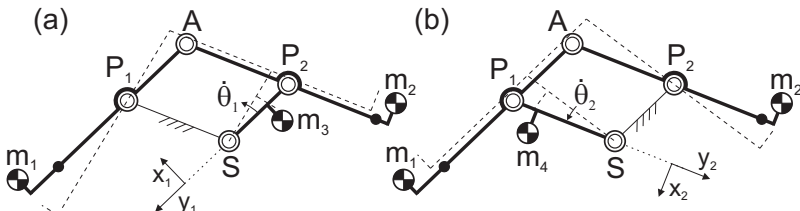


Fig. 3.3 With the linear momentum written for the motion of each DoF individually, the force balance conditions are readily obtained; a) DoF 1 with $\dot{\theta}_2 = 0$ and link P_2A solely translating; b) DoF 2 with $\dot{\theta}_1 = 0$ and link P_1A solely translating.

$$\bar{L}_2 = \begin{bmatrix} -m_2 p_2 + m_1 a_2 + m_4 p_4 \\ -m_2 q_2 + m_4 q_4 \end{bmatrix} \dot{\theta}_2 = \begin{bmatrix} 0 \\ 0 \end{bmatrix} \quad (3.4)$$

This way, the conditions (3.2) for which S is the common CoM, for which the linear momentum equations are zero for all motion, are readily found.

The main advantages of using linear momentum equations are that solely masses that move are considered, that CoM parameters in translating and immovable elements do not appear, and that each DoF can be considered individually. The latter means that as many equations are found as there are force balance conditions that determine a multi-DoF principal vector linkage. Contrary, with the equations of the CoM position only two equations are obtained for any planar multi-DoF linkage, from which the force balance conditions can be challenging to obtain.

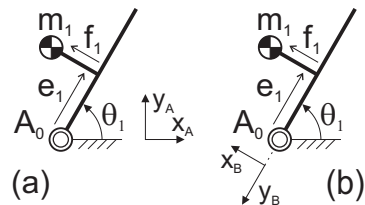
The use of relative reference frames for the linear momentum, which are aligned with the rotating link as in Fig. 3.3, simplify the equations from which the general force balance conditions are obtained. This can be shown when the linear momentum of the single rotatable link in Fig. 3.4a is written from (2.2) and with respect to fixed reference frame x_Ay_A as

$$\begin{aligned} \bar{L}_A &= \begin{bmatrix} -m_1 e_1 \sin \theta_1 - m_1 f_1 \cos \theta_1 \\ m_1 e_1 \cos \theta_1 - m_1 f_1 \sin \theta_1 \end{bmatrix} \dot{\theta}_1 = \begin{bmatrix} -\sin \theta_1 & -\cos \theta_1 \\ \cos \theta_1 & -\sin \theta_1 \end{bmatrix} \begin{bmatrix} m_1 e_1 \\ m_1 f_1 \end{bmatrix} \dot{\theta}_1 \\ &= \begin{bmatrix} -\sin \theta_1 & -\cos \theta_1 \\ \cos \theta_1 & -\sin \theta_1 \end{bmatrix} \bar{L}_B \end{aligned} \quad (3.5)$$

Here \bar{L}_B is the linear momentum of the same link but with respect to reference frame x_By_B which is aligned with the link as illustrated in Fig. 3.4b. Since for force balance the linear momentum \bar{L}_A needs to be zero for any value of the time dependent parameters, this implies that \bar{L}_B needs to be zero for any value of the time dependent parameters. Hence, using relative reference frames leads to simpler equations for deriving the force balance conditions.

For the formulation of the linear momentum it is proposed to first derive an *Equivalent Linear Momentum System* (ELMS) of the motion under investigation. Figure 3.5a shows an ELMS of the relative motion of DoF 1 in Fig. 3.3a, which is a rotational motion about principal point P_1 . This is a reduced-mass model in

Fig. 3.4 To derive the general force balance conditions, the linear momentum can be written with respect to (a) an absolute reference frame (x_Ay_A), or to (b) a relative reference frame aligned with a moving link (x_By_B). For principal vector linkages the latter approach results in the simplest equations.



which the moving masses have been projected onto a single element (the principal element) such that its linear momentum with respect to the same reference frame is equal. The ELMS in Fig. 3.5a is obtained when links P_1A and SP_2 are merged with P_1 and S coinciding. Since link P_2A solely translates, mass m_1 moves along a circular trajectory with radius a_1 as it is when projected in A . Figure 3.5b shows the ELMS of the relative motion of DoF 2, which is a rotational motion about principal point P_2 . Here links P_2A and SP_1 are merged with P_2 and S coinciding and with m_1 projected in A for equivalent linear momentum. A property of these ELMSs is that the CoM in each reduced-mass model is in its principal point P_i , which shows an alternative way to derive the force balance conditions.

From (3.2) the principal dimensions of the 2-DoF principal vector linkage in Fig. 3.2 are calculated with

$$a_1 = \frac{m_1 p_1 - m_3 p_3}{m_2} \quad a_2 = \frac{m_2 p_2 - m_4 p_4}{m_1} \quad (3.6)$$

and from $a'_1/a_1 = a_2/a'_2 = k$ principal dimensions a'_1 and a'_2 result in

$$a'_1 = \frac{m_1 p_1 - m_3 p_3}{m_1} \quad a'_2 = \frac{m_2 p_2 - m_4 p_4}{m_2} \quad (3.7)$$

with which the positions Q and R and the scaling factor $k = m_2/m_1$ of the pantograph are known. Points Q and R will be referred to as *similarity points* of the principal vector linkage. It is observed that the scaling factor does not depend on m_3 and m_4 . In chapter 4 (section 4.2) it is shown that it is not the only set of similarity points of the pantograph and in chapter 7 it is shown that multiple principal vector linkages can be combined by connecting them in these points and in S .

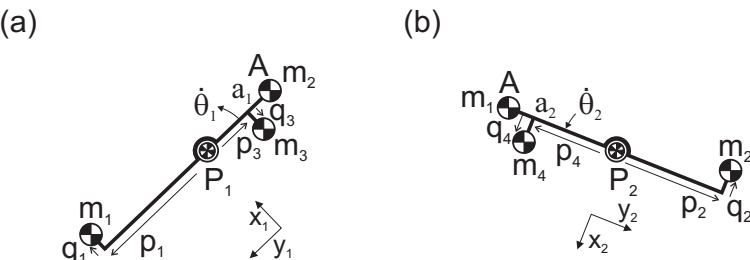


Fig. 3.5 An Equivalent Linear Momentum Systems (ELMS) is a reduced-mass model of which the linear momentum is equal to the mechanism DoF under investigation; a) ELMS of the motion of DoF 1 individually; b) ELMS of the motion of DoF 2 individually.

3.2 Principal vector linkage of three principal elements in series

The pantograph mechanism can be considered a principal vector linkage of two principal elements in series (P_1A and P_2A) with two principal vector links (SP_1 and SP_2). In this section the principal vector linkage of three principal elements in series is investigated. First it is shown that this linkage consists of a union of pantograph mechanisms and its historical development is briefly noted. Subsequently the linkage is generalized with a general CoM in each link and the principal dimensions are derived with linear momentum equations and ELMSSs. Also two kinematic variations of this principal vector linkage are investigated at the end.

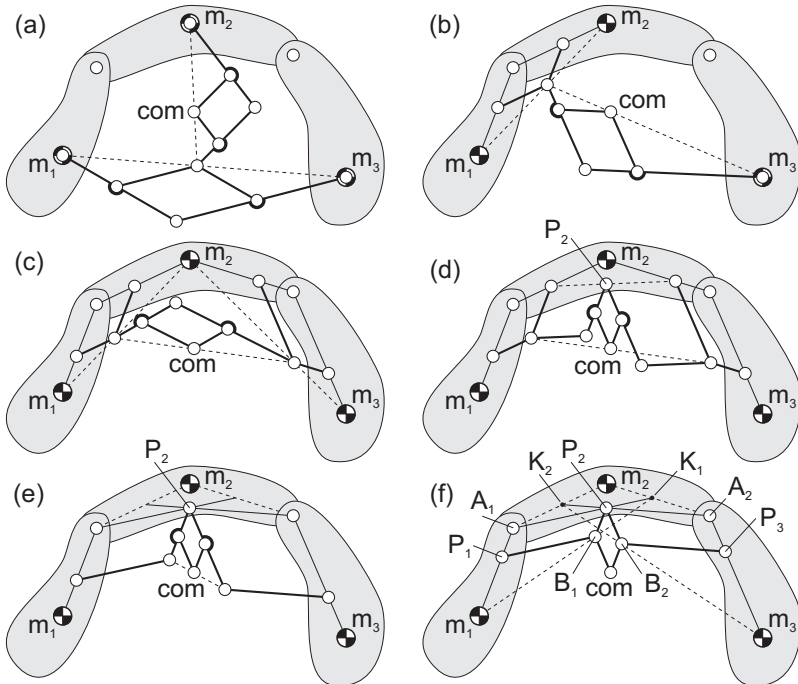


Fig. 3.6 (a) Common CoM of three elements in series traced with two auxiliary pantographs; (b) CoM traced with one incorporated pantograph and one auxiliary pantograph; (c) CoM traced with two incorporated pantographs and one auxiliary pantograph; (d) Deduced from (c) when the auxiliary pantograph is parallel to the two incorporated pantographs; (e) Deduced from (d) when parallelograms are united; (f) Specific dimensions for which the principal vector linkage is obtained.

3.2.1 Union of pantographs and Fischer's linkage

The common CoM of three elements in series can be traced with pantograph linkages in various ways as illustrated in Fig. 3.6. In Fig. 3.6a it is shown how two pantographs that are fully auxiliary can be applied. A first pantograph traces the CoM of m_1 and m_3 and a second pantograph traces the CoM of $m_1 + m_3$ and m_2 , which is the common CoM of the three elements. It is also possible (not shown) to have a first pantograph trace the CoM of m_1 and m_2 or the CoM of m_2 and m_3 . For each of the three possibilities the resulting mechanism has eleven elements.

Figure 3.6b shows a solution with two pantographs of which one traces the CoM of m_1 and m_2 and has two links incorporated in principal elements 1 and 2. The second pantograph is fully auxiliary and traces the common CoM. This solution can be applied in two different ways for which in each case the mechanism has nine elements in total.

In Fig. 3.6c three pantographs are used to trace the common CoM. Two of them have two links incorporated in the principal elements and one is fully auxiliary. The two incorporated pantographs trace the CoM of m_1 and part of m_2 , and the remaining part of m_2 and m_3 , respectively, while the auxiliary pantograph traces the common CoM. The resulting mechanism has in total eleven elements.

From the configuration in Fig. 3.6c the principal vector linkage can be obtained by unifying the three pantographs as will be explained graphically in three steps. The first step is to have the auxiliary pantograph be parallel to the other two pantographs for all motion of the linkage as shown in Fig. 3.6d. In this intermediate result the kinematics of the auxiliary pantograph remain unchanged by an additional parallelogram at each side. This implies that point P_2 is an invariant point in link 2 and therefore the parallelograms at each side of the auxiliary pantograph can be united to single parallelograms. This results in the configuration in Fig. 3.6e in which two new incorporated pantographs appear. Without affecting the kinematics, the dimensions of the links can be adapted to the configuration in Fig. 3.6f which is a 3-DoF principal vector linkage with principal points P_1 , P_2 , and P_3 .

The new incorporated pantograph on the left traces with joint B_1 the CoM of $m_2 + m_3$ in K_1 and m_1 . The new incorporated pantograph on the right traces with joint B_2 the CoM of $m_1 + m_2$ in K_2 and m_3 . K_1 and K_2 represent, respectively, the CoM of m_3 considered in A_2 and m_2 and the CoM of m_1 considered in A_1 and m_2 .

Fischer's linkage

The method of principal vectors was invented by the German physiologist, physicist, and medical doctor Otto Fischer. He was involved in studying the motion of living creatures (human beings and animals) and approached them as systems of rigid bodies. To be able to calculate by hand the internal forces and moments of muscles of bodies in motion, he was particularly interested in the division between the absolute motion of the common CoM and the relative motion of the system with

respect to the common CoM. He published various books considering these studies of which the most elaborate one in 1906 [53].

For his studies, Fischer introduced a method to geometrically trace the CoM of multiple jointed rigid elements. This method was given the name the *method of principal vectors* by Lowen and Berkof [74]. He obtained and investigated the principal vector linkage in Fig. 3.6f for mass-symmetric elements, i.e. elements of which the CoM is on the line connecting the joints. In his solution therefore m_2 is on the line A_1A_2 . The method to find the principal points he explained as that P_1 is found as the CoM of $m_2 + m_3$ in A_1 and m_1 , that P_2 is found as the CoM of m_1 in A_1 , m_3 in A_2 , and m_2 , and that P_3 is found as the CoM of $m_1 + m_2$ in A_2 and m_3 . Similar explanations have been used later on referring to the three situations as augmented bodies [105].

Fischer proved that his method works for a variety of simple and complex, open and closed chains of any number of elements. In Ref. [53] examples are shown of a chain of six elements and of a spatial system of twenty elements with multiple open and closed chains.

A thorough investigation of Fischer's work and of the historical development of his method for mechanism and machine science is presented in Appendix A. A short summary of the latter is presented here. Wittenbauer in 1923 developed Fischer's method by applying it for analysis of some more complex closed chains and by illustrating the procedure of applying the method to parallel linkages and non-symmetric links with general mass distributions [104]. Among others, Beyer [14] and Federhofer [41] summarized the method while Kreutziger [69] and Wunderlich [109] applied Fischer's method to show that the motion of the CoM of a 4R four-bar mechanism describes a curve similar to a coupler curve of the mechanism.

Fischer already related his method with shaking-force balancing and analyzed the balancing of a crank-slider mechanism [53]. In 1957, Shchepetil'nikov [87] used Fischer's method and introduced the method of double contour transformation to find auxiliary mechanisms that describe the motion of the CoM of a linkage, not being restricted to four-bar mechanisms as in [69] and [109]. His research was based on the findings of Artobolevskii in 1951 [10] who had proposed an alternative formulation of the principal vectors. These auxiliary mechanisms were force balanced with additional counter-masses in order to make the CoM of the system stationary.

Hilpert in 1965 showed how in addition to Fischer's principal vector linkage a pantograph with counter-mass can be used to bring the CoM of the mechanism to a specific stationary position in the base [61]. Shchepetil'nikov in 1975 extended his method by applying it to systems of unsymmetrical elements, i.e. elements with general CoM locations [88]. Among others, Wittenburg identified the concept of principal vectors in multi-body dynamic equations by applying concepts of graph theory, referring to the principal point as a Barycenter [105].

More recently, Agrawal et al. presented some articles, including notably Ref. [5], in which they mounted Fischer's principal vector linkage on the base with a pin in the common CoM S . The common CoM then is stationary for all motion and the mechanism has become a three-DoF force-balanced manipulator. Hereby they were the first to consider the masses of all elements of the principal vector linkage. How-

ever they limited their investigation to mass symmetric links for which they showed experimentally that these masses can be included to have S be the common CoM of all elements. Theoretically however, the problem of including these masses was not solved since their formulation of the CoM position showed to be too complex and with few physical meaning.

3.2.2 Generalization and calculation of principal dimensions with Equivalent Linear Momentum Systems

When the principal vector linkage in Fig. 3.6f is generalized such that each of the nine elements has a mass and a general CoM, then the principal vector linkage in Fig. 3.7 is obtained. Since a pantograph is a principal vector linkage that can have a general CoM in each element, also any combination of pantographs can have a general CoM in each element. The principal element P_1A_1 has a mass m_1 with its CoM in S_1 defined with p_1 and q_1 relative to P_1 and line A_1P_1 . The principal element A_1A_2 has a mass m_2 with its CoM in S_2 defined with e_2 and f_2 relative to A_1 and line A_1A_2 . The principal element A_2P_3 has a mass m_3 with its CoM in S_3 defined with p_3 and q_3 relative to P_3 and line A_2P_3 . The principal vector links have a mass m_{ij} of which the CoM is described with p_{ij} and q_{ij} relative to their links as illustrated. With respect to an arbitrary invariant link point the mechanism exhibits 3-DoF motion which is described with angles θ_1 , θ_2 , and θ_3 of the principal elements.

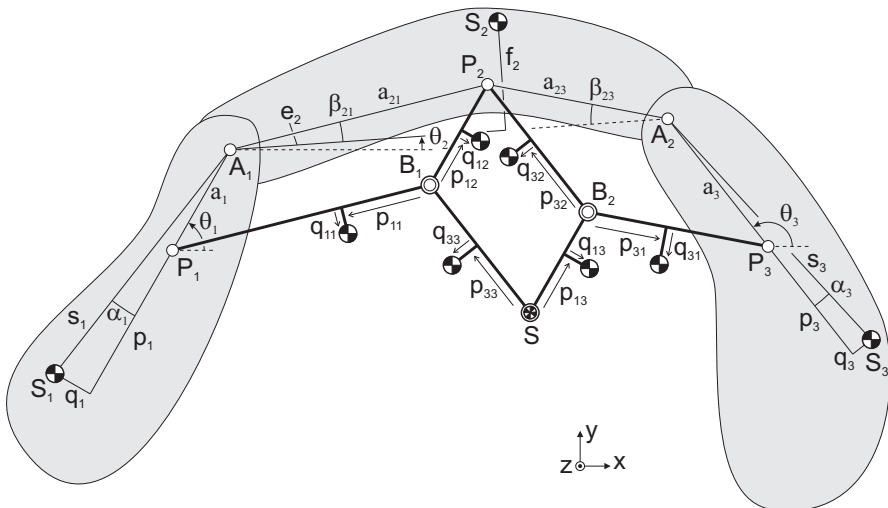


Fig. 3.7 A 3-DoF principal vector linkage of three principal elements in series jointed in A_1 and A_2 and with a general CoM in each of the nine elements. Invariant link point and joint S is the common CoM of the complete mechanism for all motion.

The principal vectors on which this mechanism is based are depicted in Fig. 3.8. These vectors describe the positions of the principal points P_1 , P_2 , and P_3 relative to the common CoM in S of which the norms are the principal dimensions a_1 , a_{21} , a_{23} , and a_3 . These vectors also describe the positions of the principal joints A_1 and A_2 . When the principal point in each principal element is known, the complete mechanism is determined for which the common CoM is in S for all motion.

Similar to the 2-DoF principal vector linkage in Fig. 3.2, the principal points of this mechanism can be calculated with linear momentum equations of each DoF individually. Figure 3.9 illustrates the relative motion of DoF 1 with $\dot{\theta}_2 = \dot{\theta}_3 = 0$. This can be regarded as principal vector links SB_1 and B_1P_1 being fixed while links 2, 3, 31, and 32 solely translate and links 1, 12, and 13 solely rotate. The linear momentum \bar{L}_1 of this motion can be written with respect to reference frame x_1y_1 , which has the y_1 -axis aligned with the principal vector \bar{a}_1 , as

$$\bar{L}_1 = \begin{bmatrix} (m_2 + m_3 + m_{31} + m_{32})a_1 + m_{12}p_{12} + m_{13}p_{13} - m_1p_1 \\ -m_{12}q_{12} - m_{13}q_{13} + m_1q_1 \end{bmatrix} \dot{\theta}_1 = \begin{bmatrix} 0 \\ 0 \end{bmatrix} \quad (3.8)$$

To facilitate the formulation of the linear momentum, an ELMS can be used which for this motion is shown in Fig. 3.11a. This reduced-mass model is obtained by merging links 1, 12, and 13 with B_1 and S coinciding with P_1 , P_2 and B_2 coinciding with A_1 , and with mass $m_2 + m_3 + m_{31} + m_{32}$ projected in A_1 . The linear momentum then is written of this model rotating about P_1 , which therefore is the CoM of the reduced-mass model.

Similarly, the linear momentum \bar{L}_3 of the relative motion of DoF 3 with $\dot{\theta}_1 = \dot{\theta}_2 = 0$ is obtained. This motion is illustrated in Fig. 3.10 and can be regarded as principal vector links SB_2 and B_2P_3 being fixed while links 1, 2, 11, and 12 solely translate and links 3, 32, and 33 solely rotate. The linear momentum \bar{L}_3 of this motion can be written with respect to reference frame x_3y_3 , which has the y_3 -axis aligned with the principal vector \bar{a}_3 , as

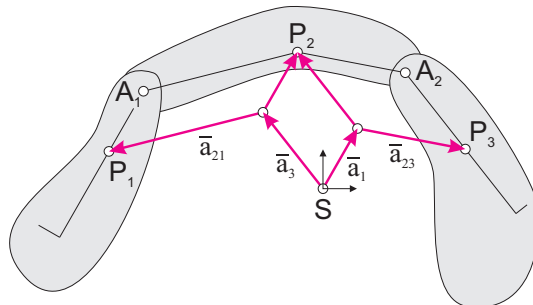


Fig. 3.8 The principal vectors \bar{a}_1 , \bar{a}_{21} , \bar{a}_{23} , and \bar{a}_3 describe the positions of the principal points P_1 , P_2 , and P_3 relative to the common CoM in S with which the principal vector linkage is fully defined.

$$\bar{L}_3 = \begin{bmatrix} (m_1 + m_2 + m_{11} + m_{12})a_3 + m_{32}p_{32} + m_{33}p_{33} - m_3p_3 \\ m_{32}q_{32} + m_{33}q_{33} - m_3q_3 \end{bmatrix} \dot{\theta}_3 = \begin{bmatrix} 0 \\ 0 \end{bmatrix} \quad (3.9)$$

The ELMS of this motion is shown in Fig. 3.11b. This reduced-mass model is obtained by merging links 3, 32, and 33 with B_2 and S coinciding with P_3 , P_2 and B_1 coinciding with A_2 , and with mass $m_1 + m_2 + m_{11} + m_{12}$ projected in A_2 . The linear momentum is written of this model rotating about P_3 , which therefore is the CoM of the reduced-mass model.

From the linear momentum equations (3.8) and (3.9) already four force balance conditions are obtained, which are

$$m_1p_1 = (m_2 + m_3 + m_{31} + m_{32})a_1 + m_{12}p_{12} + m_{13}p_{13} \quad (3.10)$$

$$m_1q_1 = m_{12}q_{12} + m_{13}q_{13} \quad (3.11)$$

$$m_3p_3 = (m_1 + m_2 + m_{11} + m_{12})a_3 + m_{32}p_{32} + m_{33}p_{33} \quad (3.12)$$

$$m_3q_3 = m_{32}q_{32} + m_{33}q_{33} \quad (3.13)$$

These are also the conditions for which P_1 and P_3 are the CoMs of their reduced-mass model in the ELMSs in Fig. 3.11. The principal dimensions a_1 and a_3 are obtained from (3.10) and (3.12) as

$$a_1 = \frac{m_1p_1 - m_{12}p_{12} - m_{13}p_{13}}{m_2 + m_3 + m_{31} + m_{32}} \quad a_3 = \frac{m_3p_3 - m_{32}p_{32} - m_{33}p_{33}}{m_1 + m_2 + m_{11} + m_{12}} \quad (3.14)$$

while q_1 and q_3 are obtained as

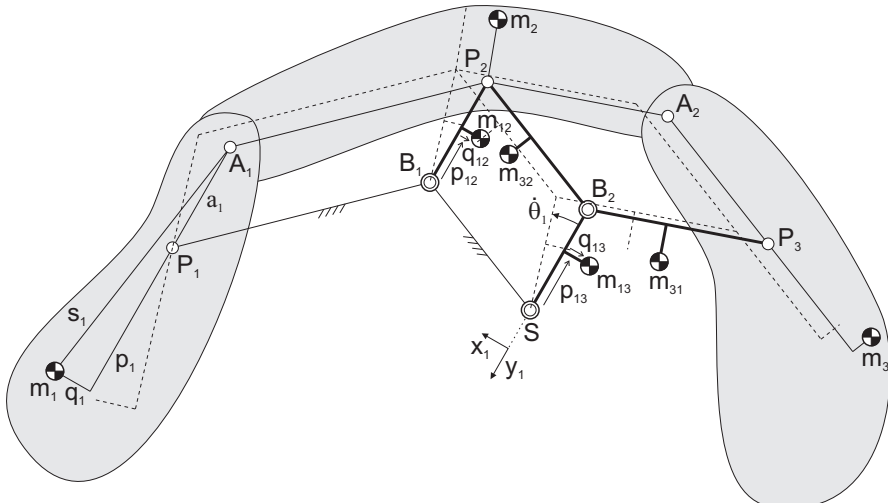


Fig. 3.9 Relative motion of DoF 1 with $\dot{\theta}_2 = \dot{\theta}_3 = 0$ for which links 2, 3, 31, and 32 solely translate and links 1, 12, and 13 solely rotate. To find P_1 the linear momentum of this motion has to be zero.

$$q_1 = \frac{m_{12}q_{12} + m_{13}q_{13}}{m_1} \quad q_3 = \frac{m_{32}q_{32} + m_{33}q_{33}}{m_3} \quad (3.15)$$

For a design it can be useful to have P_1 and P_3 defined with respect to lines s_1 and s_3 with angles α_1 and α_3 , respectively, as illustrated in Fig. 3.7. By substitution of $p_1 = s_1 \cos \alpha_1 - a_1$, $p_3 = s_3 \cos \alpha_3 - a_3$, $q_1 = s_1 \sin \alpha_1$, and $q_3 = s_3 \sin \alpha_3$, the parameters for P_1 and P_3 become

$$\begin{aligned} a_1 &= \frac{m_1 s_1 \cos \alpha_1 - m_{12} p_{12} - m_{13} p_{13}}{m_1 + m_2 + m_3 + m_{31} + m_{32}} & \alpha_1 &= \sin^{-1} \left(\frac{m_{12}q_{12} + m_{13}q_{13}}{m_1 s_1} \right) \\ a_3 &= \frac{m_3 s_3 \cos \alpha_3 - m_{32} p_{32} - m_{33} p_{33}}{m_1 + m_2 + m_3 + m_{11} + m_{12}} & \alpha_3 &= \sin^{-1} \left(\frac{m_{32}q_{32} + m_{33}q_{33}}{m_3 s_3} \right) \end{aligned}$$

and with $m_1 s_1 \cos \alpha_1 = \sqrt{m_1^2 s_1^2 (1 - \sin^2 \alpha_1)}$ and $m_3 s_3 \cos \alpha_3 = \sqrt{m_3^2 s_3^2 (1 - \sin^2 \alpha_3)}$ a_1 and a_3 are found as

$$\begin{aligned} a_1 &= \frac{\sqrt{m_1^2 s_1^2 - (m_{12}q_{12} + m_{13}q_{13})^2} - m_{12} p_{12} - m_{13} p_{13}}{m_1 + m_2 + m_3 + m_{31} + m_{32}} \\ a_3 &= \frac{\sqrt{m_3^2 s_3^2 - (m_{32}q_{32} + m_{33}q_{33})^2} - m_{32} p_{32} - m_{33} p_{33}}{m_1 + m_2 + m_3 + m_{11} + m_{12}} \end{aligned} \quad (3.16)$$

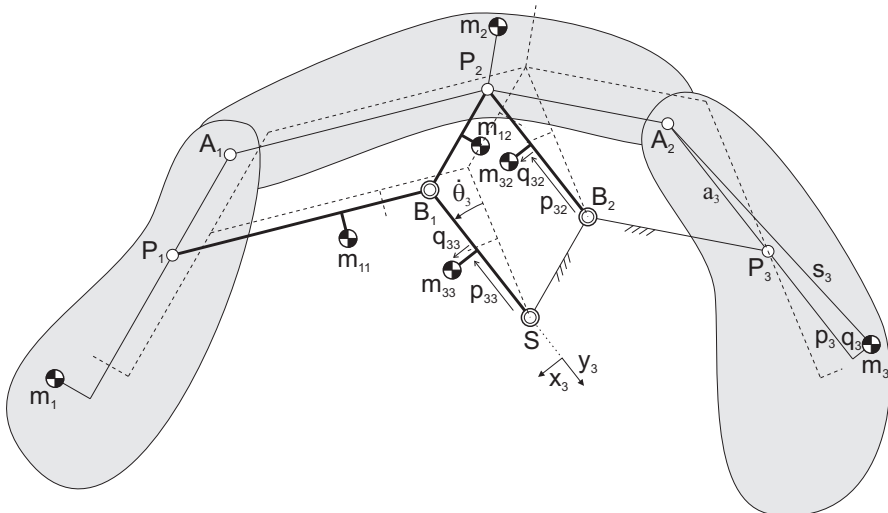


Fig. 3.10 Relative motion of DoF 3 with $\dot{\theta}_1 = \dot{\theta}_2 = 0$ for which links 1, 2, 11, and 12 solely translate and links 3, 32, and 33 solely rotate. To find P_3 the linear momentum of this motion has to be zero.

Principal point P_2 can be calculated from the linear momentum of the relative motion of DoF 2 with $\dot{\theta}_1 = \dot{\theta}_3 = 0$, which is illustrated in Fig. 3.12. This can be regarded as parallelogram $SB_1P_2B_2$ being fixed while links 1 and 3 solely translate and links 2, 11, and 31 solely rotate. For an enclosed principal element as A_1A_2 , more effort is needed to obtain the principal point and therefore an ELMS is helpful. The linear momentum of this motion can be divided such that it is written with respect to the three reference frames illustrated in Fig. 3.12. When the linear momentum of m_1 and m_{11} is written with respect to frame $x_{21}y_{21}$, the linear momentum of m_2 is written with respect to frame $x_{22}y_{22}$, and the linear momentum of m_3 and m_{31} is written with respect to frame $x_{23}y_{23}$, this results in the three sets of linear momentum equations

$$\begin{aligned}\bar{L}_{21} &= \begin{bmatrix} m_1a_{21} + m_{11}p_{11} \\ m_{11}q_{11} \end{bmatrix} \dot{\theta}_2 & \bar{L}_{22} &= \begin{bmatrix} m_2d_2 \\ 0 \end{bmatrix} \dot{\theta}_2 \\ \bar{L}_{23} &= \begin{bmatrix} m_3a_{23} + m_{31}p_{31} \\ -m_{31}q_{31} \end{bmatrix} \dot{\theta}_2\end{aligned}\quad (3.17)$$

Figure 3.13 shows the ELMS of this motion. This reduced-mass model is obtained when links 11 and 2 are merged with B_1 and P_2 coinciding, when links 31 and 2 are merged with B_2 and P_2 coinciding, and with m_1 projected in A_1 and m_3 projected in A_2 . With respect to the three reference frames the linear momentum equations of this reduced-mass model rotating about P_2 are equal. Since the linear momentum of the ELMS has to be zero, P_2 is the CoM of the reduced-mass model.

In Fig. 3.13 it is shown how m_2 can be described with respect to P_2 with a parallelogram with sides d_2^a and d_2^b . These sides are aligned with lines P_2N_1 and P_2N_2 , respectively, where N_1 is found as the CoM of m_1 and m_{11} and N_2 is found as the

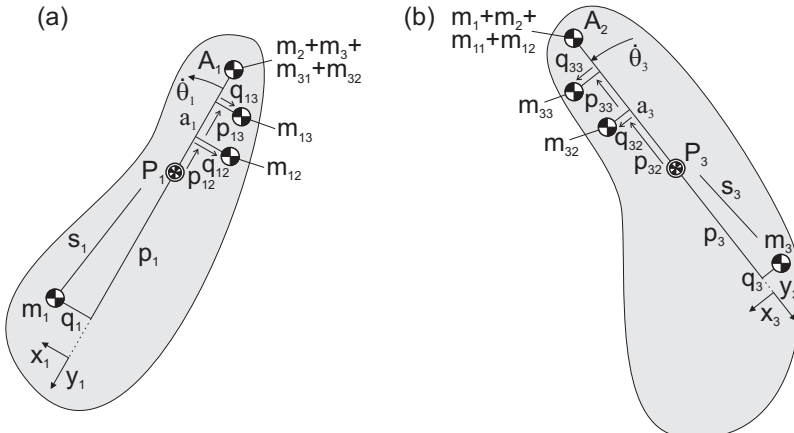


Fig. 3.11 ELMS of relative motion of (a) DoF 1 and (b) DoF 3 to facilitate the formulation of the linear momentum. These reduced-mass models have their CoM in P_1 and P_3 , respectively.

CoM of m_3 and m_{31} in the ELMS. This parallelogram can also be defined with lines p_2^a , q_2^a , p_2^b , and q_2^b as illustrated of which p_2^a is aligned with a_{21} , p_2^b is aligned with a_{23} , q_2^a is normal to p_2^a , and q_2^b is normal to p_2^b . With the parallelogram the contribution of m_2 to the force balance about P_2 of either the left side of P_2 along a_{21} and the right side of P_2 along a_{23} is determined. This can be understood when the graphical construction is regarded as a moving 2-DoF parallelogram linkage as illustrated in Fig. 3.14a. Here P_2A_1 and P_2A_2 have become links rotating about P_2 with $\dot{\theta}_{21}$ and $\dot{\theta}_{23}$, respectively. To have P_2 be the common CoM, this linkage has to be force balanced about P_2 .

The linkage in Fig. 3.14a is a pantograph and the calculations for which P_2 is the common CoM for all motion can be derived from the two relative DoFs individually as in Fig. 3.3. The ELMS of each relative DoF is shown in Fig. 3.14b and 3.14c. In Fig. 3.14b m_2 is projected at distances p_2^a and q_2^a relative to P_2 while in Fig. 3.14c m_2 is projected at distances p_2^b and q_2^b relative to P_2 , as illustrated. Of both ELMSs the linear momentum is zero when their CoMs are in P_2 which is for the force balance conditions

$$\begin{aligned} m_2 p_2^a &= m_1 a_{21} + m_{11} p_{11} & m_2 q_2^a &= m_{11} q_{11} \\ m_2 p_2^b &= m_3 a_{23} + m_{31} p_{31} & m_2 q_2^b &= m_{31} q_{31} \end{aligned} \quad (3.18)$$

Since $(d_2^a)^2 = (p_2^a)^2 + (q_2^a)^2$ and $(d_2^b)^2 = (p_2^b)^2 + (q_2^b)^2$, the four linear conditions can be reduced to the two nonlinear force balance conditions

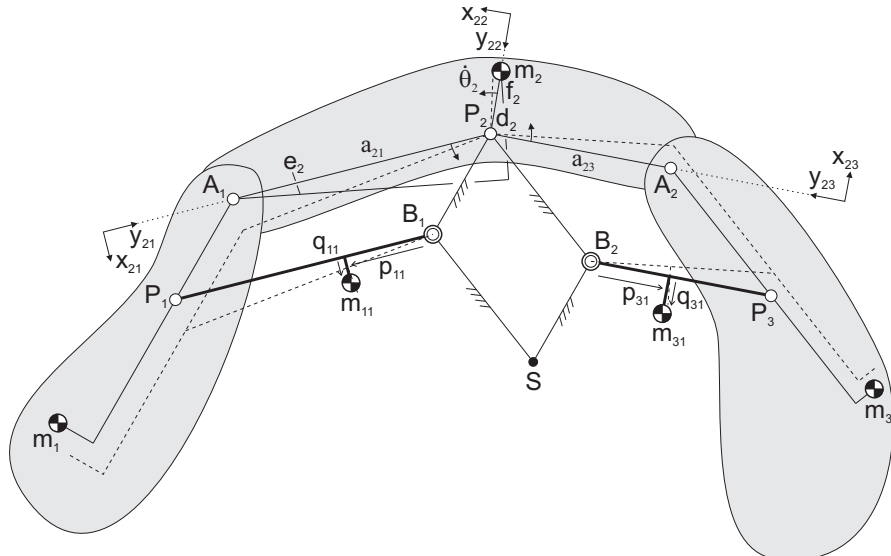


Fig. 3.12 Relative motion of DoF 2 with $\dot{\theta}_1 = \dot{\theta}_3 = 0$ for which links 1 and 3 solely translate and links 2, 11, and 31 solely rotate. To find P_2 the linear momentum of this motion has to be zero.

$$\begin{aligned}(m_2 d_2^a)^2 &= (m_1 a_{21} + m_{11} p_{11})^2 + (m_{11} q_{11})^2 \\ (m_2 d_2^b)^2 &= (m_3 a_{23} + m_{31} p_{31})^2 + (m_{31} q_{31})^2\end{aligned}\quad (3.19)$$

The principal dimensions a_{21} and a_{23} are obtained from (3.18) as

$$a_{21} = \frac{m_2 p_2^a - m_{11} p_{11}}{m_1} \quad a_{23} = \frac{m_2 p_2^b - m_{31} p_{31}}{m_3} \quad (3.20)$$

while q_2^a and q_2^b are calculated as

$$q_2^a = \frac{m_{11} q_{11}}{m_2} \quad q_2^b = \frac{m_{31} q_{31}}{m_2} \quad (3.21)$$

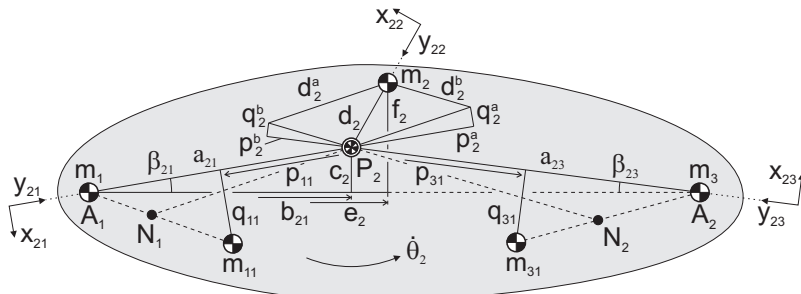


Fig. 3.13 ELMS of the relative motion of DoF 2. A parallelogram with sides d_2^a and d_2^b describes m_2 relative to P_2 . This parallelogram is defined with lines p_2^a , q_2^a , p_2^b , and q_2^b of which p_2^a is aligned with a_{21} , p_2^b is aligned with a_{23} , q_2^a is normal to p_2^a , and q_2^b is normal to p_2^b .

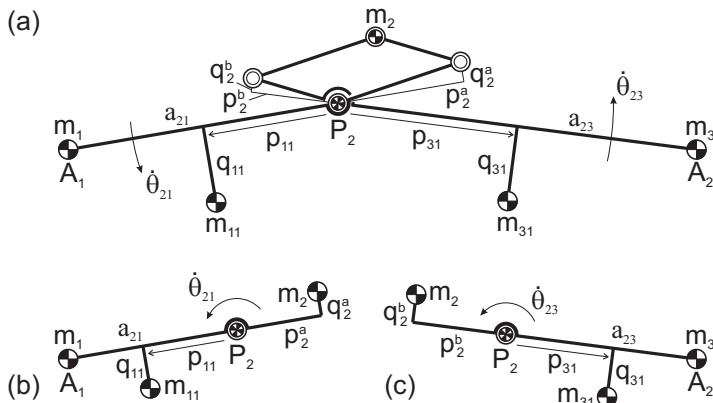


Fig. 3.14 The graphical construction in Fig. 3.13 can be considered a 2-DoF pantograph linkage (a) from which two ELMSs (b) and (c) are derived similarly to the pantograph in Fig. 3.2. The force balance conditions then are the conditions for which the ELMSs have their CoM in P_2 .

In summary, the eight force balance conditions of the 3-DoF principal vector linkage in Fig. 3.7, which define the principal dimensions for which the common CoM is in joint S for all motion, are:

$$\begin{aligned}
 m_1 p_1 &= (m_2 + m_3 + m_{31} + m_{32}) a_1 + m_{12} p_{12} + m_{13} p_{13} \\
 m_1 q_1 &= m_{12} q_{12} + m_{13} q_{13} \\
 m_2 p_2^a &= m_1 a_{21} + m_{11} p_{11} \\
 m_2 q_2^a &= m_{11} q_{11} \\
 m_2 p_2^b &= m_3 a_{23} + m_{31} p_{31} \\
 m_2 q_2^b &= m_{31} q_{31} \\
 m_3 p_3 &= (m_1 + m_2 + m_{11} + m_{12}) a_3 + m_{32} p_{32} + m_{33} p_{33} \\
 m_3 q_3 &= m_{32} q_{32} + m_{33} q_{33}
 \end{aligned} \tag{3.22}$$

The location of P_2 in $A_1 A_2$ can be found with b_{21} and c_2 with respect to A_1 and line $A_1 A_2$ as illustrated in Fig. 3.13. Therefore, the linear momenta with respect to the three reference frames $x_{21}y_{21}$, $x_{22}y_{22}$, and $x_{23}y_{23}$ need to be unified. To do this, the ELMS in Fig. 3.13 is adapted, which can be done in various ways without changing its linear momentum about P_2 . In Fig. 3.15 the mass m_{11} is projected in both points I_1 and J_1 while m_{31} is projected in both points I_2 and J_2 . J_1 is located at a distance q_{11} from P_2 normal to line $P_2 A_1$ while J_2 is located at a distance q_{31} from P_2 normal to line $P_2 A_2$, as illustrated. The linear momentum equations of this ELMS are equal to those of the ELMS in Fig. 3.13.

The ELMS in Fig. 3.15 can be adapted to the ELMS in Fig. 3.16. In this ELMS the equivalent masses $\mu_1 = m_1 + m_{11} p_{11} / a_{21}$ in A_1 and $\mu_3 = m_3 + m_{31} p_{31} / a_{23}$ in A_2 combine m_{11} in I_1 with m_1 in A_1 and m_{31} in I_2 with m_3 in A_2 , respectively. A mass $\mu_2 = m_2$ still is in S_2 while masses $v_1 = m_{11} q_{11} / a_{21}$ and $v_3 = m_{31} q_{31} / a_{23}$ are in J_1 and J_2 which now are located at distances a_{21} and a_{23} from P_2 , respectively. When these equivalent masses are substituted in (3.17) the linear momentum with respect to each of the three reference frames writes

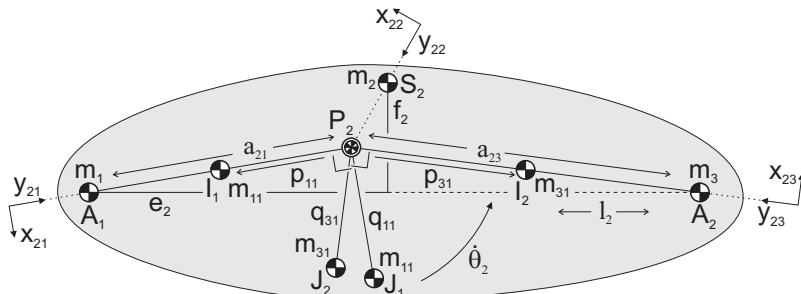


Fig. 3.15 ELMS of the relative motion of DoF 2 which is adapted from Fig. 3.13 to have a mass m_{11} in both points I_1 and J_1 and a mass m_{31} in both points I_2 and J_2 .

$$\bar{L}_{21} = \begin{bmatrix} \mu_1 \\ v_1 \end{bmatrix} a_{21} \dot{\theta}_2 \quad \bar{L}_{22} = \begin{bmatrix} \mu_2 \\ 0 \end{bmatrix} d_2 \dot{\theta}_2 \quad \bar{L}_{23} = \begin{bmatrix} \mu_3 \\ -v_3 \end{bmatrix} a_{23} \dot{\theta}_2 \quad (3.23)$$

which are equal to the linear momenta obtained from the ELMS in Fig. 3.16. From this ELMS the linear momentum \bar{L}_2 of the complete ELMS rotating about P_2 can be written with respect to reference frame x_2y_2 , which has the x_2 -axis aligned with A_1A_2 as

$$\begin{aligned} \frac{\bar{L}_2}{\dot{\theta}_2} &= \mu_1 \begin{bmatrix} c_2 \\ -b_{21} \end{bmatrix} + v_1 \begin{bmatrix} b_{21} \\ c_2 \end{bmatrix} + \mu_2 \begin{bmatrix} c_2 - f_2 \\ -(b_{21} - e_2) \end{bmatrix} + \\ &\quad \mu_3 \begin{bmatrix} c_2 \\ -(b_{21} - l_2) \end{bmatrix} - v_3 \begin{bmatrix} b_{21} - l_2 \\ c_2 \end{bmatrix} = \begin{bmatrix} 0 \\ 0 \end{bmatrix} \end{aligned} \quad (3.24)$$

The force balance conditions for the relative motion of DoF 2 then are written in terms of equivalent masses as:

$$(\mu_1 + \mu_2 + \mu_3)c_2 + (v_1 - v_3)b_{21} - \mu_2 f_2 + v_3 l_2 = 0 \quad (3.25)$$

$$-(\mu_1 + \mu_2 + \mu_3)b_{21} + (v_1 - v_3)c_2 + \mu_2 e_2 + \mu_3 l_2 = 0 \quad (3.26)$$

from which b_{21} and c_2 can be derived as

$$\begin{aligned} b_{21} &= \frac{(\mu_2 f_2 - v_3 l_2)(v_1 - v_3) + (\mu_2 e_2 + \mu_3 l_2)(\mu_1 + \mu_2 + \mu_3)}{(\mu_1 + \mu_2 + \mu_3)^2 + (v_1 - v_3)^2} \quad (3.27) \\ c_2 &= \frac{(\mu_2 f_2 - v_3 l_2)(\mu_1 + \mu_2 + \mu_3) - (\mu_2 e_2 + \mu_3 l_2)(v_1 - v_3)}{(\mu_1 + \mu_2 + \mu_3)^2 + (v_1 - v_3)^2} \end{aligned}$$

With μ_1 , μ_2 , μ_3 , v_1 , and v_2 substituted, these conditions write

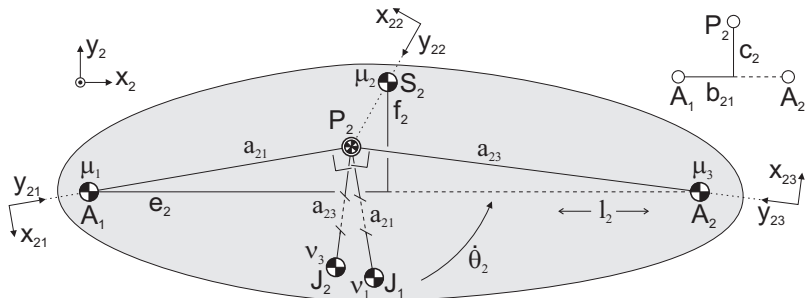


Fig. 3.16 ELMS adapted from Fig. 3.15 with masses $\mu_1 = m_1 + m_{11}p_{11}/a_{21}$ and $\mu_3 = m_3 + m_{31}p_{31}/a_{23}$ in A_1 and A_2 , respectively, a mass $\mu_2 = m_2$ in S_2 , and masses $v_1 = m_{11}q_{11}/a_{21}$ and $v_3 = m_{31}q_{31}/a_{23}$ in J_1 and J_2 , respectively.

$$\begin{aligned}
b_{21} &= \frac{(m_2 f_2 - \frac{m_{31} q_{31}}{a_{23}} l_2) (\frac{m_{11} q_{11}}{a_{21}} - \frac{m_{31} q_{31}}{a_{23}}) + (m_2 e_2 + m_3 l_2 + \frac{m_{31} p_{31}}{a_{23}} l_2) (m_1 + m_2 + m_3 + \frac{m_{11} p_{11}}{a_{21}} + \frac{m_{31} p_{31}}{a_{23}})}{(m_1 + m_2 + m_3 + \frac{m_{11} p_{11}}{a_{21}} + \frac{m_{31} p_{31}}{a_{23}})^2 + (\frac{m_{11} q_{11}}{a_{21}} - \frac{m_{31} q_{31}}{a_{23}})^2} \\
c_2 &= \frac{(m_2 f_2 - \frac{m_{31} q_{31}}{a_{23}} l_2) (m_1 + m_2 + m_3 + \frac{m_{11} p_{11}}{a_{21}} + \frac{m_{31} p_{31}}{a_{23}}) - (m_2 e_2 + m_3 l_2 + \frac{m_{31} p_{31}}{a_{23}} l_2) (\frac{m_{11} q_{11}}{a_{21}} - \frac{m_{31} q_{31}}{a_{23}})}{(m_1 + m_2 + m_3 + \frac{m_{11} p_{11}}{a_{21}} + \frac{m_{31} p_{31}}{a_{23}})^2 + (\frac{m_{11} q_{11}}{a_{21}} - \frac{m_{31} q_{31}}{a_{23}})^2} \\
\end{aligned} \tag{3.28}$$

Since in these equations $a_{21} = \sqrt{b_{21}^2 + c_2^2}$ and $a_{23} = \sqrt{(l_2 - b_{21})^2 + c_2^2}$ depend on b_{21} and c_2 , in general no closed-form expressions for b_{21} and c_2 are found. For some specific conditions however they are obtained. For instance when $\lambda_1 = p_{11}/a_{21}$, $\lambda_2 = p_{31}/a_{23}$, $\lambda_3 = q_{11}/a_{21}$, and $\lambda_4 = q_{31}/a_{23}$ are constants, then $\mu_1 = m_1 + m_{11}\lambda_1$, $\mu_2 = m_2$, $\mu_3 = m_3 + m_{31}\lambda_2$, $v_1 = m_{11}\lambda_3$, and $v_3 = m_{31}\lambda_4$ become independent of the principal dimensions. These conditions imply for instance that for $\lambda_1 = \frac{1}{2}$, m_{11} is always halfway length a_{21} . With these parameters substituted, b_{21} and c_2 are calculated from (3.28) as

$$\begin{aligned}
b_{21} &= \frac{(m_2 f_2 - m_{31} \lambda_4 l_2) (m_{11} \lambda_3 - m_{31} \lambda_4) + (m_2 e_2 + m_3 l_2 + m_{31} \lambda_2 l_2) (m_1 + m_2 + m_3 + m_{11} \lambda_1 + m_{31} \lambda_2)}{(m_1 + m_2 + m_3 + m_{11} \lambda_1 + m_{31} \lambda_2)^2 + (m_{11} \lambda_3 - m_{31} \lambda_4)^2} \\
c_2 &= \frac{(m_2 f_2 - m_{31} \lambda_4 l_2) (m_1 + m_2 + m_3 + m_{11} \lambda_1 + m_{31} \lambda_2) - (m_2 e_2 + m_3 l_2 + m_{31} \lambda_2 l_2) (m_{11} \lambda_3 - m_{31} \lambda_4)}{(m_1 + m_2 + m_3 + m_{11} \lambda_1 + m_{31} \lambda_2)^2 + (m_{11} \lambda_3 - m_{31} \lambda_4)^2} \\
\end{aligned} \tag{3.29}$$

For the specific condition $v_1 = v_3$ ($m_{11}\lambda_3 = m_{31}\lambda_4$), equations (3.27) reduce to

$$\begin{aligned}
b_{21} &= \frac{\mu_2 e_2 + \mu_3 l_2}{\mu_1 + \mu_2 + \mu_3} = \frac{m_2 e_2 + m_3 l_2 + m_{31} \lambda_2 l_2}{m_1 + m_2 + m_3 + m_{11} \lambda_1 + m_{31} \lambda_2} \\
c_2 &= \frac{\mu_2 f_2 - v_3 l_2}{\mu_1 + \mu_2 + \mu_3} = \frac{m_2 f_2 - m_{31} \lambda_4 l_2}{m_1 + m_2 + m_3 + m_{11} \lambda_1 + m_{31} \lambda_2} \\
\end{aligned} \tag{3.30}$$

while for the specific condition $v_1 = v_3 = 0$ ($\lambda_3 = \lambda_4 = 0$) these equations reduce to

$$\begin{aligned}
b_{21} &= \frac{\mu_2 e_2 + \mu_3 l_2}{\mu_1 + \mu_2 + \mu_3} = \frac{m_2 e_2 + m_3 l_2 + m_{31} \lambda_2 l_2}{m_1 + m_2 + m_3 + m_{11} \lambda_1 + m_{31} \lambda_2} \\
c_2 &= \frac{\mu_2 f_2}{\mu_1 + \mu_2 + \mu_3} = \frac{m_2 f_2}{m_1 + m_2 + m_3 + m_{11} \lambda_1 + m_{31} \lambda_2} \\
\end{aligned} \tag{3.31}$$

To go back to the linkage in Fig. 3.6f where the masses of the principal vector links are zero and only the principal elements have mass, P_2 is found with

$$b_{21} = \frac{m_2 e_2 + m_3 l_2}{m_1 + m_2 + m_3} \quad c_2 = \frac{m_2 f_2}{m_1 + m_2 + m_3} \tag{3.32}$$

From Fig. 3.13, P_2 can be found also by writing the location of m_2 as

$$\begin{aligned}
e_2 &= (a_{21} + p_2^a) \cos \beta_{21} - q_2^a \sin \beta_{21} - p_2^b \cos \beta_{23} + q_2^b \sin \beta_{23} \\
f_2 &= (a_{21} + p_2^a) \sin \beta_{21} + q_2^a \cos \beta_{21} + p_2^b \sin \beta_{23} + q_2^b \cos \beta_{23} \\
\end{aligned} \tag{3.33}$$

where $\beta_{21} \angle P_2 A_1 A_2$ and $\beta_{23} \angle P_2 A_2 A_1$. With $\cos \beta_{21} = b_{21}/a_{21}$, $\sin \beta_{21} = c_{21}/a_{21}$, $\cos \beta_{23} = (l_2 - b_{21})/a_{23}$, and $\sin \beta_{23} = c_{23}/a_{23}$ these equations become

$$\begin{aligned} e_2 &= \left(\frac{a_{21} + p_2^a}{a_{21}} + \frac{p_2^b}{a_{23}} \right) b_{21} - \left(\frac{q_2^a}{a_{21}} - \frac{q_2^b}{a_{23}} \right) c_{21} - \frac{p_2^b}{a_{23}} l_2 \\ f_2 &= \left(\frac{a_{21} + p_2^a}{a_{21}} + \frac{p_2^b}{a_{23}} \right) c_{21} + \left(\frac{q_2^a}{a_{21}} - \frac{q_2^b}{a_{23}} \right) b_{21} + \frac{q_2^b}{a_{23}} l_2 \end{aligned} \quad (3.34)$$

from which b_{21} and c_{21} are obtained in terms of principal vectors as:

$$b_{21} = \frac{\left(\frac{a_{21} + p_2^a}{a_{21}} + \frac{p_2^b}{a_{23}} \right) (e_2 + \frac{p_2^b}{a_{23}} l_2) + \left(\frac{q_2^a}{a_{21}} - \frac{q_2^b}{a_{23}} \right) (f_2 - \frac{q_2^b}{a_{23}} l_2)}{\left(\frac{a_{21} + p_2^a}{a_{21}} + \frac{p_2^b}{a_{23}} \right)^2 + \left(\frac{q_2^a}{a_{21}} - \frac{q_2^b}{a_{23}} \right)^2} \quad (3.35)$$

$$c_{21} = \frac{\left(\frac{a_{21} + p_2^a}{a_{21}} + \frac{p_2^b}{a_{23}} \right) (f_2 - \frac{q_2^b}{a_{23}} l_2) - \left(\frac{q_2^a}{a_{21}} - \frac{q_2^b}{a_{23}} \right) (e_2 + \frac{p_2^b}{a_{23}} l_2)}{\left(\frac{a_{21} + p_2^a}{a_{21}} + \frac{p_2^b}{a_{23}} \right)^2 + \left(\frac{q_2^a}{a_{21}} - \frac{q_2^b}{a_{23}} \right)^2} \quad (3.36)$$

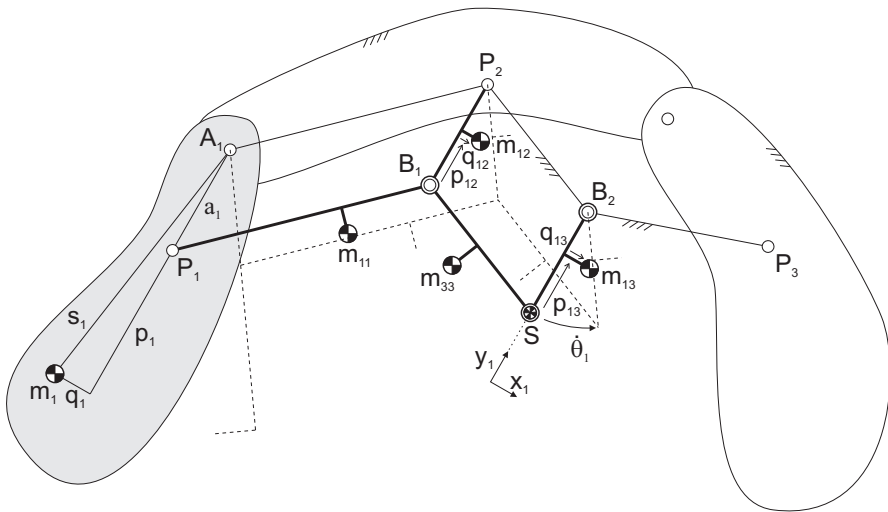


Fig. 3.17 Investigation of the relative motion of DoF 1 by rotation of principal element 1 about principal joint A_1 , where links 1, 12, and 13 solely rotate, links 11 and 33 solely translate, and the other links are fixed. Here the linear momentum of the moving masses equals the linear momentum of the total mass moving in S , from which the conditions for force balance are found.

3.2.3 Method of rotations about the principal joints

The relative motions of DoF 1 and of DoF 3 can also be investigated as illustrated for the relative motion of DoF 1 in Fig. 3.17. Here principal element 1 rotates about the principal joint A_1 while all other principal elements are fixed. While principal element 1 and links 12, and 13 solely rotate, links 11 and 33 solely translate and all other links are fixed. Since links 13 and 33 move, also joint S moves. This means that to have S be the common CoM, the linear momentum of the moving masses has to be equal to the linear momentum of the total mass m_{tot} moving in S . The linear momentum \bar{L}_1 of this motion can be written with respect to reference frame x_1y_1 , which has the y_1 -axis aligned with principal vector \bar{a}_1 , as

$$\begin{aligned}\bar{L}_1 &= \begin{bmatrix} (m_{11} + m_{33})a_1 + m_1(a_1 + p_1) + m_{12}(a_1 - p_{12}) + m_{13}(a_1 - p_{13}) \\ m_{12}q_{12} + m_{13}q_{13} - m_1q_1 \end{bmatrix} \dot{\theta}_1 \\ &= \begin{bmatrix} m_{tot}a_1 \\ 0 \end{bmatrix} \dot{\theta}_1\end{aligned}\quad (3.37)$$

with $m_{tot} = m_1 + m_2 + m_3 + m_{11} + m_{12} + m_{13} + m_{31} + m_{32} + m_{33}$. It is verified that the resulting force balance conditions (3.10) and (3.11) are also obtained this way.

3.2.4 Kinematic variations of the principal vector linkage

An alternative kinematic solution of a principal vector linkage with mass-symmetric elements was proposed by Artobolevskii [10], see Fig. A.8a. When this solution is generalized as a mechanism with a general CoM in each of the nine elements, the mechanism in Fig. 3.18 is obtained where joint S is the common CoM. Here the links are arranged such that P_2 is not used as a joint and B_2 is linked with A_2 and is a joint in link $P_1B_1B_2$.

Similar to the linkage in Fig. 3.7, the locations of P_1 and P_3 can be derived from the linear momentum of the relative motion of DoF 1 and DoF 3, respectively. For the relative motion of DoF 1 with $\dot{\theta}_2 = \dot{\theta}_3 = 0$ links SB_1 , SB_3 , B_2B_3 , and $P_1B_1B_2$ can be regarded as fixed while links P_1A_1 , B_2A_2 , and B_3P_3 solely rotate and links A_1A_2 and A_2P_3 solely translate. The linear momentum \bar{L}_1 with respect to reference frame x_1y_1 then is written as

$$\bar{L}_1 = \begin{bmatrix} (m_2 + m_3)a_1 + m_{12}p_{12} + m_{13}p_{13} - m_1p_1 \\ -m_{12}q_{12} - m_{13}q_{13} + m_1q_1 \end{bmatrix} \dot{\theta}_1 = \begin{bmatrix} 0 \\ 0 \end{bmatrix}\quad (3.38)$$

For the relative motion of DoF 3 with $\dot{\theta}_1 = \dot{\theta}_2 = 0$ links SB_3 and B_3P_3 can be regarded as fixed while links A_2P_3 , B_2B_3 , and B_1S solely rotate and links P_1A_1 , A_1A_2 , $P_1B_1B_2$, and B_2A_2 solely translate. The linear momentum \bar{L}_3 then is written with respect to reference frame x_3y_3 as

$$\bar{L}_3 = \begin{bmatrix} (m_1 + m_2 + m_{11} + m_{12})a_3 + m_{32}p_{32} + m_{33}p_{33} - m_3p_3 \\ m_{32}q_{32} + m_{33}q_{33} - m_3q_3 \end{bmatrix} \dot{\theta}_3 = \begin{bmatrix} 0 \\ 0 \end{bmatrix} \quad (3.39)$$

To find P_2 , the ELMS of the relative motion of DoF 2 is shown in Fig. 3.19. This ELMS is similar to the ELMS in Fig. 3.13 with as only difference a mass $m_3 + m_{12} + m_{13} + m_{32}$ in A_2 . The derivation of the conditions for which the linear momentum of the relative motion of DoF 2 is zero, i.e. for which P_2 is the CoM of this reduced-mass model, is similar to Fig. 3.14. Then together with \bar{L}_1 and \bar{L}_3 , the complete set of eight force balance conditions of the 3-DoF principal vector linkage in Fig. 3.18 becomes:

$$\begin{aligned} m_1p_1 &= (m_2 + m_3)a_1 + m_{12}p_{12} + m_{13}p_{13} \\ m_1q_1 &= m_{12}q_{12} + m_{13}q_{13} \\ m_2p_2^a &= m_1a_{21} + m_{11}p_{11} \\ m_2q_2^a &= m_{11}q_{11} \\ m_2p_2^b &= (m_3 + m_{12} + m_{13} + m_{32})a_{23} + m_{31}p_{31} \\ m_2q_2^b &= m_{31}q_{31} \\ m_3p_3 &= (m_1 + m_2 + m_{11} + m_{12})a_3 + m_{32}p_{32} + m_{33}p_{33} \\ m_3q_3 &= m_{32}q_{32} + m_{33}q_{33} \end{aligned} \quad (3.40)$$

From these conditions the principal dimensions a_1, a_{21}, a_{23}, a_3 are obtained. Parameters b_{21} and c_2 of the location of P_2 with respect to line A_1A_2 can be found

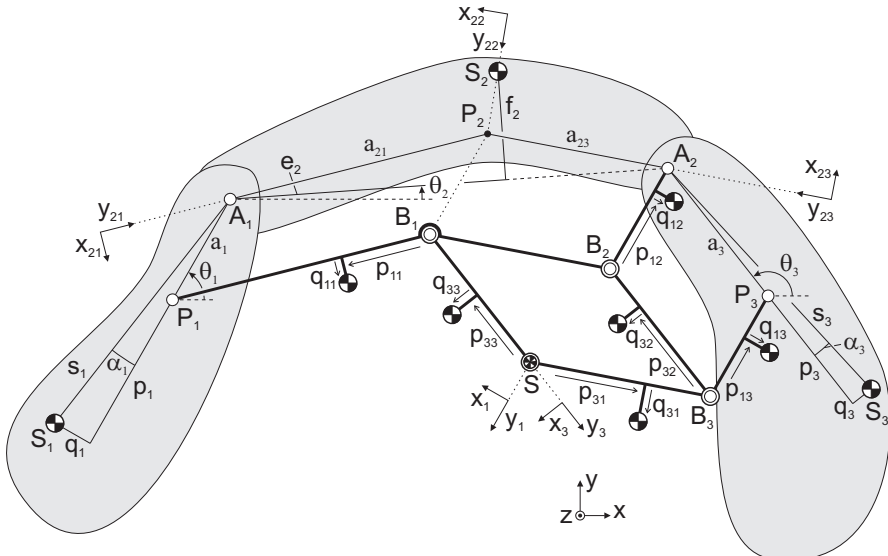


Fig. 3.18 Kinematic variation of a principal vector linkage by generalization of Artobolevski's solution of three principal elements in series with a general CoM in each of the nine elements and S as common CoM.

with (3.25) and (3.26) with $\mu_1 = m_1 + m_{11}p_{11}/a_{21}$, $\mu_2 = m_2$, $\mu_3 = m_3 + m_{12} + m_{13} + m_{32} + m_{31}p_{31}/a_{23}$, $v_1 = m_{11}q_{11}/a_{21}$, and $v_3 = m_{31}q_{31}/a_{23}$, comparable with the ELMS in Fig. 3.16 and with the linear momentum \bar{L}_2 about P_2 written as in (3.24). They can also be derived from (3.35) and (3.36).

Another kind of kinematic variation of the principal vector linkage is obtained with various designs of the principal vector links of which Fig. 3.20 illustrates a few possibilities. Here links 1 and 11 are not pivoted in P_1 but in T_6 , which is at a distance t_1 from P_1 along P_1A_1 , link 33 is pivoted with links 12 and 13 in T_2 and T_3 , which are at distances t_2 and t_3 with respect to B_1 and T_1 as illustrated, and link 31 is pivoted with link 32 in T_4 and with link 3 in T_5 , which are at distances t_4 and t_5 with respect to B_2 and P_3 as illustrated. The common CoM in S is an invariant link point in link 33 and is defined with o_1 and o_2 relative to T_3 as illustrated.

Various other changes can be made. Important for any of them is that to maintain a principal vector linkage, the mechanism needs to remain movable with the same relative motions per DoF. This means that the parallelograms of the principal vectors have to remain parallelograms for all motion. Therefore all elements still need to be arranged kinematically as parallelograms.

To find P_1 , Fig. 3.21 shows the relative motion of DoF 1. With respect to Fig. 3.9, here also links 11 and 33 move in pure translation while solely points P_1 , B_1 , and T_1 can be regarded as fixed points. This means that the common CoM in S is movable too and that, similar to Fig. 3.17, the linear momentum of the moving masses has to be equal to the linear momentum of the total mass moving in S . The linear momentum \bar{L}_1 therefore is written with respect to reference frame x_1y_1 as

$$\begin{aligned}\frac{\bar{L}_1}{\dot{\theta}_1} &= \begin{bmatrix} (m_2 + m_3 + m_{31} + m_{32})a_1 + m_{12}p_{12} + m_{13}p_{13} - m_1p_1 + m_{11}t_1 - m_{33}t_2 \\ -m_{12}q_{12} - m_{13}q_{13} + m_1q_1 + m_{33}t_3 \end{bmatrix} \\ &= \begin{bmatrix} -m_{tot}t_2 \\ m_{tot}t_3 \end{bmatrix}\end{aligned}\quad (3.41)$$

with $m_{tot} = m_1 + m_2 + m_3 + m_{11} + m_{12} + m_{13} + m_{31} + m_{32} + m_{33}$.

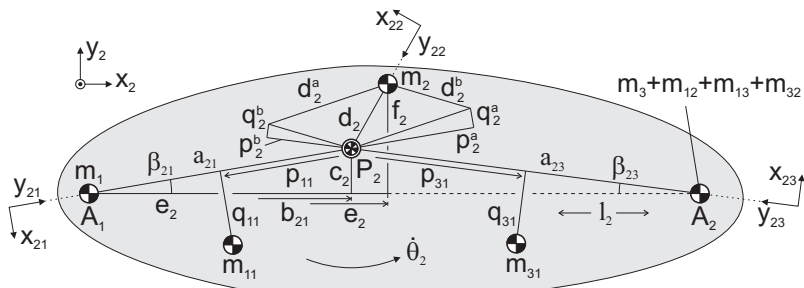


Fig. 3.19 ELMS of the relative motion of DoF 2 of the principal vector linkage in Fig. 3.18. P_2 is the CoM of this reduced-mass model with mass $m_3 + m_{12} + m_{13} + m_{32}$ in A_2 .

Figure 3.22 shows the relative motion of DoF 3. As compared to the motion in Fig. 3.10, here also link 31 moves in pure translation while solely points P_3 , B_2 , and T_1 can be regarded as fixed points. The linear momentum \bar{L}_3 of this motion is written with respect to reference frame x_3y_3 as

$$\begin{aligned}\frac{\bar{L}_3}{\theta_1} &= \begin{bmatrix} (m_1 + m_2 + m_{11} + m_{12})a_3 + m_{32}p_{32} + m_{33}p_{33} - m_3p_3 + m_{31}t_5 \\ m_{32}q_{32} + m_{33}q_{33} - m_3q_3 - m_{31}t_5 \end{bmatrix} \\ &= \begin{bmatrix} m_{tot}o_1 \\ m_{tot}o_2 \end{bmatrix} \quad (3.42)\end{aligned}$$

From \bar{L}_1 and \bar{L}_3 , four force balance conditions are derived as

$$\begin{aligned}m_1p_1 &= (m_{tot} - m_{33})t_2 + (m_2 + m_3 + m_{31} + m_{32})a_1 + m_{12}p_{12} + m_{13}p_{13} + m_{11}t_1 \\ m_1q_1 &= (m_{tot} - m_{33})t_3 + m_{12}q_{12} + m_{13}q_{13} \\ m_3p_3 &= -m_{tot}o_1 + (m_1 + m_2 + m_{11} + m_{12})a_3 + m_{32}p_{32} + m_{33}p_{33} + m_{31}t_4 \\ m_3q_3 &= -m_{tot}o_2 + m_{32}q_{32} + m_{33}q_{33} - m_{31}t_5\end{aligned}$$

The linear momentum of the relative motion of DoF 2 is equal to that of the motion in Fig. 3.12. The ELMS of this motion therefore is equal to Fig. 3.13 and the force balance conditions of DoF 2 are equal to (3.18). The eight force balance conditions of the principal vector linkage in Fig. 3.20 then become:

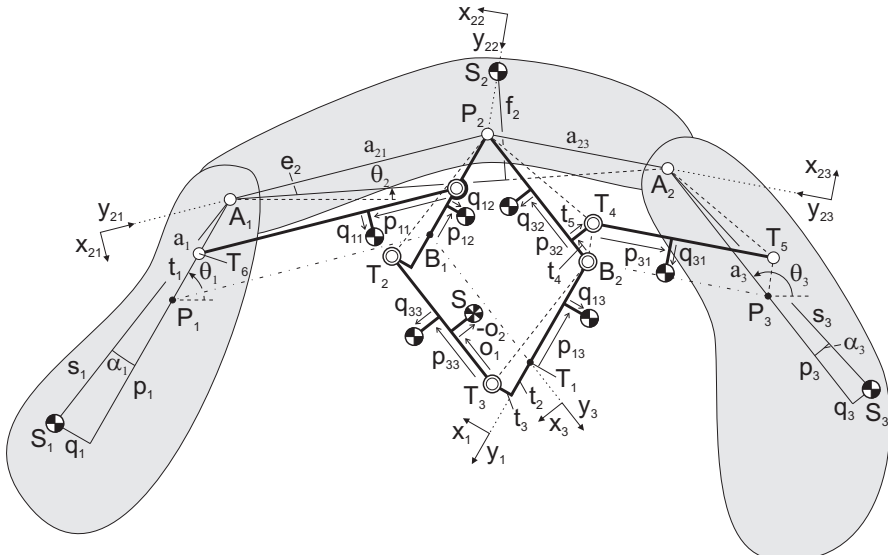


Fig. 3.20 Variations of the principal vector linkage in Fig. 3.7 where link 11 is pivoted with link 1 in T_6 , link 33 is pivoted with links 12 and 13 in T_2 and T_3 , respectively, and link 31 is pivoted with links 32 and 3 in T_4 and T_5 , respectively. Invariant link point S is the common CoM of the mechanism for all motion and is defined with o_1 and o_2 relative to T_3 .

$$\begin{aligned}
m_1 p_1 &= (m_{tot} - m_{33})t_2 + (m_2 + m_3 + m_{31} + m_{32})a_1 + m_{12}p_{12} + m_{13}p_{13} + m_{11}t_1 \\
m_1 q_1 &= (m_{tot} - m_{33})t_3 + m_{12}q_{12} + m_{13}q_{13} \\
m_2 p_2^a &= m_1 a_{21} + m_{11}p_{11} \\
m_2 q_2^a &= m_{11}q_{11} \\
m_2 p_2^b &= m_3 a_{23} + m_{31}p_{31} \\
m_2 q_2^b &= m_{31}q_{31} \\
m_3 p_3 &= -m_{tot}o_1 + (m_1 + m_2 + m_{11} + m_{12})a_3 + m_{32}p_{32} + m_{33}p_{33} + m_{31}t_4 \\
m_3 q_3 &= -m_{tot}o_2 + m_{32}q_{32} + m_{33}q_{33} - m_{31}t_5
\end{aligned} \tag{3.43}$$

The principal dimensions a_1 and a_3 are calculated as

$$a_1 = \frac{m_1 p_1 - (m_{tot} - m_{33})t_2 - m_{12}p_{12} - m_{13}p_{13} - m_{11}t_1}{m_2 + m_3 + m_{31} + m_{32}} \tag{3.44}$$

$$a_3 = \frac{m_3 p_3 + m_{tot}o_1 - m_{32}p_{32} - m_{33}p_{33} - m_{31}t_4}{m_1 + m_2 + m_{11} + m_{12}} \tag{3.45}$$

Parameters b_{21} and c_2 of the location of P_2 with respect to line A_1A_2 can be found from the ELMS in Fig. 3.16 with (3.25) and (3.26) with $\mu_1 = m_1 + m_{11}p_{11}/a_{21}$, $\mu_2 = m_2$, $\mu_3 = m_3 + m_{31}p_{31}/a_{23}$, $v_1 = m_{11}q_{11}/a_{21}$, and $v_3 = m_{31}q_{31}/a_{23}$ and they can be calculated with (3.35) and (3.36).

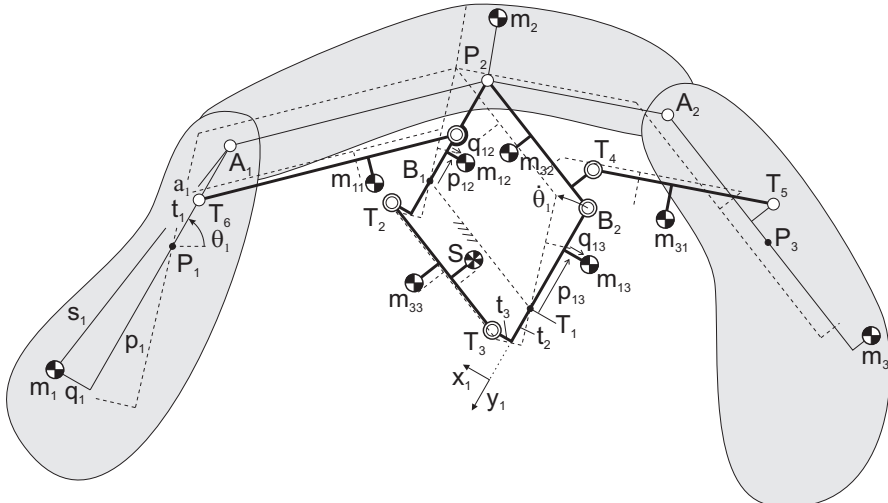


Fig. 3.21 Relative motion of DoF 1 where link 1 rotates about P_1 , link 12 rotates about B_1 , and link 13 rotates about T_1 with P_1 , B_1 , and T_1 as fixed points. All other elements solely translate.

3.3 Principal vector linkage of four principal elements in series

The theory in the previous section is also applicable to series of more than three principal elements. In this section a 4-DoF principal vector linkage with four principal elements in series is investigated, which is shown in Fig. 3.23 and has in total sixteen elements with a general CoM. The common CoM of all elements is in joint S for all motion.

As for three elements in series in Fig. 3.6f, also the principal vector linkage of four elements in series can be considered a union of pantographs. It is illustrated in Fig. 3.24a that the common CoM of a chain of four elements can be traced with in total six pantographs. Three of these pantographs have each two links incorporated in the principal elements as explained for Fig. 3.6c. With the procedure of Fig. 3.6d-e-f the pantographs can be united such that the principal vector linkage in Fig. 3.24b is obtained. Here the left incorporated pantograph traces the CoM of m_1 and $m_2 + m_3 + m_4$ in K_1 , the centered incorporated pantograph traces the CoM of $m_1 + m_2$ in K_2 and $m_3 + m_4$ in K_3 , and the right incorporated pantograph traces the CoM of $m_1 + m_2 + m_3$ in K_4 and m_4 . K_1 is derived as the CoM of m_2 and $m_3 + m_4$ in A_2 , K_2 is derived as the CoM of m_1 in A_1 and m_2 , K_3 is derived as the CoM of m_3 and m_4 in A_3 , and K_4 is derived as the CoM of $m_1 + m_2$ in A_2 and m_3 .

Figure 3.25 shows the principal vectors on which the 4-DoF principal vector linkage is based. These six vectors $\bar{a}_1, \bar{a}_{21}, \bar{a}_{23}, \bar{a}_{32}, \bar{a}_{34}$, and \bar{a}_4 describe the positions of principal points P_1, P_2, P_3 , and P_4 relative to the common CoM in S . When

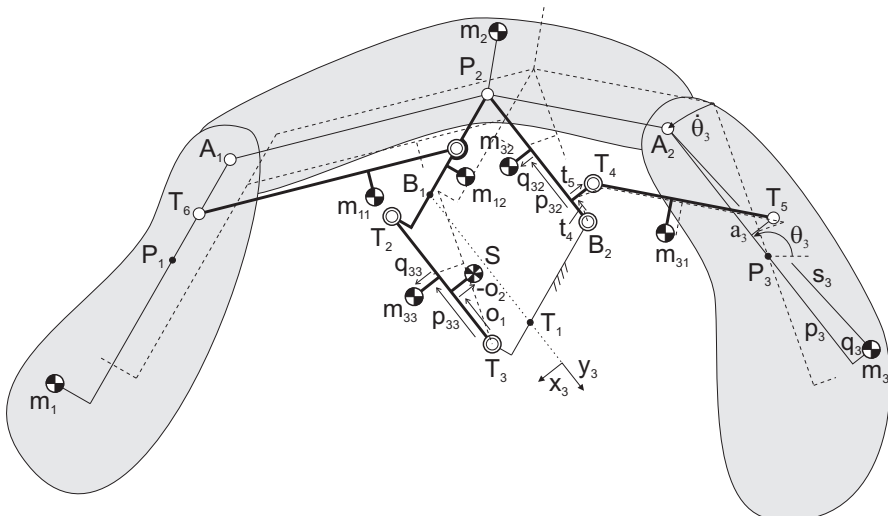


Fig. 3.22 Relative motion of DoF 3 where link 3 rotates about P_3 , link 32 rotates about B_2 , and link 33 rotates about T_3 with P_3, B_2 , and T_3 as fixed points. All other links solely translate.

these points are known, the principal vector linkage is fully determined with the six principal dimensions $a_1, a_{21}, a_{23}, a_{32}, a_{34}$, and a_4 .

Principal points P_1 and P_4 can be derived with the linear momentum of the relative motion of DoF 1 and of DoF 4, respectively, similarly as P_1 and P_3 in Fig. 3.7. Both P_2 and P_3 can be obtained with an ELMS of their respective relative motion as for P_2 in Fig. 3.16.

The relative motion of DoF 1 is illustrated in Fig. 3.26 where principal vector links SC_1 , C_1B_1 , and B_1P_1 can be regarded as fixed while links 1, 12, 13, and 14 solely rotate and the other links solely translate. The linear momentum \bar{L}_1 of this motion can be written with respect to reference frame x_1y_1 as

$$\frac{\bar{L}_1}{\dot{\theta}_1} = \begin{bmatrix} m_{T1}a_1 + m_{12}p_{12} + m_{13}p_{13} + m_{14}p_{14} - m_1p_1 \\ -m_{12}q_{12} - m_{13}q_{13} - m_{14}q_{14} + m_1q_1 \end{bmatrix} = \begin{bmatrix} 0 \\ 0 \end{bmatrix} \quad (3.46)$$

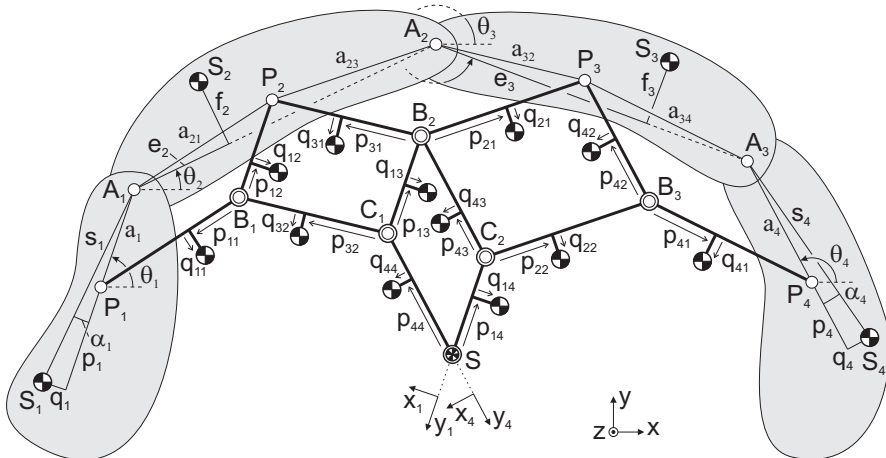


Fig. 3.23 A 4-DoF principal vector linkage of four principal elements in series. All elements have a general CoM and the common CoM of the linkage is in S for all motion.

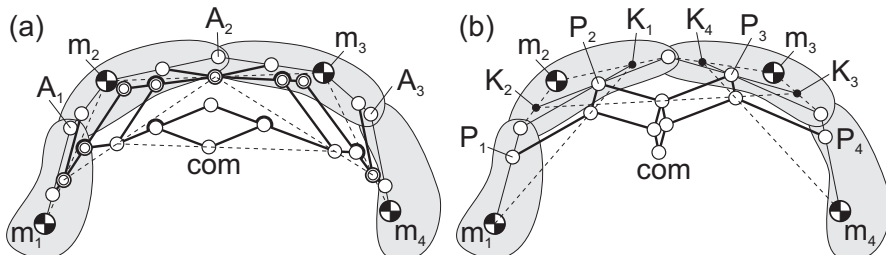


Fig. 3.24 a) The common CoM of four elements in series can be traced with six pantographs of which three have each two links incorporated in the principal elements and three are fully auxiliary; b) A 4-DoF principal vector linkage is obtained when the six pantographs are united.

with $m_{T1} = m_2 + m_3 + m_4 + m_{21} + m_{22} + m_{31} + m_{41} + m_{42} + m_{43}$. The force balance conditions are readily obtained as

$$\begin{aligned} m_1 p_1 &= m_{T1} a_1 + m_{12} p_{12} + m_{13} p_{13} + m_{14} p_{14} \\ m_1 q_1 &= m_{12} q_{12} + m_{13} q_{13} + m_{14} q_{14} \end{aligned} \quad (3.47)$$

from which the principal dimension a_1 and q_1 are calculated as

$$\begin{aligned} a_1 &= \frac{m_1 p_1 - m_{12} p_{12} - m_{13} p_{13} - m_{14} p_{14}}{m_2 + m_3 + m_4 + m_{21} + m_{22} + m_{31} + m_{41} + m_{42} + m_{43}} \\ q_1 &= \frac{m_{12} q_{12} + m_{13} q_{13} + m_{14} q_{14}}{m_1} \end{aligned} \quad (3.48)$$

Similarly to (3.16), a_1 can be found also by substituting $m_1 p_1 = m_1(s_1 \cos \alpha_1 - a_1) = \sqrt{m_1^2 s_1^2(1 - \sin^2 \alpha_1)} - m_1 a_1$ with $\sin \alpha_1 = q_1/s_1$ as

$$a_1 = \frac{\sqrt{m_1^2 s_1^2 - (m_{12} q_{12} + m_{13} q_{13} + m_{14} q_{14})^2} - m_{12} p_{12} - m_{13} p_{13} - m_{14} p_{14}}{m_1 + m_2 + m_3 + m_4 + m_{21} + m_{22} + m_{31} + m_{41} + m_{42} + m_{43}} \quad (3.49)$$

For the relative motion of DoF 4 principal vector links SC_2 , C_2B_3 , and B_3P_4 can be regarded as fixed while links 4, 42, 43, and 44 solely rotate and the other links solely translate. The linear momentum \bar{L}_4 of this motion can be written with respect to reference frame x_4y_4 as

$$\bar{\theta}_4 = \begin{bmatrix} m_{T4} a_4 + m_{42} p_{42} + m_{43} p_{43} + m_{44} p_{44} - m_4 p_4 \\ m_{42} q_{42} + m_{43} q_{43} + m_{44} q_{44} - m_4 q_4 \end{bmatrix} = \begin{bmatrix} 0 \\ 0 \end{bmatrix} \quad (3.50)$$

with $m_{T4} = m_1 + m_2 + m_3 + m_{11} + m_{12} + m_{13} + m_{21} + m_{31} + m_{32}$. Here the force balance conditions are readily obtained as

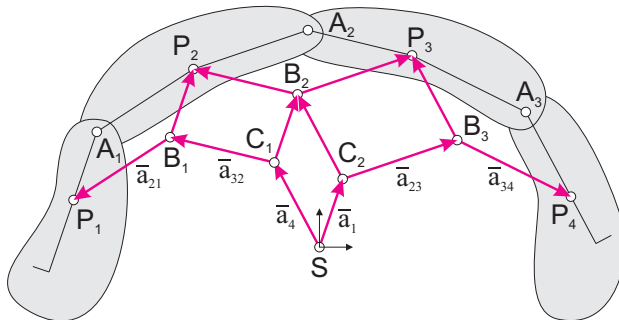


Fig. 3.25 The 4-dof principal vector linkage in Fig. 3.23 is based on six principal vectors that describe the positions of the principal points P_1 , P_2 , P_3 , and P_4 relative to S .

$$\begin{aligned} m_4 p_4 &= m_{T4} a_4 + m_{42} p_{42} + m_{43} p_{43} + m_{44} p_{44} \\ m_4 q_4 &= m_{42} q_{42} + m_{43} q_{43} + m_{44} q_{44} \end{aligned} \quad (3.51)$$

from which the principal dimension a_4 and q_4 are calculated as

$$\begin{aligned} a_4 &= \frac{m_4 p_4 - m_{42} p_{42} - m_{43} p_{43} - m_{44} p_{44}}{m_1 + m_2 + m_3 + m_{11} + m_{12} + m_{13} + m_{21} + m_{31} + m_{32}} \\ q_4 &= \frac{m_{42} q_{42} + m_{43} q_{43} + m_{44} q_{44}}{m_4} \end{aligned} \quad (3.52)$$

By substituting $m_4 p_4 = m_4 (s_4 \cos \alpha_4 - a_4) = \sqrt{m_4^2 s_4^2 (1 - \sin^2 \alpha_4)} - m_4 a_4$ with $\sin \alpha_4 = q_4 / s_4$, a_4 can be found also as

$$a_4 = \frac{\sqrt{m_4^2 s_4^2 - (m_{42} q_{42} + m_{43} q_{43} + m_{44} q_{44})^2} - m_{42} p_{42} - m_{43} p_{43} - m_{44} p_{44}}{m_1 + m_2 + m_3 + m_4 + m_{11} + m_{12} + m_{13} + m_{21} + m_{31} + m_{32}} \quad (3.53)$$

The relative motion of DoF 2 is illustrated in Fig. 3.27. Here points S , C_1 , C_2 , B_1 , B_2 , and P_2 can be regarded as fixed for which links 2, 11, 21, and 22 solely rotate and the remaining movable links solely translate. As for the enclosed principal element in Fig. 3.12, the linear momentum of this enclosed principal element can be written with respect to the three reference frames $x_{21}y_{21}$, $x_{22}y_{22}$, and $x_{23}y_{23}$ as illustrated in Fig. 3.27 as

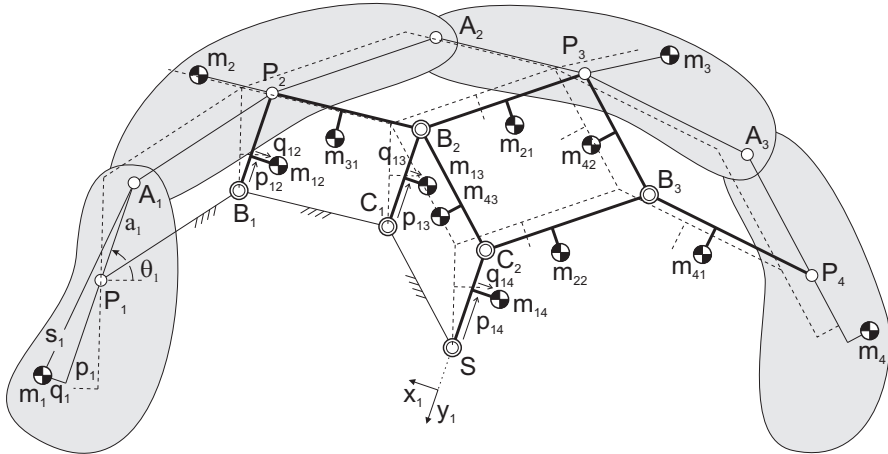


Fig. 3.26 Relative motion of DoF 1 where links SC_1 , C_1B_1 , and B_1P_1 can be regarded as fixed while links 1, 12, 13, and 14 solely rotate and the other links solely translate.

$$\begin{aligned}\bar{L}_{21} &= \begin{bmatrix} m_1 a_{21} + m_{11} p_{11} \\ m_{11} q_{11} \end{bmatrix} \dot{\theta}_2 & \bar{L}_{22} &= \begin{bmatrix} m_2 d_2 \\ 0 \end{bmatrix} \dot{\theta}_2 \\ \bar{L}_{23} &= \begin{bmatrix} (m_3 + m_4 + m_{41} + m_{42}) a_{23} + m_{21} p_{21} + m_{22} p_{22} \\ -m_{21} q_{21} - m_{22} q_{22} \end{bmatrix} \dot{\theta}_2\end{aligned}\quad (3.54)$$

or as

$$\bar{L}_{21} = \begin{bmatrix} \mu_1 \\ v_1 \end{bmatrix} a_{21} \dot{\theta}_2 \quad \bar{L}_{22} = \begin{bmatrix} \mu_2 \\ 0 \end{bmatrix} d_2 \dot{\theta}_2 \quad \bar{L}_{23} = \begin{bmatrix} \mu_3 \\ -v_3 \end{bmatrix} a_{23} \dot{\theta}_2 \quad (3.55)$$

with equivalent masses $\mu_1 = m_1 + m_{11} p_{11}/a_{21}$, $\mu_2 = m_2$, $\mu_3 = m_3 + m_4 + m_{41} + m_{42} + (m_{21} p_{21} + m_{22} p_{22})/a_{23}$, $v_1 = m_{11} q_{11}/a_{21}$, and $v_3 = (m_{21} q_{21} + m_{22} q_{22})/a_{23}$. The ELMS of this motions is shown in Fig. 3.28a and is similar to the ELMS in Fig. 3.16. As in Fig. 3.14, the force balance conditions for this DoF can be found with a parallelogram that is defined with p_2^a , q_2^a , p_2^b , and q_2^b with which they result in

$$\begin{aligned}\mu_2 p_2^a &= \mu_1 a_{21} & \mu_2 q_2^a &= v_1 a_{21} \\ \mu_2 p_2^b &= \mu_3 a_{23} & \mu_2 q_2^b &= v_3 a_{23}\end{aligned}\quad (3.56)$$

With μ_1 , μ_2 , μ_3 , v_1 , and v_3 substituted, the force balance conditions become

$$\begin{aligned}m_2 p_2^a &= m_1 a_{21} + m_{11} p_{11} \\ m_2 q_2^a &= m_{11} q_{11} \\ m_2 p_2^b &= (m_3 + m_4 + m_{41} + m_{42}) a_{23} + m_{21} p_{21} + m_{22} p_{22} \\ m_2 q_2^b &= m_{21} q_{21} + m_{22} q_{22}\end{aligned}\quad (3.57)$$

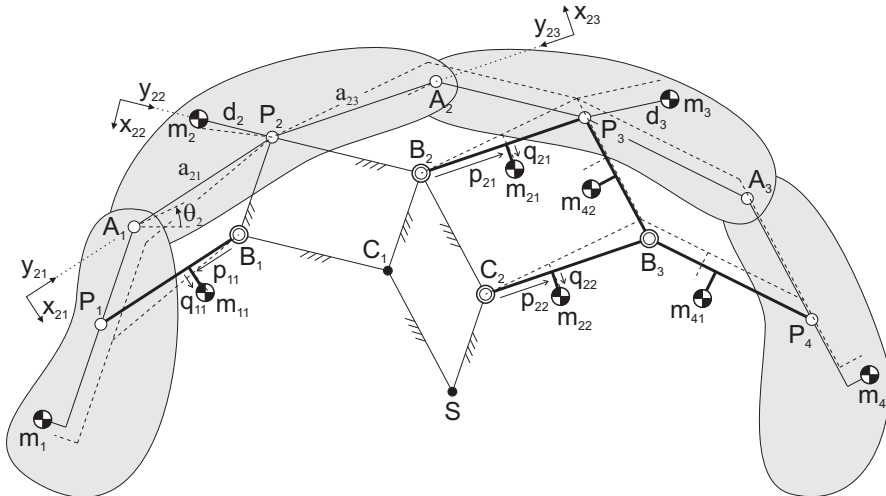


Fig. 3.27 Relative motion of DoF 2 where points S , C_1 , C_2 , B_1 , B_2 , and P_2 are regarded as fixed for which links 2, 11, 21, and 22 solely rotate and the remaining movable links solely translate.

from which the principal dimensions a_{21} and a_{23} are calculated as

$$a_{21} = \frac{m_2 p_2^a - m_{11} p_{11}}{m_1} \quad a_{23} = \frac{m_2 p_2^b - m_{21} p_{21} - m_{22} p_{22}}{m_3 + m_4 + m_{41} + m_{42}} \quad (3.58)$$

The derivation of P_3 is similar to the derivation of P_2 . For the relative motion of DoF 3 the points S , C_1 , C_2 , B_2 , B_3 , and P_3 can be regarded as fixed for which links 3, 31, 32, and 41 solely rotate and the remaining movable links solely translate. The linear momentum of this motion can be written with respect to the three reference frames $x_{32}y_{32}$, $x_{33}y_{33}$, and $x_{34}y_{34}$ as illustrated in the ELMS in Fig. 3.28b and write

$$\begin{aligned} \bar{L}_{32} &= \begin{bmatrix} (m_1 + m_2 + m_{11} + m_{12})a_{32} + m_{31}p_{31} + m_{32}p_{32} \\ m_{31}q_{31} + m_{32}q_{32} \end{bmatrix} \dot{\theta}_3 & (3.59) \\ \bar{L}_{33} &= \begin{bmatrix} m_3 d_3 \\ 0 \end{bmatrix} \dot{\theta}_3 \quad \bar{L}_{34} = \begin{bmatrix} m_4 a_{34} + m_{41}p_{41} \\ -m_{41}q_{41} \end{bmatrix} \dot{\theta}_3 \end{aligned}$$

or

$$\bar{L}_{32} = \begin{bmatrix} \mu_4 \\ v_4 \end{bmatrix} a_{32} \dot{\theta}_3 \quad \bar{L}_{33} = \begin{bmatrix} \mu_5 \\ 0 \end{bmatrix} d_3 \dot{\theta}_3 \quad \bar{L}_{34} = \begin{bmatrix} \mu_6 \\ -v_6 \end{bmatrix} a_{34} \dot{\theta}_3 \quad (3.60)$$

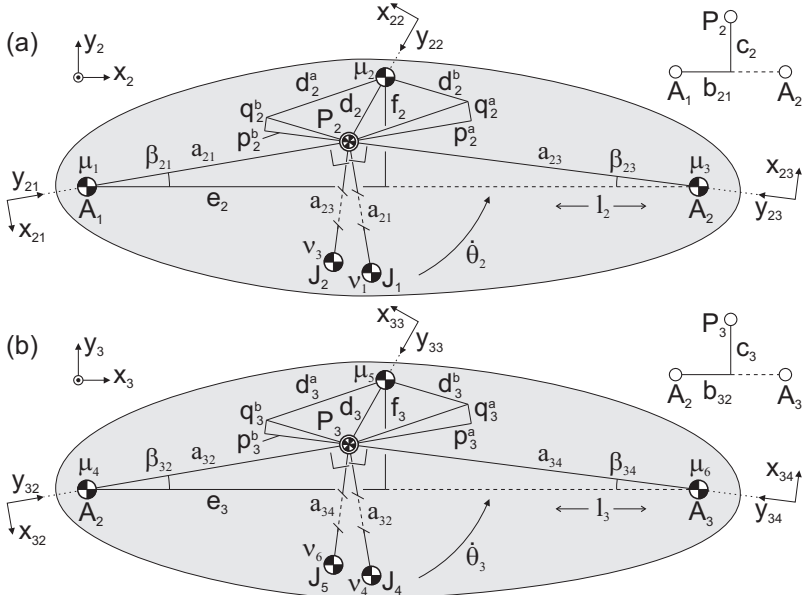


Fig. 3.28 Equivalent Linear Momentum Systems for the relative motion of (a) DoF 2 to find P_2 and (b) DoF 3 to find P_3 . Principal points P_2 and P_3 are the CoMs of the reduced-mass models.

with equivalent masses $\mu_4 = m_1 + m_2 + m_{11} + m_{12} + (m_{31}p_{31} + m_{32}p_{32})/a_{32}$, $\mu_5 = m_3$, $\mu_6 = m_4 + m_{41}p_{41}/a_{34}$, $v_4 = (m_{31}q_{31} + m_{32}q_{32})/a_{32}$, and $v_6 = m_{41}q_{41}/a_{34}$. The force balance conditions for this DoF are found with the parallelogram defined with p_3^a , q_3^a , p_3^b , and q_3^b and result in

$$\begin{aligned}\mu_5 p_3^a &= \mu_4 a_{32} & \mu_5 q_3^a &= v_4 a_{32} \\ \mu_5 p_3^b &= \mu_6 a_{34} & \mu_5 q_3^b &= v_6 a_{34}\end{aligned}\quad (3.61)$$

With μ_4 , μ_5 , μ_6 , v_4 , and v_6 substituted, the force balance conditions result in

$$m_3 p_3^a = (m_1 + m_2 + m_{11} + m_{12})a_{32} + m_{31}p_{31} + m_{32}p_{32} \quad (3.62)$$

$$m_3 q_3^a = m_{31}q_{31} + m_{32}q_{32} \quad (3.63)$$

$$m_3 p_3^b = m_4 a_{34} + m_{41}p_{41} \quad (3.64)$$

$$m_3 q_3^b = m_{41}q_{41} \quad (3.65)$$

from which the principal dimensions a_{32} and a_{34} are calculated as

$$a_{32} = \frac{m_3 p_3^a - m_{31}p_{31} - m_{32}p_{32}}{m_1 + m_2 + m_{11} + m_{12}} \quad a_{34} = \frac{m_3 p_3^b - m_{41}p_{41}}{m_4} \quad (3.66)$$

In summary, the twelve force balance conditions of the 4-DoF principal vector linkage in Fig. 3.23, which define the principal dimensions for which the common CoM is in joint S for all motion, are:

$$\begin{aligned}m_1 p_1 &= (m_2 + m_3 + m_4 + m_{21} + m_{22} + m_{31} + m_{41} + m_{42} + m_{43})a_1 + \\ &\quad m_{12}p_{12} + m_{13}p_{13} + m_{14}p_{14} \\ m_1 q_1 &= m_{12}q_{12} + m_{13}q_{13} + m_{14}q_{14} \\ m_2 p_2^a &= m_1 a_{21} + m_{11}p_{11} \\ m_2 q_2^a &= m_{11}q_{11} \\ m_2 p_2^b &= (m_3 + m_4 + m_{41} + m_{42})a_{23} + m_{21}p_{21} + m_{22}p_{22} \\ m_2 q_2^b &= m_{21}q_{21} + m_{22}q_{22} \\ m_3 p_3^a &= (m_1 + m_2 + m_{11} + m_{12})a_{32} + m_{31}p_{31} + m_{32}p_{32} \\ m_3 q_3^a &= m_{31}q_{31} + m_{32}q_{32} \\ m_3 p_3^b &= m_4 a_{34} + m_{41}p_{41} \\ m_3 q_3^b &= m_{41}q_{41} \\ m_4 p_4 &= (m_1 + m_2 + m_3 + m_{11} + m_{12} + m_{13} + m_{21} + m_{31} + m_{32})a_{44} + \\ &\quad m_{42}p_{42} + m_{43}p_{43} + m_{44}p_{44} \\ m_4 q_4 &= m_{42}q_{42} + m_{43}q_{43} + m_{44}q_{44}\end{aligned}\quad (3.67)$$

The parameters b_{21} and c_2 of the location of P_2 in A_1A_2 can be obtained from the linear momentum \bar{L}_2 about P_2 , which is written as in (3.24). The force balance conditions then become as in (3.25) and (3.26) and in (3.35) and (3.36).

The parameters b_{32} and c_3 of the location of P_3 in A_2A_3 can be obtained by writing the linear momentum \bar{L}_3 of the ELMS in Fig. 3.28b about P_3 with respect to reference frame x_3y_3 as

$$\begin{aligned} \frac{\bar{L}_3}{\dot{\theta}_3} &= \mu_4 \begin{bmatrix} c_3 \\ -b_{32} \end{bmatrix} + v_4 \begin{bmatrix} b_{32} \\ c_3 \end{bmatrix} + \mu_5 \begin{bmatrix} c_3 - f_3 \\ -(b_{32} - e_3) \end{bmatrix} + \\ &\quad \mu_6 \begin{bmatrix} c_3 \\ -(b_{32} - l_3) \end{bmatrix} - v_6 \begin{bmatrix} b_{32} - l_2 \\ c_3 \end{bmatrix} = \begin{bmatrix} 0 \\ 0 \end{bmatrix} \end{aligned} \quad (3.68)$$

The force balance conditions for the individual motion of DoF 3 from which b_{32} and c_3 can be calculated then result in terms of equivalent masses as:

$$(\mu_4 + \mu_5 + \mu_6)c_3 + (v_4 - v_6)b_{32} - \mu_5f_3 + v_6l_6 = 0 \quad (3.69)$$

$$-(\mu_4 + \mu_5 + \mu_6)b_{32} + (v_4 - v_6)c_3 + \mu_5e_3 + \mu_6l_6 = 0 \quad (3.70)$$

It is also possible to write the position of m_3 as

$$e_3 = (a_{32} + p_3^a) \cos \beta_{32} - q_3^a \sin \beta_{32} - p_3^b \cos \beta_{34} + q_3^b \sin \beta_{34} \quad (3.71)$$

$$f_3 = (a_{32} + p_3^a) \sin \beta_{32} + q_3^a \cos \beta_{32} + p_3^b \sin \beta_{34} + q_3^b \cos \beta_{34}$$

where $\beta_{32} \angle P_3A_2A_3$ and $\beta_{34} \angle P_3A_3A_2$. With $\cos \beta_{32} = b_{32}/a_{32}$, $\sin \beta_{32} = c_3/a_{32}$, $\cos \beta_{34} = (l_3 - b_{32})/a_{34}$, and $\sin \beta_{34} = c_3/a_{34}$ these equations become

$$e_3 = \left(\frac{a_{32} + p_3^a}{a_{32}} + \frac{p_3^b}{a_{34}} \right) b_{32} - \left(\frac{q_3^a}{a_{32}} - \frac{q_3^b}{a_{34}} \right) c_3 - \frac{p_3^b}{a_{34}} l_3 \quad (3.72)$$

$$f_3 = \left(\frac{a_{32} + p_3^a}{a_{32}} + \frac{p_3^b}{a_{34}} \right) c_3 + \left(\frac{q_3^a}{a_{32}} - \frac{q_3^b}{a_{34}} \right) b_{32} + \frac{q_3^b}{a_{34}} l_3$$

from which b_{32} and c_3 are obtained in terms of principal vectors as:

$$b_{32} = \frac{\left(\frac{a_{32} + p_3^a}{a_{32}} + \frac{p_3^b}{a_{34}} \right) (e_3 + \frac{p_3^b}{a_{34}} l_3) + \left(\frac{q_3^a}{a_{32}} - \frac{q_3^b}{a_{34}} \right) (f_3 - \frac{q_3^b}{a_{34}} l_3)}{\left(\frac{a_{32} + p_3^a}{a_{32}} + \frac{p_3^b}{a_{34}} \right)^2 + \left(\frac{q_3^a}{a_{32}} - \frac{q_3^b}{a_{34}} \right)^2} \quad (3.73)$$

$$c_3 = \frac{\left(\frac{a_{32} + p_3^a}{a_{32}} + \frac{p_3^b}{a_{34}} \right) (f_3 - \frac{q_3^b}{a_{34}} l_3) - \left(\frac{q_3^a}{a_{32}} - \frac{q_3^b}{a_{34}} \right) (e_3 + \frac{p_3^b}{a_{34}} l_3)}{\left(\frac{a_{32} + p_3^a}{a_{32}} + \frac{p_3^b}{a_{34}} \right)^2 + \left(\frac{q_3^a}{a_{32}} - \frac{q_3^b}{a_{34}} \right)^2} \quad (3.74)$$

In this section the principal vector linkage of four principal elements in series was studied. The variations in the design of the principal vector linkage as in section 3.2.4 are also applicable here. The common CoM can be an invariant point in link SC_1 or in link SC_2 , not necessarily being S . When another principal element is added, a principal vector linkage of five principal elements in series is obtained. Figure 3.29 shows a physical model of such a mechanism that was developed and is shown in various poses. The principal elements have a length of 60 mm and are multi-layered of 4 mm thick steel segments. The masses of the principal elements 1 to 5 were designed to be 120.61 g, 34.46 g, 17.23 g, 34.46 g and 120.61 g, respectively, which varies to have the dimensions of the parallelograms not be too small.

After production, these elements had a deviation of -1.27 g, 0.12 g, -0.12 g, -0.11 g, and -1.29 g, respectively. The principal vector links are made of Ø 4 mm welding rod with shiny copper-brown appearance and are dual for rigidity. The joint axles are made of Ø 2 mm welding rod. The total mass of the moving elements after production is $428.21 - 2.67 = 425.54$ g of which the five principal elements weight together $327.37 - 2.67 = 324.7$ g and the principal vector links weight together 100.84 g.

This model was, as all other models in this book, first simulated in Matlab and designed in CAD-software SolidWorks in which the common CoM can be verified. In experiments, the mechanism remains steady in every pose. The stick-slip friction about the axle at the base was determined with measurement weights being 0.00045 Nm maximally. This implies that the maximal error of the common CoM with the center of the joint with the base can be $0.00045 \text{Nm} / (0.42821 \text{kg} * 9.81 \text{ms}^{-2}) = 0.11$ mm to have the mechanism still remain steady.

3.4 Principal vector linkage of four principal elements in parallel

Instead of multiple principal elements in series, principal vector linkages can also consist of multiple principal elements jointed in a parallel manner. Figure 3.30 shows such a linkage with a central principal element 1 to which the three principal elements 11, 21, and 31 are connected with revolute pairs, all having a general CoM. The motion of this 4-DoF principal vector linkage is described with angles θ_{11} , θ_{21} , θ_{31} , and θ_1 about the four principal points P_{11} , P_{21} , P_{31} , and P_1 , respec-

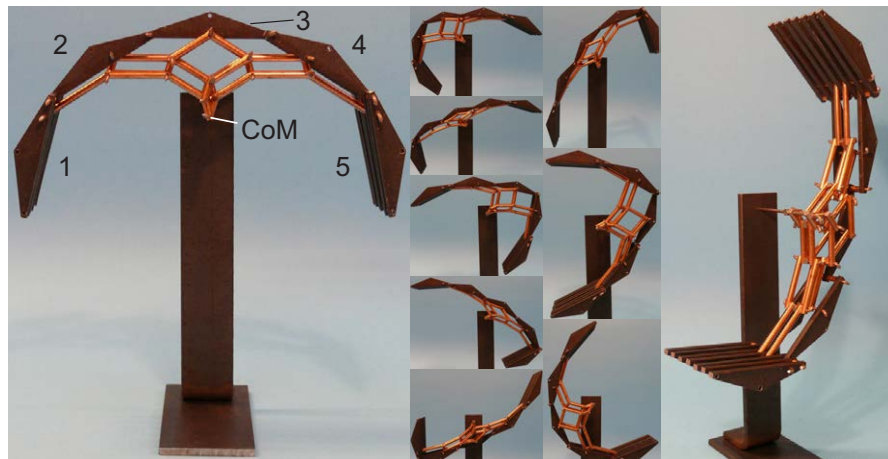


Fig. 3.29 Physical model of a principal vector linkage of five principal elements in series, shown in various poses. The principal elements are made of steel while the principal vector links are made of shiny copper-brown Ø 4 mm welding rod. (see video at: www.kineticart.nl)

tively. The common CoM for all motion is in joint S of the principal vector links and is drawn to float above principal element 1.

Also this principal vector linkage consists of a union of pantographs which is illustrated in Fig. 3.31 where six pantographs together trace the common CoM in S of which three have each two links incorporated in the principal elements and the other three are fully auxiliary. When these pantographs are united the principal vector linkage in Fig. 3.30 is obtained where new incorporated pantographs appear. Pantograph $B_1P_{11}A_1P_1$ traces with B_1 the CoM of m_{11} and $m_1 + m_{21} + m_{31}$ in K_1 . Pantograph $B_2P_{21}A_2P_1$ traces with B_2 the CoM of m_{21} and $m_1 + m_{11} + m_{31}$ in K_2 . Pantograph $B_3P_{31}A_3P_1$ traces with B_3 the CoM of m_{31} and $m_1 + m_{11} + m_{21}$ in K_3 . K_1 is found as the CoM of m_1, m_{21} in A_2 , and m_{31} in A_3 . K_2 is found as the CoM of m_1, m_{11} in A_1 , and m_{31} in A_3 . K_3 is found as the CoM of m_1, m_{11} in A_1 , and m_{21} in A_2 . For maximal clarity Fig. 3.30 is not made proportionate.

The six pantographs in Fig. 3.31 are centered about principal element 11, which is one of the three solutions for this mechanism to trace the common CoM in S . It is also possible to trace the common CoM with six pantographs centered about principal elements 21 or 31 of which the results look similar. When the pantographs of all three solutions together are united, this results in the planar principal vector linkage in Fig. 3.32 which is overconstraint but movable. In this linkage also a general CoM in each of the nineteen elements can be considered. Figure 3.33 shows the

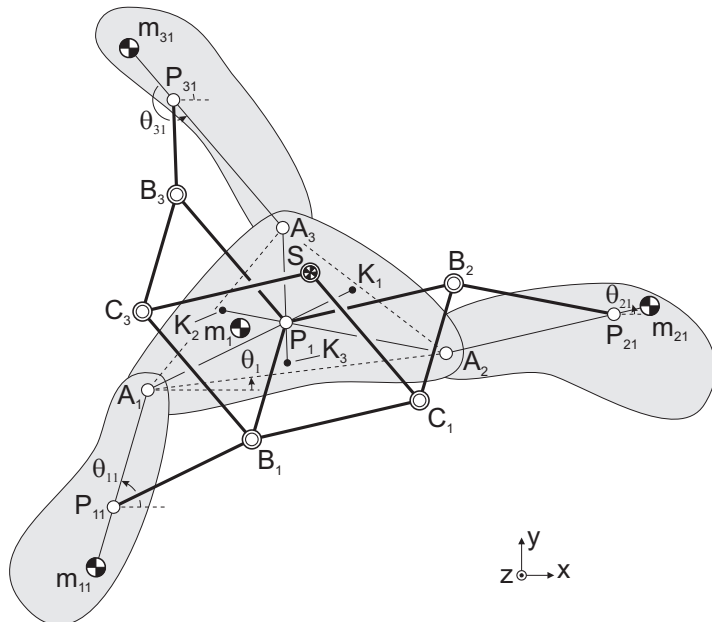


Fig. 3.30 Planar 4-DoF principal vector linkage with four principal elements of which the three elements 11, 21, and 31 are arranged in parallel. The common CoM of the four elements for all motion is in joint S , which is drawn to float above principal element 1.

six principal vectors \bar{a}_{11} , \bar{a}_{21} , \bar{a}_{31} , \bar{a}_{111} , \bar{a}_{121} , and \bar{a}_{131} on which this mechanism is based and with which the positions of the principal points are described relative to S .

To find the principal points and to calculate the principal dimensions a_{11} , a_{21} , a_{31} , a_{111} , a_{121} , and a_{131} , the method of rotations about the principal joints A_1 , A_2 , and A_3 in section 3.2.3 is the clearest to illustrate. For simplicity therefore, the CoM of all the principal vector links that are based on the vectors \bar{a}_{11} , \bar{a}_{21} , and \bar{a}_{31} are defined with parameters p_{ijk} from opposite direction as compared to the linkages in Figs. 3.7 and 3.23.

The relative motion of DoF 1 is illustrated in Fig. 3.34 where $\dot{\theta}_{21} = \dot{\theta}_{31} = \dot{\theta}_1 = 0$ and points P_1 , A_1 , B_2 , B_3 , and C_2 can be regarded as fixed while links 11, 112, 113, 114, and 115 solely rotate and links 111, 313, 314, 214, and 215 (i.e. link $P_{11}B_1$ and rectangle $SC_3B_1C_1$) solely translate. The linear momentum \bar{L}_{111} of this motion can be written with respect to reference frame $x_{111}y_{111}$ as

$$\begin{aligned}\bar{L}_{111} &= \begin{bmatrix} m_{T11}a_{11} + m_{112}p_{112} + m_{113}p_{113} + m_{114}p_{114} + m_{115}p_{115} + m_{11}(a_{11} + p_{11}) \\ m_{112}q_{112} + m_{113}q_{113} + m_{114}q_{114} + m_{115}q_{115} - m_{11}q_{11} \end{bmatrix} \\ &= \begin{bmatrix} m_{tot}a_{11} \\ 0 \end{bmatrix}\end{aligned}\quad (3.75)$$

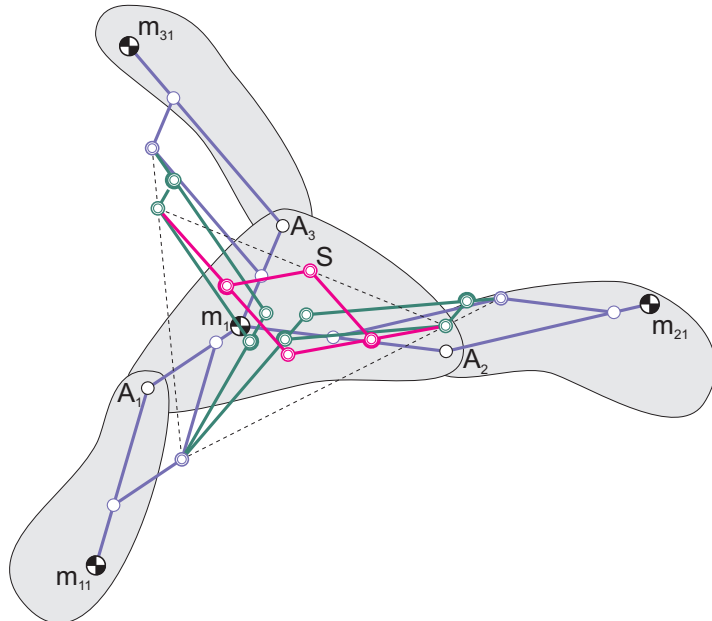


Fig. 3.31 The common CoM in S of the four masses can be traced with six pantographs of which three have each two links incorporated in the principal elements. Here the pantographs are centered about principal element 11 and when united the linkage in Fig. 3.30 is obtained.

with $m_{T11} = m_{111} + m_{313} + m_{314} + m_{214} + m_{215}$ and $m_{tot} = m_1 + m_{11} + m_{21} + m_{31} + \sum_{k=1}^5 (m_{11k} + m_{21k} + m_{31k})$. Principal point P_{11} can be found with respect to line $S_{11}A_1$ wheb $a_{11} + p_{11} = s_{11} \cos \alpha_{11}$ and $q_{11} = s_{11} \sin \alpha_{11}$ are substituted such that the principal dimension a_{11} and angle α_{11} are calculated as

$$a_{11} = \frac{m_{11}s_{11} \cos \alpha_{11} + m_{112}p_{112} + m_{113}p_{113} + m_{114}p_{114} + m_{115}p_{115}}{m_{tot} - m_{111} - m_{214} - m_{215} - m_{313} - m_{314}} \quad (3.76)$$

$$\alpha_{11} = \sin^{-1} \left(\frac{m_{112}q_{112} + m_{113}q_{113} + m_{114}q_{114} + m_{115}q_{115}}{m_{11}s_{11}} \right)$$

Similarly the linear momentum \bar{L}_{211} of the relative motion of DoF 2 and the linear momentum \bar{L}_{311} of the relative motion of DoF 3 are obtained. For the relative motion of DoF 2 where $\dot{\theta}_{11} = \dot{\theta}_{31} = \dot{\theta}_1 = 0$, points P_1, A_2, B_1, B_3 , and C_3 can be regarded as fixed while links 21, 212, 213, 214, and 215 solely rotate and links 211, 113, 114, 314, and 315 (i.e. link P_2B_2 and rectangle $SC_1B_2C_2$) solely translate. The linear momentum can be written with respect to reference frame $x_{211}y_{211}$ as

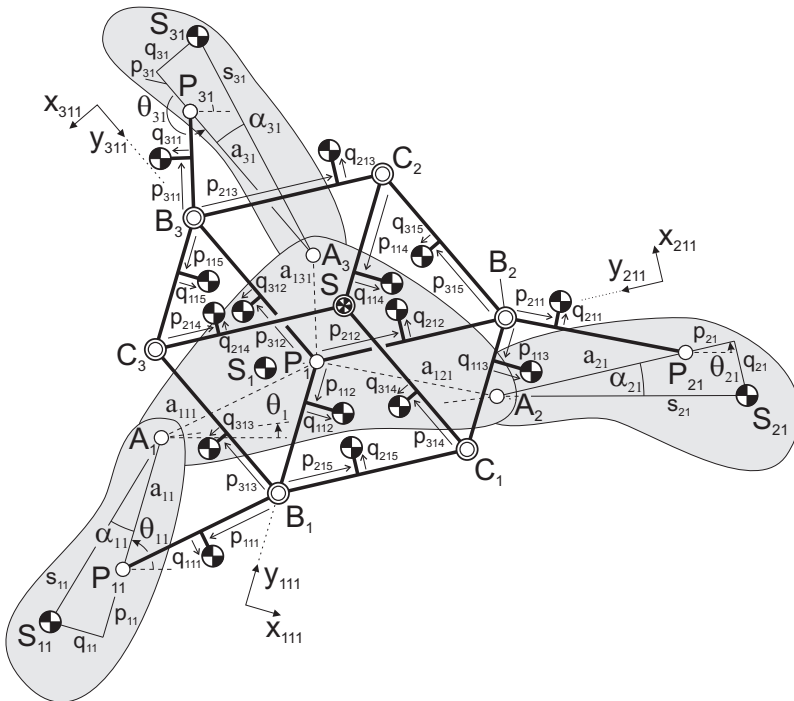


Fig. 3.32 Planar 4-DoF overconstraint principal vector linkage obtained from the union of the three solutions of pantographs to trace the common CoM in S . Each of the nineteen elements has a general CoM and angles $\theta_{11}, \theta_{21}, \theta_{31}$, and θ_1 describe the four relative DoFs.

$$\begin{aligned}\bar{\dot{L}}_{211} = & \begin{bmatrix} m_{T21}a_{21} + m_{212}p_{212} + m_{213}p_{213} + m_{214}p_{214} + m_{215}p_{215} + m_{21}(a_{21} + p_{21}) \\ m_{212}q_{212} + m_{213}q_{213} + m_{214}q_{214} + m_{215}q_{215} - m_{21}q_{21} \end{bmatrix} \\ = & \begin{bmatrix} m_{tot}a_{21} \\ 0 \end{bmatrix}\end{aligned}\quad (3.77)$$

with $m_{T21} = m_{211} + m_{113} + m_{114} + m_{314} + m_{315}$. Principal point P_{21} is found with respect to line $S_2 A_2$ where $a_{21} + p_{21} = s_{21} \cos \alpha_{21}$ and $q_{21} = s_{21} \sin \alpha_{21}$ are substituted such that the principal dimension a_{21} and angle α_{21} are calculated as

$$\begin{aligned}a_{21} &= \frac{m_{21}s_{21} \cos \alpha_{21} + m_{212}p_{212} + m_{213}p_{213} + m_{214}p_{214} + m_{215}p_{215}}{m_{tot} - m_{211} - m_{314} - m_{315} - m_{113} - m_{114}} \quad (3.78) \\ \alpha_{21} &= \sin^{-1} \left(\frac{m_{212}q_{212} + m_{213}q_{213} + m_{214}q_{214} + m_{215}q_{215}}{m_{21}s_{21}} \right)\end{aligned}$$

For the relative motion of DoF 3 where $\dot{\theta}_{11} = \dot{\theta}_{21} = \dot{\theta}_1 = 0$ points P_1 , A_3 , B_1 , B_2 , and C_1 can be regarded as fixed while links 31, 312, 313, 314, and 315 solely rotate and links 311, 213, 214, 114, and 115 (link $P_{31}B_3$ and rectangle $SC_2B_3C_3$) solely translate. The linear momentum of this motion can be written with respect to

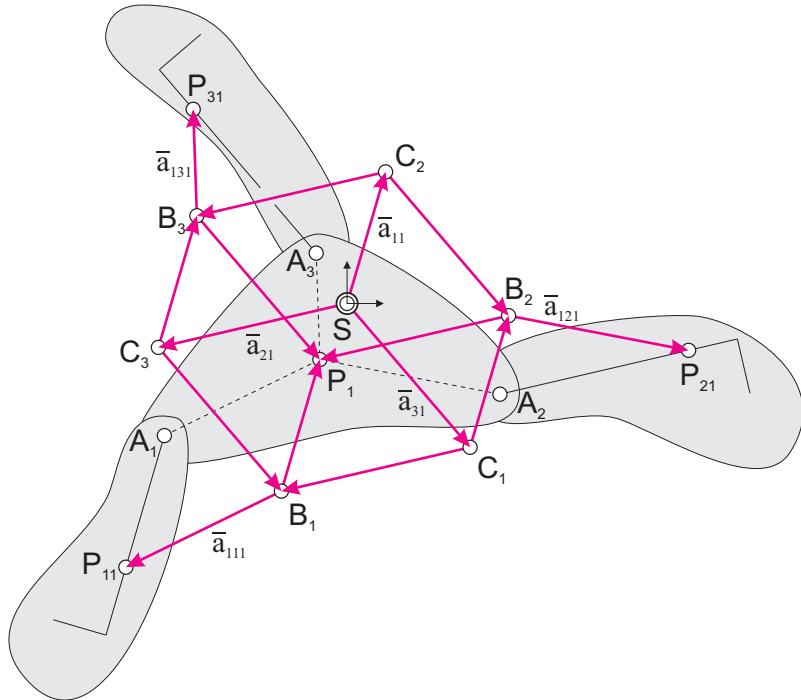


Fig. 3.33 The six principal vectors \bar{a}_{111} , \bar{a}_{211} , \bar{a}_{31} , \bar{a}_{1111} , \bar{a}_{2111} , and \bar{a}_{3111} describe the positions of principal points P_{11} , P_{21} , P_{31} , and P_1 relative to S .

reference frame $x_{311}y_{311}$ as

$$\begin{aligned}\bar{L}_{311} &= \begin{bmatrix} m_{T31}a_{31} + m_{312}p_{312} + m_{313}p_{313} + m_{314}p_{314} + m_{315}p_{315} + m_{31}(a_{31} + p_{31}) \\ m_{312}q_{312} + m_{313}q_{313} + m_{314}q_{314} + m_{315}q_{315} - m_{31}q_{31} \end{bmatrix} \\ &= \begin{bmatrix} m_{tot}a_{31} \\ 0 \end{bmatrix}\end{aligned}\quad (3.79)$$

with $m_{T31} = m_{311} + m_{213} + m_{214} + m_{114} + m_{115}$. Principal point P_{31} is found with respect to line S_3A_3 when $a_{31} + p_{31} = s_{31} \cos \alpha_{31}$ and $q_{31} = s_{31} \sin \alpha_{31}$ are substituted such that the principal dimension a_{31} and angle α_{31} are calculated as

$$\begin{aligned}a_{31} &= \frac{m_{31}s_{31} \cos \alpha_{31} + m_{312}p_{312} + m_{313}p_{313} + m_{314}p_{314} + m_{315}p_{315}}{m_{tot} - m_{311} - m_{114} - m_{115} - m_{213} - m_{214}} \quad (3.80) \\ \alpha_{31} &= \sin^{-1} \left(\frac{m_{312}q_{312} + m_{313}q_{313} + m_{314}q_{314} + m_{315}q_{315}}{m_{31}s_{31}} \right)\end{aligned}$$

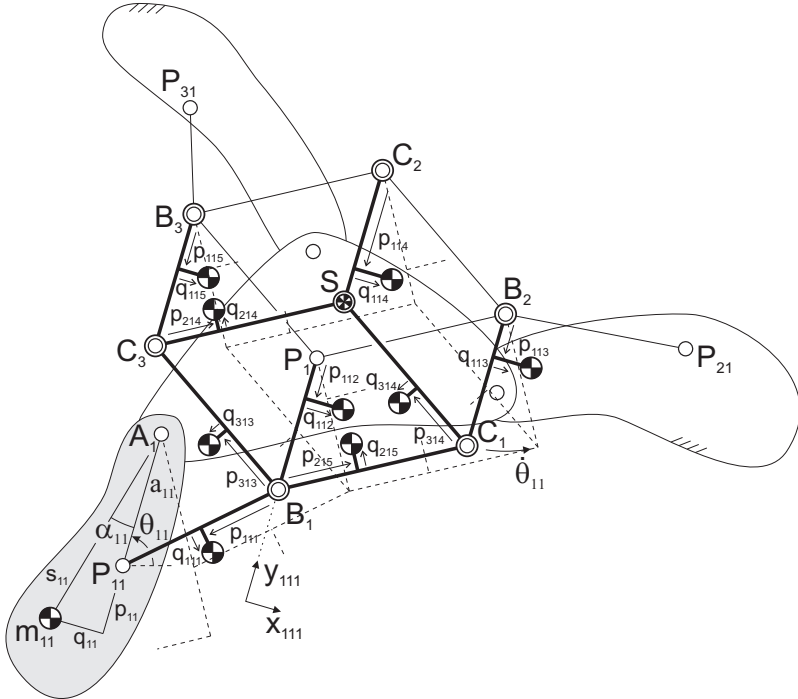


Fig. 3.34 Relative motion of DoF 1 with rotation about principal joint A_1 and where $\dot{\theta}_{21} = \dot{\theta}_{31} = \dot{\theta}_1 = 0$. To find P_{11} , the linear momentum of the moving masses equals the linear momentum of the total mass moving in S .

The relative motion of DoF 4 to find P_1 is illustrated in Fig. 3.35 where $\dot{\theta}_{11} = \dot{\theta}_{21} = \dot{\theta}_{31} = 0$. Here points P_1 , B_1 , B_2 , B_3 , C_1 , C_2 , C_3 , and S can be regarded as fixed while links 1, 111, 211, and 311 solely rotate and links 11, 21, and 31 solely translate. The linear momentum of this motion can be written with respect to the four reference frames $x_{10}y_{10}$, $x_{11}y_{11}$, $x_{12}y_{12}$, and $x_{13}y_{13}$. Then the linear momentum of m_1 is written with respect to frame $x_{10}y_{10}$, of m_{11} and m_{111} with respect to frame $x_{11}y_{11}$, of m_{21} and m_{211} with respect to frame $x_{12}y_{12}$, and of m_{31} and m_{311} with respect to frame $x_{13}y_{13}$. The four sets of linear momentum equations then result in

$$\begin{aligned}\bar{L}_{10} &= \begin{bmatrix} m_1 d_1 \\ 0 \end{bmatrix} \dot{\theta}_1 & \bar{L}_{11} &= \begin{bmatrix} m_{11} a_{111} + m_{111} p_{111} \\ m_{111} q_{111} \end{bmatrix} \dot{\theta}_1 \quad (3.81) \\ \bar{L}_{12} &= \begin{bmatrix} m_{21} a_{121} + m_{211} p_{211} \\ m_{211} q_{211} \end{bmatrix} \dot{\theta}_1 & \bar{L}_{13} &= \begin{bmatrix} m_{31} a_{131} + m_{311} p_{311} \\ m_{311} q_{311} \end{bmatrix} \dot{\theta}_1\end{aligned}$$

The force balance conditions for the relative motion of DoF 4 can be found from the ELMS of this motion in Fig. 3.36 where m_1 is described relative to P_1 with a construction of three parallelograms as illustrated. This is an extension of the construction with a single parallelogram in Fig. 3.13. The parallelograms are defined

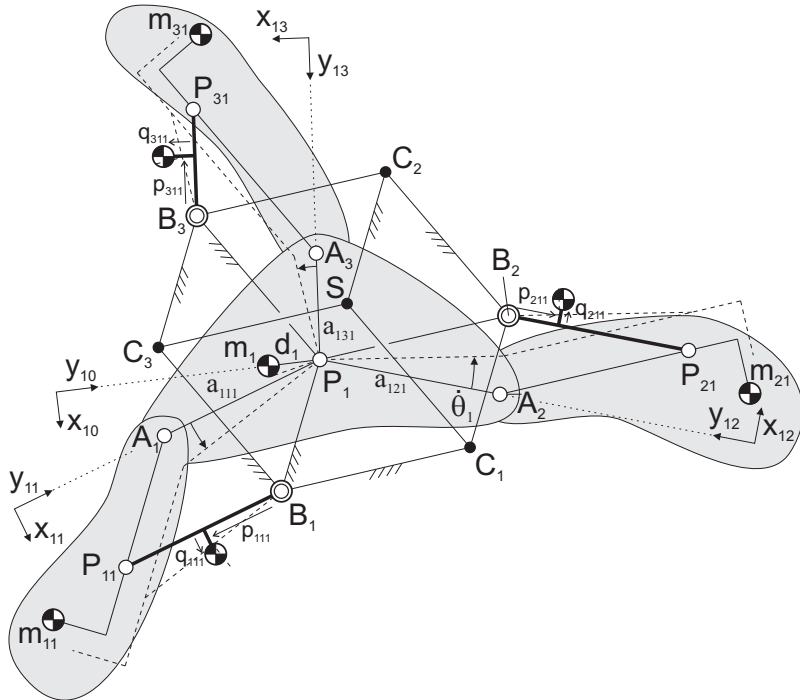


Fig. 3.35 Relative motion of DoF 4 where $\dot{\theta}_{11} = \dot{\theta}_{21} = \dot{\theta}_{31} = 0$ to find P_1 . Links 1, 111, 211, and 311 solely rotate and links 11, 21, and 31 solely translate.

with d_1^a along the line P_1N_1 , d_1^b along the line P_1N_2 , and d_1^c along the line P_1N_3 in opposite direction of P_1 . Here N_1 is the CoM of m_{11} and m_{111} , N_2 is the CoM of m_{21} and m_{211} , and N_3 is the CoM of m_{31} and m_{311} .

Similar to Fig. 3.14, Fig. 3.37 shows this construction as a 3-DoF pantographic mechanism in which P_1 is the common CoM. The force balance conditions of this mechanism can be derived from the motion of each DoF individually, resulting in the three ELMSs in Fig. 3.38. Also here m_1 can be defined in each model with parameters $p_1^{\{a,b,c\}}$ and $q_1^{\{a,b,c\}}$ with respect to the principal dimensions \bar{a}_{i11} , as illustrated. P_1 is found as the CoM of each of these reduced-mass models which results in the six force balance conditions

$$m_1 p_1^a = m_{11} a_{111} + m_{111} p_{111} \quad m_1 q_1^a = m_{111} q_{111}$$

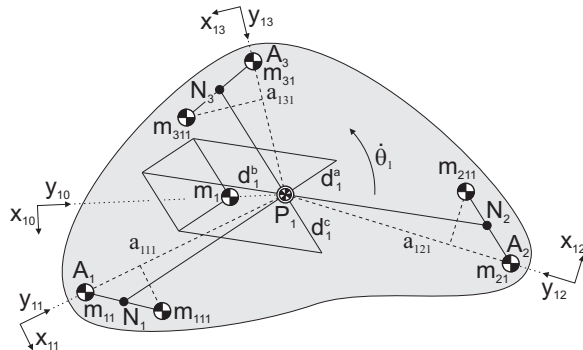


Fig. 3.36 ELMS of the relative motion of DoF 4 where P_1 is the CoM of the reduced-mass model. To obtain the force balance conditions, m_1 is described with a construction of three parallelograms with sides d_1^a , d_1^b , and d_1^c relative to P_1 as illustrated, which is an extension of the construction with a single parallelogram in Fig. 3.13.

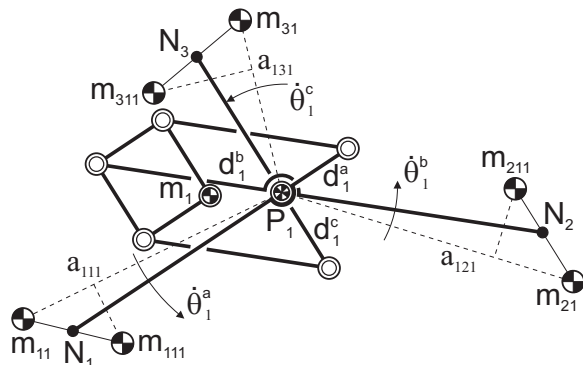


Fig. 3.37 The graphical construction in Fig. 3.36 can be regarded as a 3-DoF force-balanced parallelogram linkage from which the force balance conditions can be derived.

$$\begin{aligned} m_1 p_1^b &= m_{21} a_{121} + m_{211} p_{211} & m_1 q_1^b &= m_{211} q_{211} \\ m_1 p_1^c &= m_{31} a_{131} + m_{311} p_{311} & m_1 q_1^c &= m_{311} q_{311} \end{aligned} \quad (3.82)$$

In summary, from (3.75), (3.77), (3.79), and (3.82) the twelve force balance conditions of the 4-DoF principal vector linkage in Fig. 3.32 are:

$$\begin{aligned} (m_{tot} - m_{T11} - m_{11})a_{11} &= m_{112} p_{112} + m_{113} p_{113} + m_{114} p_{114} + m_{115} p_{115} + m_{11} p_{11} \\ m_{11} q_{11} &= m_{112} q_{112} + m_{113} q_{113} + m_{114} q_{114} + m_{115} q_{115} \\ (m_{tot} - m_{T21} - m_{21})a_{21} &= m_{212} p_{212} + m_{213} p_{213} + m_{214} p_{214} + m_{215} p_{215} + m_{21} p_{21} \\ m_{21} q_{21} &= m_{212} q_{212} + m_{213} q_{213} + m_{214} q_{214} + m_{215} q_{215} \\ (m_{tot} - m_{T31} - m_{31})a_{31} &= m_{312} p_{312} + m_{313} p_{313} + m_{314} p_{314} + m_{315} p_{315} + m_{31} p_{31} \\ m_{31} q_{31} &= m_{312} q_{312} + m_{313} q_{313} + m_{314} q_{314} + m_{315} q_{315} \\ m_1 p_1^a &= m_{11} a_{111} + m_{111} p_{111} \\ m_1 q_1^a &= m_{111} q_{111} \\ m_1 p_1^b &= m_{21} a_{121} + m_{211} p_{211} \\ m_1 q_1^b &= m_{211} q_{211} \\ m_1 p_1^c &= m_{31} a_{131} + m_{311} p_{311} \\ m_1 q_1^c &= m_{311} q_{311} \end{aligned} \quad (3.83)$$

with

$$\begin{aligned} m_{T11} &= m_{111} + m_{313} + m_{314} + m_{214} + m_{215} \\ m_{T21} &= m_{211} + m_{113} + m_{114} + m_{314} + m_{315} \\ m_{T31} &= m_{311} + m_{213} + m_{214} + m_{114} + m_{115} \\ m_{tot} &= m_1 + m_{11} + m_{21} + m_{31} + \sum_{k=1}^5 (m_{11k} + m_{21k} + m_{31k}) \end{aligned} \quad (3.84)$$

With equivalent masses $\mu_1 = m_{11} + m_{111} p_{111} / a_{111}$, $\mu_2 = m_{21} + m_{211} p_{211} / a_{121}$, $\mu_3 = m_{31} + m_{311} p_{311} / a_{131}$, $\mu_4 = m_1$, $v_1 = m_{111} q_{111} / a_{111}$, $v_2 = m_{211} q_{211} / a_{121}$, and

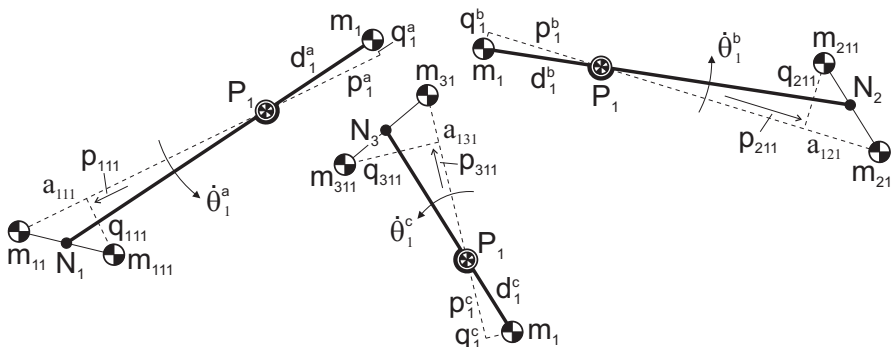


Fig. 3.38 ELMSSs of the parallelogram linkage in Fig. 3.37 to derive the force balance conditions where P_1 is the CoM in each model.

$v_3 = m_{311}q_{311}/a_{131}$, the linear momenta equations in (3.81) are written as

$$\begin{aligned}\bar{L}_{10} &= \begin{bmatrix} \mu_4 \\ 0 \end{bmatrix} d_1 \dot{\theta}_1 & \bar{L}_{11} &= \begin{bmatrix} \mu_1 \\ v_1 \end{bmatrix} a_{111} \dot{\theta}_1 \\ \bar{L}_{12} &= \begin{bmatrix} \mu_2 \\ v_2 \end{bmatrix} a_{121} \dot{\theta}_1 & \bar{L}_{13} &= \begin{bmatrix} \mu_3 \\ v_3 \end{bmatrix} a_{131} \dot{\theta}_1\end{aligned}\quad (3.85)$$

and Fig. 3.39 shows the representing ELMS. When the location of P_1 is described with respect to A_1 with parameters b_1 along line A_1A_2 and c_1 from line A_1A_2 and the location of A_3 with respect to A_1 is defined similarly with parameters h_1 and h_2 , as illustrated, then the linear momentum \bar{L}_1 of the ELMS rotating about P_1 can be written with respect to reference frame x_1y_1 as

$$\begin{aligned}\frac{\bar{L}_1}{\dot{\theta}_1} &= \mu_1 \begin{bmatrix} c_1 \\ -b_1 \end{bmatrix} + v_1 \begin{bmatrix} b_1 \\ c_1 \end{bmatrix} + \mu_2 \begin{bmatrix} c_1 \\ -(b_1 - l_1) \end{bmatrix} + v_2 \begin{bmatrix} b_1 - l_1 \\ c_1 \end{bmatrix} + \\ &\quad \mu_3 \begin{bmatrix} c_1 - h_2 \\ -(b_1 - h_1) \end{bmatrix} + v_3 \begin{bmatrix} b_1 - h_1 \\ c_1 - h_2 \end{bmatrix} + \mu_4 \begin{bmatrix} c_1 - f_1 \\ -(b_1 - e_1) \end{bmatrix} = \begin{bmatrix} 0 \\ 0 \end{bmatrix}\end{aligned}\quad (3.86)$$

where l_1 is the distance between A_1 and A_2 . The conditions from which b_1 and c_1 are calculated then become:

$$(\mu_1 + \mu_2 + \mu_3 + \mu_4)c_1 + (v_1 + v_2 + v_3)b_1 - v_2l_1 - \mu_3h_2 - v_3h_1 - \mu_4f_1 = 0 \quad (3.87)$$

$$-(\mu_1 + \mu_2 + \mu_3 + \mu_4)b_1 + (v_1 + v_2 + v_3)c_1 + \mu_2l_1 + \mu_3h_1 - v_3h_2 + \mu_4e_1 = 0 \quad (3.88)$$

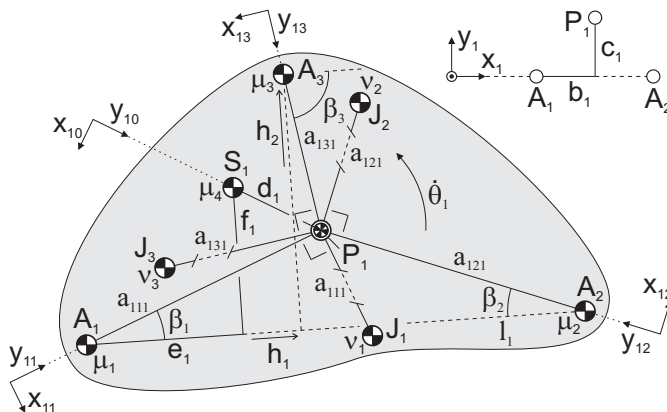


Fig. 3.39 ELMS of the relative motion of DoF 4 where P_1 is the CoM of the reduced-mass model. P_1 can be found with respect to A_1 and line A_1A_2 with parameters b_1 and c_1 .

It is also possible to find P_2 by writing the position of m_1 from Fig. 3.36 and Fig. 3.39 as:

$$\begin{aligned} e_1 &= (a_{111} + p_1^a) \cos \beta_1 - q_1^a \sin \beta_1 - p_1^b \cos \beta_2 - q_1^b \sin \beta_2 + p_1^c \cos \beta_3 + q_1^c \sin \beta_3 \\ f_1 &= (a_{111} + p_1^a) \sin \beta_1 + q_1^a \cos \beta_1 + p_1^b \sin \beta_2 - q_1^b \cos \beta_2 - p_1^c \sin \beta_3 + q_1^c \cos \beta_3 \end{aligned}$$

with $\cos \beta_1 = b_1/a_{111}$, $\sin \beta_1 = c_1/a_{111}$, $\cos \beta_2 = (l_1 - b_1)/a_{121}$, $\sin \beta_2 = c_1/a_{121}$, $\cos \beta_3 = (b_1 - h_1)/a_{131}$, and $\sin \beta_3 = (h_2 - c_1)/a_{131}$. When substituted, these equations write

$$\begin{aligned} e_1 &= \left(\frac{a_{111} + p_1^a}{a_{111}} + \frac{p_1^b}{a_{121}} + \frac{p_1^c}{a_{131}} \right) b_1 - \left(\frac{q_1^a}{a_{111}} + \frac{q_1^b}{a_{121}} + \frac{q_1^c}{a_{131}} \right) c_1 - \frac{p_1^b}{a_{121}} l_1 - \frac{p_1^c}{a_{131}} h_1 + \frac{q_1^c}{a_{131}} h_2 \\ f_1 &= \left(\frac{a_{111} + p_1^a}{a_{111}} + \frac{p_1^b}{a_{121}} + \frac{p_1^c}{a_{131}} \right) c_1 + \left(\frac{q_1^a}{a_{111}} + \frac{q_1^b}{a_{121}} + \frac{q_1^c}{a_{131}} \right) b_1 - \frac{q_1^b}{a_{121}} l_1 - \frac{p_1^c}{a_{131}} h_2 - \frac{q_1^c}{a_{131}} h_1 \end{aligned}$$

from which b_1 and c_1 are obtained in terms of principal vectors as:

$$\begin{aligned} b_1 &= \frac{\left(\frac{a_{111} + p_1^a}{a_{111}} + \frac{p_1^b}{a_{121}} + \frac{p_1^c}{a_{131}} \right) \left(\frac{p_1^b}{a_{121}} l_1 + \frac{p_1^c}{a_{131}} h_1 - \frac{q_1^c}{a_{131}} h_2 + e_1 \right)}{\left(\frac{a_{111} + p_1^a}{a_{111}} + \frac{p_1^b}{a_{121}} + \frac{p_1^c}{a_{131}} \right)^2 + \left(\frac{q_1^a}{a_{111}} + \frac{q_1^b}{a_{121}} + \frac{q_1^c}{a_{131}} \right)^2} \\ &\quad + \frac{\left(\frac{q_1^a}{a_{111}} + \frac{q_1^b}{a_{121}} + \frac{q_1^c}{a_{131}} \right) \left(\frac{q_1^b}{a_{121}} l_1 + \frac{p_1^c}{a_{131}} h_2 + \frac{q_1^c}{a_{131}} h_1 + f_1 \right)}{\left(\frac{a_{111} + p_1^a}{a_{111}} + \frac{p_1^b}{a_{121}} + \frac{p_1^c}{a_{131}} \right)^2 + \left(\frac{q_1^a}{a_{111}} + \frac{q_1^b}{a_{121}} + \frac{q_1^c}{a_{131}} \right)^2} \quad (3.89) \end{aligned}$$

$$\begin{aligned} c_1 &= \frac{\left(\frac{a_{111} + p_1^a}{a_{111}} + \frac{p_1^b}{a_{121}} + \frac{p_1^c}{a_{131}} \right) \left(\frac{q_1^b}{a_{121}} l_1 + \frac{p_1^c}{a_{131}} h_2 + \frac{q_1^c}{a_{131}} h_1 + f_1 \right)}{\left(\frac{a_{111} + p_1^a}{a_{111}} + \frac{p_1^b}{a_{121}} + \frac{p_1^c}{a_{131}} \right)^2 + \left(\frac{q_1^a}{a_{111}} + \frac{q_1^b}{a_{121}} + \frac{q_1^c}{a_{131}} \right)^2} \\ &\quad - \frac{\left(\frac{q_1^a}{a_{111}} + \frac{q_1^b}{a_{121}} + \frac{q_1^c}{a_{131}} \right) \left(\frac{p_1^b}{a_{121}} l_1 + \frac{p_1^c}{a_{131}} h_1 - \frac{q_1^c}{a_{131}} h_2 + e_1 \right)}{\left(\frac{a_{111} + p_1^a}{a_{111}} + \frac{p_1^b}{a_{121}} + \frac{p_1^c}{a_{131}} \right)^2 + \left(\frac{q_1^a}{a_{111}} + \frac{q_1^b}{a_{121}} + \frac{q_1^c}{a_{131}} \right)^2} \quad (3.90) \end{aligned}$$

3.5 The spatial principal vector linkage

Fischer showed that the method of principal vectors also applies to spatial systems [52, 53]. He analyzed a spatial system of twenty elements with spherical joints for which the principal points were determined. He also analyzed the spatial motion of two mass-symmetric links connected with a spherical joint, for which the kinetic energy equations were derived and with the lagrange equations of motions the inverse dynamics of the linkage in motion were obtained based on the principal vectors.

In this section, Fischer's theory is extended for the design of spatial force-balanced principal vector linkages where each line of the graphical solution is a real element with a general CoM. Also spatial principal vector linkages consist of pantograph mechanisms which then are spatial too. Figure 3.40 shows such a spatial force-balanced 3-DoF pantograph. This mechanism consists of four elements of which the opposite elements remain parallel in each direction, i.e. elements 1 and 3 remain parallel and elements 2 and 4 remain parallel for all motion. Elements 1 and 3 also remain in the same plane as shown in Fig. 3.40b while this is not true for elements 2 and 4.

The spatial motion of the spatial pantograph must not be confused with the spatial motion of a planar pantograph mechanism. A 2-DoF planar pantograph mechanism may be rotated out of its plane in its entirety as in [25], while in a spatial 3-DoF pantograph the elements exhibit spatial motion relatively. The elements in a planar 2-DoF pantograph solely have planar motion relatively.

The force balance conditions of the spatial 3-DoF principal vector linkage of two principal elements in series in Fig. 3.40 are equal to the force balance conditions of the planar 2-DoF principal vector linkage in Fig. 3.2. To have the common CoM of all elements be in the joint of element 3 and 4, the force balance conditions (3.2) must hold within the plane of the front view in Fig. 3.40c. In addition, two conditions

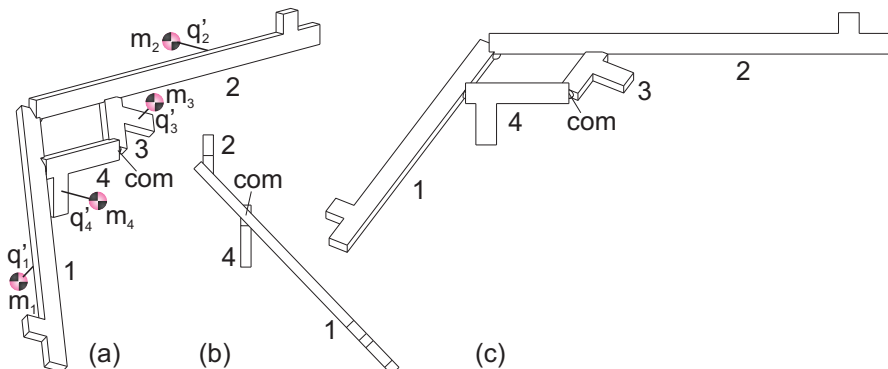


Fig. 3.40 Dimetric view (a), side view (b), and front view (c) of a force-balanced spatial 3-DoF pantograph where opposite elements remain parallel in each direction for all motion. The conditions for force balance are equal to the planar pantograph with two additional conditions.

determine the out-of-plane location of the CoM with

$$m_1 q'_1 = m_3 q'_3 \quad m_2 q'_2 = m_4 q'_4 \quad (3.91)$$

These are comparable to the second and fourth equation in (3.2) where q'_i defines the CoM of element i with respect to the plane of the element through the joints, as illustrated in Fig. 3.40a.

To find the right type of joints for the spatial pantograph to move correctly is challenging. Since spherical joints or universal joints in each of the four connections cannot constrain the mechanism to move correctly, additional elements are likely to be needed. Figure 3.41 shows a solution of a functional spatial pantograph, which is applied as an arm of the delta robot for force balance. Parallelogram 1 represents principal element 1 and is connected with two spherical joints to both element 2 and 4. Parallelogram 3 represents element 3 and is also connected with two spherical joints to both element 2 and 4. To synchronize the motions out of plane of parallelogram 1 and parallelogram 3, a torsion bar 5 is jointed with revolute pairs on each side of element 4 around the spherical joints. This is possible since elements 1 and 3 remain in the same plane for all motion.

With the spatial pantograph, the delta robot is force balanced as schematically shown in Fig. 3.42a, where arm 1 is replaced with the spatial pantograph as compared to Fig. 2.12. Mass m_{12} then is not determined for force balance and can freely located. Countermass m_{BAL} and m_{11} are applied to force balance arm 1 together



Fig. 3.41 Force-balanced Blueprint Automation delta robot of which one arm is a spatial 3-DoF pantograph with a countermass on elements 2 and 4. Parallelogram 3 remains parallel to parallelogram 1 with a torsion bar 5 on each side of the actuated element 4 with which the rotational motions of parallelograms 1 and 3 are synchronized. (patented [100])

with the platform and parts of the lower links of the other arms as illustrated in Fig. 3.42b. The common CoM of these elements is in the pivot with the base. It is possible to solely apply m_{BAL} for force balance for which m_{11} is the mass of its link only. However, applying m_{11} as a countermass as in Fig. 2.12 is dynamically advantageous since it is located about a fixed pivot and the countermass m_{BAL} is reduced significantly.

In general, the synthesis of spatial principal vector linkages can be approached as creating unions of spatial pantographs. Figure 3.43 shows how, similarly to the synthesis of the planar 3-DoF principal vector linkage in Fig. 3.7, a spatial 6-DoF principal vector linkage of three principal elements in series is obtained from a union of three spatial pantographs. Also for this linkage it is required that, to remain a principal vector linkage, the pantograph relations must be maintained for all motion. This means that elements 1, 12, and 13 have to remain parallel in each direction for all motions, which is also required for elements 3, 31, and 32, and for elements 2, 11, and 31. For force balance about the joint of elements 13 and 33, the force balance conditions (3.22) must hold within the plane of the front view of the mechanism and in addition there are three conditions that determine the common CoM in the out-of-plane location, which are similar to (3.91).

In Ref. [4] a spatial linkage was developed which is can be regarded as a reduced case of the spatial principal vector linkage in Fig. 3.43. Derived from complex mathematics, their mechanism was developed with mass-symmetric links with solely revolute pairs such that elements 1 and 3 in Fig. 3.43 were limited to move in planes perpendicular to the front plane of element 2. Since for mass-symmetric links rotational motion about their longitudinal axes does not affect the force balance, the parallel relations of these elements do not need to be maintained.

To have the linkage in Fig. 3.43 move correctly with spherical or universal joints in all connections, also here torsion bars could be used to synchronize the out-of-plane motions of elements 1 and 12 and of elements 3 and 32. Then also elements

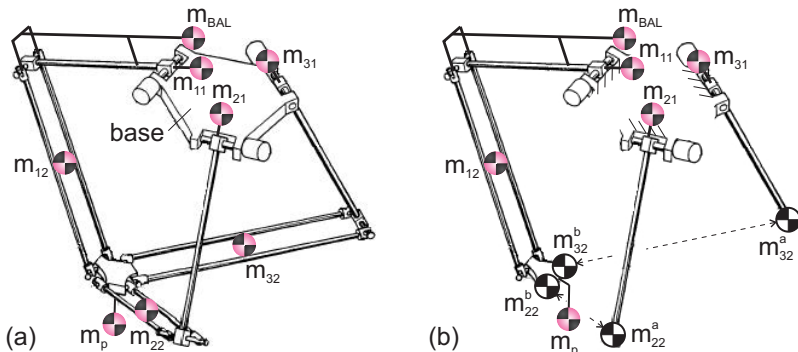


Fig. 3.42 a) Schematic overview of the force balanced delta robot with arm 1 as a spatial pantograph in Fig. 3.41. b) Illustration of the force balance of each arm where m_{BAL} and m_{11} balance arm 1, the platform, and parts of the lower links of the other arms.

2, 11, and 31 move correctly. To synchronize the motions of elements 13 and 33, a more sophisticated solution is required.

It is also possible to obtain a force-balanced delta robot by transforming the complete mechanism into a spatial principal vector linkage as illustrated in Fig. 3.44a. Figure 3.44b shows how the mechanism is constructed of the spatial version of the principal vector linkage in Fig. 3.32 with the mass of the upper links being distributed equivalently to their joints A_i and B_i . Then together with the solution proposed by Hilpert, the CoM of the mechanism is an invariant point in the base with a planar pantograph with countermass [61]. The choice of the right type of joints still may be challenging, however advantage can be taken of the overconstraint design and of mass-symmetric links. When all links are mass symmetric, then with the force balance conditions (3.83) this complete spatial linkage is force balanced.

3.6 Discussion and conclusion

In this section the method of principal vectors was investigated for the development of principal vector linkages. While invented and applied mainly for dynamic analysis, here the method is used as a fundament in the design of force-balanced mechanism architectures. A principal vector linkage has the common CoM of all elements in an invariant point in one of the links for all motion. When this point is made stationary, principal vector linkages are shaking-force-balanced mechanisms.

It has been shown that both planar and spatial principal vector linkages consist of unions of pantographs, with which the physical meaning of the principal points has become clear. A more fundamental approach for the calculations of the principal points and the principal dimensions, as compared to known from literature, was

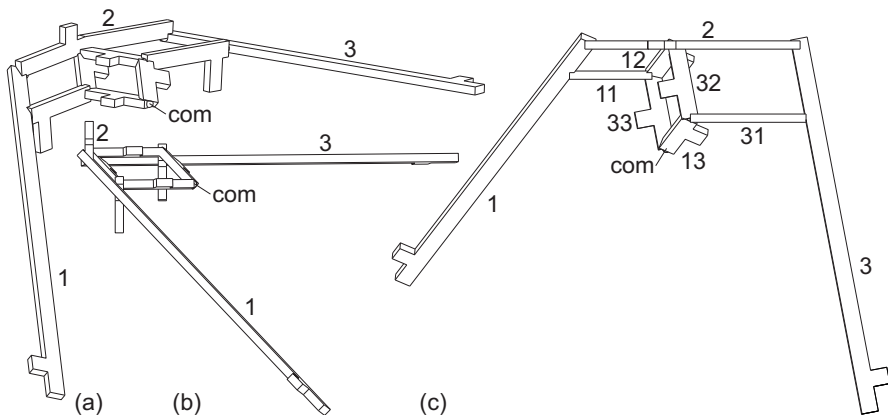


Fig. 3.43 Force-balanced 6-DoF spatial principal vector linkage of three principal elements in series found as an union of three spatial pantographs. a) dimetric view; b) side view; c) top view.

proposed and applied to multi-DoF planar serial and parallel chains of principal elements. This approach is based on linear momentum equations, with which each DoF of the linkage can be investigated individually. Equivalent linear momentum systems were proposed to facilitate the calculations and to use different convenient reference frames together.

The reduced mass models from the equivalent linear momentum systems are comparable with the augmented bodies as found, among others, in [105]. Also this concept is explained in literature as a trick, comparable to the original explanation of the method of principal vectors. With the linear momentum equations however they are obtained naturally. Including the mass of the principal vector links is challenging with the explanation in literature. With linear momentum equations including these masses is not a problem.

The principal vector linkages in this chapter can be extended by adding principal elements either in series or in parallel. For the synthesis of inherently force-balanced mechanisms, various solutions can be derived from principal vector linkages by changing the link design and organisation, adding elements, exchanging links with gears, replacing joints with other types of joints, etc. As long as the essential kinematic conditions are maintained, for all derived results inherent balance can be obtained. Some kinematic variations of the principal vector links were investigated for the 3-DoF principal vector linkage in Fig. 3.18 and Fig. 3.20. More of the synthesis with principal vector linkages is investigated in chapter 7.

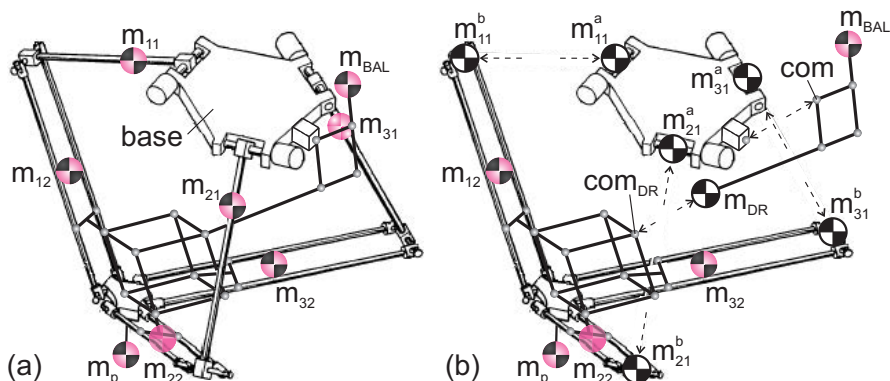


Fig. 3.44 Force-balanced delta robot where the lower part of the robot is a spatial version of the principal vector linkage in Fig. 3.32 and a planar pantograph is used to have the common CoM stationary with respect to the base.

Chapter 4

Closed-chain principal vector linkages

Abstract Closed-chain principal vector linkages can be obtained by closing the chain of principal elements of an open-chain principal vector linkage. This is named here an *open-chain method* where the loop closure relations are not considered. It is shown that the loop closure relations can be considered when a closed chain is modeled as a *mass equivalent principal open chain* of one element less. Therefore one of the elements in the closed chain is taken out and modeled with three equivalent masses of which two are real and one is virtual. The remaining elements define a principal vector linkage on which the three equivalent masses are projected to become a mass equivalent principal open chain. This is shown for a closed chain of four elements and is generalized for closed chains with a higher number of elements.

4.1 Approaches for synthesis of closed-chain principal vector linkages

The principal vector linkages in chapter 3 consist of an open chain of principal elements. It is also possible to find principal vector linkages that consist of closed chains of elements. One approach is to simply close an open-chain principal vector linkage by connecting elements together with a movable joint. Comparable with chapter 2, this is referred to as an *open-chain method* to derive closed-chain principal vector linkages. Such an approach was used by Fischer and Wittenbauer for analysis of closed kinematic chains with principal vectors [53, 104]. This method is also applicable for synthesis of closed-chain principal vector linkages with a general CoM in each of the elements, which is investigated in the first part of this chapter.

As in chapter 2, the loop closure relations are not considered with the open chain method. Therefore general solutions, in this case a general closed-chain principal vector linkage, can not be found with this method. Since the motion of one element in a closed chain depends fully on the motion of the other elements, it can be derived that the general solution of, for instance, a closed chain of four elements is an

open-chain principal vector linkage of three principal elements of which the outer elements are linked with a fourth element with movable joints.

To find the general solution, an approach is proposed where one element in a closed chain is taken out and its mass is modeled with equivalent masses which then are included in the calculations of the open-chain principal vector linkage of the remaining elements. Therefore the equivalent masses are projected on the open chain of principal elements which then is referred to as a *mass equivalent principal chain* (MEPC). For elements with a CoM along the line through the two joints it is well known that it can be modeled with two equivalent masses, one in each joint, when their sum equals the mass of the element and their combined CoM is at the same location as the element CoM, as was shown for the four-bar linkage in Fig. 2.7 and for the delta robot in Fig. 2.12. How to model an element with a general CoM that is not along the line through the two joints however is not known.

In this chapter it is derived and shown that such an element can be modeled with the two known equivalent masses in the joints and, in addition, a third equivalent mass located elsewhere. Whereas the two equivalent masses in the joints determine the element CoM along the line through the joints, the third equivalent mass determines the element CoM with respect to this line.

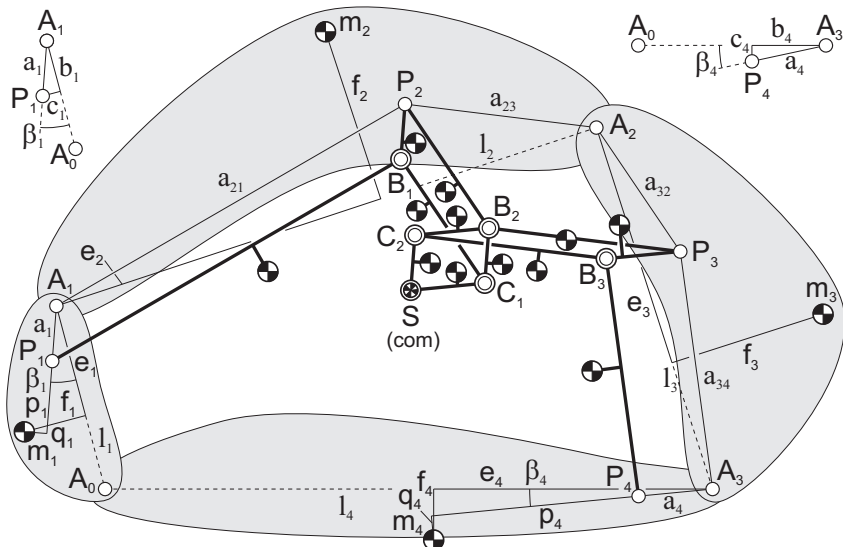


Fig. 4.1 Closed-chain principal vector linkage of four principal elements obtained by closing an open-chain principal vector linkage of four principal elements with revolute pairs in A_0 .

4.2 Closed chain of four elements with Open Chain Method

Figure 4.1 shows a closed-chain principal vector linkage of four principal elements that is obtained by closing the open-chain principal vector linkage in Fig. 3.23. Elements 1 and 4 here have a common joint of revolute pairs in A_0 , which can be in an arbitrary point in each of the two elements. The common CoM of all elements is in joint S for all motion of the closed chain for the conditions (3.67).

As a specific case, it is possible to have the common CoM in S be an invariant point in element A_0A_3 . This is illustrated in Fig. 4.2 where the mechanism can be said to be force balanced with respect to A_0A_3 . This means that S can have revolute pairs directly with A_0A_3 and since SC_1 is parallel to P_4A_3 and therefore is fixed in A_0A_3 , also C_1 can have revolute pairs directly with A_0A_3 . Then the mechanism becomes overconstraint but it remains movable since quadrilaterals $C_1B_2P_3A_3$, $A_0P_1B_1C_1$, and $A_0A_1A_2A_3$ are similar of shape. The necessity of this similarity follows from the parallelograms $P_1A_1P_2B_1$, $P_2B_2C_1B_1$, and $P_3B_2C_2B_3$ that remain movable too. The conditions of the similar quadrilaterals $C_1B_2P_3A_3 \sim A_0P_1B_1C_1$ and $C_1B_2P_3A_3 \sim A_0A_1A_2A_3$ can be written as

$$\frac{a_1}{a'_1} = \frac{a_{23}}{a_{21}} = \frac{a_{34}}{a_{32}} = \frac{a''_3}{a''_1} \quad \frac{a_1}{l_1} = \frac{a_{23}}{l_2} = \frac{a_{34}}{l_3} = \frac{a''_3}{l_4} \quad (4.1)$$

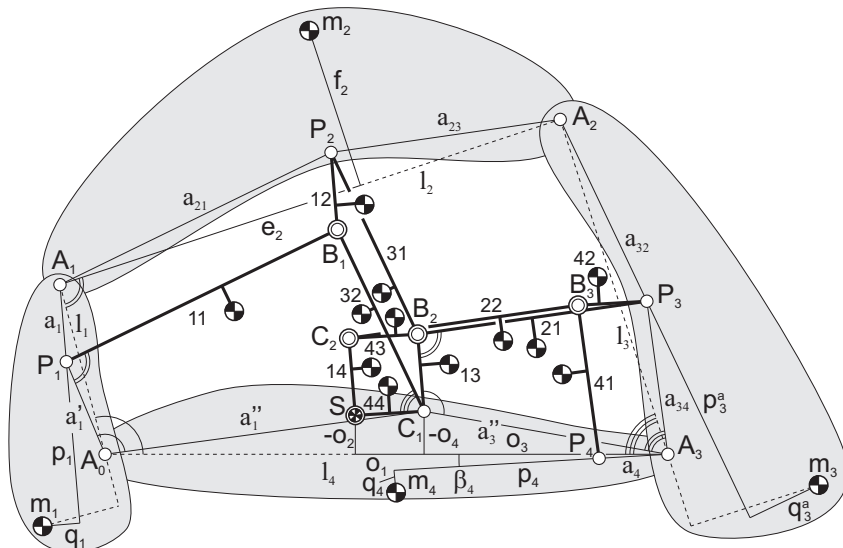


Fig. 4.2 For the similarity conditions $C_1B_2P_3A_3 \sim A_0P_1B_1C_1$ and $C_1B_2P_3A_3 \sim A_0A_1A_2A_3$, joint C_1 and the common CoM in joint S are invariant points in A_0A_3 and the mechanisms is force balanced with respect to A_0A_3 .

with a'_1 , a''_1 , and a''_3 the distances P_1A_0 , A_0C_1 , and A_3C_1 , respectively, and with the principal dimensions $a_1, a_{21}, a_{23}, a_{32}, a_{34}$, and a_4 calculated from (3.67). With length l_i of each link, a'_1 , a''_1 , and a''_3 are calculated as:

$$\begin{aligned} a'_1 &= \frac{a_1 a_{21}}{a_{23}} = \frac{a_1 a_{32}}{a_{34}} & a''_3 &= \frac{a_1 l_4}{l_1} = \frac{a_{23} l_4}{l_2} = \frac{a_{34} l_4}{l_3} \\ a''_1 &= \frac{a_1 a_{32} l_4}{a_{34} l_1} = \frac{a_1 a_{21} l_4}{a_{23} l_1} = \frac{a_{23} a_{32} l_4}{a_{34} l_2} = \frac{a_{21} l_4}{l_2} = \frac{a_{32} l_4}{l_3} = \frac{a_{21} a_{34} l_4}{a_{23} l_3} \end{aligned} \quad (4.2)$$

with which the positions of A_0 and C_1 are determined. With point C_1 defined with o_3 and o_4 within A_0A_3 as illustrated, these parameters can be calculated from the intersection of a circle with radius a''_3 and origin in A_3 with a circle with radius a''_1 and origin in A_0 . This results in

$$o_3 = \frac{l_4^2 - a''_1^2 + a''_3^2}{2l_4} \quad o_4 = -\sqrt{a''_3^2 - \left(\frac{l_4^2 - a''_1^2 + a''_3^2}{2l_4} \right)^2} \quad (4.3)$$

After substituting $a''_1 = a_{21}l_4/l_2$ and $a''_3 = a_{23}l_4/l_2$, o_3 and o_4 become:

$$\begin{aligned} o_3 &= \frac{l_4}{2} \left(1 - \frac{a_{21}^2}{l_2^2} + \frac{a_{23}^2}{l_2^2} \right) \\ o_4 &= -\frac{l_4}{2} \sqrt{\frac{4a_{23}^2}{l_2^2} - \left(1 - \frac{a_{21}^2}{l_2^2} + \frac{a_{23}^2}{l_2^2} \right)^2} \end{aligned} \quad (4.4)$$

Subsequently the location of the common CoM in S is found as

$$o_1 = o_3 + b_4 \quad o_2 = o_4 + c_4 \quad (4.5)$$

where parameters b_4 and c_4 define P_4 with respect to A_3 and line A_3A_0 as illustrated in Fig. 4.1 with $\cos \beta_4 = b_4/a_4$ and $\sin \beta_4 = c_4/a_4$. To derive these parameters, the position of m_4 can be written with e_4 and f_4 relative to A_3 and to line A_3A_0 as

$$\begin{aligned} e_4 &= (a_4 + p_4) \cos \beta_4 - q_4 \sin \beta_4 = \left(1 + \frac{p_4}{a_4} \right) b_4 - \frac{q_4}{a_4} c_4 \\ f_4 &= (a_4 + p_4) \sin \beta_4 + q_4 \cos \beta_4 = \left(1 + \frac{p_4}{a_4} \right) c_4 + \frac{q_4}{a_4} b_4 \end{aligned}$$

Then b_4 and c_4 are obtained as:

$$b_4 = a_4 \frac{(a_4 + p_4)e_4 + q_4f_4}{(a_4 + p_4)^2 + q_4^2} \quad c_4 = a_4 \frac{(a_4 + p_4)f_4 - q_4e_4}{(a_4 + p_4)^2 + q_4^2} \quad (4.6)$$

Together with (4.4) o_1 and o_2 then are written as:

$$\begin{aligned} o_1 &= \frac{l_4}{2} \left(1 - \frac{a_{21}^2}{l_2^2} + \frac{a_{23}^2}{l_2^2} \right) + a_4 \frac{(a_4 + p_4)e_4 + q_4f_4}{(a_4 + p_4)^2 + q_4^2} \\ o_2 &= -\frac{l_4}{2} \sqrt{\frac{4a_{23}^2}{l_2^2} - \left(1 - \frac{a_{21}^2}{l_2^2} + \frac{a_{23}^2}{l_2^2} \right)^2} + a_4 \frac{(a_4 + p_4)f_4 - q_4e_4}{(a_4 + p_4)^2 + q_4^2} \end{aligned} \quad (4.7)$$

The location of P_2 in A_1A_2 is obtained with (3.25-3.26) or (3.35-3.36) and the location of P_3 in A_2A_3 is obtained with (3.69-3.70) or (3.73-3.74). The location of P_1 can be defined with b_1 and c_1 relative to A_1 and to line A_1A_0 as illustrated in Fig. 4.1. With $\cos \beta_1 = b_1/a_1$ and $\sin \beta_1 = c_1/a_1$, the position of m_1 can be written with e_1 and f_1 relative to A_1 and to line A_1A_0 as

$$\begin{aligned} e_1 &= (a_1 + p_1)\cos \beta_1 - q_1 \sin \beta_1 = (1 + \frac{p_1}{a_1})b_1 - \frac{q_1}{a_1}c_1 \\ f_1 &= (a_1 + p_1)\sin \beta_1 + q_1 \cos \beta_1 = (1 + \frac{p_1}{a_1})c_1 + \frac{q_1}{a_1}b_1 \end{aligned}$$

from which b_1 and c_1 are found as:

$$b_1 = a_1 \frac{(a_1 + p_1)e_1 + q_1f_1}{(a_1 + p_1)^2 + q_1^2} \quad c_1 = a_1 \frac{(a_1 + p_1)f_1 - q_1e_1}{(a_1 + p_1)^2 + q_1^2} \quad (4.8)$$

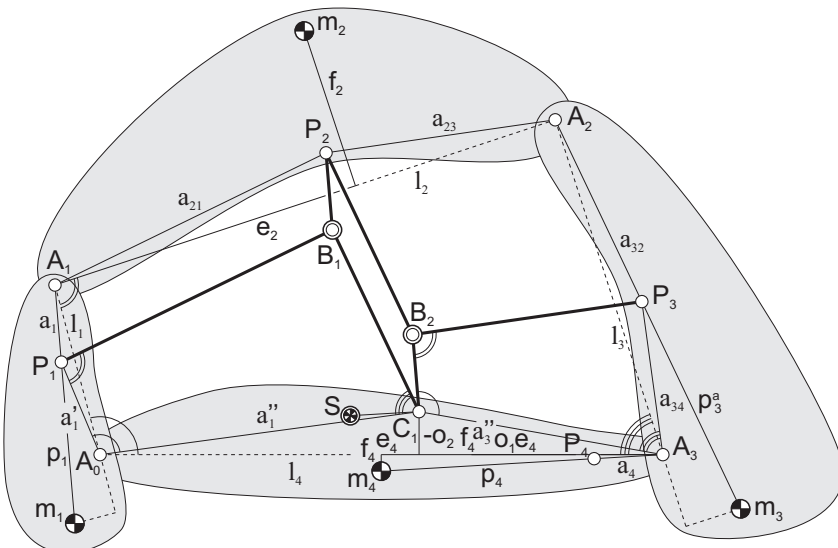


Fig. 4.3 Configuration with massless principal vector links to derive the force balance conditions of the general 4R four-bar linkage.

When the masses of the principal vector links in Fig. 4.2 are zero and links SC_2 , B_2C_2 , B_3C_2 , P_3B_3 , and P_4B_3 are left out, the mechanism in Fig. 4.3 is obtained. This mechanism is comparable with the 4R four-bar mechanism in Fig. 2.14b and it will be shown that the obtained conditions are equal to the force balance conditions (2.29).

With $q_1 = q_4 = q_2^a = q_2^b = q_3^a = q_3^b = 0$, the conditions (3.67) for which S is the common CoM of the mechanism in Fig. 4.3 can be written as

$$\begin{aligned} p_1 &= \frac{(m_2 + m_3 + m_4)a_1}{m_1} & p_2^a &= \frac{m_1 a_{21}}{m_2} & p_2^b &= \frac{(m_3 + m_4)a_{23}}{m_2} \\ p_3^a &= \frac{(m_1 + m_2)a_{32}}{m_3} & p_3^b &= \frac{m_4 a_{34}}{m_3} & p_4 &= \frac{(m_1 + m_2 + m_3)a_4}{m_4} \end{aligned} \quad (4.9)$$

When these equations are substituted in (3.35), (3.36), (3.73), (3.74), (4.6), and (4.8) the parameters of the principal points are obtained as

$$\begin{aligned} b_1 &= \frac{m_1 e_1}{m_1 + m_2 + m_3 + m_4} & c_1 &= \frac{m_1 f_1}{m_1 + m_2 + m_3 + m_4} \\ b_{21} &= \frac{m_2 e_2 + (m_3 + m_4)l_2}{m_1 + m_2 + m_3 + m_4} & c_2 &= \frac{m_2 f_2}{m_1 + m_2 + m_3 + m_4} \\ b_{32} &= \frac{m_3 e_3 + m_4 l_3}{m_1 + m_2 + m_3 + m_4} & c_3 &= \frac{f_3}{m_1 + m_2 + m_3 + m_4} \\ b_4 &= \frac{m_4 e_4}{m_1 + m_2 + m_3 + m_4} & c_4 &= \frac{m_4 f_4}{m_1 + m_2 + m_3 + m_4} \end{aligned} \quad (4.10)$$

Parameters b_1 , c_1 , b_{32} , and c_3 can also be derived from the relations

$$\begin{aligned} b_1^2 + c_1^2 &= a_1^2 & b_{32}^2 + c_3^2 &= a_{32}^2 \\ (l_1 - b_1)^2 + c_1^2 &= a_1^2 & (l_3 - b_{32})^2 + c_3^2 &= a_{32}^2 \end{aligned} \quad (4.11)$$

where the principal dimensions can be written from (4.1) to depend on a_{21} and a_{23} as

$$a_1 = \frac{a_{23}l_1}{l_2} \quad a_{32} = \frac{a_{21}l_3}{l_2} \quad a'_1 = \frac{a_{21}l_1}{l_2} \quad a_{34} = \frac{a_{23}l_3}{l_2} \quad (4.12)$$

for which they can be found as

$$\begin{aligned} b_1 &= \frac{l_1}{2} \left(1 - \frac{a_{21}^2}{l_2^2} + \frac{a_{23}^2}{l_2^2} \right) & c_1 &= \frac{l_1}{2} \sqrt{\frac{4a_{23}^2}{l_2^2} - \left(1 - \frac{a_{21}^2}{l_2^2} + \frac{a_{23}^2}{l_2^2} \right)^2} \\ b_{32} &= \frac{l_3}{2} \left(1 + \frac{a_{21}^2}{l_2^2} - \frac{a_{23}^2}{l_2^2} \right) & c_3 &= \frac{l_3}{2} \sqrt{\frac{4a_{21}^2}{l_2^2} - \left(1 + \frac{a_{21}^2}{l_2^2} - \frac{a_{23}^2}{l_2^2} \right)^2} \end{aligned} \quad (4.13)$$

The principal dimensions a_{21} and a_{23} are calculated as

$$a_{21}^2 = b_{21}^2 + c_2^2 = \frac{(m_2 e_2 + (m_3 + m_4)l_2)^2 + m_2^2 f_2^2}{(m_1 + m_2 + m_3 + m_4)^2} \quad (4.14)$$

$$a_{23}^2 = (l_2 - b_{21})^2 + c_2^2 = \frac{(m_1 l_2 + m_2(l_2 - e_2))^2 + m_2^2 f_2^2}{(m_1 + m_2 + m_3 + m_4)^2} \quad (4.15)$$

which leads after substitution in (4.4), (4.5), and (4.13) to

$$\begin{aligned} b_1 &= l_1 \frac{m_1 + m_2(1 - \frac{e_2}{l_2})}{m_1 + m_2 + m_3 + m_4} & c_1 &= l_1 \frac{m_2 \frac{f_2}{l_2}}{m_1 + m_2 + m_3 + m_4} \\ b_{32} &= l_3 \frac{m_2 \frac{e_2}{l_2} + m_3 + m_4}{m_1 + m_2 + m_3 + m_4} & c_3 &= l_3 \frac{m_2 \frac{f_2}{l_2}}{m_1 + m_2 + m_3 + m_4} \\ o_1 &= l_4 \frac{m_1 + m_2(1 - \frac{e_2}{l_2})}{m_1 + m_2 + m_3 + m_4} + b_4 & o_2 &= -l_4 \frac{m_2 \frac{f_2}{l_2}}{m_1 + m_2 + m_3 + m_4} + c_4 \end{aligned} \quad (4.16)$$

Combining (4.10) and (4.16) then leads to the equations

$$\begin{aligned} m_1(l_1 - e_1) + m_2(1 - \frac{e_2}{l_2})l_1 &= 0 & m_1 f_1 - m_2 \frac{f_2}{l_2} l_1 &= 0 \\ m_3(l_3 - e_3) + m_2 \frac{e_2}{l_2} l_3 &= 0 & m_3 f_3 - \frac{m_2 f_2}{l_2} l_3 &= 0 \\ m_{tot}(l_4 - o_1) - m_2 \frac{e_2}{l_2} l_4 - m_3 l_4 - m_4(l_4 - e_4) &= 0 & m_{tot} o_2 + m_2 \frac{f_2}{l_2} l_4 - m_4 f_4 &= 0 \end{aligned} \quad (4.17)$$

with $m_{tot} = m_1 + m_2 + m_3 + m_4$. These equations are equal to the force balance conditions (2.29), taking into account that e_1 is defined differently here.

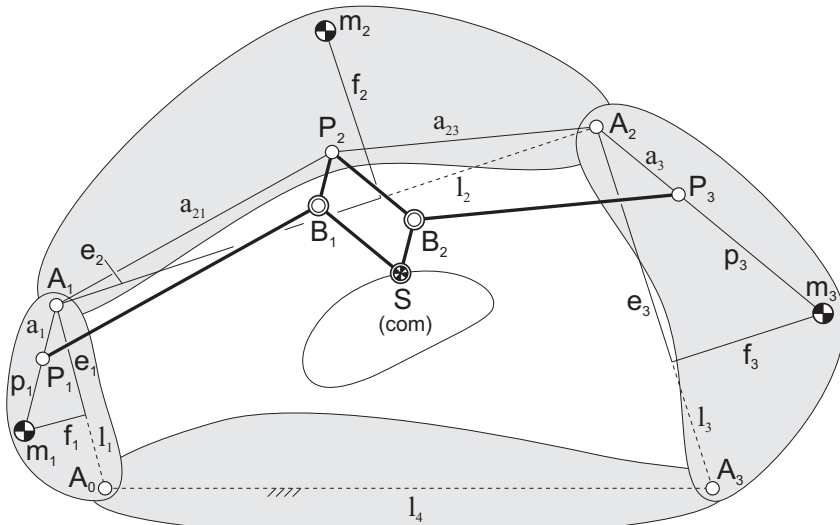


Fig. 4.4 Open-chain principal vector linkage of three principal elements and massless principal vector links that is closed with a massless element as base.

It is interesting to consider the case that also A_0A_3 is massless, i.e. $m_4 = 0$. The resulting mechanism can be regarded as the open-chain principal vector linkage in Fig. 3.6f with three principal elements that is closed with a massless element (e.g. a base of which the mass is not moving) and connected with revolute pairs in A_0 and A_3 , as illustrated in Fig. 4.4. It can be said that S traces the common CoM of m_1 , m_2 , and m_3 with respect to A_0A_3 of which the relative trajectory is illustrated. In literature this 4R four-bar linkage with massless principal vector links is found as a graphical method for dynamic analysis of the motion of the common CoM of closed-loop mechanisms [15, 53, 61, 69, 79, 87, 104].

Comparable with Fig. 4.3, S is an invariant point in A_0A_3 when the quadrilaterals $A_0A_1A_2A_3$, $A_0P_1B_1S$, and $SB_2P_3A_3$ in Fig. 4.5 are similar for all motion. Then the mechanism is force balanced with respect to A_0A_3 . The conditions for the similarities $SB_2P_3A_3 \sim A_0P_1B_1S$ and $SB_2P_3A_3 \sim A_0A_1A_2A_3$ can be written as

$$\frac{a_1}{a'_1} = \frac{a_{23}}{a_{21}} = \frac{a'_3}{a_3} = \frac{a''_3}{a''_1} \quad \frac{a_1}{l_1} = \frac{a_{23}}{l_2} = \frac{a'_3}{l_3} = \frac{a''_3}{l_4} \quad (4.18)$$

with a'_1 , a'_3 , a''_1 , and a''_3 the distances P_1A_0 , P_3A_3 , SA_0 , and SA_3 , respectively, which are derived as:

$$a'_1 = \frac{a_1 a_{21}}{a_{23}} \quad a'_3 = \frac{a_3 a_{23}}{a_{21}} \quad a''_1 = \frac{a_{21} l_4}{l_2} \quad a''_3 = \frac{a_{23} l_4}{l_2} \quad (4.19)$$

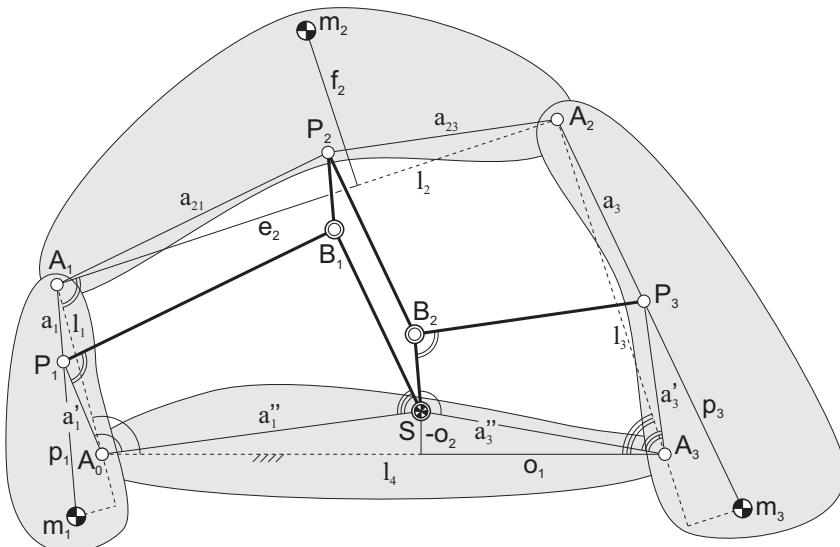


Fig. 4.5 Configuration where common CoM S is an invariant point in A_0A_3 from which the force balance conditions of the general 4R four-bar linkage are derived in terms of principal dimensions.

The principal dimensions a_1 , a_{21} , a_{23} , and a_3 are calculated from (3.22) as:

$$a_1 = \frac{m_1 p_1}{m_2 + m_3} \quad a_{21} = \frac{m_2 p_2^a}{m_1} \quad a_{23} = \frac{m_2 p_2^b}{m_3} \quad a_3 = \frac{m_3 p_3}{m_1 + m_2} \quad (4.20)$$

with p_2^a and p_2^b as in Fig. 3.13 and link lengths l_1 and l_3 derived as:

$$l_1 = \frac{a_1 l_2}{a_{23}} \quad l_3 = \frac{a_3 l_2}{a_{21}} \quad (4.21)$$

Together, these are the force balance conditions of the 4R four-bar linkage in terms of principal dimensions since they define the locations of A_0 and A_3 for which the common CoM in S is an invariant point in base $A_0 A_3$. As can be noticed and as expected, l_4 does not affect these locations and can have any chosen value.

The parameters o_1 and o_2 can be found as the intersection of a circle with radius a_3'' centered in A_3 and a circle with radius a_1'' centered in A_0 , of which the equations are equal to the equations for o_3 and o_4 in (4.3), respectively. After substituting a_1'' and a_3'' they are written in terms of the principal dimensions and dimensions l_2 and l_4 as:

$$o_1 = \frac{l_4}{2} \left(1 + \frac{a_{23}^2 - a_{21}^2}{l_2^2} \right) \quad o_2 = -\frac{l_4}{2} \sqrt{\frac{4a_{23}^2}{l_2^2} - \left(1 + \frac{a_{23}^2 - a_{21}^2}{l_2^2} \right)^2} \quad (4.22)$$

When the masses of all principal vector links are included, each with a general CoM, then the linkage in Fig. 4.6 is obtained. Also here the similarity relations $SB_2P_3A_3 \sim A_0P_1B_1S$ and $SB_2P_3A_3 \sim A_0A_1A_2A_3$ of the quadrilaterals hold, which means that for the conditions in (4.18) also here S is the common CoM for all motion and an invariant point in link A_0A_3 with o_1 and o_2 of (4.22) and with the principal dimensions a_1 , a_{21} , a_{23} , and a_3 from (3.22).

The principal dimensions a'_1 and a'_3 in (4.19) depend solely on the principal dimensions a_1 , a_{21} , a_{23} , and a_3 , comparable with the 2-DoF pantograph in Fig. 3.2. In fact, they describe the positions of A_0 and A_3 which are the *similarity points* of the 3-DoF open-chain principal vector linkage of three principal elements. Here the scaling factor can be written from (4.18) as $k = a'_1/a'_3 = a_3 l_1 / a_1 l_3$ and is constant for any value of l_4 .

From the configuration in Fig. 4.6 also the general similarity points of the 2-DoF pantograph can be derived. When $m_3 = m_{13} = m_{31} = m_{32} = m_{33} = 0$, then a_3 becomes zero with which joints S and B_1 coincide and joints B_2 and P_2 coincide as shown in Fig. 4.7. Then links 3, 13, 32, and 33 disappear. The result is a general pantograph of which the joints A_0 and A_2 are the similarity points. Here the conditions of similarity of the triangles $SP_2A_2 \sim A_0P_1S$ and $SP_2A_2 \sim A_0A_1A_2$ are obtained from (4.18) as

$$\frac{a_1}{a'_1} = \frac{a_{23}}{a_{21}} = \frac{a''_3}{a''_1} \quad \frac{a_1}{l_1} = \frac{a_{23}}{l_2} = \frac{a''_3}{l_4} \quad (4.23)$$

The similarity points in Fig. 4.7 are general while in Fig. 3.2 a specific set of similarity points of the 2-DoF pantograph was found. The principal dimensions a'_1 , a''_1 , and a''_3 are obtained here as in (4.19). The scaling factor is obtained as $k = a''_1/a''_3 = a_{21}/a_{23}$. In chapter 7 it is shown how the similarity points can be used for synthesis of balanced mechanisms.

4.3 Mass equivalent model of a general element in a closed chain

The force balance conditions (2.29) or (4.17) of the four-bar linkage in Fig. 2.14b or Fig. 4.5 can be represented graphically in an interesting way when the terms $m_2^a = m_2(1 - e_2/l_2)$, $m_2^b = m_2e_2/l_2$, and $m_2^c = m_2f_2/l_2$ are considered equivalent masses. Then when link 1 is investigated individually as in Fig. 4.8b, it shows that from the equations that depend on e_1 and f_1 , the common CoM of m_1 , m_2^a in A_1 , and m_2^c in J_1 is in A_0 . The location of J_1 is at a distance l_1 from A_0 , normal to line A_0A_1 as illustrated. Similarly, link 3 can be investigated individually as in Fig. 4.8c showing that from the equations that depend on e_3 and f_3 the common CoM of m_3 , m_2^b in A_2 , and m_2^c in J_3 is in A_3 . The location of J_3 is at a distance l_3 from A_3 , normal

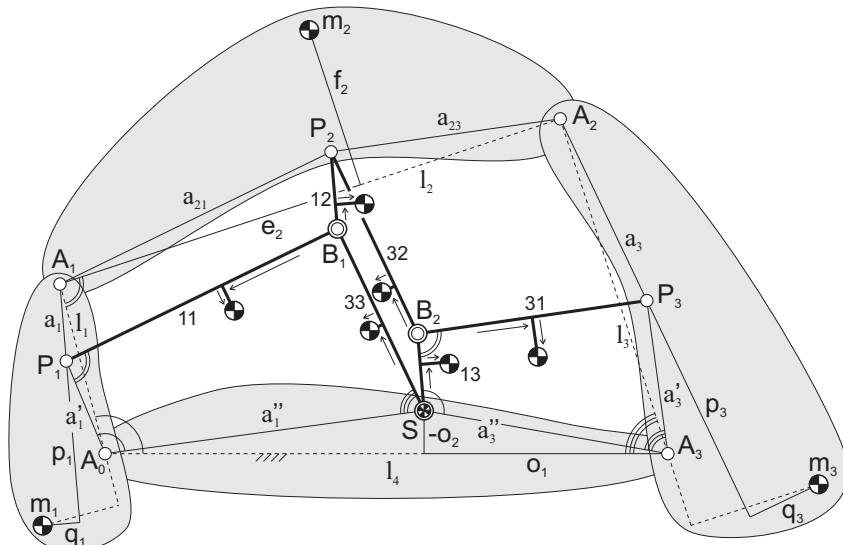


Fig. 4.6 The principal dimensions a'_1 and a'_3 determine together with l_1 and l_3 the locations of A_0 and A_3 , which are the similarity points of the 3-DoF open-chain principal vector linkage of three principal elements.

to line A_2A_3 as illustrated. For link 4 the two force balance conditions that depend on o_1 and o_2 can be represented with $m_1 + m_2^a$ in A_0 , $m_3 + m_2^b$ in A_3 , and m_2^c in J_4 as illustrated in Fig. 4.8d. The common CoM of these masses and m_4 is in S and the location of J_4 is at a distance l_4 from S , normal to line A_0A_3 as shown.

When link 2 is considered, it is shown in Fig. 4.8a that the common CoM of equivalent masses m_2^a in A_1 , m_2^b in A_2 , and m_2^c in J_2 is in the same point as the element CoM S_2 . The location of J_2 is at a distance l_2 from S_2 normal to line A_1A_2 as illustrated. Since there are only equivalent masses involved, Fig. 4.8a can be regarded a *mass equivalent model* of link 2. Equivalent masses m_2^a and m_2^b determine the location of the CoM along the line A_1A_2 with $m_2^a e_2 = m_2^b(l_2 - e_2)$ and are the commonly known equivalent masses as used e.g. in Fig. 2.7, Fig. 2.12, and in Ref. [108, 29]. Their sum equals the mass of the element as $m_2^a + m_2^b = m_2$. Equivalent mass m_2^c however is new and determines the location of the CoM normal to the line A_1A_2 with $m_2^c l_2 = (m_2^a + m_2^b) f_2$.

With m_2^c , the total mass of the mass equivalent model of link 2 in Fig. 4.8a is $m_2^a + m_2^b + m_2^c = m_2(1 + f_2/l_2)$, which can be more or less than the real value of m_2 . Since m_2^c does not represent a real mass, it is regarded a *virtual equivalent mass* while m_2^a and m_2^b both are regarded a *real equivalent mass*.

The mass equivalent model in Fig. 4.8a can also be constructed as in Fig. 4.9a. Here a virtual equivalent mass m_2^c is located in both J_{21} and J_{22} with J_{21} at a distance $s_{21} = \sqrt{e_2^2 + f_2^2}$ from S_2 normal to line A_1S_2 and J_{22} at a distance

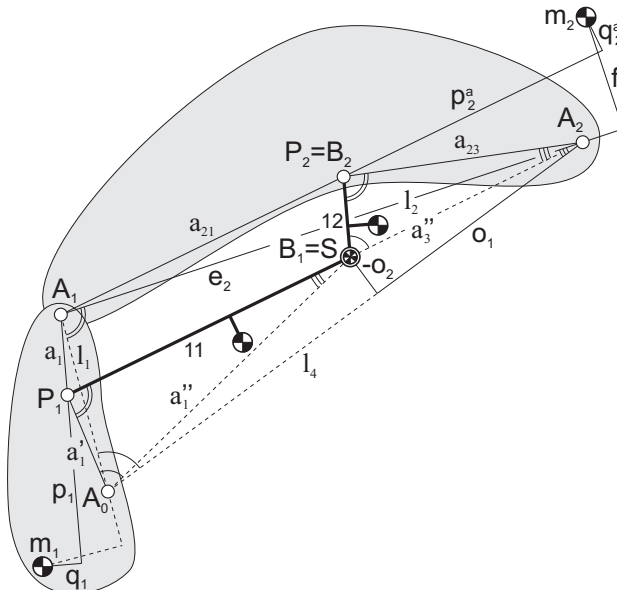


Fig. 4.7 The general similarity points A_0 and A_2 of the 2-DoF pantograph obtained by reducing the 3-DoF principal vector linkage in Fig. 4.6.

$s_{22} = \sqrt{(l_2 - e_2)^2 + f_2^2}$ from S_2 normal to line S_2A_2 , as illustrated. Since the CoM of both virtual equivalent masses ($2m_2^c$) is located along the line through S_2 that is normal to line A_1A_2 (the dashed line) and is located at a distance $l_2/2$ from S_2 , the conditions for mass equivalence are equal to the model in Fig. 4.8a with $m_2^a e_2 + m_2^b (l_2 - e_2) = m_2^c l_2 = (m_2^a + m_2^b) f_2$. Therefore Fig. 4.8a and Fig. 4.9a are mass equivalent models of the same element.

Similarly, the model of link 4 in Fig. 4.8d can be constructed with two virtual equivalent masses as shown in Fig. 4.9d. Here a virtual equivalent mass m_2^c is located in both J_{41} and J_{42} which are at a distance $g_1 = \sqrt{o_1^2 + o_2^2}$ and $g_2 = \sqrt{(l_4 - o_1)^2 + o_2^2}$ from S , respectively, as illustrated.

In Fig. 4.9 the locations of the virtual equivalent mass in each of the models show some general characteristics. The location of each virtual equivalent mass in the mass equivalent model of link 2 in Fig. 4.9a can be characterized as: The virtual equivalent mass (m_2^c) is located at a distance from the CoM of the model (S_2) that is equal to the distance between the CoM of the model and the real equivalent mass (distance s_{21} to m_2^a for J_{21} and distance s_{22} to m_2^b for J_{22}) and normal to the line through the CoM of the model and the real equivalent mass in the direction towards

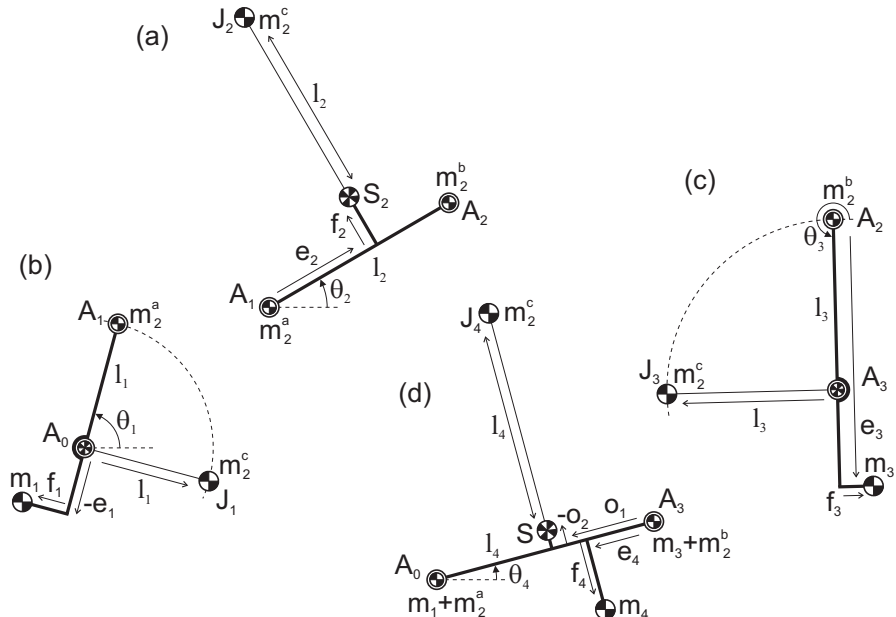


Fig. 4.8 a) Mass equivalent model of link 2 of the four-bar linkage in Fig. 2.14b with real equivalent masses m_2^a and m_2^b and virtual equivalent mass m_2^c of which the CoM is in S_2 ; b-c-d) Graphical representation of the force balance conditions (2.29) for each link with the three equivalent masses with which the CoM of each model is in A_0 , A_3 , and S , respectively.

the positive side (side of positive f_2) of the line through the two real equivalent masses (line A_1A_2).

From the mass equivalent model then the location of the virtual equivalent mass in Fig. 4.9b, 4.9c, and 4.9d can be derived as: The virtual equivalent mass (m_2^c) is located at a distance from the CoM of the model (A_0 in Fig. 4.9b, A_3 in Fig. 4.9c, and S in Fig. 4.9d) that is equal to the distance between the CoM of the model and the real equivalent mass (l_1 to m_2^a in Fig. 4.9b, l_3 to m_2^b in Fig. 4.9c, and g_1 to m_2^b for J_{41} and g_2 to m_2^a for J_{42} in Fig. 4.9d) and normal to the line through the CoM of the model and the real equivalent mass in the same direction as in the mass equivalent model (same direction with respect to the line from the CoM of the model to the real equivalent mass). For instance, the direction in Fig. 4.9b can be found when the mass equivalent model in Fig. 4.9a is considered superimposed on link 1 with their joint in A_1 and subsequently rotated such that the lines from each CoM to real equivalent mass are aligned. In Fig. 4.9c it is found when the mass equivalent model in Fig. 4.9a is considered superimposed on link 3 with their joint in A_2 and subsequently rotated such that the lines from each CoM to real equivalent mass are aligned.

Characteristic of the locations of the real equivalent masses in each of the models in Fig. 4.9 is that (1) they are always in a joint; (2) they follow in the joints of the subsequent elements in the loop, each along their own side (m_2^a appears in A_1 and

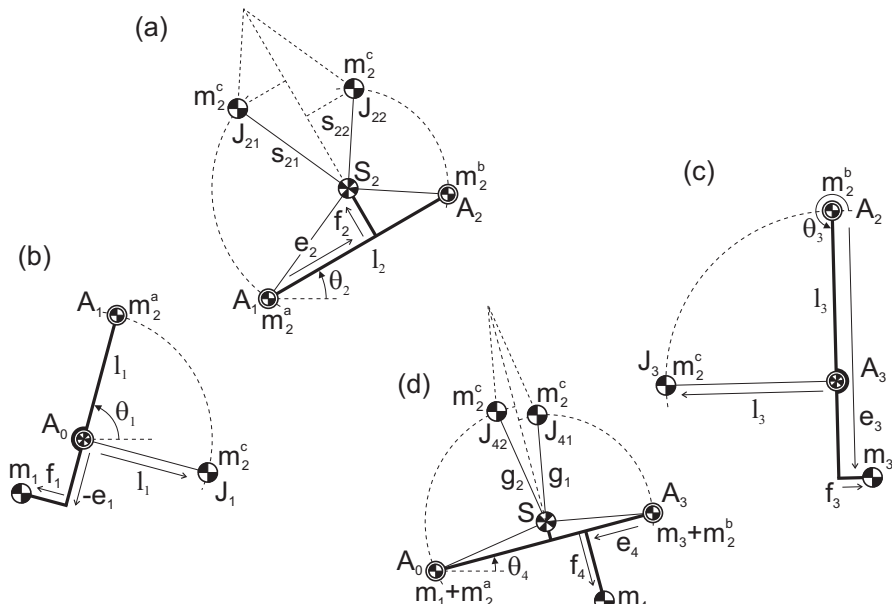


Fig. 4.9 Graphical representation of the force balance conditions (2.29) with (a) a mass equivalent model of link 2 with a virtual equivalent mass m_2^c in both J_{21} and J_{22} and CoM in S_2 and (d) link 4 with a virtual equivalent mass m_2^c in both J_{41} and J_{42} and CoM in S .

A_0 , m_2^b appears in A_2 and A_3). In addition, from the models in Fig. 4.9 it can be said that the mass equivalent model consists of two sets of a real and a virtual equivalent mass which follow in the subsequent elements in the loop, each set along each of the two sides of the loop.

To conclude so far:

A mass equivalent model of an element (i) with a general CoM (defined in Fig. 4.10a with e_i , f_i , and l_i) can be constructed with two real equivalent masses (m_i^a and m_i^b) and a virtual equivalent mass (m_i^c) for the conditions:

$$m_i^a e_i = m_i^b (l_i - e_i) \quad (4.24)$$

$$m_i^c l_i = (m_i^a + m_i^b) f_i \quad (4.25)$$

$$m_i^a + m_i^b = m_i \quad (4.26)$$

Such a mass equivalent model can be constructed as in Fig. 4.10b and as in Fig. 4.10c, of which both will show their usefulness for the modeling of balanced mechanisms.

4.4 Mass equivalent principal open chain of three elements

Figure 4.11 shows an inherent closed-chain principal vector linkage of an open-chain principal vector linkage of three principal elements that is closed with an element 4 with mass m_4 which has joints with element 1 in A_0 and with element 3 in A_3 . To derive the conditions for which the common CoM of the ten elements is in joint S for all motion of the mechanism, element 4 is modeled with equiva-

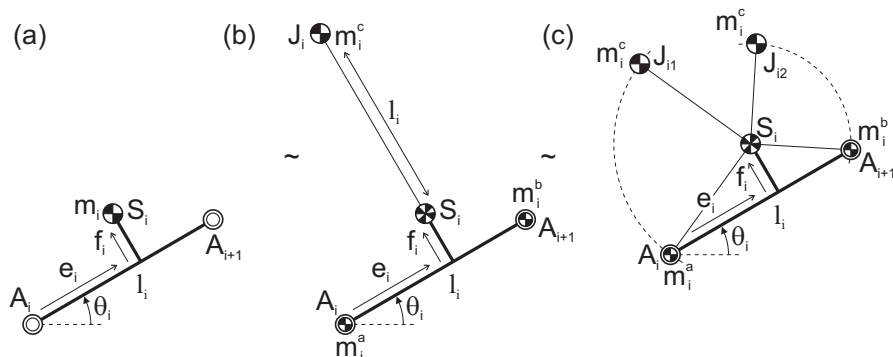


Fig. 4.10 An element with a generally located CoM (a), can be modeled mass-equivalently with two real equivalent masses m_i^a and m_i^b and a virtual equivalent mass m_i^c , of which the virtual equivalent mass can be located (b) in J_i or (c) in both J_{i1} and J_{i2} .

lent masses as in Fig. 4.10b. Figure 4.12b shows the mass equivalent model where, according the conditions (4.24-4.26), a real equivalent mass $m_4^a = m_4(1 - e_4/l_4)$ is located in A_3 , a real equivalent mass $m_4^b = m_4e_4/l_4$ is located in A_0 , and a virtual equivalent mass $m_4^c = m_4f_4/l_4$ is located in both J_{41} and J_{42} , which are at a distance a''_3 and a''_1 from S_4 as illustrated.

With the three equivalent masses the mechanism in Fig. 4.11 can be analyzed as an open-chain principal vector linkage without element 4 on which the equivalent masses are projected. The result will be named a *mass equivalent principal open chain* (MEPC) and is shown in Fig. 4.12a. When the description of the locations of the equivalent masses in section 4.3 is followed, then the real equivalent masses m_4^a and m_4^b are located in the joints A_3 and A_0 , respectively, while the virtual equivalent masses are located about the principal points P_1 , P_2 , and P_3 , which are the CoMs of the reduced mass models of the ELMS of each relative DoF. The directions of the locations are as in the mass equivalent model of element 4 in Fig. 4.12b. It is observed that one virtual equivalent mass follows the chain from the right side with distances a'_3 , a_{23} , and a_1 , while the second virtual equivalent mass follows the chain from the left side with distances a'_1 , a_{21} , and a_3 .

The ELMS of each DoF can be derived from the relative motions of the MEPC as in Fig. 3.9, Fig. 3.10, and Fig. 3.12. Therefore an important property of the virtual equivalent mass is that:

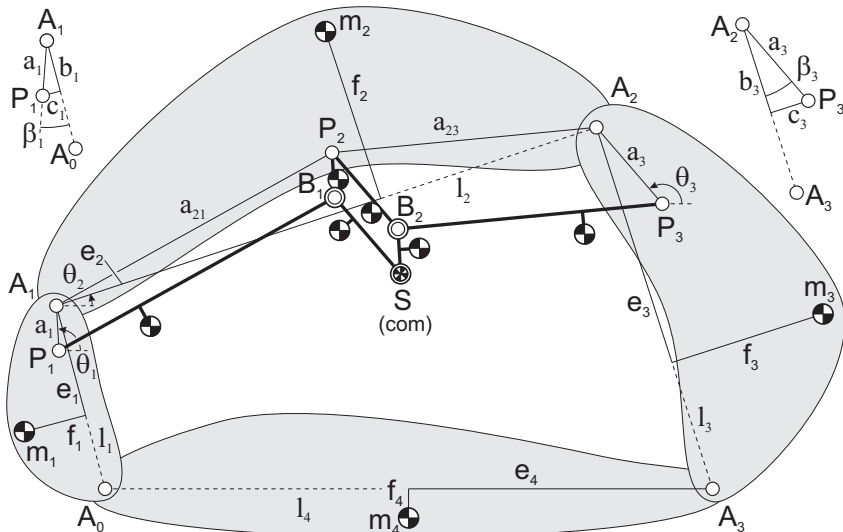


Fig. 4.11 Closed-chain principal vector linkage of an open-chain principal vector linkage of three principal elements that is closed with a fourth element pivoted to element 1 in A_0 and to element 3 in A_3 . The common CoM of all elements is in S for all motion of the mechanism.

A virtual equivalent mass acts as a real mass for rotational motion while it is massless for translational motion of the element on which it is projected.

In other words, a virtual equivalent mass has linear momentum only when the element on which it is projected rotates while for translational motion of the element its linear momentum is zero.

With this property and when the mass of the principal vector links are not considered, the ELMS of each DoF of the MEPC in Fig. 4.12a becomes as in Fig. 4.13. For DoF 1 the ELMS in Fig. 4.13b has $m_2 + m_3 + m_4^a$ located in A_1 , m_4^b located A_0 , and m_4^c located twice about P_1 . Since for this relative motion elements 2 and 3 solely translate, the virtual equivalent masses in these elements are zero. For DoF 3 the ELMS in Fig. 4.13c has $m_1 + m_2 + m_4^b$ located in A_2 , m_4^a located A_3 , and m_4^c located twice about P_3 . Since for this relative motion elements 1 and 2 solely translate, the virtual equivalent masses in these elements are zero. For DoF 2 the ELMS in Fig. 4.13a has $m_1 + m_4^b$ located in A_1 , $m_3 + m_4^a$ located A_2 , and m_4^c located twice

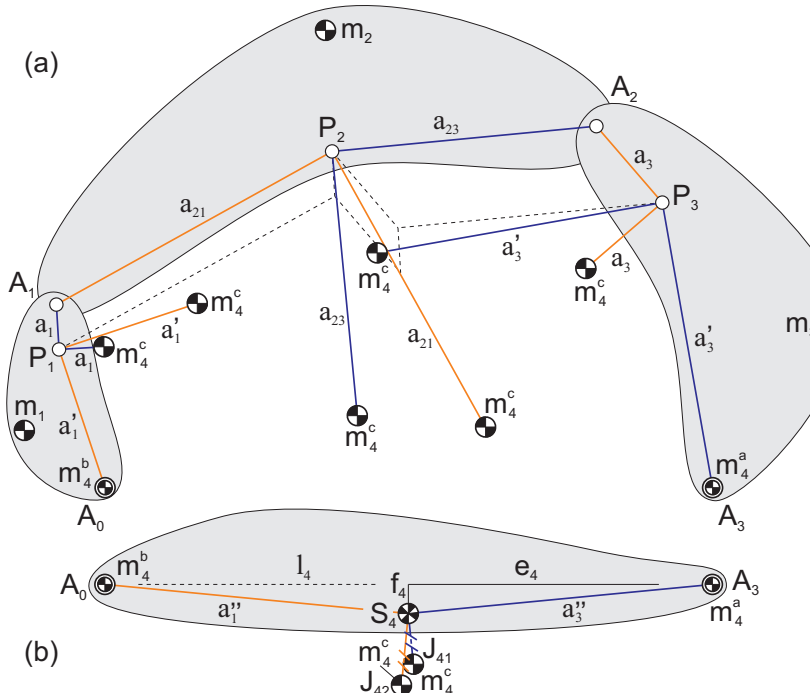


Fig. 4.12 a) Mass equivalent principal open chain where the equivalent masses m_4^a , m_4^b , and m_4^c are projected on the principal open chain. b) Mass equivalent model of element 4 with real equivalent masses m_4^a and m_4^b in joints A_3 and A_0 , respectively, and a virtual equivalent mass in both J_{41} and J_{42} of which the common CoM is in S_4 .

about P_2 . Since for this relative motion elements 1 and 3 solely translate, the virtual equivalent masses in these elements are zero. Also in Fig. 4.13 the principal point is the CoM of each mass model.

If the case is considered that in the limits $a_1 \rightarrow 0$ and $a_3 \rightarrow 0$, which means that S becomes an invariant point in element A_1A_2 (and the principal vector linkage becomes infinitely slim), then the ELMS of each DoF becomes as in Fig. 4.14. While the ELMS of DoF 2 remains equal to Fig. 4.13a, the ELMS of DoF 1 and of DoF 3 changes where P_1 and P_3 coincide with A_1 and A_2 , respectively. When compared with Fig. 4.9, the results are similar. In both elements 1 and 3 one virtual equivalent mass vanishes together with the masses in A_1 and A_2 , respectively, and one virtual equivalent mass is located at a distance equal to the link length from the principal joints. To have the CoM of the models be in the principal joints A_1 and A_2 , for this case m_1 and m_3 cannot be located freely within their elements but need to be located under the conditions in Fig. 4.9.

Since the ELMSs in Fig. 4.14b and Fig. 4.14c rotate about the principal joints A_1 and A_2 , it is possible to analyze the MEPC with the initial principal vector linkage with the method of rotations about the principal joints from section 3.2.3 where m_1 and m_3 are freely located within their elements. This will show to be the shortest way to derive the force balance conditions for DoF 1 and DoF 3. Since then all masses in element 1 are defined with respect to line A_1A_0 , it is possible to combine them as shown in Fig. 4.15b with $m'_1 = m_1 + m_4^b + m_4^c$ of which the CoM S'_1 can be defined with e'_1 and f'_1 as illustrated, which are calculated as

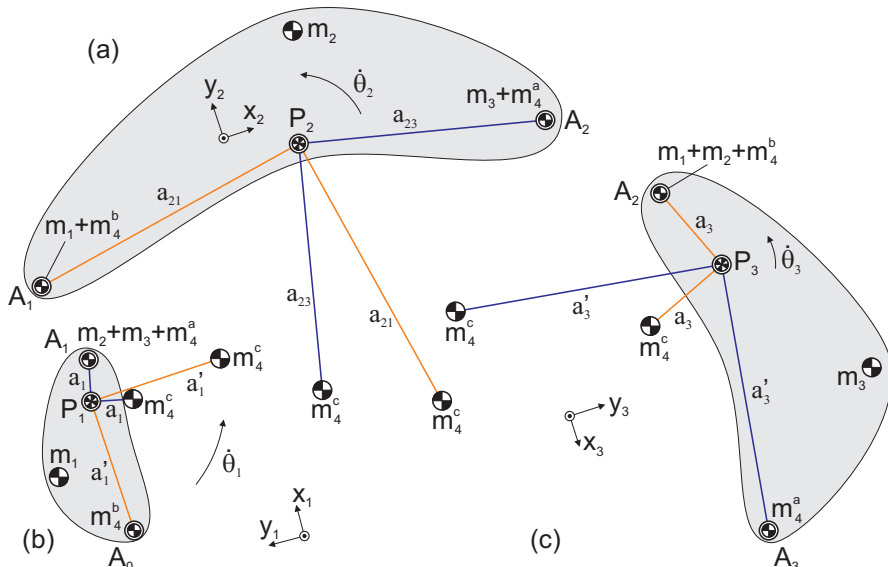


Fig. 4.13 The ELMS of each relative DoF of the MEPC has the two real equivalent masses located in the joints and has two virtual equivalent masses that are located about the principal point.

$$e'_1 = \frac{m_1 e_1 + m_4^b l_1}{m_1 + m_4^b + m_4^c} \quad f'_1 = \frac{m_1 f_1 - m_4^c l_1}{m_1 + m_4^b + m_4^c} \quad (4.27)$$

Similarly, the masses in element 3 can be combined as shown in Fig. 4.15c with $m'_3 = m_3 + m_4^a + m_4^c$ of which the CoM S'_3 can be defined with e'_3 and f'_3 as illustrated, which are calculated as

$$e'_3 = \frac{m_3 e_3 + m_4^a l_3}{m_3 + m_4^a + m_4^c} \quad f'_3 = \frac{m_3 f_3 - m_4^c l_3}{m_3 + m_4^a + m_4^c} \quad (4.28)$$

With these combined masses, the mechanism of the relative motion of DoF 1 with the masses of the principal vector links included is shown in Fig. 4.16. The linear momentum of this motion can be written with respect to the x_1y_1 -frame as

$$\frac{\bar{L}_1}{\dot{\theta}_1} = \begin{bmatrix} m'_1(a_1 + p_1) + (m_{11} + m_{33})a_1 + \\ m_{12}(a_1 - p_{12}) + m_{13}(a_1 - p_{13}) \\ -m'_1 q_1 + m_{12}q_{12} + m_{13}q_{13} \end{bmatrix} = \begin{bmatrix} m_{tot}a_1 \\ 0 \end{bmatrix} \quad (4.29)$$

with $m_{tot} = m_1 + m_2 + m_3 + m_4 + m_{11} + m_{12} + m_{13} + m_{31} + m_{32} + m_{33}$ the total mass of the mechanism. From these equations two force balance conditions are obtained as

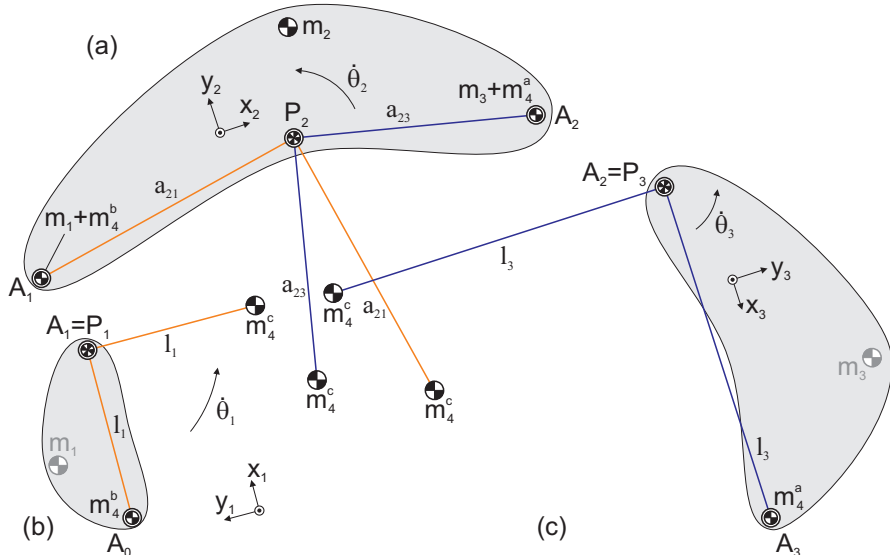


Fig. 4.14 ELMSSs when $a_1 \rightarrow 0$ and $a_3 \rightarrow 0$ for which S becomes an invariant point in A_1A_2 . The results show the projection of the virtual equivalent mass for analysis with method of rotations about principal joints A_1 and A_2 .

$$\begin{aligned} m'_1 p_1 &= (m_1 - m'_1 + m_2 + m_3 + m_4 + m_{31} + m_{32}) a_1 + m_{12} p_{12} + m_{13} p_{13} \\ m'_1 q_1 &= m_{12} q_{12} + m_{13} q_{13} \end{aligned} \quad (4.30)$$

The relative motion for DoF 3 is shown in Fig. 4.17 of which the linear momentum can be written with respect to the x_3y_3 -frame as

$$\frac{\bar{L}_3}{\dot{\theta}_3} = \begin{bmatrix} m'_3(a_3 + p_3) + (m_{31} + m_{13})a_3 + \\ m_{32}(a_3 - p_{32}) + m_{33}(a_3 - p_{33}) \\ m'_3 q_3 - m_{32} q_{32} - m_{33} q_{33} \end{bmatrix} = \begin{bmatrix} m_{tot} a_1 \\ 0 \end{bmatrix} \quad (4.31)$$

with which the two force balance conditions for DoF 3 become

$$\begin{aligned} m'_3 p_3 &= (m_1 + m_2 + m_3 - m'_3 + m_4 + m_{11} + m_{12}) a_1 + m_{32} p_{32} + m_{33} p_{33} \\ m'_3 q_3 &= m_{32} q_{32} + m_{33} q_{33} \end{aligned} \quad (4.32)$$

The relative motion of DoF 2 is shown in Fig. 4.18. The ELMS for this motion can be derived as shown in Fig. 4.19, where the linear momentum of m_1 , m_4^b , m_{11} , and m_4^c in J_{21} are equal with respect to the $x_{21}y_{21}$ -frame, the linear momentum of m_3 , m_4^a , m_{31} , and m_4^c in J_{22} are equal with respect to the $x_{23}y_{23}$ -frame, and the linear momentum of m_2 is equal with respect to the x_2y_2 -frame for rotation of the ELMS about P_2 .

Since the linear momentum of DoF 2 is zero for force balance, in Fig. 4.19 P_2 is the CoM of all masses. As compared to Fig. 3.13, here N_1 is the CoM of $m_1 + m_4^b$ in A_1 , m_4^c in J_{21} , and m_{11} and N_2 is the CoM of $m_3 + m_4^a$ in A_2 , m_4^c in J_{22} , and m_{31} . Both points lay on lines extended from the parallelogram between P_2 and m_2 . The conditions for force balance for this DoF can be found from Fig. 4.19 as in Fig. 3.14 and write

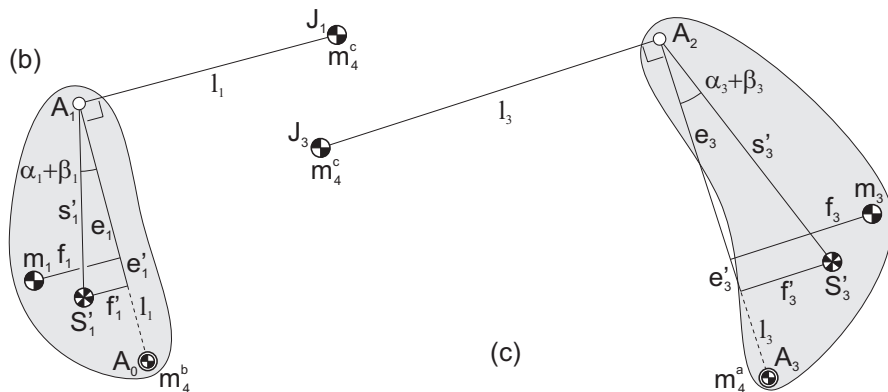


Fig. 4.15 For analysis of DoF 1 and DoF 3 with the method of rotations about principal joints, the masses in element 1 and in element 3 can be combined.

$$\begin{aligned} m_2 p_2^a &= (m_1 + m_4^b) a_{21} + m_{11} p_{11} & m_2 q_2^a &= m_{11} q_{11} + m_4^c a_{21} \\ m_2 p_2^b &= (m_3 + m_4^a) a_{23} + m_{31} p_{31} & m_2 q_2^b &= m_{31} q_{31} + m_4^c a_{23} \end{aligned} \quad (4.33)$$

With m'_1 , m'_3 , m'_4^a , m'_4^b , and m'_4^c substituted in (4.30), (4.32), and in the four linear conditions (4.33), the eight force balance conditions of the mechanism in Fig. 4.11 result in:

$$\begin{aligned} (m_1 + m_4(\frac{e_4}{l_4} + \frac{f_4}{l_4})) p_1 &= (m_2 + m_3 + m_{31} + m_{32} + m_4(1 - \frac{e_4}{l_4} - \frac{f_4}{l_4})) a_1 + \\ &\quad m_{12} p_{12} + m_{13} p_{13} \\ (m_1 + m_4(\frac{e_4}{l_4} + \frac{f_4}{l_4})) q_1 &= m_{12} q_{12} + m_{13} q_{13} \\ m_2 p_2^a &= (m_1 + m_4 \frac{e_4}{l_4}) a_{21} + m_{11} p_{11} \\ m_2 q_2^a &= m_{11} q_{11} + m_4 \frac{f_4}{l_4} a_{21} \\ m_2 p_2^b &= (m_3 + m_4(1 - \frac{e_4}{l_4})) a_{23} + m_{31} p_{31} \\ m_2 q_2^b &= m_{31} q_{31} + m_4 \frac{f_4}{l_4} a_{23} \\ (m_3 + m_4(1 - \frac{e_4}{l_4} + \frac{f_4}{l_4})) p_3 &= (m_1 + m_2 + m_{11} + m_{12} + m_4(\frac{e_4}{l_4} - \frac{f_4}{l_4})) a_3 + \\ &\quad m_{32} p_{32} + m_{33} p_{33} \\ (m_3 + m_4(1 - \frac{e_4}{l_4} + \frac{f_4}{l_4})) q_3 &= m_{32} q_{32} + m_{33} q_{33} \end{aligned} \quad (4.34)$$

Similarly to (3.16), with $s_1'^2 = e_1'^2 + f_1'^2$ and $s_3'^2 = e_3'^2 + f_3'^2$ a_1 and a_3 can be derived as

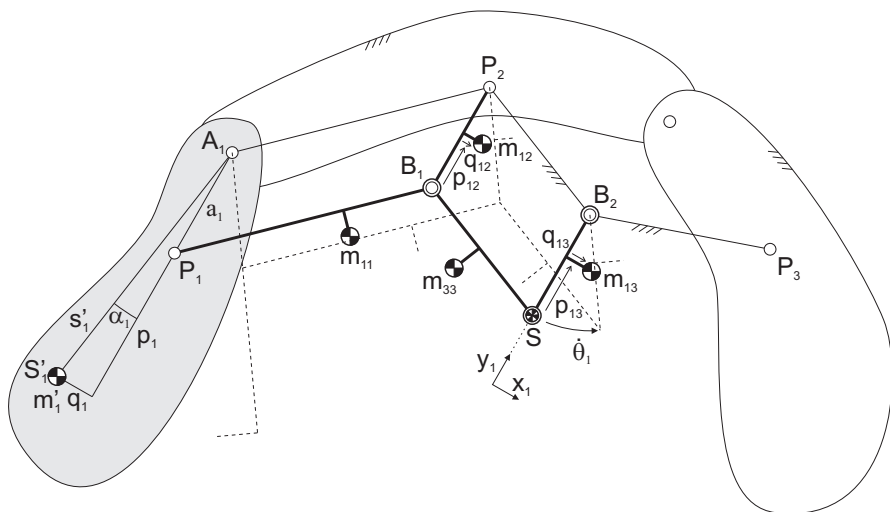


Fig. 4.16 Relative motion of MEPC DoF 1 of which the linear momentum of the moving masses equals the linear momentum of the total mass moving in S to obtain two force balance conditions.

$$a_1 = \frac{\sqrt{m_1'^2 s_1'^2 - (m_{12}q_{12} + m_{13}q_{13})^2} - m_{12}p_{12} - m_{13}p_{13}}{m_1 + m_2 + m_3 + m_4 + m_{31} + m_{32}} \quad (4.35)$$

$$a_3 = \frac{\sqrt{m_3'^2 s_3'^2 - (m_{32}q_{32} + m_{33}q_{33})^2} - m_{32}p_{32} - m_{33}p_{33}}{m_1 + m_2 + m_3 + m_4 + m_{11} + m_{12}}$$

and the location of P_1 in A_0A_1 can be obtained similarly to (4.8) as:

$$b_1 = a_1 \frac{(a_1 + p_1)e'_1 + q_1 f'_1}{(a_1 + p_1)^2 + q_1^2} \quad c_1 = a_1 \frac{(a_1 + p_1)f'_1 - q_1 e'_1}{(a_1 + p_1)^2 + q_1^2} \quad (4.36)$$

while the location of P_3 in A_2A_3 is found as:

$$b_3 = a_3 \frac{(a_3 + p_3)e'_3 + q_3 f'_3}{(a_3 + p_3)^2 + q_3^2} \quad c_3 = a_3 \frac{(a_3 + p_3)f'_3 - q_3 e'_3}{(a_3 + p_3)^2 + q_3^2} \quad (4.37)$$

With $s'_1 \cos(\alpha_1) = a_1 + p_1$, $s'_1 \sin(\alpha_1) = q_1$, $s'_1'^2 = (a_1 + p_1)^2 + q_1^2$, $s'_3 \cos(\alpha_3) = a_3 + p_3$, $s'_3 \sin(\alpha_3) = q_3$, and $s'_3'^2 = (a_3 + p_3)^2 + q_3^2$, parameters b_1 , c_1 , b_3 , and c_3 can also be found as

$$b_1 = a_1 \frac{\cos(\alpha_1)e'_1 + \sin(\alpha_1)f'_1}{s'_1} \quad c_1 = a_1 \frac{\cos(\alpha_1)f'_1 - \sin(\alpha_1)e'_1}{s'_1} \quad (4.38)$$

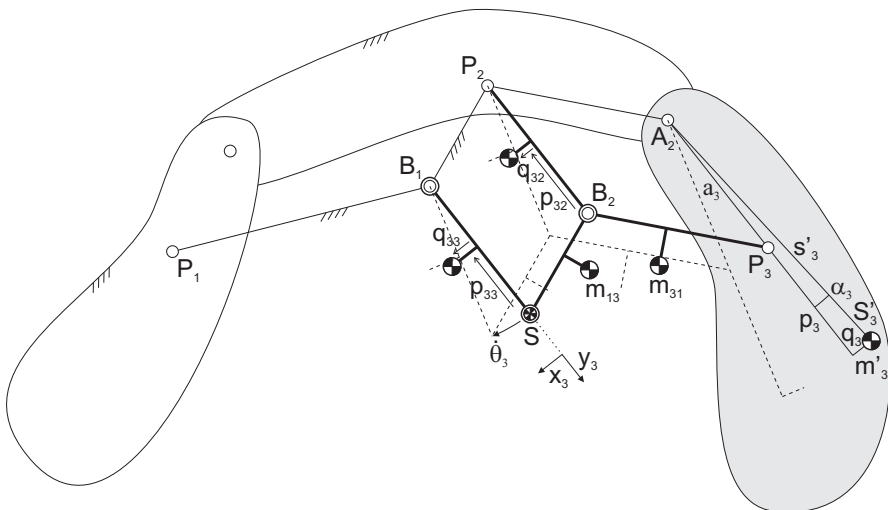


Fig. 4.17 Relative motion of MEPC DoF 3 of which the linear momentum of the moving masses equals the linear momentum of the total mass moving in S to obtain two force balance conditions.

$$b_3 = a_3 \frac{\cos(\alpha_3)e'_3 + \sin(\alpha_3)f'_3}{s'_3} \quad c_3 = a_3 \frac{\cos(\alpha_3)f'_3 - \sin(\alpha_3)e'_3}{s'_3}$$

with

$$\alpha_1 = \sin^{-1} \left(\frac{m_{12}q_{12} + m_{13}q_{13}}{m'_1 s'_1} \right) \quad \alpha_3 = \sin^{-1} \left(\frac{m_{32}q_{32} + m_{33}q_{33}}{m'_3 s'_3} \right) \quad (4.39)$$

To find the location of P_2 in A_1A_2 with b_{21} and c_2 , the linear momentum of the ELMS in Fig. 4.19 rotating about P_2 with respect to reference frame x_2y_2 , which has the x_2 -axis aligned with A_1A_2 , is written as

$$\begin{aligned} \frac{\bar{L}_2}{\dot{\theta}_2} &= \mu_{21} \begin{bmatrix} c_2 \\ -b_{21} \end{bmatrix} + v_{21} \begin{bmatrix} b_{21} \\ c_2 \end{bmatrix} + \mu_{22} \begin{bmatrix} c_2 - f_2 \\ -(b_{21} - e_2) \end{bmatrix} + \\ &\quad \mu_{23} \begin{bmatrix} c_2 \\ -(b_{21} - l_2) \end{bmatrix} - v_{23} \begin{bmatrix} b_{21} - l_2 \\ c_2 \end{bmatrix} = \begin{bmatrix} 0 \\ 0 \end{bmatrix} \end{aligned} \quad (4.40)$$

with $\mu_{21} = m_1 + m_4^b + m_{11}p_{11}/a_{21}$, $\mu_{22} = m_2$, $\mu_{23} = m_3 + m_4^a + m_{31}p_{31}/a_{23}$, $v_{21} = m_4^c + m_{11}q_{11}/a_{21}$, and $v_{23} = m_4^c + m_{31}q_{31}/a_{23}$. From these two equations the two linear force balance conditions for DoF 2 become

$$\begin{aligned} (\mu_{21} + \mu_{22} + \mu_{23})c_2 + (v_{21} - v_{23})b_{21} - \mu_{22}f_2 + v_{23}l_2 &= 0 \\ -(\mu_{21} + \mu_{22} + \mu_{23})b_{21} + (v_{21} - v_{23})c_2 + \mu_{22}e_2 + \mu_{23}l_2 &= 0 \end{aligned} \quad (4.41)$$

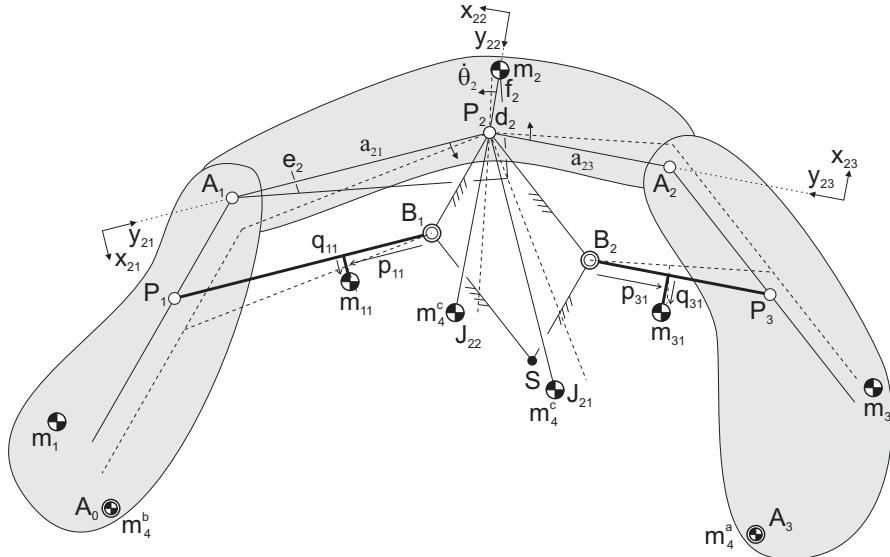


Fig. 4.18 Relative motion of MEPC DoF 2 of which the linear momentum of the moving masses equals zero to obtain the remaining force balance conditions.

from which b_{21} and c_2 result in

$$b_{21} = \frac{(\mu_{22}f_2 - v_{23}l_2)(v_{21} - v_{23}) + (\mu_{22}e_2 + \mu_{23}l_2)(\mu_{21} + \mu_{22} + \mu_{23})}{(\mu_{21} + \mu_{22} + \mu_{23})^2 + (v_{21} - v_{23})^2} \quad (4.42)$$

$$c_2 = \frac{(\mu_{22}f_2 - v_{23}l_2)(\mu_{21} + \mu_{22} + \mu_{23}) - (\mu_{22}e_2 + \mu_{23}l_2)(v_{21} - v_{23})}{(\mu_{21} + \mu_{22} + \mu_{23})^2 + (v_{21} - v_{23})^2}$$

With (3.35) and (3.36) b_{21} and c_2 are found in terms of principal vectors too.

So far, the analysis of the relative DoFs in this section was considered with rotations of DoF 1 and DoF 3 about the principal joints. If the individual motions of DoF 1 and DoF 3 are analyzed with rotations about the principal points P_1 and P_3 as in Fig. 3.9 and Fig. 3.10, respectively, then the ELMS of each DoF becomes as in Fig. 4.20. In addition to the ELMSs in Fig. 4.13b and Fig. 4.13c, for DoF 1 in Fig. 4.20a m_{12} and m_{13} are included and for DoF 3 in Fig. 4.20b m_{32} and m_{33} are included.

These ELMSs are of similar composition as the ELMS of DoF 2 in Fig. 4.19. The force balance conditions for DoF 1 can be obtained from the linear momentum equations of the ELMS in Fig. 4.20a rotating about P_1 , which writes with respect to reference frame x_1y_1 , which has the x_1 -axis aligned with A_0A_1 , as

$$\frac{\bar{L}_1}{\dot{\theta}_1} = \mu_{11} \begin{bmatrix} c_1 \\ b_1 - l_1 \end{bmatrix} + \mu_{12} \begin{bmatrix} c_1 - f_1 \\ b_1 - e_1 \end{bmatrix} + v_{12} \begin{bmatrix} l_1 \\ 0 \end{bmatrix} + \mu_{13} \begin{bmatrix} c_1 \\ b_1 \end{bmatrix} - v_{13} \begin{bmatrix} -b_1 \\ c_1 \end{bmatrix} = \begin{bmatrix} 0 \\ 0 \end{bmatrix} \quad (4.43)$$

with $\mu_{11} = m_4^b$, $\mu_{12} = m_1$, $\mu_{13} = m_2 + m_3 + m_{31} + m_{32} + m_4^a + m_{12}p_{12}/a_1 + m_{13}p_{13}/a_1$, $v_{12} = m_4^c$, and $v_{13} = m_{12}q_{12}/a_1 + m_{13}q_{13}/a_1$. The force balance conditions for DoF 3 can be obtained from the linear momentum equations of the ELMS in Fig. 4.20b rotating about P_3 , which writes with respect to reference frame x_3y_3 , which has the x_3 -axis aligned with A_2A_3 , as

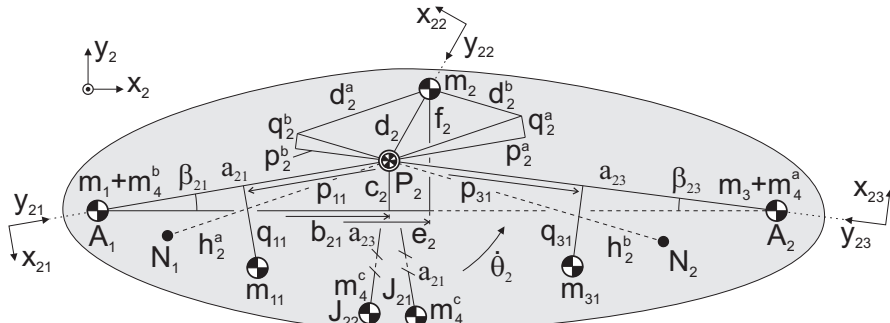


Fig. 4.19 ELMS of the relative motion of DoF 2. N_1 is the CoM of $m_1 + m_4^b$ in A_1 , m_4^c in J_{21} and m_{11} and N_2 is the CoM of $m_3 + m_4^a$ in A_2 , m_4^c in J_{22} , and m_{31} . With P_2 as CoM of the model, from the parallelogram with sides d_2^a and d_2^b the force balance conditions can be written directly.

$$\begin{aligned} \bar{\theta}_3 &= \mu_{31} \begin{bmatrix} c_3 \\ -b_3 \end{bmatrix} + v_{31} \begin{bmatrix} b_3 \\ c_3 \end{bmatrix} + \mu_{32} \begin{bmatrix} c_3 - f_3 \\ e_3 - b_3 \end{bmatrix} + v_{32} \begin{bmatrix} l_3 \\ 0 \end{bmatrix} + \mu_{33} \begin{bmatrix} c_3 \\ l_3 - b_3 \end{bmatrix} = \begin{bmatrix} 0 \\ 0 \end{bmatrix} \end{aligned} \quad (4.44)$$

with $\mu_{31} = m_1 + m_2 + m_{11} + m_{12} + m_4^b + m_{32}p_{32}/a_3 + m_{33}p_{33}/a_3$, $\mu_{32} = m_3$, $\mu_{33} = m_4^a$, $v_{31} = m_{32}q_{32}/a_3 + m_{33}q_{33}/a_3$, and $v_{32} = m_4^c$. From these linear momentum equations and (4.40) the force balance conditions of the mechanism in Fig. 4.11 are obtained with analysis of the relative motions about the principal points as:

$$\begin{aligned} (\mu_{11} + \mu_{12} + \mu_{13})c_1 + v_{13}b_1 - \mu_{12}f_1 + v_{12}l_1 &= 0 \\ (\mu_{11} + \mu_{12} + \mu_{13})b_1 - v_{13}c_1 - \mu_{12}e_1 - \mu_{11}l_1 &= 0 \\ (\mu_{21} + \mu_{22} + \mu_{23})c_2 + (v_{21} - v_{23})b_{21} - \mu_{22}f_2 + v_{23}l_2 &= 0 \quad (4.45) \\ -(\mu_{21} + \mu_{22} + \mu_{23})b_{21} + (v_{21} - v_{23})c_2 + \mu_{22}e_2 + \mu_{23}l_2 &= 0 \\ (\mu_{31} + \mu_{32} + \mu_{33})c_3 + v_{31}b_3 - \mu_{32}f_3 + v_{32}l_3 &= 0 \\ -(\mu_{31} + \mu_{32} + \mu_{33})b_3 + v_{31}c_3 + \mu_{32}e_3 + \mu_{33}l_3 &= 0 \end{aligned}$$

From these conditions b_1 and c_1 can be derived as

$$\begin{aligned} b_1 &= \frac{(\mu_{12}f_1 - v_{12}l_1)v_{13} + (\mu_{12}e_1 + \mu_{11}l_1)(\mu_{11} + \mu_{12} + \mu_{13})}{(\mu_{11} + \mu_{12} + \mu_{13})^2 + v_{13}^2} \quad (4.46) \\ c_1 &= \frac{(\mu_{12}f_1 - v_{12}l_1)(\mu_{11} + \mu_{12} + \mu_{13}) - (\mu_{12}e_1 + \mu_{11}l_1)v_{13}}{(\mu_{11} + \mu_{12} + \mu_{13})^2 + v_{13}^2} \end{aligned}$$

and b_3 and c_3 can be derived as

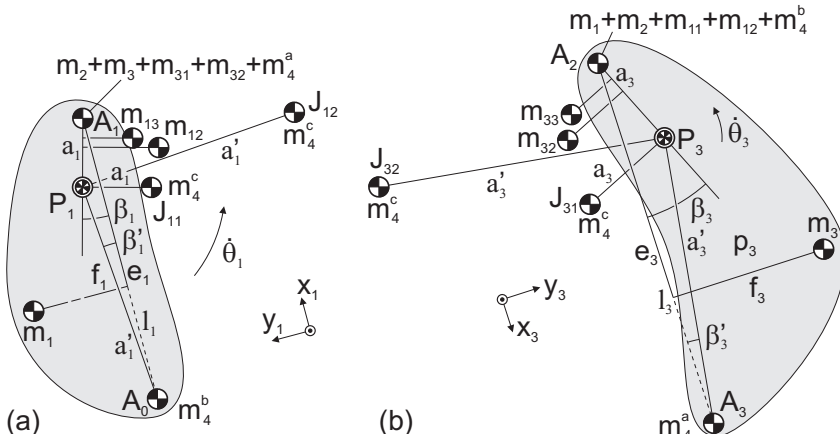


Fig. 4.20 ELMS for analysis of rotations about the principal points (a) P_1 and (b) P_3 , which are of similar structure as the ELMS of DoF 2 in Fig. 4.19.

$$b_3 = \frac{(\mu_{32}f_3 - v_{32}l_3)v_{31} + (\mu_{32}e_3 + \mu_{33}l_3)(\mu_{31} + \mu_{32} + \mu_{33})}{(\mu_{31} + \mu_{32} + \mu_{33})^2 + v_{31}^2} \quad (4.47)$$

$$c_3 = \frac{(\mu_{32}f_3 - v_{32}l_3)(\mu_{31} + \mu_{32} + \mu_{33}) - (\mu_{32}e_3 + \mu_{33}l_3)v_{31}}{(\mu_{31} + \mu_{32} + \mu_{33})^2 + v_{31}^2}$$

To validate the results, the principal vector linkage in Fig. 4.11 was modeled with the multi-body dynamic simulation software package Spacar¹. With Matlab the parameters of the mechanism were calculated as in Table 4.1. The parameters in the first four columns were chosen with which the parameters in the last column were calculated. With SpaScripting the parameters were transformed from Matlab into a dynamic model in Spacar in which the only connection with the base is a pivot in S.

The simulation of the dynamic model is illustrated in Fig. 4.21 with two poses of the mechanism. For the simulation time of 0.5 seconds a torque $\tau_1 = 50 \cos(4\pi t)$ Nm was applied to element SB_1 and a torque $\tau_2 = -\tau_1$ was applied to element SB_2 . The dynamics were solved with solver ODE45 (Dormand-Prince) with a maximal step size of 0.0001 s and with a relative tolerance of $1e^{-12}$ m. The reaction forces in the pivot with the base were recorded and are displayed in Fig. 4.22. These shaking forces are expected to be zero for force balance and show an error which is about the computation accuracy. Figure 4.23 shows the linear momentum of the mechanism in both x and y-direction which are also expected to be zero for force balance and have an error which is about the computation accuracy.

In the remainder of this section it is shown that when S of the mechanism in Fig. 4.11 is an invariant point in A_0A_3 as in Fig. 4.24, from the force balance conditions (4.34) the force balance conditions (2.29/4.17) of the 4R four-bar mechanism can be derived.

As in Fig. 4.5, for movability of the mechanism in Fig. 4.24 the quadrilaterals $A_0A_1A_2A_3$, $A_0P_1B_1S$, and $SB_2P_3A_3$ are similar with the conditions (4.18). With massless principal vector links and $q_1 = q_3 = 0$, the force balance conditions (4.34) can be rewritten as

Table 4.1 Parameters of the principal vector linkage in Fig. 4.11 for simulation

[m]	[kg]	[m]	[m]	[m]
$l_1 = 1.0$	$m_1 = 2.10$	$e_1 = 0.69$	$f_1 = 0.21$	$a_1 = 0.2206$
$l_2 = 3.0$	$m_2 = 3.00$	$e_2 = 1.80$	$f_2 = 0.93$	$b_1 = 0.2161$
$l_3 = 2.0$	$m_3 = 2.20$	$e_3 = 1.30$	$f_3 = 0.84$	$c_1 = 0.0439$
$l_4 = 3.2$	$m_4 = 1.10$	$e_4 = 1.312$	$f_4 = 0.10$	$a_{21} = 1.6838$
	$m_{11} = 0.20$	$p_{11} = 1.00$	$q_{11} = 0.20$	$a_{23} = 1.3770$
	$m_{12} = 0.10$	$p_{12} = 0.12$	$q_{12} = 0.09$	$b_{21} = 1.6565$
	$m_{13} = 0.11$	$p_{13} = 0.10$	$q_{13} = 0.10$	$c_2 = 0.3018$
	$m_{31} = 0.20$	$p_{31} = 0.85$	$q_{31} = 0.20$	$a_3 = 0.5140$
	$m_{32} = 0.105$	$p_{32} = 0.25$	$q_{32} = 0.08$	$b_3 = 0.4734$
	$m_{33} = 0.09$	$p_{33} = 0.27$	$q_{33} = 0.10$	$c_3 = 0.2004$

¹ <http://www.spacar.nl/>

$$\begin{aligned}
p_1 &= \frac{(m_2 + m_3 + m_4(1 - \frac{e_4}{l_4} - \frac{f_4}{l_4}))a_1}{m_1 + m_4(\frac{e_4}{l_4} + \frac{f_4}{l_4})} & p_3 &= \frac{(m_1 + m_2 + m_4(\frac{e_4}{l_4} - \frac{f_4}{l_4}))a_3}{m_3 + m_4(1 - \frac{e_4}{l_4} + \frac{f_4}{l_4})} \\
p_2^a &= \frac{(m_1 + m_4 \frac{e_4}{l_4})a_{21}}{m_2} & q_2^a &= \frac{m_4 \frac{f_4}{l_4}a_{21}}{m_2} \\
p_2^b &= \frac{(m_3 + m_4(1 - \frac{e_4}{l_4}))a_{23}}{m_2} & q_2^b &= \frac{m_4 \frac{f_4}{l_4}a_{23}}{m_2}
\end{aligned} \tag{4.48}$$

When these equations are substituted in (3.35), (3.36), (4.36), and (4.37), parameters b_1 , c_1 , b_{21} , c_2 , b_3 , and c_3 become

$$\begin{aligned}
b_1 &= \frac{m_1 e_1 + m_4 \frac{e_4}{l_4} l_1}{m_1 + m_2 + m_3 + m_4} & c_1 &= \frac{m_1 f_1 - m_4 \frac{f_4}{l_4} l_1}{m_1 + m_2 + m_3 + m_4} \\
b_{21} &= \frac{m_2 e_2 + m_3 l_2 + m_4(1 - \frac{e_4}{l_4})l_2}{m_1 + m_2 + m_3 + m_4} & c_2 &= \frac{m_2 f_2 - m_4 \frac{f_4}{l_4} l_2}{m_1 + m_2 + m_3 + m_4} \\
b_3 &= \frac{m_3 e_3 + m_4(1 - \frac{e_4}{l_4})l_3}{m_1 + m_2 + m_3 + m_4} & c_3 &= \frac{m_3 f_3 - m_4 \frac{f_4}{l_4} l_3}{m_1 + m_2 + m_3 + m_4}
\end{aligned} \tag{4.49}$$

Parameters b_1 , c_1 , b_3 , and c_3 can also be derived from the relations

$$\begin{aligned}
b_1^2 + c_1^2 &= a_1^2 & b_3^2 + c_3^2 &= a_3^2 \\
(l_1 - b_1)^2 + c_1^2 &= a_1'^2 & (l_3 - b_3)^2 + c_3^2 &= a_3'^2
\end{aligned} \tag{4.50}$$

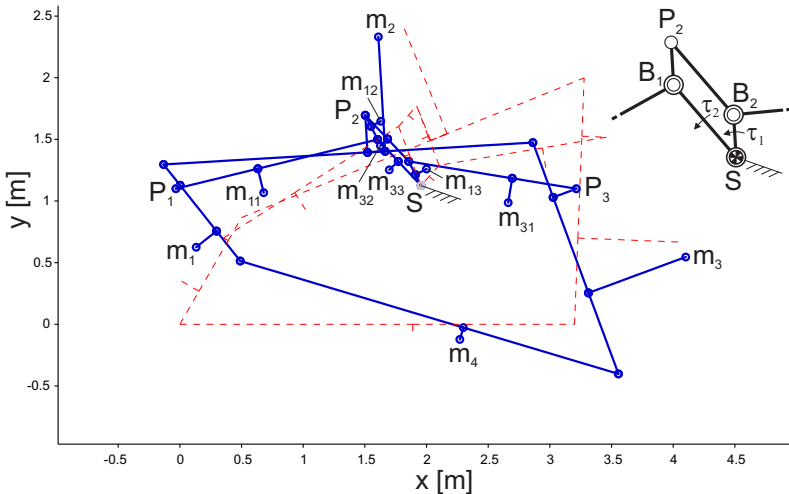


Fig. 4.21 Dynamic simulation in Spacar of the mechanism in Fig. 4.11 where S is a pivot with the base. A torque τ_1 was applied to element SB_1 and a torque τ_2 was applied to element SB_2 .

where the principal dimensions can be written from (4.18) to depend on a_{21} and a_{23} as

$$a_1 = \frac{a_{23}l_1}{l_2} \quad a_3 = \frac{a_{21}l_3}{l_2} \quad a'_1 = \frac{a_{21}l_1}{l_2} \quad a'_3 = \frac{a_{23}l_3}{l_2} \quad (4.51)$$

for which these parameters result in

$$\begin{aligned} b_1 &= \frac{l_1}{2} \left(1 - \frac{a_{21}^2}{l_2^2} + \frac{a_{23}^2}{l_2^2} \right) & c_1 &= \frac{l_1}{2} \sqrt{\frac{4a_{23}^2}{l_2^2} - \left(1 - \frac{a_{21}^2}{l_2^2} + \frac{a_{23}^2}{l_2^2} \right)^2} \\ b_3 &= \frac{l_3}{2} \left(1 + \frac{a_{21}^2}{l_2^2} - \frac{a_{23}^2}{l_2^2} \right) & c_3 &= \frac{l_3}{2} \sqrt{\frac{4a_{21}^2}{l_2^2} - \left(1 + \frac{a_{21}^2}{l_2^2} - \frac{a_{23}^2}{l_2^2} \right)^2} \end{aligned} \quad (4.52)$$

The principal dimensions a_{21} and a_{23} are calculated as

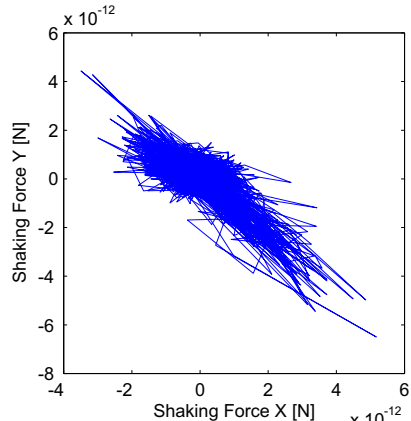


Fig. 4.22 The resulting shaking forces in pivot S show that the mechanism is force balanced about S .

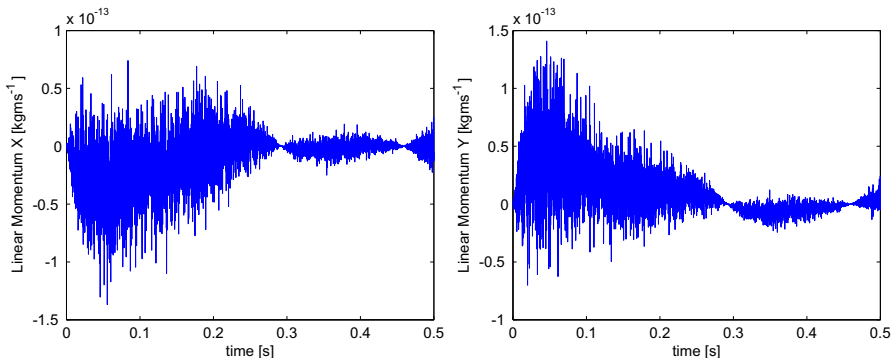


Fig. 4.23 The linear momentum in both x and y -direction, which were calculated from the simulated motion, show force balance about S .

$$a_{21}^2 = b_{21}^2 + c_2^2 = \frac{(m_2 e_2 + m_3 l_2 + m_4(1 - \frac{e_4}{l_4})l_2)^2 + (m_2 f_2 - m_4 \frac{f_4}{l_4}l_2)^2}{(m_1 + m_2 + m_3 + m_4)^2} \quad (4.53)$$

$$a_{23}^2 = (l_2 - b_{21})^2 + c_2^2 = \frac{((m_1 + m_4 \frac{e_4}{l_4})l_2 + m_2(l_2 - e_2))^2 + (m_2 f_2 - m_4 \frac{f_4}{l_4}l_2)^2}{(m_1 + m_2 + m_3 + m_4)^2}$$

which leads after substitution in (4.22) and (4.52) to

$$\begin{aligned} b_1 &= l_1 \frac{m_1 + m_2(1 - \frac{e_2}{l_2}) + m_4 \frac{e_4}{l_4}}{m_1 + m_2 + m_3 + m_4} & c_1 &= l_1 \frac{m_2 \frac{f_2}{l_2} - m_4 \frac{f_4}{l_4}}{m_1 + m_2 + m_3 + m_4} \\ b_3 &= l_3 \frac{m_2 \frac{e_2}{l_2} + m_3 + m_4(1 - \frac{e_4}{l_4})}{m_1 + m_2 + m_3 + m_4} & c_3 &= l_3 \frac{m_2 \frac{f_2}{l_2} - m_4 \frac{f_4}{l_4}}{m_1 + m_2 + m_3 + m_4} \\ o_1 &= l_4 \frac{m_1 + m_2(1 - \frac{e_2}{l_2}) + m_4 \frac{e_4}{l_4}}{m_1 + m_2 + m_3 + m_4} & o_2 &= -l_4 \frac{m_2 \frac{f_2}{l_2} - m_4 \frac{f_4}{l_4}}{m_1 + m_2 + m_3 + m_4} \end{aligned} \quad (4.54)$$

Combining (4.52) and (4.54) then leads to the equations

$$\begin{aligned} m_1(l_1 - e_1) + m_2(1 - \frac{e_2}{l_2})l_1 &= 0 & m_1 f_1 - m_2 \frac{f_2}{l_2} l_1 &= 0 \\ m_3(l_3 - e_3) + m_2 \frac{e_2}{l_2} l_3 &= 0 & m_3 f_3 - \frac{m_2 f_2}{l_2} l_3 &= 0 \\ m_{tot}(l_4 - o_1) - m_2 \frac{e_2}{l_2} l_4 - m_3 l_4 - m_4(l_4 - e_4) &= 0 & m_{tot} o_2 + m_2 \frac{f_2}{l_2} l_4 - m_4 f_4 &= 0 \end{aligned} \quad (4.55)$$

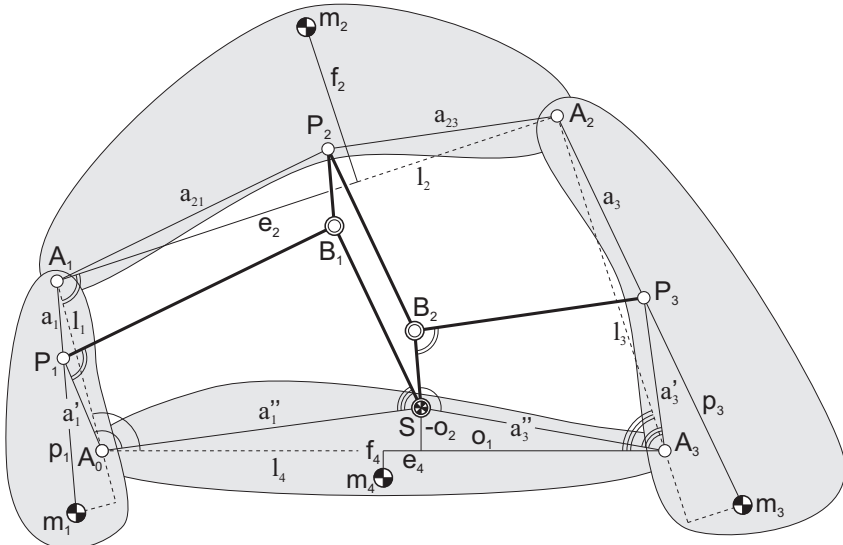


Fig. 4.24 With the common CoM S of the four elements as invariant point in element A_0A_3 , the linkage in Fig. 4.11 represents a generally force-balanced four-bar linkage.

with $m_{tot} = m_1 + m_2 + m_3 + m_4$. It is verified that these equations are equal to the force balance conditions (4.17).

4.5 Principal vector linkages of closed chains of n elements

In the previous section a closed-chain principal vector linkage of four elements was analyzed as a MEPC of three principal elements. This method can also be applied to closed chains of higher number of elements. In general, a principal vector linkage of a closed chain of n elements can be analyzed as an open-chain principal vector linkage of $n - 1$ principal elements, which is illustrated in Fig. 4.25. Therefore element n is taken out of the chain and is modeled with the three equivalent masses m_n^a , m_n^b , and m_n^c according to Fig. 4.10. These equivalent masses are projected on the open-chain principal vector linkage of $n - 1$ principal elements as in Fig. 4.12a which then becomes a MEPC. Then real equivalent mass m_n^a is located in joint A_{n-1} , real equivalent mass m_n^b is located in joint A_0 , and virtual equivalent mass m_n^c is located once about each principal point according to Fig. 4.10b, or twice about each principal point according to Fig. 4.10c. Herewith element n is included for the calculation of the principal dimensions and the location of the principal points P_i for each relative DoF i .

In the ELMS of each relative DoF the equivalent masses appear systematically as shown in Fig. 4.26. Practically it can be regarded also as that a set of m_n^b and m_n^c follows the loop from the left side, appearing similarly in each subsequent ELMS, and that a set of m_n^a and m_n^c follows the loop from the right side, also appearing similarly in each subsequent ELMS.

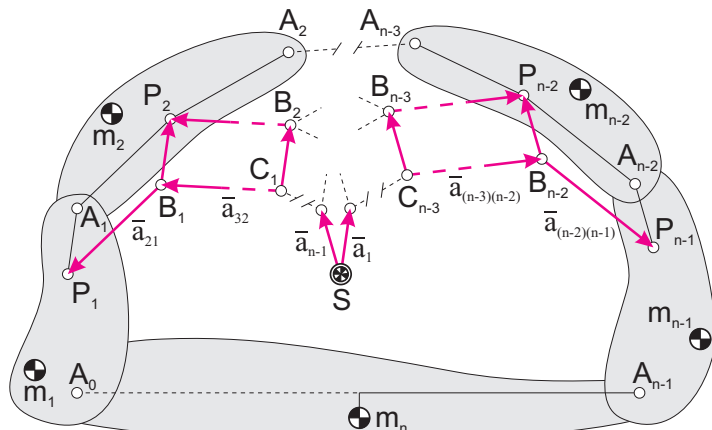


Fig. 4.25 Closed chains of n elements can be analyzed as an open-chain principal vector linkage of $n - 1$ principal elements.

When for the analysis of relative DoF 1 and relative DoF $n - 1$ the method of rotations about the principal joints A_1 and A_{n-1} is used, then the virtual equivalent mass in principal element 1 and $n - 1$ has a location which does not depend on the principal vectors as shown in Fig. 4.27. Therefore it can be combined with the other masses in the element as in Fig. 4.15, which showed a convenient way to derive the force balance conditions.

4.6 Discussion and conclusion

In this chapter principal vector linkages of closed kinematic chains were found and investigated. With the open-chain method, closed-chain principal vector linkages were obtained by closing open-chain principal vector linkages. This was shown for an open-chain principal vector linkage of four principal elements of which the outer principal elements were connected with a pivot. This is also possible for principal vector linkages of higher number of principal elements. In addition, with the open-chain method it is also possible to connect the outer principal elements to inner principal elements or to principal vector links or to connect inner elements together, especially for mechanisms with many DoFs. Instead of connecting elements with a pivot, also other connections such as sliders are possible without affecting the force balance.

The method of mass equivalent principal chains was proposed to find inherent closed-chain principal vector linkages where the loop closure relations are considered. Therefore it was proposed to model an element with a general CoM with

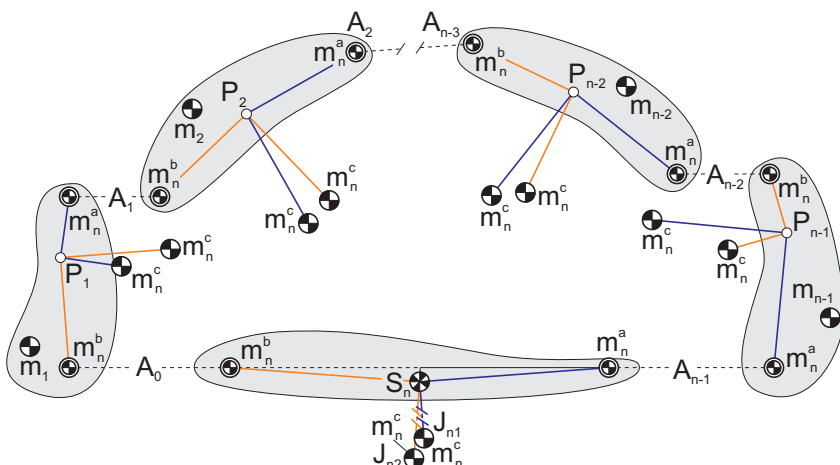


Fig. 4.26 Appearance of the equivalent masses m_n^a , m_n^b , and m_n^c of element n in the ELMS of each relative DoF i for analysis with rotations about the principal points P_i .

equivalent masses of which two are referred to as a real equivalent mass and one is referred to as a virtual equivalent mass. Then one of the elements can be taken out of the closed chain by projecting its equivalent masses on the open-chain principal vector linkage of the remaining elements, which then is a mass equivalent principal chain.

For analysis of each DoF individually of the mass equivalent principal chain, the virtual equivalent mass has the property that it acts as a real mass in elements for rotational motion, while it has no mass in elements for translational motion. This property implies that the virtual equivalent mass is solely related to rotational motion. This can also be observed from the equivalent mass model. For translational motion an element with a general CoM can be modeled solely with one or more real equivalent masses and no virtual equivalent mass is required. For rotational motion however a virtual equivalent mass is required to model an element with a general CoM with two joints.

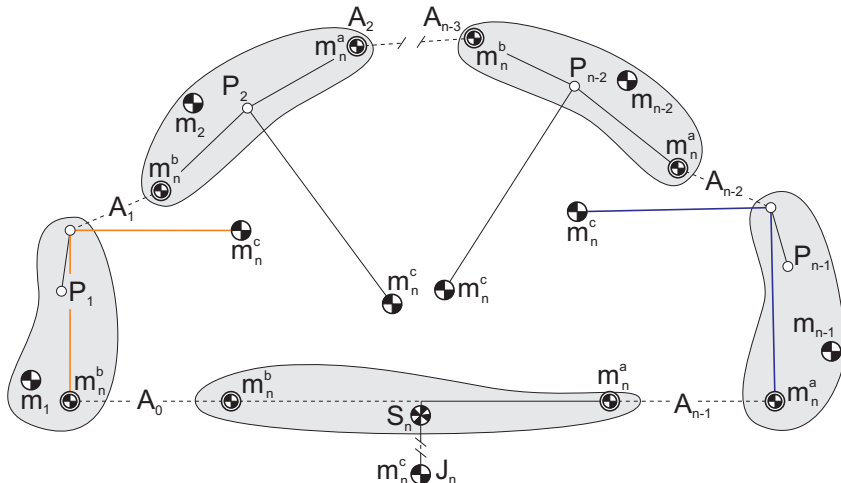
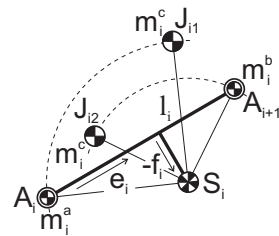


Fig. 4.27 Appearance of the equivalent masses of element n in the ELMS of the first and the last relative DoF for analysis with rotations about principal joints A_1 and A_{n-2} .

Fig. 4.28 Illustration of a mass equivalent model of which parameter f_i has a negative value. Then also m_i^c is negative and the CoM of the model still is in S_i .



When parameter f_i in Fig. 4.10 has a negative value, the mass equivalent model of Fig. 4.10c becomes as in Fig. 4.28. Since from (4.25) the value for m_i^c then is also negative, the CoM of the model still is in S_i .

With a multi-body dynamic simulation the results were verified. From the closed-chain principal vector linkages the force balance conditions of the general planar 4R four-bar mechanism were derived, both as they are known and in terms of principal dimensions.

Also inherent closed-chain principal vector linkages with principal elements in parallel are possible. Figure 4.29 shows how the principal vector linkage in Fig. 3.30 is closed with element A_4A_5 between principal elements 11 and 12, and with element A_6A_7 between principal elements 12 and 13. The principal elements are arranged as a six-bar linkage with two closed loops. To find the force balance conditions, each loop can be considered independently as a single closed chain where elements A_4A_5 and A_6A_7 can be modeled with equivalent masses. The projection of the equivalent masses then will show that about the principal points P_1 and P_{21} two different virtual equivalent masses are modeled, one from each closed chain.

Also for inherent closed-chain principal vector linkages it is possible to have inner and outer elements connected with various means. The following chapter will

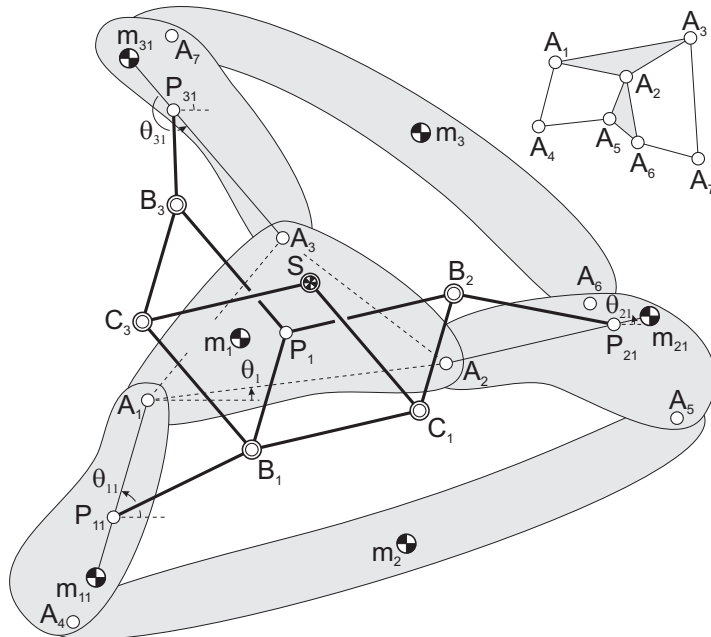


Fig. 4.29 The principal vector linkage in Fig. 3.30 can be closed with the two elements A_4A_5 and A_6A_7 which can be modeled with equivalent masses to obtain the force balance conditions of this closed-chain principal vector linkage of a six-bar linkage with two closed loops.

show a specific example of this where multiple closed loops of inner and outer elements are considered.

Chapter 5

Principal vector linkage architecture with similar linkages

Abstract The motion of the CoM of a mechanism can be described with a point in a mechanism similar to it. In this chapter the principal vector linkage of a closed chain of four elements is combined with such a similar mechanism with which various theories from literature come together and are generalized. The conditions for similarity of this principal vector linkage architecture are derived in terms of principal dimensions. Subsequently the principal dimensions are calculated by means of a mass equivalent principal chain. For three closed loops, three elements are modeled with each two real equivalent masses and one virtual equivalent mass. With this it is shown that also elements with more than two joints are modeled with only two real equivalent masses, which are located in the joints of the considered loop.

5.1 Architecture with CoM in invariant point in a similar linkage

It is shown by Kreutzinger [69] that the common CoM of the three moving links of a 4R four-bar linkage with mass-symmetric links describes a curve with respect to the base link that is similar to a coupler curve of the mechanism. The common CoM therefore is a coupler point in a similar 4R four-bar linkage moving synchronously (see Fig. A.7b). Wunderlich [109] extended this theory by showing that in general the common CoM of the three moving links of a 4R four-bar linkage with general mass distributions describes a curve similar to a coupler curve of the mechanism. This is illustrated in Fig. 5.1 where S is the common CoM of m_1 , m_2 , and m_3 and is an invariant point in element A_5A_6 of the four-bar linkage $A_4A_5A_6A_7$, which is similar and moves synchronously with the four-bar linkage $A_0A_1A_2A_3$. The trajectory of S with respect to base link A_0A_3 is similar to the trajectory of point T in element A_1A_2 .

With respect to linkage $A_0A_1A_2A_3$, linkage $A_4A_5A_6A_7$ is similar and is scaled with a factor η and is rotated with an angle γ . With angle $\rho = \angle TA_1A_2 = \angle SA_5A_6$, point T is located in element A_1A_2 at a distance εl_2 from A_1 and at an angle ρ relative to

line A_1A_2 , while point S is located in element A_5A_6 at a distance $\eta \varepsilon l_2 = \varepsilon l_6$ from A_5 at an angle ρ relative to line A_5A_6 .

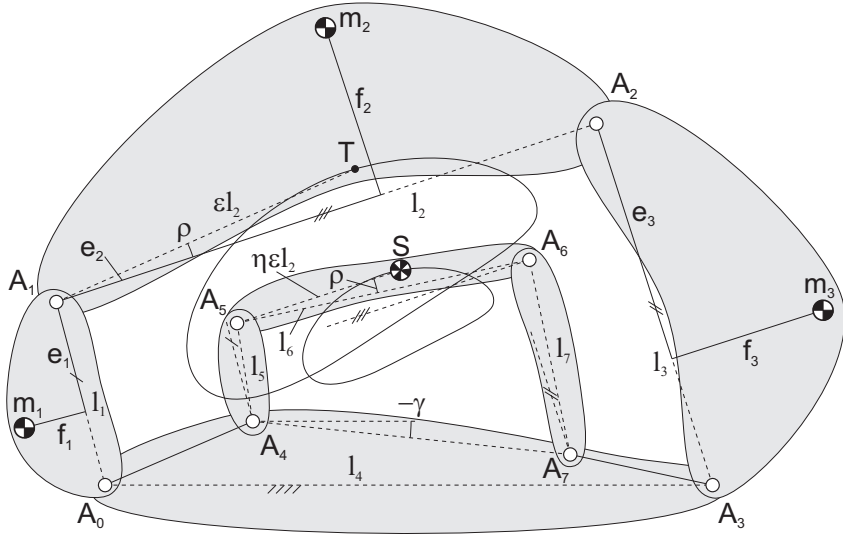


Fig. 5.1 The CoM of general 4R four-bar linkage is an invariant point in the coupler link of a similar 4R four-bar linkage moving synchronously which describes a curve similar to the curve of point T in A_1A_2 .

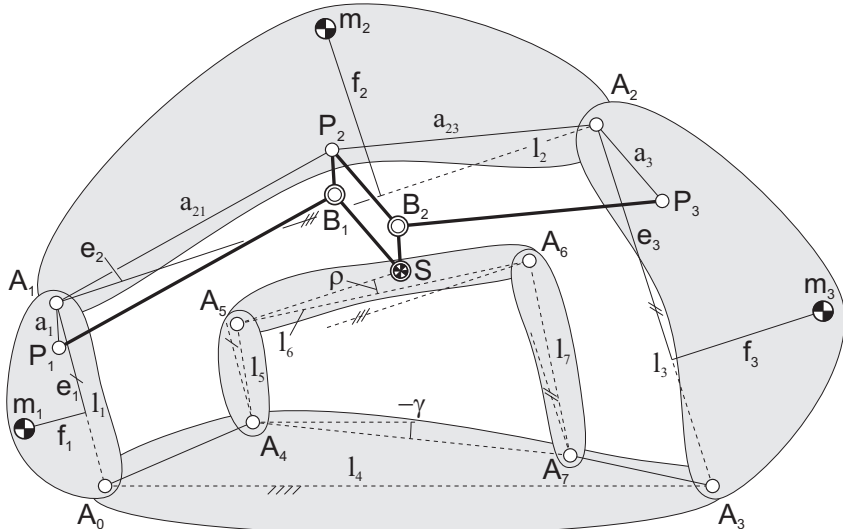


Fig. 5.2 Combination of the similar linkage and the principal vector linkage which have a common joint in the common CoM in S with which the linkage has one DoF with respect to A_0A_3 .

Kreutzinger [69] derived his finding by using a graphical construction of principal vectors. When this graphical construction is transformed into a linkage and is generalized for a 4R four-bar linkage with elements with general CoM, the combined mechanism of a principal vector linkage and a similar linkage is obtained as illustrated in Fig. 5.2. With S as a common joint between the principal vector linkage and the similar linkage, the complete mechanism has one DoF with respect to A_0A_3 .

Shchepetil'nikov [87] proposed a method that he named the *method of double contour transformation* to construct similar linkages for accurate graphical analysis of the motion of the common CoM. This method is based on principal vectors too and it was applied to linkages with mass-symmetric links. When generalized for elements with general CoM, one solution of a *double contour* is illustrated in Fig. 5.3. Here principal vector link P_1B_1 is extended with B_1C_1 to obtain parallelogram $SB_1C_1A_6$ where C_1 is a joint with element A_6A_7 and distance A_6C_1 equals principal dimension a_3 . Linkages $P_1C_1A_7$ and $A_6A_5A_4$ then are the said *double contours* of the initial linkage $A_0A_1A_2A_3$ with which similar linkage $A_4A_5A_6A_7$ is obtained. A second solution of a double contour linkage is shown in Fig. 5.4 where principal vector link P_3B_2 is extended with B_2C_2 to obtain parallelogram $SA_5C_2B_2$ where C_2 is a joint with element A_4A_5 and distance A_5C_2 equals principal dimension a_1 .

To constrain the motion of the linkages to be similar, it is also possible to include elements D_8E_8 or D_9E_9 as illustrated in Fig. 5.5. Points D_8 and E_8 can be located arbitrarily within elements A_0A_1 and A_4A_5 , respectively, as long as $A_0D_8E_8A_4$ is a

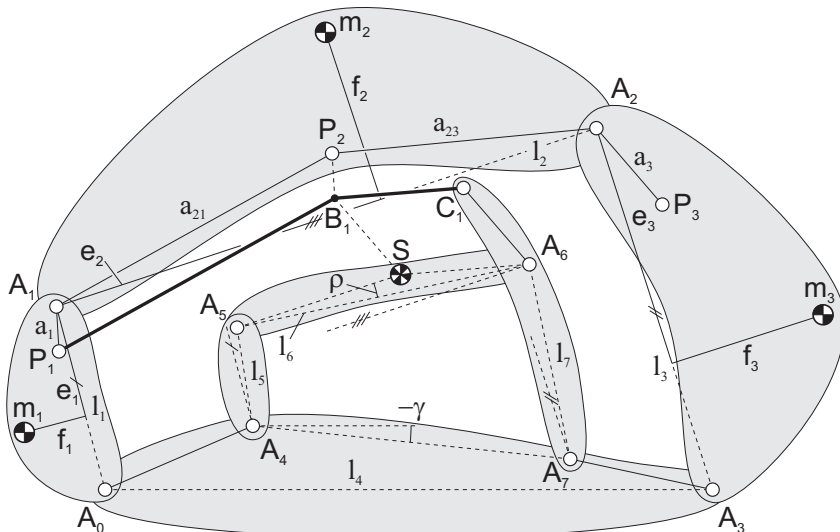


Fig. 5.3 Generalized double contour linkage where principal vector link P_1B_1 is extended with B_1C_1 where C_1 is a joint with element A_6A_7 .

parallelogram and points D_9 and E_9 can be located arbitrarily within elements A_2A_3 and A_6A_7 , respectively, as long as $A_3A_7E_9D_9$ is a parallelogram.

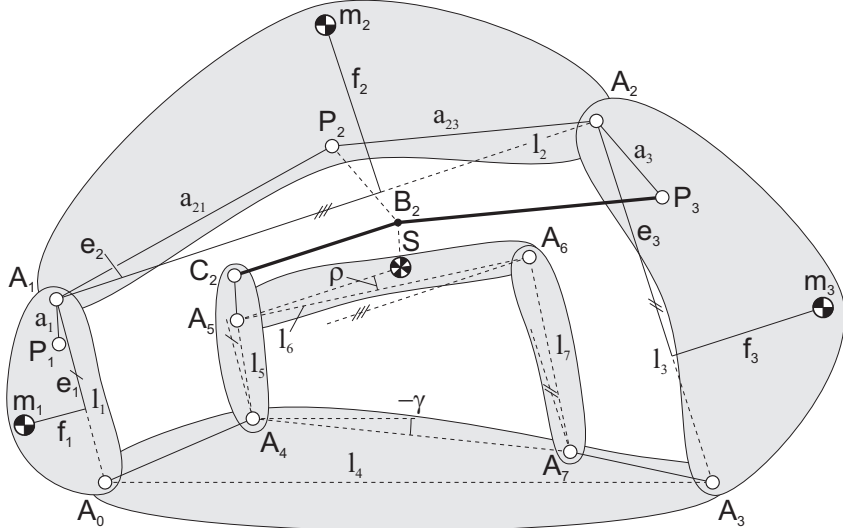


Fig. 5.4 A second solution of a generalized double contour linkage where principal vector link P_3B_2 is extended with B_2C_2 where C_2 is a joint with element A_4A_5 .

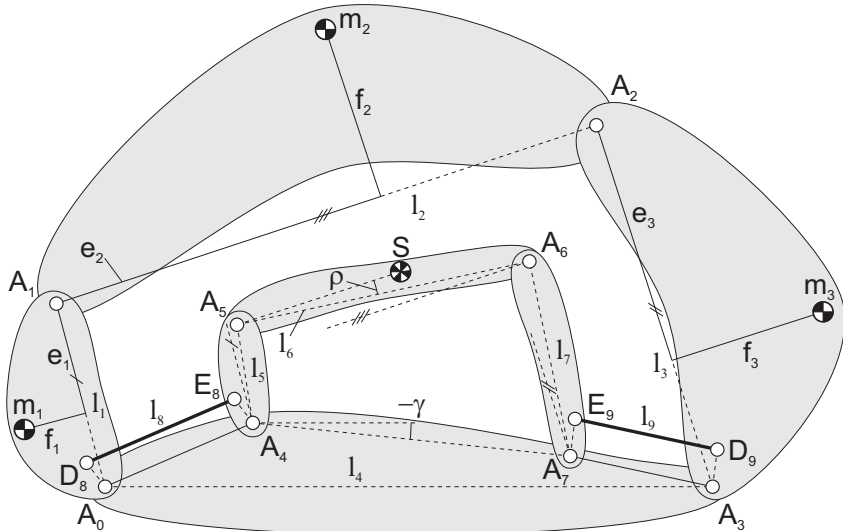


Fig. 5.5 To constrain the motion of the linkages to be similar, also a link D_8E_8 or a link D_9E_9 can be included which form the parallelograms $A_0D_8E_8A_4$ and $A_3A_7E_9D_9$, respectively.

5.2 Conditions for similarity

In this section the conditions for similarity of the two linkages are derived in terms of principal dimensions. When the principal dimensions then are calculated from the mass properties of each element, the design of the principal vector linkage architecture is determined.

Figure 5.6 shows how the position of S can be described along a closed loop with the complex vectors \bar{u}_i , \bar{v}_i , and \bar{w}_i as

$$\overline{A_0S} = \bar{v}_1\bar{u}_1 + \bar{v}_2\bar{u}_2 + \bar{v}_3\bar{u}_3 = \bar{w}_1\bar{u}_4 + \bar{w}_2\bar{u}_1 + \bar{w}_3\bar{u}_2 \quad (5.1)$$

Vectors \bar{u}_i are the time dependent vectors that describe the motion of the relative positions of joints A_0, A_1, A_2 , and A_3 and vectors \bar{v}_i are the principal vectors $\bar{v}_1 = \bar{d}'_1$, $\bar{v}_2 = -\bar{a}_{21}$, and $\bar{v}_3 = -\bar{a}_3$. Vectors \bar{w}_i describe the size and the pose of the similar linkage with respect to linkage $A_0A_1A_2A_3$. From Fig. 5.6 the principal vectors can be written as

$$\begin{aligned}\bar{v}_1 &= \frac{l_1 - a_1 \cos \beta_1}{l_1} + \frac{a_1 \sin \beta_1}{l_1} i = \frac{l_1 - b_1}{l_1} + \frac{c_1}{l_1} i \\ \bar{v}_2 &= \frac{a_{21} \cos \beta_{21}}{l_2} + \frac{a_{21} \sin \beta_{21}}{l_2} i = \frac{b_{21}}{l_2} + \frac{c_2}{l_2} i \\ \bar{v}_3 &= \frac{a_3 \cos \beta_3}{l_3} + \frac{a_3 \sin \beta_3}{l_3} i = \frac{b_3}{l_3} + \frac{c_3}{l_3} i\end{aligned} \quad (5.2)$$

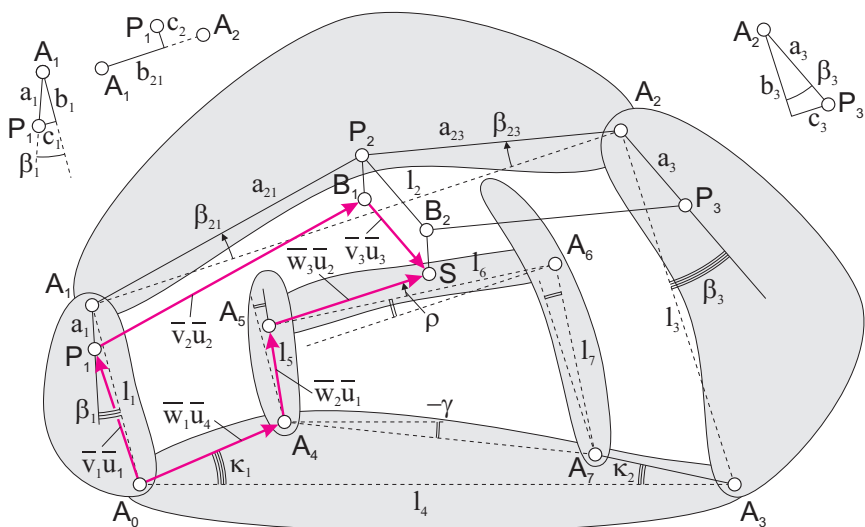


Fig. 5.6 The position of S is described with principal vectors \bar{v}_i , time dependent vectors \bar{u}_i , and similar linkage vectors \bar{w}_i .

with $\cos \beta_1 = b_1/a_1$, $\sin \beta_1 = c_1/a_1$, $\cos \beta_{21} = b_{21}/a_{21}$, $\sin \beta_{21} = c_{21}/a_{21}$, $\cos \beta_3 = b_3/a_3$, and $\sin \beta_3 = c_3/a_3$. The vectors of the similar linkage \bar{w}_i can be written as

$$\bar{w}_1 = \kappa_1^R + \kappa_1^I i \quad \bar{w}_2 = \gamma^R + \gamma^I i \quad \bar{w}_3 = \bar{w}_2(\rho^R + \rho^I i) \quad (5.3)$$

where κ_1^R and κ_1^I are the real and imaginary part of angle $\kappa_1 = \angle A_4A_0A_3$, γ^R and γ^I are the real and imaginary part of angle γ , and ρ^R and ρ^I are the real and imaginary part of angle ρ . The loop closure equation can be written as $\bar{u}_1 + \bar{u}_2 + \bar{u}_3 = \bar{u}_4$ and when substituted for \bar{u}_4 , (5.1) can be rewritten as

$$(\bar{v}_1 - \bar{w}_1 - \bar{w}_2)\bar{u}_1 + (\bar{v}_2 - \bar{w}_1 - \bar{w}_3)\bar{u}_2 + (\bar{v}_3 - \bar{w}_1)\bar{u}_3 = 0 \quad (5.4)$$

After substitution of (5.2) and (5.3) this equation results in

$$\begin{aligned} & \left\{ \left(1 - \frac{a_1 \cos \beta_1}{l_1} - \kappa_1^R - \gamma^R \right) + \left(\frac{a_1 \sin \beta_1}{l_1} - \kappa_1^I - \gamma^I \right) i \right\} \bar{u}_1 + \\ & \left\{ \left(\frac{a_{21} \cos \beta_{21}}{l_2} - \kappa_1^R - \gamma^R \rho^R + \gamma^I \rho^I \right) + \left(\frac{a_{21} \sin \beta_{21}}{l_2} - \kappa_1^I - \gamma^R \rho^I - \gamma^I \rho^R \right) i \right\} \bar{u}_2 + \\ & \left\{ \left(\frac{a_3 \cos \beta_3}{l_3} - \kappa_1^R \right) + \left(\frac{a_3 \sin \beta_3}{l_3} - \kappa_1^I \right) i \right\} \bar{u}_3 = 0 \end{aligned} \quad (5.5)$$

From this equation all conditions for similarity can be derived. Since in general the time dependent vectors \bar{u}_i are not linearly related or zero, this equation only holds when each of the three terms is zero. This means that each of the three real parts and each of the three imaginary parts are zero. From the term of \bar{u}_3 then κ_1^R , κ_1^I , and κ_1 are derived as

$$\begin{aligned} \kappa_1^R &= \frac{a_3 \cos \beta_3}{l_3} = \frac{b_3}{l_3} \quad \kappa_1^I = \frac{a_3 \sin \beta_3}{l_3} = \frac{c_3}{l_3} \\ \kappa_1 &= \tan^{-1} \left(\frac{\kappa_1^I}{\kappa_1^R} \right) = \tan^{-1} \left(\frac{c_3}{b_3} \right) = \beta_3 \end{aligned} \quad (5.6)$$

As a result, κ_1 is found to be equal to β_3 . By substituting these results in the term of \bar{u}_1 , from this term being zero γ^R , γ^I , and γ are found as

$$\begin{aligned} \gamma^R &= 1 - \frac{a_1 \cos \beta_1}{l_1} - \frac{a_3 \cos \beta_3}{l_3} = 1 - \frac{b_1}{l_1} - \frac{b_3}{l_3} \\ \gamma^I &= \frac{a_1 \sin \beta_1}{l_1} - \frac{a_3 \sin \beta_3}{l_3} = \frac{c_1}{l_1} - \frac{c_3}{l_3} \\ \gamma &= \tan^{-1} \left(\frac{\gamma^I}{\gamma^R} \right) = \tan^{-1} \left(\frac{\frac{a_1}{l_1} \sin \beta_1 - \frac{a_3}{l_3} \sin \beta_3}{1 - \frac{a_1}{l_1} \cos \beta_1 - \frac{a_3}{l_3} \cos \beta_3} \right) = \tan^{-1} \left(\frac{\frac{c_1}{l_1} - \frac{c_3}{l_3}}{1 - \frac{b_1}{l_1} - \frac{b_3}{l_3}} \right) \end{aligned} \quad (5.7)$$

With γ^R and γ^I the scale factor η of the similar linkage is calculated as

$$\begin{aligned}\eta &= \sqrt{(\gamma^R)^2 + (\gamma^I)^2} = \sqrt{(1 - \frac{a_1}{l_1} \cos \beta_1 - \frac{a_3}{l_3} \cos \beta_3)^2 + (\frac{a_1}{l_1} \sin \beta_1 - \frac{a_3}{l_3} \sin \beta_3)^2} \\ &= \frac{\sqrt{((l_3 - b_3)l_1 - b_1l_3)^2 + (c_1l_3 - c_3l_1)^2}}{l_1l_3}\end{aligned}\quad (5.8)$$

The lengths of the links of the similar linkage then are related as

$$\eta = \frac{l_5}{l_1} = \frac{l_6}{l_2} = \frac{l_7}{l_3} = \frac{\|\overline{A_4A_7}\|}{l_4} \quad (5.9)$$

By substituting κ_1^R , κ_1^I , γ^R , and γ^I in the term of \bar{u}_2 , from this term being zero ρ^R , ρ^I , and ρ are obtained as

$$\begin{aligned}\rho^R &= \frac{(1 - \frac{a_1 \cos \beta_1}{l_1} - \frac{a_3 \cos \beta_3}{l_3})(\frac{a_{21} \cos \beta_{21}}{l_2} - \frac{a_3 \cos \beta_3}{l_3}) + (\frac{a_1 \sin \beta_1}{l_1} - \frac{a_3 \sin \beta_3}{l_3})(\frac{a_{21} \sin \beta_{21}}{l_2} - \frac{a_3 \sin \beta_3}{l_3})}{(1 - \frac{a_1 \cos \beta_1}{l_1} - \frac{a_3 \cos \beta_3}{l_3})^2 + (\frac{a_1 \sin \beta_1}{l_1} - \frac{a_3 \sin \beta_3}{l_3})^2} \\ \rho^I &= \frac{(1 - \frac{a_1 \cos \beta_1}{l_1} - \frac{a_3 \cos \beta_3}{l_3})(\frac{a_{21} \sin \beta_{21}}{l_2} - \frac{a_3 \sin \beta_3}{l_3}) - (\frac{a_1 \sin \beta_1}{l_1} - \frac{a_3 \sin \beta_3}{l_3})(\frac{a_{21} \cos \beta_{21}}{l_2} - \frac{a_3 \cos \beta_3}{l_3})}{(1 - \frac{a_1 \cos \beta_1}{l_1} - \frac{a_3 \cos \beta_3}{l_3})^2 + (\frac{a_1 \sin \beta_1}{l_1} - \frac{a_3 \sin \beta_3}{l_3})^2} \\ \rho &= \tan^{-1} \left(\frac{\rho^I}{\rho^R} \right)\end{aligned}\quad (5.10)$$

or

$$\begin{aligned}\rho^R &= \frac{(1 - \frac{b_1}{l_1} - \frac{b_3}{l_3})(\frac{b_{21}}{l_2} - \frac{b_3}{l_3}) + (\frac{c_1}{l_1} - \frac{c_3}{l_3})(\frac{c_{21}}{l_2} - \frac{c_3}{l_3})}{(1 - \frac{b_1}{l_1} - \frac{b_3}{l_3})^2 + (\frac{c_1}{l_1} - \frac{c_3}{l_3})^2} \\ \rho^I &= \frac{(1 - \frac{b_1}{l_1} - \frac{b_3}{l_3})(\frac{c_{21}}{l_2} - \frac{c_3}{l_3}) - (\frac{c_1}{l_1} - \frac{c_3}{l_3})(\frac{b_{21}}{l_2} - \frac{b_3}{l_3})}{(1 - \frac{b_1}{l_1} - \frac{b_3}{l_3})^2 + (\frac{c_1}{l_1} - \frac{c_3}{l_3})^2} \\ \rho &= \tan^{-1} \left(\frac{(1 - \frac{b_1}{l_1} - \frac{b_3}{l_3})(\frac{c_{21}}{l_2} - \frac{c_3}{l_3}) - (\frac{c_1}{l_1} - \frac{c_3}{l_3})(\frac{b_{21}}{l_2} - \frac{b_3}{l_3})}{(1 - \frac{b_1}{l_1} - \frac{b_3}{l_3})(\frac{b_{21}}{l_2} - \frac{b_3}{l_3}) + (\frac{c_1}{l_1} - \frac{c_3}{l_3})(\frac{c_{21}}{l_2} - \frac{c_3}{l_3})} \right)\end{aligned}\quad (5.11)$$

With ρ^R and ρ^I the distance ε in Fig. 5.1 is calculated as

$$\varepsilon = \sqrt{(\rho^R)^2 + (\rho^I)^2} \quad (5.12)$$

and with κ_1 and γ known, from polygon $A_0A_3A_7A_4$ angle $\kappa_2 = \angle A_7A_3A_0$ can be derived as

$$\begin{aligned}\kappa_2^R &= 1 - \kappa_1^R - \gamma^R = \frac{a_1 \cos \beta_1}{l_1} = \frac{b_1}{l_1} \quad \kappa_2^I = \kappa_1^I + \gamma^I = \frac{a_1 \sin \beta_1}{l_1} = \frac{c_1}{l_1} \\ \kappa_2 &= \tan^{-1} \left(\frac{\kappa_2^I}{\kappa_2^R} \right) = \tan^{-1} \left(\frac{c_1}{b_1} \right) = \beta_1\end{aligned}\quad (5.13)$$

5.3 Force balance conditions from mass equivalent principal chain

The linkage architecture in Fig. 5.7 is obtained when the elements in Fig. 5.2-5.5 are combined and each element has a general CoM. For simplicity joint D_8 is chosen to be on the line A_0A_1 at a distance d_8 from A_0 and joint D_9 is chosen to be on the line A_2A_3 at a distance d_9 from A_3 . Then joint E_8 is located in A_4A_5 at a distance d_8 from A_4 such that $A_0D_8E_8A_4$ is a parallelogram and joint E_9 is located in A_6A_7 at a distance d_9 from A_7 such that $A_3A_7E_9D_9$ is a parallelogram. The linkage is five times overconstrained but because of its specific dimensions it has a mobility of one. From overconstrained balanced architectures a variety of inherently balanced mechanisms can be synthesized as will be shown in chapter 7.

The mass parameters of the closed-chain principal vector linkage are equal to Fig. 4.11. In addition, element A_4A_5 has a mass m_5 with its CoM defined with parameters e_5 and f_5 relative to A_5 and the line A_5A_4 , element A_5A_6 has a mass m_6 with its CoM defined with parameters e_6 and f_6 relative to A_5 and the line A_5A_6 , element A_6A_7 has a mass m_7 with its CoM defined with parameters e_7 and f_7 relative to A_6 and the line A_6A_7 , element D_8E_8 has a mass m_8 with its CoM defined with parameters e_8 and f_8 relative to D_8 and the line D_8E_8 , and element D_9E_9 has a mass m_9 with its CoM defined with parameters e_9 and f_9 relative to D_9 and the line D_9E_9 , as illustrated.

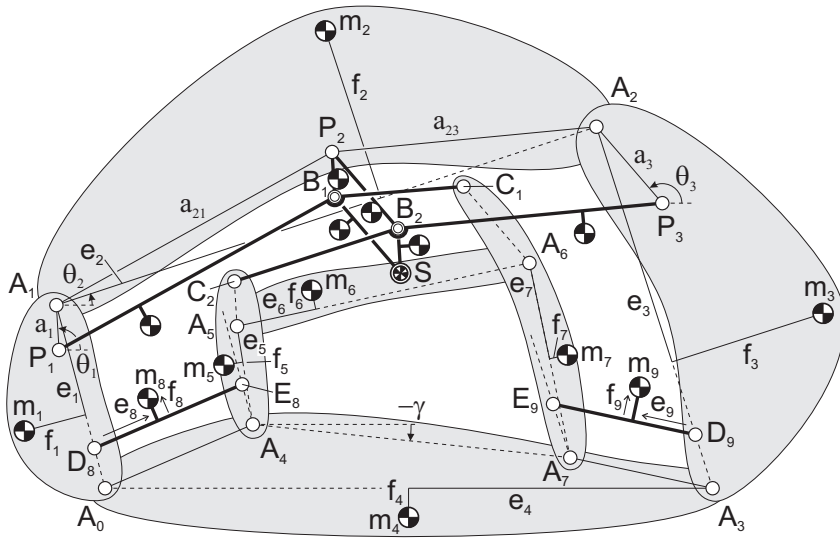


Fig. 5.7 Inherently balanced linkage architecture by combining the elements in Fig. 5.2-5.5 with each a general CoM. For all motion the common CoM of the linkage is in joint S , which is an invariant point in elements B_1S , B_2S , and A_5A_6 .

The force balance conditions can be derived following the same approach as in section 4.4 by analysis of the mass equivalent principal chain. Therefore elements that do not move similar to the principal elements, here elements A_0A_3 , D_8E_8 , and D_9E_9 , are modeled with equivalent masses while the similarly moving elements A_4A_5 , A_5A_6 , and A_6A_7 become part of the mass equivalent principal chain. Without the three mass equivalently modeled elements, the linkage in Fig. 5.7 has only closed loops of parallelograms that are related to the principal chain.

Fig. 5.8a shows how element D_8E_8 is modeled with a real equivalent mass $m_8^a = m_8(1 - e_8/l_8)$ located in joint D_8 , a real equivalent mass $m_8^b = m_8e_8/l_8$ located in joint E_8 , and a virtual equivalent mass $m_8^c = m_8f_8/l_8$ located in both J_{81} and J_{82} , according to the model in Fig. 4.10c. Similarly, Fig. 5.8b shows how element D_9E_9 is modeled with a real equivalent mass $m_9^a = m_9(1 - e_9/l_9)$ located in joint D_9 , a real equivalent mass $m_9^b = m_9e_9/l_9$ located in joint E_9 , and a virtual equivalent mass $m_9^c = m_9f_9/l_9$ located in both J_{91} and J_{92} . The mass equivalent model of element A_0A_3 is shown in Fig. 5.8c and is equal to the model in Fig. 4.12b with a real equivalent mass $m_4^a = m_4(1 - e_4/l_4)$ located in joint A_3 , a real equivalent mass $m_4^b = m_4e_4/l_4$ located in joint A_0 , and a virtual equivalent mass $m_4^c = m_4f_4/l_4$ located in both J_{41} and J_{42} .

The equivalent masses are projected on the open-chain principal vector linkage as illustrated in Fig. 5.9. The projection of m_4^a , m_4^b , and m_4^c are equal to Fig. 4.12a with m_4^a in joint A_3 , m_4^b in joint A_0 , and m_4^c twice about each principal point P_1 , P_2 , and P_3 . Equivalent masses m_8^a , m_8^b , m_9^a , and m_9^b are projected in joints D_8 , E_8 , D_9 , and E_9 , respectively. Following the loop on the left side from D_8 , virtual equivalent mass m_8^c is projected about P_1 and about P_2 as illustrated. Following the loop on the right side along $E_8A_5SB_2P_2P_1$, virtual equivalent mass m_8^c is projected about A_5 , S , B_2 , P_2 , and P_1 as illustrated. It is also possible to follow the loop along B_1 instead of

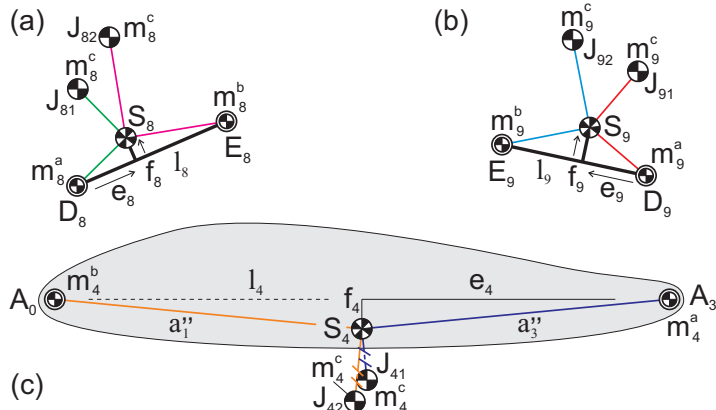


Fig. 5.8 Mass equivalent models of elements A_0A_3 , D_8E_8 , and D_9E_9 according to Fig. 4.10b with real equivalent masses m_4^a , m_4^b , m_8^a , m_8^b , m_9^a , and m_9^b and virtual equivalent masses m_4^c , m_8^c , and m_9^c .

B_2 which is effectively the same. As a result m_8^c is located twice about the principal points P_1 and P_2 .

Similarly the virtual equivalent mass of element D_9E_9 is projected. Following the loop on the right side from D_9 , m_9^c is projected about P_3 and about P_2 as illustrated. Following the loop on the left side along $E_9A_6SB_2P_2P_3$, m_9^c is projected about A_6 , S , B_2 , P_2 , and P_3 as illustrated. About P_2 and P_3 then m_9^c is located twice.

For analysis with the method of rotations about the principal joints A_1 and A_2 as a short way to derive the force balance conditions for DoF 1 and DoF 3, Fig. 5.10 shows the reduced projection of the virtual equivalent masses, derived similarly as in Fig. 4.14. In element 1 then one m_4^c and one m_8^c are located about A_1 and in element 3 one m_4^c and one m_9^c are located about A_2 .

Figure 5.11 shows for the relative motion of DoF 1 the virtual equivalent masses of the rotating elements A_0A_1 , A_4A_5 , and SB_2 which act as a real mass, while all other virtual masses are zero since elements A_5A_6 and A_6A_7 solely translate and elements A_1A_2 , A_2A_3 , and P_2B_2 are not moving. For the relative motion of DoF 3, Fig. 5.12 shows the virtual equivalent masses of the rotating elements A_2A_3 , A_6A_7 , and B_2P_2 which act as a real mass while all other virtual masses are zero since elements B_2S , A_5A_6 , and A_4A_5 solely translate and elements A_0A_1 and A_1A_2 are not moving. For the relative motion of DoF 2, Fig. 5.13 shows the virtual equivalent masses of the rotating elements A_1A_2 and A_4A_6 which act as a real mass while all other virtual masses are zero since elements A_0A_1 , A_2A_3 , A_4A_5 , and A_6A_7 solely translate and elements P_2B_2 and B_2S do not move.

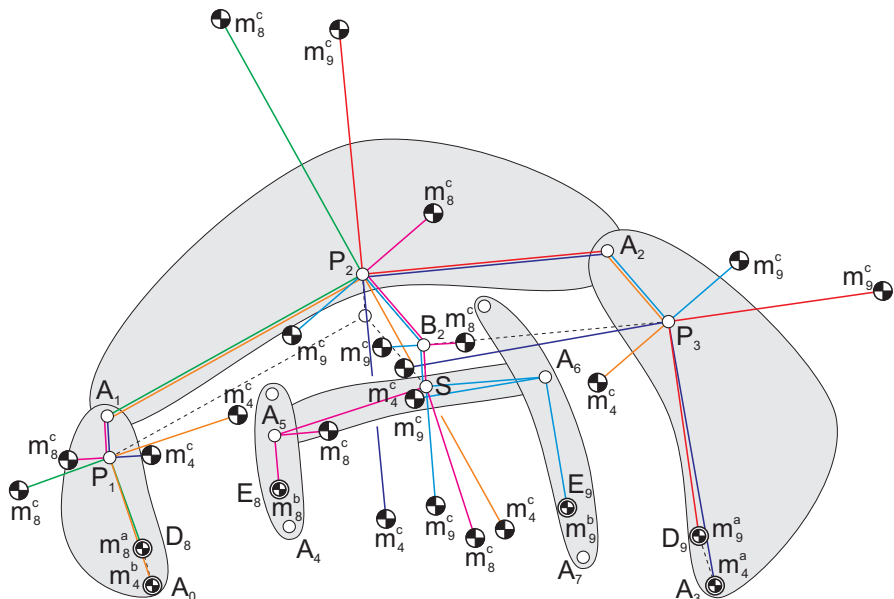


Fig. 5.9 Mass equivalent principal chain with the projection of the equivalent masses.

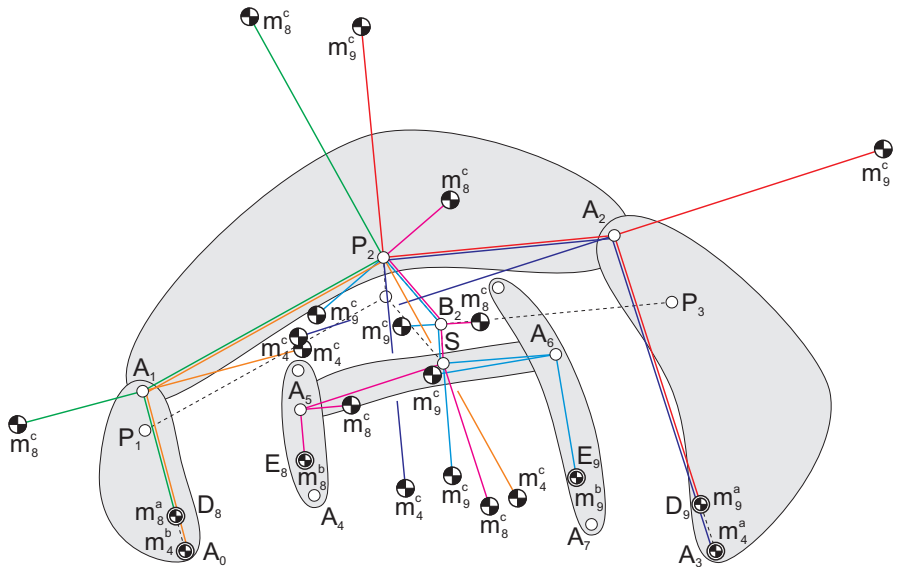


Fig. 5.10 Reduced projection of the virtual equivalent masses for analysis with the method of rotations about the principal joints A_1 and A_2 .

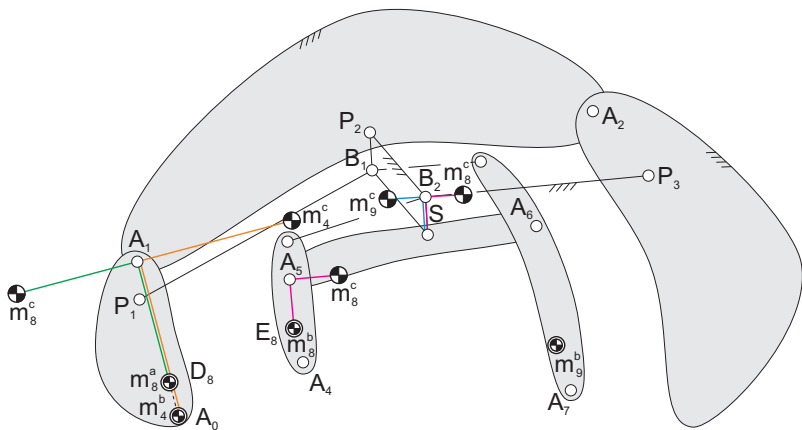


Fig. 5.11 Virtual equivalent masses that are nonzero for the relative motion of DoF 1.

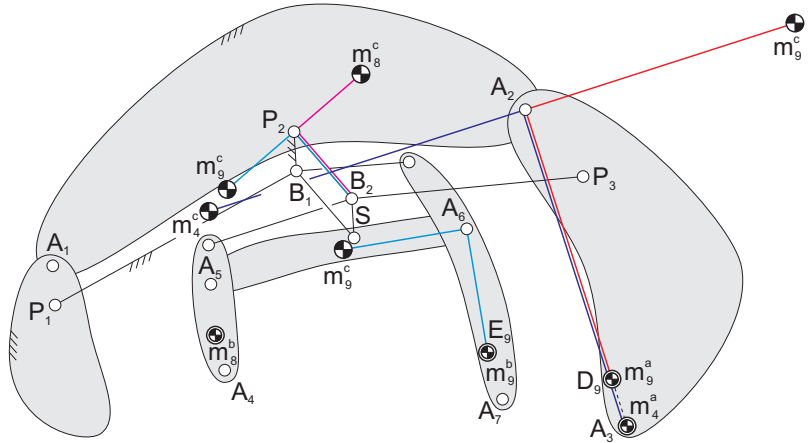


Fig. 5.12 Virtual equivalent masses that are nonzero for the relative motion of DoF 3.

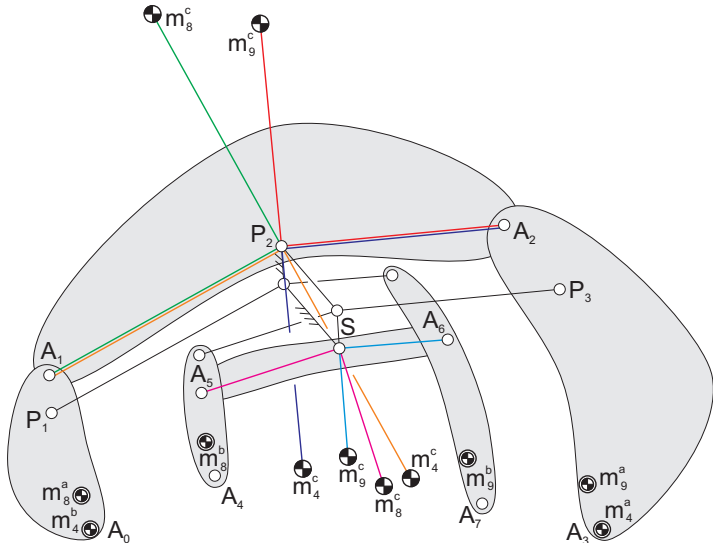


Fig. 5.13 Virtual equivalent masses that are nonzero for the relative motion of DoF 2.

Subsequently, the masses in element 1 for DoF 1 can be combined as shown in Fig. 5.14a. Then the mass $m'_1 = m_1 + m_4^b + m_4^c + m_8^a + m_8^c$ has its CoM in S'_1 , which is defined with e'_1 and f'_1 relative to A_1 and the line A_1A_0 as illustrated. These parameters are calculated as

$$e'_1 = \frac{m_1 e_1 + m_4^b l_1 + m_8^a (l_1 - d_8)}{m'_1} \quad f'_1 = \frac{m_1 f_1 - m_4^c l_1 + m_8^c (l_1 - d_8)}{m'_1} \quad (5.14)$$

When the masses in element 3 for DoF 3 are combined as in Fig. 5.14b, then the mass $m'_3 = m_3 + m_4^a + m_4^c + m_9^a + m_9^c$ has its CoM in S'_3 , which is defined with e'_3 and f'_3 relative to A_2 and the line A_2A_3 as illustrated. These parameters are calculated as

$$e'_3 = \frac{m_3 e_3 + m_4^a l_3 + m_9^a (l_3 - d_9)}{m'_3} \quad f'_3 = \frac{m_3 f_3 - m_4^c l_3 + m_9^c (l_3 - d_9)}{m'_3} \quad (5.15)$$

It is also possible to combine the masses in element 5 for DoF 1 as shown in Fig. 5.15a where the mass $m'_5 = m_5 + m_8^b + m_8^c$ has its CoM in S'_5 . When S'_5 is defined with e'_5 and f'_5 relative to A_5 and the line A_5A_4 , as illustrated, these parameters are calculated as

$$e'_5 = \frac{m_5 e_5 + m_8^b (l_5 - d_8 \cos \gamma) - m_8^c d_8 \sin \gamma}{m'_5} \quad (5.16)$$

$$f'_5 = \frac{m_5 f_5 - m_8^b d_8 \sin \gamma - m_8^c (l_5 - d_8 \cos \gamma)}{m'_5} \quad (5.17)$$

Similarly the masses in element 7 for DoF 3 can be combined as shown in Fig. 5.15b where the mass $m'_7 = m_7 + m_9^b + m_9^c$ has its CoM in S'_7 . When S'_7 is defined with e'_7

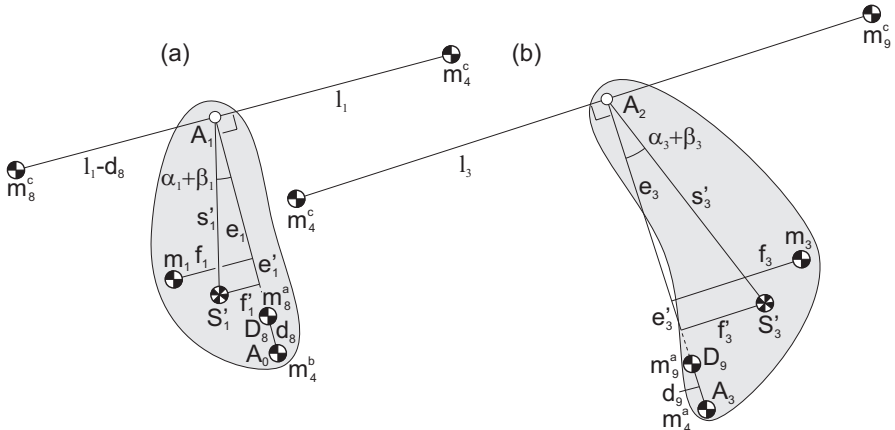


Fig. 5.14 Combination of the masses (a) in element 1 for DoF 1 where $m'_1 = m_1 + m_4^b + m_4^c + m_8^a + m_8^c$ is in S'_1 and (b) in element 3 for DoF 3 where $m'_3 = m_3 + m_4^a + m_4^c + m_9^a + m_9^c$ is located in S'_3 .

and f'_7 relative to A_6 and the line A_6A_7 , as illustrated, these parameters are calculated as

$$e'_7 = \frac{m_7 e_7 + m_9^b (l_7 - d_9 \cos \gamma) + m_9^c d_9 \sin \gamma}{m'_7} \quad (5.18)$$

$$f'_7 = \frac{m_7 f_7 + m_9^b d_9 \sin \gamma - m_9^c (l_7 - d_9 \cos \gamma)}{m'_7} \quad (5.19)$$

With these combined masses, the relative motion of DoF 1 can be illustrated as in Fig. 5.16, where from Fig. 5.15a p_5 and q_5 can be obtained as

$$\begin{aligned} p_5 &= e'_5 \cos(\beta_1 + \gamma) + f'_5 \sin(\beta_1 + \gamma) \\ q_5 &= e'_5 \sin(\beta_1 + \gamma) - f'_5 \cos(\beta_1 + \gamma) \end{aligned} \quad (5.20)$$

or from

$$\begin{aligned} p_5 \cos \beta_1 + q_5 \sin \beta_1 &= e'_5 \cos \gamma + f'_5 \sin \gamma \\ p_5 \sin \beta_1 - q_5 \cos \beta_1 &= -e'_5 \sin \gamma + f'_5 \cos \gamma \end{aligned} \quad (5.21)$$

as

$$\begin{aligned} p_5 &= \cos \beta_1 (e'_5 \cos \gamma + f'_5 \sin \gamma) - \sin \beta_1 (e'_5 \sin \gamma - f'_5 \cos \gamma) \\ q_5 &= \sin \beta_1 (e'_5 \cos \gamma + f'_5 \sin \gamma) + \cos \beta_1 (e'_5 \sin \gamma - f'_5 \cos \gamma) \end{aligned} \quad (5.22)$$

The linear momentum of the relative motion of DoF 1 can be written with respect to the reference frame x_1y_1 as

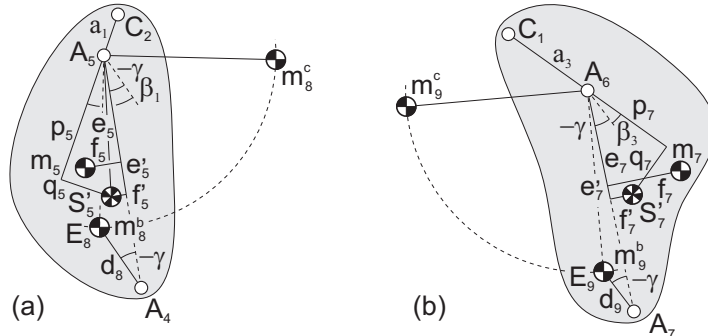


Fig. 5.15 Combination of the masses (a) in element 5 for DoF 1 where $m'_5 = m_5 + m_8 + m_9^c$ is in S'_5 and (b) in element 7 for DoF 3 where $m'_7 = m_7 + m_9^b + m_9^c$ is located in S'_7 .

$$\frac{\bar{L}_1}{\dot{\theta}_1} = \begin{bmatrix} m'_1(a_1 + p_1) + m'_5 p_5 + (m_{11} + m_{33})a_1 + m_{12}(a_1 - p_{12}) + \\ m_{13}(a_1 - p_{13}) + (m_5 + m_6 + m_7 + m_8^b + m_9^b)a_1 \\ -m'_1 q_1 + m'_5 q_5 + m_{12}q_{12} + m_{13}q_{13} + (m_8^c - m_9^c)a_1 \end{bmatrix} = \begin{bmatrix} m_{tot}a_1 \\ 0 \end{bmatrix} \quad (5.23)$$

with the total mass of the linkage $m_{tot} = m_1 + m_2 + m_3 + m_4 + m_5 + m_6 + m_7 + m_8 + m_9 + m_{11} + m_{12} + m_{13} + m_{31} + m_{32} + m_{33}$. Here elements P_1A_1 , P_2B_1 , and B_2S solely rotate and elements A_5SA_6 , $P_1B_1C_1$, A_6C_1 , and B_1S solely translate. Since A_5 , about which m_8^c is modeled, is moving, element A_5C_2 both translates and rotates. This means that for the rotational motion the linear momentum of m'_5 is considered, while for the translational motion the linear momentum of $m_5 + m_8^b$ is considered since therefore $m_8^c = 0$. For DoF 1 then the force balance conditions are found as

$$\begin{aligned} m'_1 p_1 + m'_5 p_5 &= (m_1 - m'_1 + m_2 + m_3 + m_4 + m_8^a + m_9^a + m_{31} + m_{32})a_1 + \\ &\quad m_{12}p_{12} + m_{13}p_{13} \\ m'_1 q_1 - m'_5 q_5 &= (m_8^c - m_9^c)a_1 + m_{12}q_{12} + m_{13}q_{13} \end{aligned} \quad (5.24)$$

The relative motion of DoF 3 is illustrated in Fig. 5.17 where elements P_3A_2 , P_2B_2 , and B_1S solely rotate, elements A_5SA_6 , $P_3B_2C_2$, A_5C_2 , and B_2S solely translate, and element A_6C_1 both translates and rotates. From Fig. 5.15b p_7 and q_7 can be obtained as

$$\begin{aligned} p_7 &= e'_7 \cos(\beta_3 - \gamma) + f'_7 \sin(\beta_3 - \gamma) \\ q_7 &= e'_7 \sin(\beta_3 - \gamma) - f'_7 \cos(\beta_3 - \gamma) \end{aligned} \quad (5.25)$$

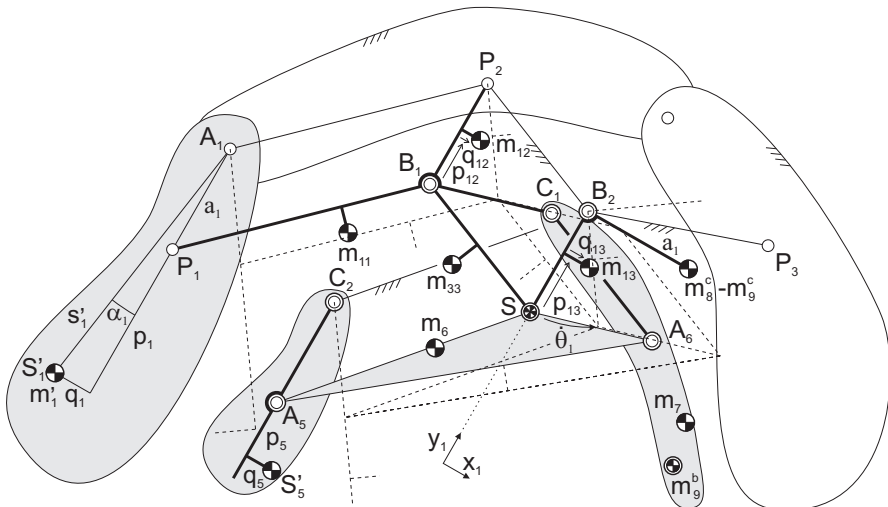


Fig. 5.16 Relative motion of DoF 1 to derive the linear momentum equations.

or from

$$\begin{aligned} p_7 \cos \beta_3 + q_7 \sin \beta_3 &= e'_7 \cos \gamma - f'_7 \sin \gamma \\ p_7 \sin \beta_3 - q_7 \cos \beta_3 &= e'_7 \sin \gamma + f'_7 \cos \gamma \end{aligned} \quad (5.26)$$

as

$$\begin{aligned} p_7 &= \cos \beta_3 (e'_7 \cos \gamma - f'_7 \sin \gamma) + \sin \beta_3 (e'_7 \sin \gamma + f'_7 \cos \gamma) \\ q_7 &= \sin \beta_3 (e'_7 \cos \gamma - f'_7 \sin \gamma) - \cos \beta_3 (e'_7 \sin \gamma + f'_7 \cos \gamma) \end{aligned} \quad (5.27)$$

The linear momentum of this motion can be written with respect to the reference frame x_3y_3 as

$$\frac{\bar{L}_3}{\dot{\theta}_3} = \begin{bmatrix} m'_3(a_3 + p_3) + m'_7p_7 + (m_{13} + m_{31})a_3 + m_{32}(a_3 - p_{32}) + \\ m_{33}(a_3 - p_{33}) + (m_5 + m_6 + m_7 + m_8^b + m_9^b)a_3 \\ m'_3q_3 - m'_7q_7 - m_{32}q_{32} - m_{33}q_{33} + (m_8^c - m_9^c)a_3 \end{bmatrix} = \begin{bmatrix} m_{tot}a_3 \\ 0 \end{bmatrix} \quad (5.28)$$

from which the force balance conditions for DoF 3 are found as

$$\begin{aligned} m'_3p_3 + m'_7p_7 &= (m_1 + m_2 + m_3 - m'_3 + m_4 + m_8^a + m_9^a + m_{11} + m_{12})a_3 + \\ &\quad m_{32}p_{32} + m_{33}p_{33} \\ m'_3q_3 - m'_7q_7 &= -(m_8^c - m_9^c)a_3 + m_{32}q_{32} + m_{33}q_{33} \end{aligned} \quad (5.29)$$

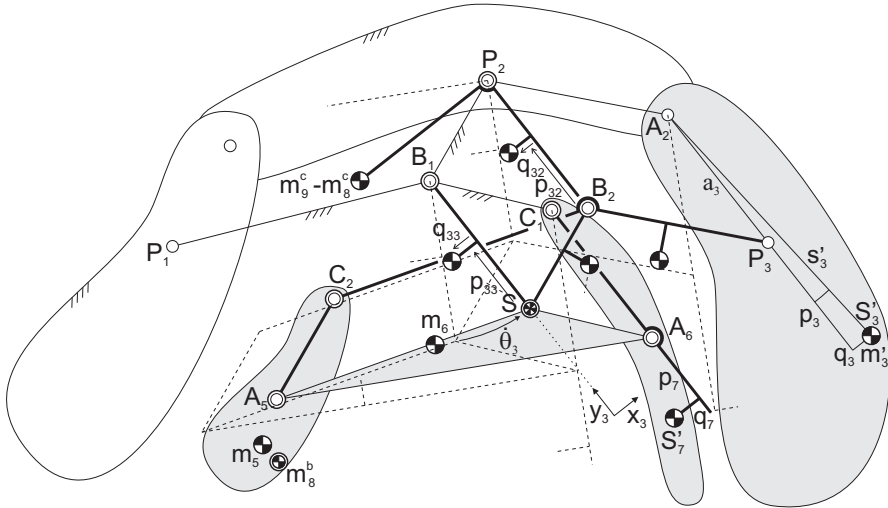


Fig. 5.17 Relative motion of DoF 3 to derive the linear momentum equations.

The relative motion of DoF 2 is illustrated in Fig. 5.18 where elements A_1A_2 , A_5A_6 , $P_1B_1C_1$, and $P_3B_2C_2$ solely rotate and elements P_1A_1 , P_3A_2 , A_5C_2 , and A_6C_1 solely translate. Figure 5.19 shows the ELMS of this motion with

$$\begin{aligned}\mu_1 &= m_1 + m_{11}p_{11}/a_{21} + m_4^b + m_8^a, & v_1 &= m_4^c + m_{11}q_{11}/a_{21} \\ \mu_3 &= m_3 + m_{31}p_{31}/a_{23} + m_4^a + m_9^a, & v_2 &= m_4^c + m_{31}q_{31}/a_{23} \\ \mu_2 &= m_2, \quad \mu_4 = m_5 + m_8^b, & v_3 &= m_8^c \\ \mu_5 &= m_7 + m_9^b, \quad \mu_6 = m_6, & v_4 &= m_9^c\end{aligned}\quad (5.30)$$

This ELMS is obtained as in Fig. 3.13 to which the linear momentum of elements A_5C_2 , A_5SA_6 , and A_6C_1 is added by superimposing element A_5SA_6 with S and P_2 coinciding. From the ELMS the linear momentum of DoF 2 can be written with respect to the reference frame x_2y_2 as

$$\begin{aligned}\frac{\bar{L}_2}{\dot{\theta}_2} &= \mu_1 \begin{bmatrix} c_2 \\ -b_{21} \end{bmatrix} + v_1 \begin{bmatrix} b_{21} \\ c_2 \end{bmatrix} + \mu_2 \begin{bmatrix} c_2 - f_2 \\ -(b_{21} - e_2) \end{bmatrix} - v_2 \begin{bmatrix} b_{21} - l_2 \\ c_2 \end{bmatrix} + \mu_3 \begin{bmatrix} c_2 \\ -(b_{21} - l_2) \end{bmatrix} + \\ &\quad \mu_4 \eta l_2 \epsilon \begin{bmatrix} \sin(\gamma + \rho) \\ -\cos(\gamma + \rho) \end{bmatrix} + \mu_5 \eta l_2 \begin{bmatrix} \epsilon \sin(\gamma + \rho) - \sin(\gamma) \\ -\epsilon \cos(\gamma + \rho) + \cos(\gamma) \end{bmatrix} + \\ &\quad \mu_6 \begin{bmatrix} \eta l_2 \epsilon \sin(\gamma + \rho) - e_6 \sin(\gamma) - f_6 \cos(\gamma) \\ -\eta l_2 \epsilon \cos(\gamma + \rho) + e_6 \cos(\gamma) - f_6 \sin(\gamma) \end{bmatrix} + v_3 \begin{bmatrix} -b_{21} \\ -c_2 \end{bmatrix} + \\ &\quad v_3 \eta l_2 \epsilon \begin{bmatrix} \cos(\gamma + \rho) \\ \sin(\gamma + \rho) \end{bmatrix} + v_4 \begin{bmatrix} -(l_2 - b_{21}) \\ c_2 \end{bmatrix} + v_4 \eta l_2 \begin{bmatrix} -\epsilon \cos(\gamma + \rho) + \cos(\gamma) \\ -\epsilon \sin(\gamma + \rho) + \sin(\gamma) \end{bmatrix} = \begin{bmatrix} 0 \\ 0 \end{bmatrix}\end{aligned}\quad (5.31)$$

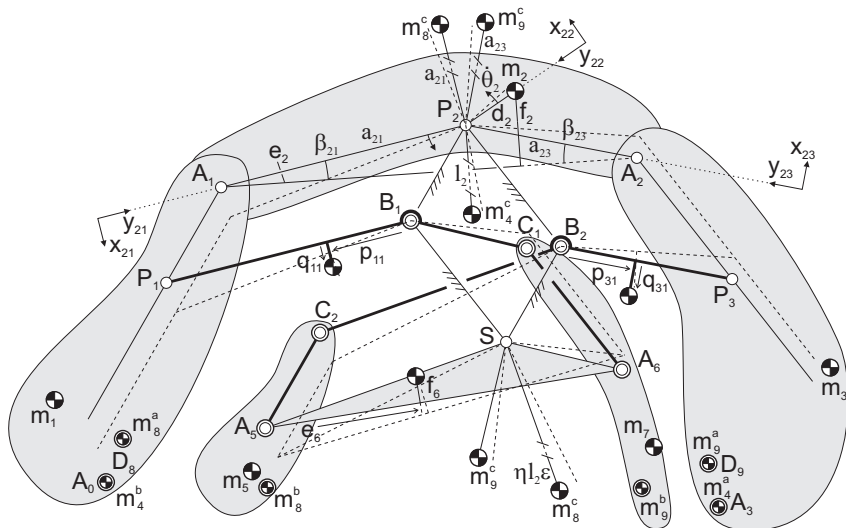


Fig. 5.18 Relative motion of DoF 2 to derive the linear momentum equations.

The force balance conditions for DoF 2 then are found as

$$\begin{aligned}
 & (\mu_1 + \mu_2 + \mu_3)c_2 + (v_1 - v_2 - v_3 + v_4)b_{21} - \mu_2 f_2 + (v_2 - v_4)l_2 + \\
 & (\mu_4 + \mu_5 + \mu_6)\eta l_2 \epsilon \sin(\gamma + \rho) + (v_3 - v_4)\eta l_2 \epsilon \cos(\gamma + \rho) - \\
 & (\mu_5 \eta l_2 + \mu_6 e_6) \sin \gamma + (v_4 \eta l_2 - \mu_6 f_6) \cos \gamma = 0 \quad (5.32) \\
 & (-\mu_1 - \mu_2 - \mu_3)b_{21} + (v_1 - v_2 - v_3 + v_4)c_2 + \mu_2 e_2 + \mu_3 l_2 + \\
 & (-\mu_4 - \mu_5 - \mu_6)\eta l_2 \epsilon \cos(\gamma + \rho) + (v_3 - v_4)\eta l_2 \epsilon \sin(\gamma + \rho) + \\
 & (\mu_5 \eta l_2 + \mu_6 e_6) \cos \gamma + (v_4 \eta l_2 - \mu_6 f_6) \sin \gamma = 0
 \end{aligned}$$

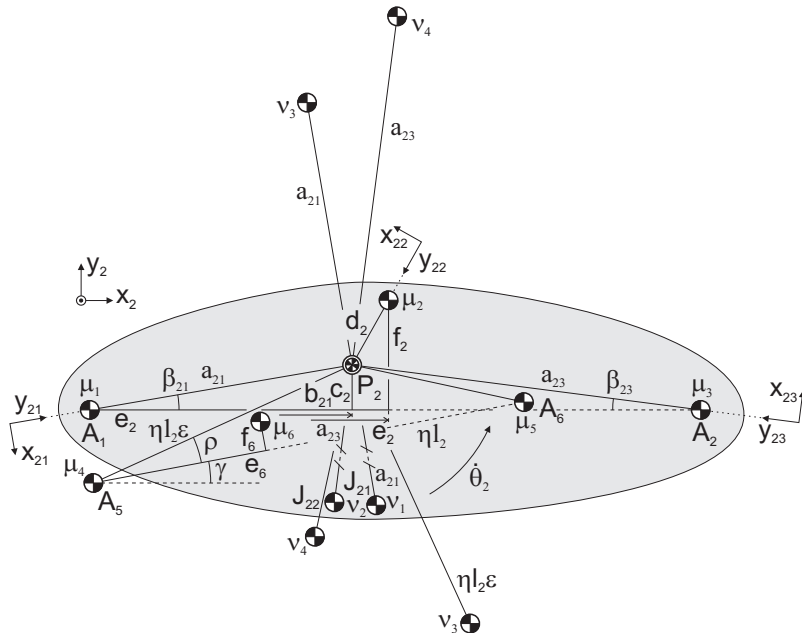


Fig. 5.19 ELMS of relative motion of DoF 2 where the linear momentum of elements A_5C_2, A_5SA_6 , and A_6C_1 is added by superimposing element A_5SA_6 on A_1A_2 with S and P_2 coinciding.

Altogether, the force balance conditions of the inherently balanced linkage architecture in Fig. 5.7 are obtained from (5.24), (5.29), and (5.32) as:

$$\begin{aligned}
& (m_2 + m_3 + m_4(1 - \frac{e_4}{l_4} - \frac{f_4}{l_4}) - m_8 \frac{f_8}{l_8} + m_9(1 - \frac{e_9}{l_9}) + m_{31} + m_{32})a_1 - \\
& (m_1 + m_4(\frac{e_4}{l_4} + \frac{f_4}{l_4}) + m_8(1 - \frac{e_8}{l_8} + \frac{f_8}{l_8}))p_1 + m_{12}p_{12} + \\
& m_{13}p_{13} - (m_5 + m_8(\frac{e_8}{l_8} + \frac{f_8}{l_8}))p_5 = 0 \\
& m_{12}q_{12} + m_{13}q_{13} - (m_1 + m_4(\frac{e_4}{l_4} + \frac{f_4}{l_4}) + m_8(1 - \frac{e_8}{l_8} + \frac{f_8}{l_8}))q_1 + \\
& (m_5 + m_8(\frac{e_8}{l_8} + \frac{f_8}{l_8}))q_5 + (m_8 \frac{f_8}{l_8} - m_9 \frac{f_9}{l_9})a_1 = 0 \\
& (\mu_1 + \mu_2 + \mu_3)c_2 + (v_1 - v_2 - v_3 + v_4)b_{21} - \mu_2 f_2 + (v_2 - v_4)l_2 + \\
& (\mu_4 + \mu_5 + \mu_6)\eta l_2 \epsilon \sin(\gamma + \rho) + (v_3 - v_4)\eta l_2 \epsilon \cos(\gamma + \rho) - \\
& (\mu_5 \eta l_2 + \mu_6 e_6) \sin \gamma + (v_4 \eta l_2 - \mu_6 f_6) \cos \gamma = 0 \\
& (-\mu_1 - \mu_2 - \mu_3)b_{21} + (v_1 - v_2 - v_3 + v_4)c_2 + \mu_2 e_2 + \mu_3 l_2 + \\
& (-\mu_4 - \mu_5 - \mu_6)\eta l_2 \epsilon \cos(\gamma + \rho) + (v_3 - v_4)\eta l_2 \epsilon \sin(\gamma + \rho) + \\
& (\mu_5 \eta l_2 + \mu_6 e_6) \cos \gamma + (v_4 \eta l_2 - \mu_6 f_6) \sin \gamma = 0 \\
& (m_1 + m_2 + m_4(\frac{e_4}{l_4} - \frac{f_4}{l_4}) + m_8(1 - \frac{e_8}{l_8}) - m_9 \frac{f_9}{l_9} + m_{11} + m_{12})a_3 - \\
& (m_3 + m_4(1 - \frac{e_4}{l_4} + \frac{f_4}{l_4}) + m_9(1 - \frac{e_9}{l_9} + \frac{f_9}{l_9}))p_3 + m_{32}p_{32} + \\
& m_{33}p_{33} - (m_7 + m_9(\frac{e_9}{l_9} + \frac{f_9}{l_9}))p_7 = 0 \\
& m_{32}q_{32} + m_{33}q_{33} - (m_3 + m_4(1 - \frac{e_4}{l_4} + \frac{f_4}{l_4}) + m_9(1 - \frac{e_9}{l_9} + \frac{f_9}{l_9}))q_3 + \\
& (m_7 + m_9(\frac{e_9}{l_9} + \frac{f_9}{l_9}))q_7 - (m_8 \frac{f_8}{l_8} - m_9 \frac{f_9}{l_9})a_3 = 0
\end{aligned} \tag{5.33}$$

with (5.30) and where $m'_1, m'_3, m'_5, m'_7, m'_4, m^a_4, m^b_4, m^c_4, m^a_8, m^b_8, m^c_8, m^a_9, m^b_9, m^c_9$ were substituted.

Since the force balance conditions depend on the similarity parameters γ, ρ, ϵ , and η , the principal dimensions are to be found in an iterative way. With $s'_1'^2 = e'_1'^2 + f'_1'^2 = (a_1 + p_1)^2 + q_1^2$ and $s'_3'^2 = e'_3'^2 + f'_3'^2 = (a_3 + p_3)^2 + q_3^2$, from (5.24) and (5.29) the equations for a_1 and a_3 can be written as

$$\begin{aligned}
a_1 &= \frac{\sqrt{m'_1'^2 s'_1'^2 - (m_{12}q_{12} + m_{13}q_{13} + m'_5 q_5 + (m^c_8 - m^c_9)a_1)^2} - m_{12}p_{12} - m_{13}p_{13} + m'_5 p_5}{m_1 + m_2 + m_3 + m_4 + m^a_4 + m^a_8 + m_{31} + m_{32}} \\
a_3 &= \frac{\sqrt{m'_3'^2 s'_3'^2 - (m_{32}q_{32} + m_{33}q_{33} + m'_7 q_7 + (m^c_9 - m^c_8)a_3)^2} - m_{32}p_{32} - m_{33}p_{33} + m'_7 p_7}{m_1 + m_2 + m_3 + m_4 + m^a_8 + m^a_9 + m_{11} + m_{12}}
\end{aligned} \tag{5.34}$$

and the locations of P_1 in A_0A_1 and P_3 in A_2A_3 can be obtained as

$$b_1 = a_1 \cos \beta_1 \quad c_1 = a_1 \sin \beta_1 \quad b_3 = a_3 \cos \beta_3 \quad c_1 = a_3 \sin \beta_3 \tag{5.35}$$

with

$$\beta_1 = \sin^{-1}(\frac{f'_1}{s'_1}) - \alpha_1 = \sin^{-1}(\frac{m_1 f_1 - m^c_4 l_1 + m^c_8(l_1 - d_8)}{m'_1 s'_1}) - \alpha_1 \tag{5.36}$$

$$\beta_3 = \sin^{-1}(\frac{f'_3}{s'_3}) - \alpha_3 = \sin^{-1}(\frac{m_3 f_3 - m^c_4 l_3 + m^c_9(l_3 - d_9)}{m'_3 s'_3}) - \alpha_3$$

in which

$$\begin{aligned}\alpha_1 &= \sin^{-1} \left(\frac{m_{12}q_{12} + m_{13}q_{13} + m'_5q_5 + (m_8^c - m_9^c)a_1}{m'_1s'_1} \right) \\ \alpha_3 &= \sin^{-1} \left(\frac{m_{32}q_{32} + m_{33}q_{33} + m'_7q_7 + (m_9^c - m_8^c)a_3}{m'_3s'_3} \right)\end{aligned}\quad (5.37)$$

They can also be found with (4.36), (4.37), and with (4.38).

For validation of the results, a simulation with a dynamic model of the mechanism in Fig. 5.7 was made in which the only connection with the base is with a pivot in S . The parameters of the mechanism are the same as in the first four columns of Table 4.1, except for f_4 which was chosen to be negative here, with in addition the parameters in Table 5.1. The parameters in the last three columns of Table 5.1 were calculated.

The simulation of the dynamic model is illustrated in Fig. 5.20 with two poses of the mechanism. For the simulation time of 0.5 seconds a torque $\tau_1 = 50 \cos(4\pi t)$ Nm was applied to element SB_1 and a torque $\tau_2 = -\tau_1$ was applied to element SB_2 . The dynamics were solved with solver ODE45 (Dormand-Prince) with a maximal step size of 0.0001 s and with a relative tolerance of $1e^{-12}$ m. The reaction forces in the pivot with the base were recorded and are displayed in Fig. 5.21. These shaking forces are expected to be zero for force balance and show an error which is about the computation accuracy. Figure 5.22 shows the linear momentum of the mechanism in both x and y -direction which are also expected to be zero for force balance and have an error which is about the computation accuracy.

To demonstrate the feasibility of producing such a linkage architecture in real, Fig. 5.23 shows a physical model of stainless steel in various poses. Here the principal vector links were assumed massless and in the two pictures on top they were added as made of paper.

Table 5.1 Parameters in addition to Table 4.1 of the inherently balanced architecture in Fig. 5.7 for simulation.

	[kg]	[m]	[m]	[m]	[m]	[.]
			$f_4 = -0.13$		$a_1 = 0.2477$	$\gamma = -0.1079$
$m_5 = 0.2$	$e_5 = 0.20$	$f_5 = 0.11$	$l_5 = 0.4853$	$b_1 = 0.2396$	$\eta = 0.4853$	
$m_6 = 0.5$	$e_6 = 0.43$	$f_6 = 0.10$	$l_6 = 1.4560$	$c_1 = 0.0629$	$\rho = 0.0806$	
$m_7 = 0.8$	$e_7 = 0.32$	$f_7 = 0.18$	$l_7 = 0.9706$	$a_{21} = 1.6946$		
$m_8 = 0.6$	$e_8 = 0.55$	$f_8 = 0.22$	$l_8 = 0.9625$	$a_{23} = 1.3748$		
$m_9 = 0.7$	$e_9 = 0.44$	$f_9 = 0.19$	$l_9 = 0.7927$	$b_{21} = 1.6636$		
		$d_8 = 0.21$		$c_2 = 0.3226$		
		$d_9 = 0.32$		$a_3 = 0.6016$		
				$b_3 = 0.5558$		
				$c_3 = 0.2302$		

5.4 Discussion and conclusion

In this chapter it was shown that the motion of the common CoM of a 4R four-bar linkage with its principal vector linkage and its similar linkage can be described with a point in this similar linkage. Therefore various theories from literature were generalized, extended, and combined. The conditions for similarity of the resulting principal vector linkage architecture were derived and the force balance conditions were calculated by means of a mass equivalent principal chain.

It was shown that multiple closed loops can be considered by equivalent modeling of one element in each closed loop. In addition, with element $A_0A_3A_4A_7$ in Fig. 5.7 it was shown that an element with more than two joints is modeled mass equivalently also with only two real masses and a virtual equivalent mass of which the real masses are projected in the two joints of the considered closed loop (here A_0 and A_3). This means that such an element can be considered in multiple ways, for instance for the closed loop $A_4A_5A_6A_7$, element $A_0A_3A_4A_7$ would be modeled such that the two real equivalent masses are projected in joints A_4 and A_7 . The obtained force balance conditions are independent of this choice. Since modeling along the closed loop $A_4A_5A_6A_7$ through S to P_2 is longer than modeling along the closed loop $A_0A_1A_2A_3$ where the equivalent masses are projected in the principal elements directly, the latter approach is more convenient.

Instead of constructing the principal vector linkage on the opposite side of the similar linkage as in Fig. 5.7, it is also possible to have them on the same side as

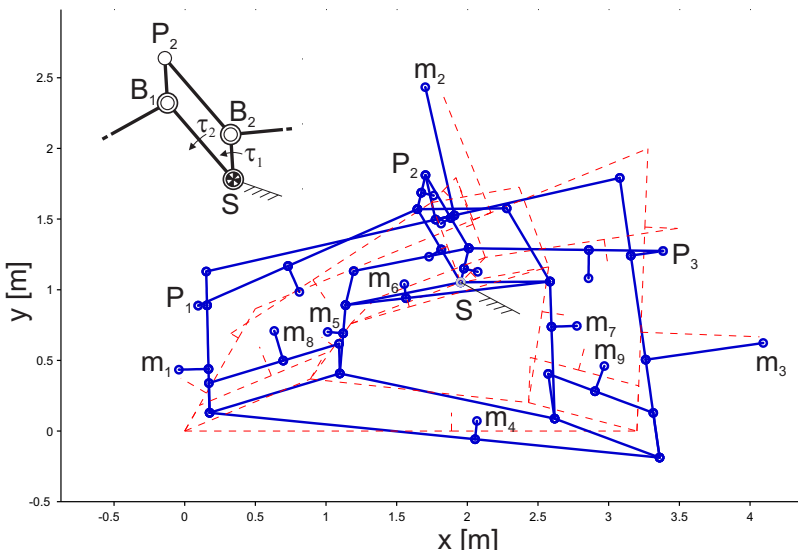


Fig. 5.20 Dynamic simulation in Spacar where S is a pivot with the base, a torque τ_1 is applied to element SB_1 , and a torque τ_2 is applied to element SB_2 .

shown in Fig. 5.24. The similar linkage then shares the central principal element (here A_0A_3). It is also possible to construct them as in Fig. 5.25, where the similar linkage shares one of the outer principal elements (here A_2A_3). To derive the force balance conditions for these constructions, in Fig. 5.24 elements A_1A_2 and A_5A_6 can be modeled mass equivalently while in Fig. 5.25 elements A_0A_1 and A_4A_5 can be modeled mass equivalently.

There are numerous other possibilities and variations on these types of principal vector linkage architectures. For instance the variation of the principal vector linkage in Fig. 3.18 can be combined with the similar linkage, or the adapted principal vector linkage in Fig. 3.20 can be combined with the similar linkage in which the common CoM in joint S does not necessarily need to be an invariant point in A_5A_6 , leaving the initial motivation for designing a similar linkage. Figure 5.26 shows a variation where two similar linkages are combined, which can be analyzed by using the principal vector linkages in Fig. 5.24 and Fig. 5.25.

It is also possible to find similar linkages of linkages other than four-bar mechanisms. For instance a principal vector linkage architecture of similar 5R five-bar

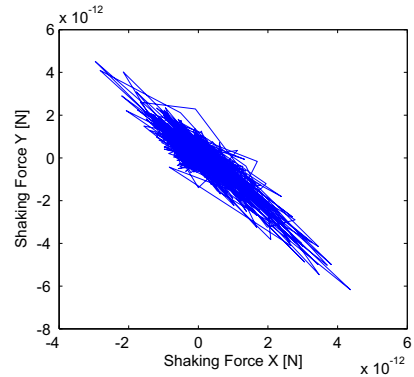


Fig. 5.21 The resulting shaking forces in pivot S show that the mechanism is force balanced about S .

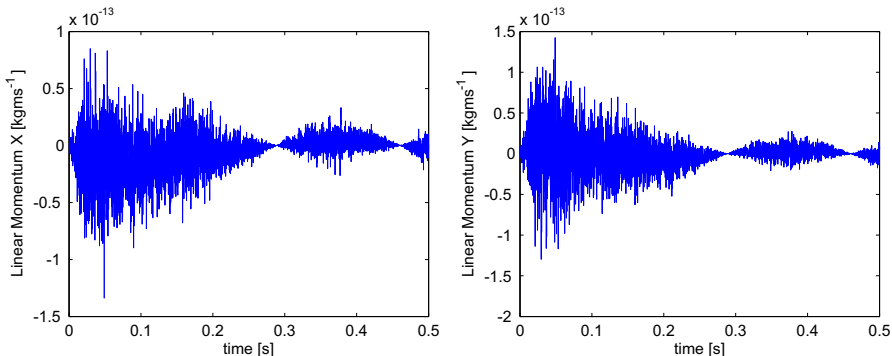


Fig. 5.22 The linear momentum in both x and y -direction, which were calculated from the simulated motion, show force balance about S .

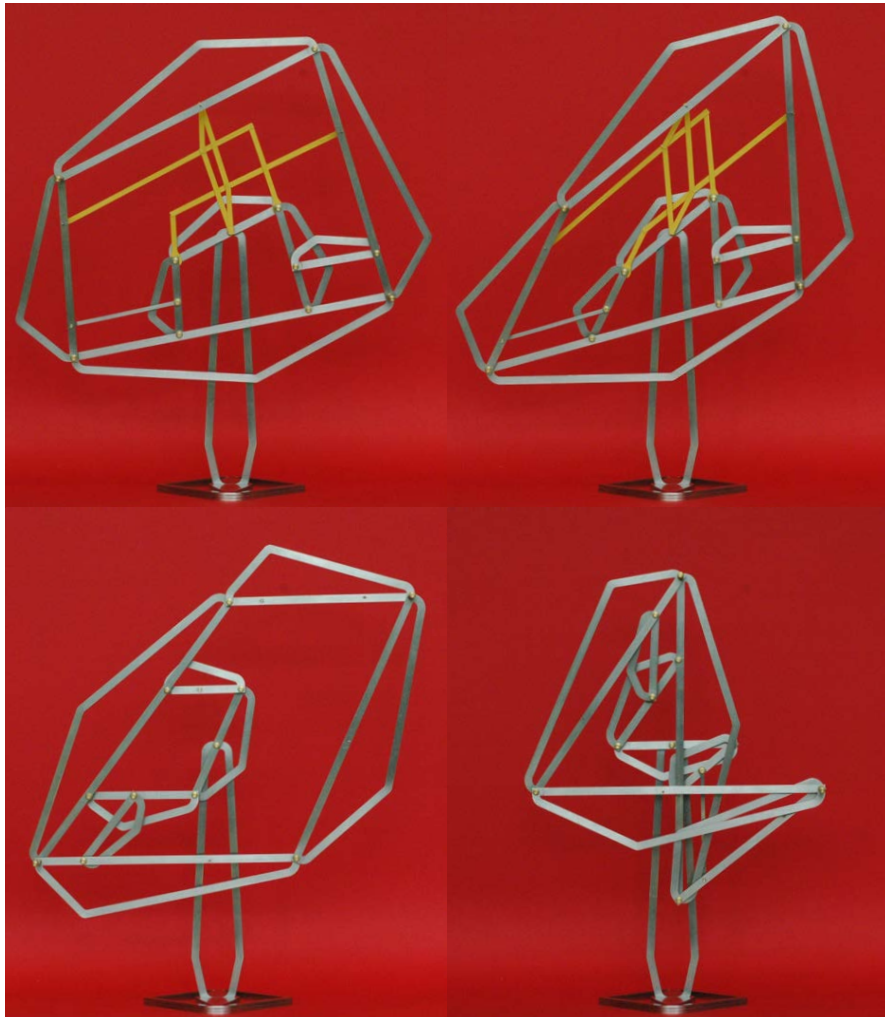


Fig. 5.23 Physical model of a force-balanced mechanism of two similar four-bar linkages in four poses. In the images on top an assumed massless principal vector linkage made of paper was added. (see model in motion at: www.kineticart.nl)

linkages can be obtained by generalizing the theory in [87] following the theory in this chapter, and similarly it can be extended to principal vector linkage architectures of similar 6R six-bar linkages.

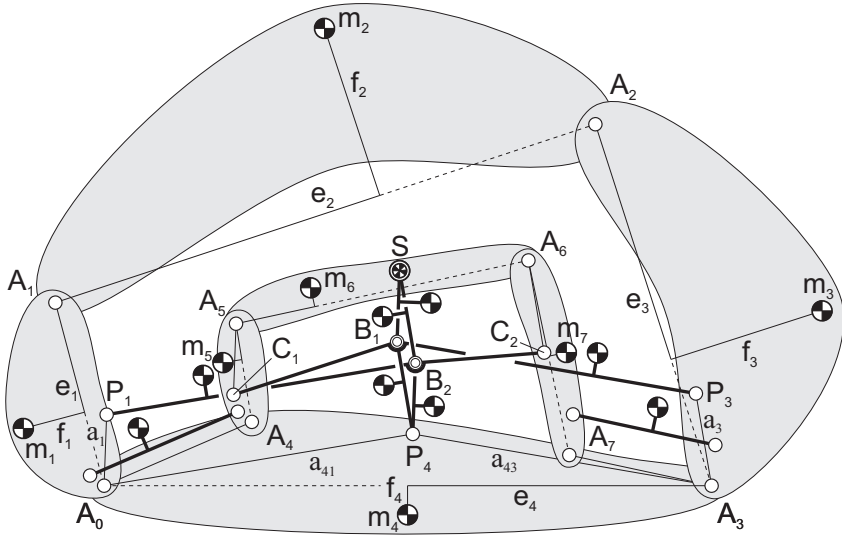


Fig. 5.24 Principal vector linkage architecture with the principal vector linkage and the similar linkage on the same side.

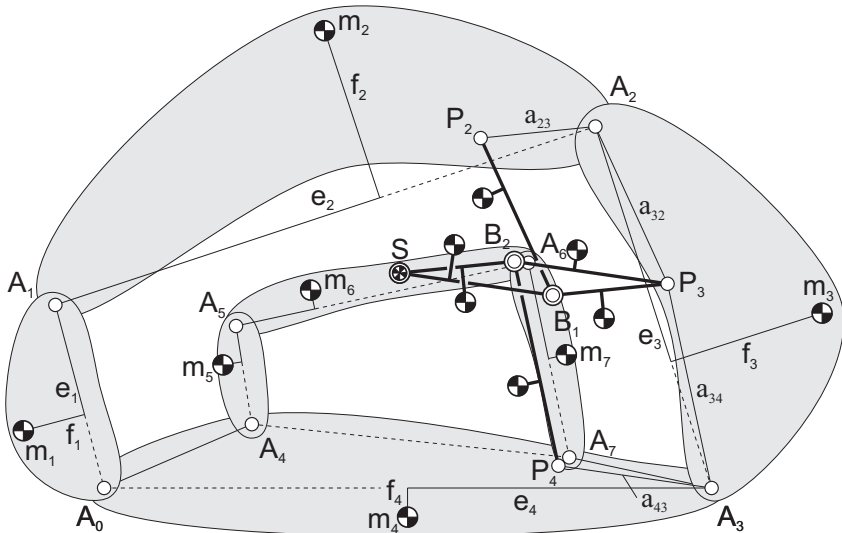


Fig. 5.25 Principal vector linkage architecture with differently orientated principal vector linkage and similar linkage.

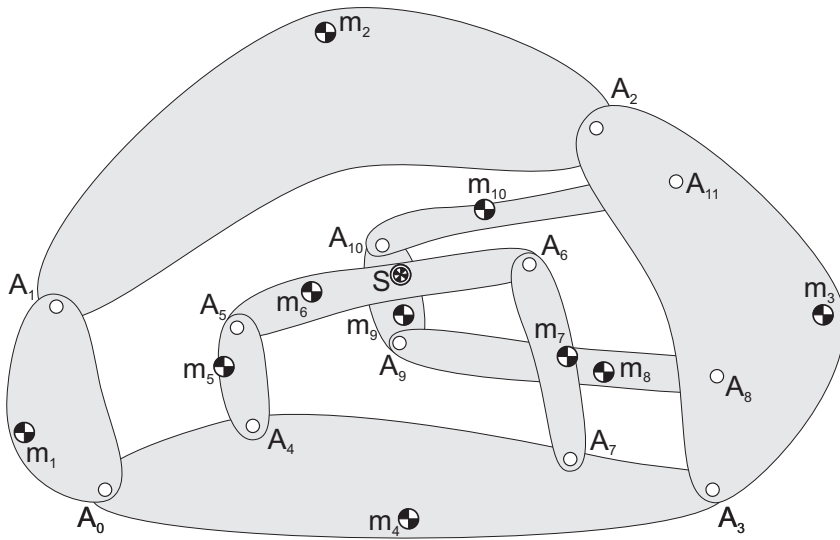


Fig. 5.26 Principal vector linkage architecture with two similar linkages.

Chapter 6

Principal vector linkages for inherent shaking moment balance

Abstract In this chapter the method of principal vectors is investigated for inherent shaking moment balancing. Since in general the angular momentum of a principal vector linkage is not zero, shaking moment balance can only be obtained by reduction of the degrees of freedom. Therefore it is shown that the angular momentum of a principal vector linkage about its center of mass can be written compactly such that the moment balance solutions can be derived. Also closed-chain principal vector linkages are considered, where the angular momentum of a mass equivalent principal chain was found only for the specific case that the inertia of the equivalently modeled element equals the inertia of the two real equivalent masses about their center of mass.

6.1 Moment balance conditions of open-chain principal vector linkages

For the design of dynamically balanced linkages the shaking moments also need to be considered. Therefore the angular momentum of a principal vector linkage about its common CoM can be investigated which for shaking moment balance needs to be constant for all motion.

The use of principal vectors for shaking moment balancing is not found in literature. Originally, Fisher developed the method to derive the kinetic energy equations of a linkage in motion. With principal vectors it was shown that the kinetic energy of a linkage can be formulated compactly to solely depend on the total mass, reduced inertia terms, the principal dimensions, and the time dependent angles of each relative DoF [53]. Although kinetic energy equations are essentially different from angular momentum equations, they share similarities. It will be shown in this section that also the angular momentum of a linkage can be formulated compactly with the same characteristics.

It will be shown how from the angular momentum equation the moment balance conditions of a principal vector linkage are derived. The angular momentum

equation of the 2-DoF pantograph in Fig. 3.2, the 3-DoF principal vector linkage in Fig. 3.7, and the 4-DoF principal vector linkage in Fig. 3.23 are derived and moment balance solutions are investigated.

6.1.1 Moment balance of a 2-DoF pantograph

Figure 6.1 shows the general planar pantograph or planar 2-DoF principal vector linkage of Fig. 3.2 with common CoM in S . Each element has an arbitrary mass distribution with link mass m_i and link inertia I_i in and about link CoM S_i . Generally, the angular momentum of the linkage within the xy -plane about the common CoM in S can be written as

$$H_S = (I_1 + I_3)\dot{\theta}_1 + (I_2 + I_4)\dot{\theta}_2 + m_1(\bar{r}_1 \times \dot{\bar{r}}_1)_z + m_2(\bar{r}_2 \times \dot{\bar{r}}_2)_z + m_3(\bar{r}_3 \times \dot{\bar{r}}_3)_z + m_4(\bar{r}_4 \times \dot{\bar{r}}_4)_z \quad (6.1)$$

where z indicates the z -component of the cross-products. Vectors \bar{r}_i describe the positions of the link CoMs S_i relative to the common CoM in S and can be written with the principal vectors as

$$\bar{r}_1 = a_2 \begin{bmatrix} \cos \theta_2 \\ \sin \theta_2 \\ 0 \end{bmatrix} - p_1 \begin{bmatrix} \cos \theta_1 \\ \sin \theta_1 \\ 0 \end{bmatrix} + q_1 \begin{bmatrix} -\sin \theta_1 \\ \cos \theta_1 \\ 0 \end{bmatrix} \quad (6.2)$$

$$\bar{r}_2 = a_1 \begin{bmatrix} \cos \theta_1 \\ \sin \theta_1 \\ 0 \end{bmatrix} - p_2 \begin{bmatrix} \cos \theta_2 \\ \sin \theta_2 \\ 0 \end{bmatrix} - q_2 \begin{bmatrix} -\sin \theta_2 \\ \cos \theta_2 \\ 0 \end{bmatrix} \quad (6.3)$$

$$\bar{r}_3 = p_3 \begin{bmatrix} \cos \theta_1 \\ \sin \theta_1 \\ 0 \end{bmatrix} - q_3 \begin{bmatrix} -\sin \theta_1 \\ \cos \theta_1 \\ 0 \end{bmatrix} \quad (6.4)$$

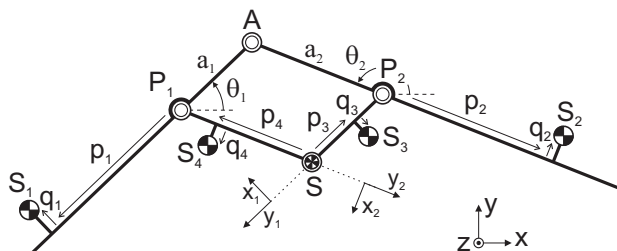


Fig. 6.1 General pantograph or 2-DoF principal vector linkage with common CoM in S . Each element has an arbitrary mass distribution with link mass m_i in and link inertia I_i about link CoM S_i .

$$\bar{r}_4 = p_4 \begin{bmatrix} \cos \theta_2 \\ \sin \theta_2 \\ 0 \end{bmatrix} + q_4 \begin{bmatrix} -\sin \theta_2 \\ \cos \theta_2 \\ 0 \end{bmatrix} \quad (6.5)$$

When vectors \bar{r}_i and their derivatives $\dot{\bar{r}}_i$ are substituted, the angular momentum becomes

$$\begin{aligned} H_S = & (I_1 + I_3 + m_1(p_1^2 + q_1^2) + m_2a_1^2 + m_3(p_3^2 + q_3^2))\dot{\theta}_1 + \\ & (I_2 + I_4 + m_1a_2^2 + m_2(p_2^2 + q_2^2) + m_4(p_4^2 + q_4^2))\dot{\theta}_2 - \\ & (m_1a_2p_1 + m_2a_1p_2)\cos(\theta_1 - \theta_2)(\dot{\theta}_1 + \dot{\theta}_2) - \\ & (m_1a_2q_1 + m_2a_1q_2)\sin(\theta_1 - \theta_2)(\dot{\theta}_1 + \dot{\theta}_2) \end{aligned} \quad (6.6)$$

Subsequently, the force balance conditions (3.2) can be substituted for m_1p_1 , m_2p_2 , m_1q_1 , and m_2q_2 , which leads to the angular momentum equation

$$\begin{aligned} H_S = & (I_1 + I_3 + m_1(p_1^2 + q_1^2) + m_2a_1^2 + m_3(p_3^2 + q_3^2))\dot{\theta}_1 + \\ & (I_2 + I_4 + m_1a_2^2 + m_2(p_2^2 + q_2^2) + m_4(p_4^2 + q_4^2))\dot{\theta}_2 - \\ & (m_{tot}a_1a_2 - m_3a_2(a_1 - p_3) - m_4a_1(a_1 - p_4))\cos(\theta_1 - \theta_2)(\dot{\theta}_1 + \dot{\theta}_2) - \\ & (m_3a_2q_3 + m_4a_1q_4)\sin(\theta_1 - \theta_2)(\dot{\theta}_1 + \dot{\theta}_2) \end{aligned} \quad (6.7)$$

with $m_{tot} = m_1 + m_2 + m_3 + m_4$. With the linkage inertia written with its radius of gyration κ_i as $I_i = m_{tot}\kappa_i^2$ and with the reduced inertia terms written as $m_{tot}\xi_i^2$, the angular momentum can be written in its final compact form as

$$\begin{aligned} H_S = & m_{tot}\{\chi_1^2\dot{\theta}_1 + \chi_2^2\dot{\theta}_2 - a_1a_2\cos(\theta_1 - \theta_2)(\dot{\theta}_1 + \dot{\theta}_2)\} + \\ & (m_3a_2(a_1 - p_3) + m_4a_1(a_2 - p_4))\cos(\theta_1 - \theta_2)(\dot{\theta}_1 + \dot{\theta}_2) - \\ & (m_3a_2q_3 + m_4a_1q_4)\sin(\theta_1 - \theta_2)(\dot{\theta}_1 + \dot{\theta}_2) \end{aligned} \quad (6.8)$$

in which $\chi_i^2 = \kappa_i^2 + \xi_i^2$ are the radii of the reduced inertias with the reduced inertias written as

$$\begin{aligned} m_{tot}\chi_1^2 &= I_1 + I_3 + m_1(p_1^2 + q_1^2) + m_2a_1^2 + m_3(p_3^2 + q_3^2) \\ m_{tot}\chi_2^2 &= I_2 + I_4 + m_1a_2^2 + m_2(p_2^2 + q_2^2) + m_4(p_4^2 + q_4^2) \end{aligned} \quad (6.9)$$

These reduced inertia terms can be found also from the ELMSs of the individual motions of DoF 1 and DoF 2 (Fig. 3.5) which are shown in Fig. 6.2. They are calculated as the inertia of the masses in each ELMS about the principal point together with the link inertias. The first line of the angular momentum equation depends solely on the total mass, the reduced inertias, the principal dimensions, and the time dependent angles of each relative DoF. This is the angular momentum of mainly the principal elements. The last two lines of the angular momentum equation depend on the masses m_3 and m_4 of the principal vector links 3 and 4. When the method of principal vectors is solely used to analyze the motion of the principal elements (i.e. $m_3 = 0$, $m_4 = 0$, $I_3 = 0$, and $I_4 = 0$), then the angular momentum reduces to

$$H_S = m_{tot}(\chi_1^2 \dot{\theta}_1 + \chi_2^2 \dot{\theta}_2 - a_1 a_2 \cos(\theta_1 - \theta_2)(\dot{\theta}_1 + \dot{\theta}_2)) \quad (6.10)$$

with the reduced inertias written as

$$\begin{aligned} m_{tot} \chi_1^2 &= I_1 + m_1 p_1^2 + m_2 a_1^2 \\ m_{tot} \chi_2^2 &= I_2 + m_1 a_2^2 + m_2 p_2^2 \end{aligned} \quad (6.11)$$

For the principal vector linkage in Fig. 6.1, moment balance is obtained when the angular momentum (6.8) is constant, which is for the moment balance condition:

$$\begin{aligned} m_{tot} \{ \chi_1^2 \dot{\theta}_1 + \chi_2^2 \dot{\theta}_2 - a_1 a_2 \cos(\theta_1 - \theta_2)(\dot{\theta}_1 + \dot{\theta}_2) \} + \\ (m_3 a_2(a_1 - p_3) + m_4 a_1(a_2 - p_4)) \cos(\theta_1 - \theta_2)(\dot{\theta}_1 + \dot{\theta}_2) - \\ (m_3 a_2 q_3 + m_4 a_1 q_4) \sin(\theta_1 - \theta_2)(\dot{\theta}_1 + \dot{\theta}_2) = \Lambda \end{aligned} \quad (6.12)$$

with constant $\Lambda \in \Re$.

Moment balance solutions

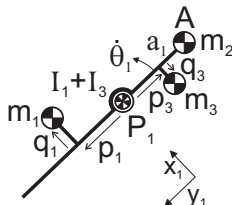
In general, the moment balance condition (6.12) is not constant or zero for all motion. It can only be constant for specific relations among the individual relative motions, which means for reduced cases. For instance for $\Lambda = 0$, a possible solution is the set of two moment balance conditions

$$\begin{aligned} \dot{\theta}_1 + \dot{\theta}_2 &= 0 \\ \chi_1^2 &= \chi_2^2 \end{aligned} \quad (6.13)$$

of which the latter results in

$$\begin{aligned} I_1 + I_3 + m_1(p_1^2 + q_1^2) + m_2 a_1^2 + m_3(p_3^2 + q_3^2) = \\ I_2 + I_4 + m_1 a_2^2 + m_2(p_2^2 + q_2^2) + m_4(p_4^2 + q_4^2) \end{aligned} \quad (6.14)$$

(a)



(b)

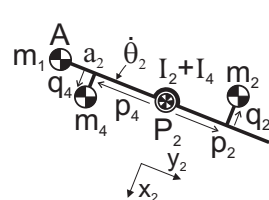


Fig. 6.2 ELMSs of individual motions of a) DoF 1 and b) DoF 2, including the link inertias from which the reduced inertia terms are obtained as the inertia of these reduced mass models.

Then the two relative motions are equal and in opposite direction.

In general, a linear relation between the motion of the two relative DoFs can be written with $\theta_2 = t_1 - t_2 \theta_1$ with arbitrary constants t_1 and t_2 . Together with its derivative $\dot{\theta}_2 = -t_2 \dot{\theta}_1$, then the moment balance condition (6.12) reduces to

$$\begin{aligned} m_{tot}(\chi_1^2 - t_2 \chi_2^2 - a_1 a_2 (1 - t_2) \cos((1 + t_2) \theta_1 - t_1)) + \\ (m_3 a_2 (a_1 - p_3) + m_4 a_1 (a_2 - p_4))(1 - t_2) \cos((1 + t_2) \theta_1 - t_1) - \\ (m_3 a_2 q_3 + m_4 a_1 q_4)(1 - t_2) \sin((1 + t_2) \theta_1 - t_1) = 0 \end{aligned} \quad (6.15)$$

The general set of moment balance conditions for linear relations between the motion of the two relative DoFs then is found as

$$\begin{aligned} \theta_2 &= t_1 - t_2 \theta_1 \\ \dot{\theta}_2 &= -t_2 \dot{\theta}_1 \\ m_{tot} \chi_1^2 - m_{tot} t_2 \chi_2^2 + (-a_1 a_2 m_{tot} + m_3 a_2 (a_1 - p_3) + \\ m_4 a_1 (a_2 - p_4))(1 - t_2) \cos((1 + t_2) \theta_1 - t_1) - \\ (m_3 a_2 q_3 + m_4 a_1 q_4)(1 - t_2) \sin((1 + t_2) \theta_1 - t_1) &= 0 \end{aligned} \quad (6.16)$$

Two subsets of moment balance conditions can be derived from these equations. The subset of moment balance conditions for $t_2 = 1$ was shown in (6.13) and a second subset of moment balance conditions is found as

$$\begin{aligned} \theta_2 &= t_1 - t_2 \theta_1 \\ \dot{\theta}_2 &= -t_2 \dot{\theta}_1 \\ \chi_1^2 &= t_2 \chi_2^2 \\ -a_1 a_2 m_{tot} + m_3 a_2 (a_1 - p_3) + m_4 a_1 (a_2 - p_4) &= 0 \\ m_3 a_2 q_3 + m_4 a_1 q_4 &= 0 \end{aligned} \quad (6.17)$$

Here the two relative motions are in opposite direction but with different angular velocities. Moment balance solutions for nonlinear relations between the two relative DoFs can be found in a similar way.

6.1.2 Moment balance of three principal elements in series

Figure 6.3 shows the planar open-chain 3-DoF principal vector linkage of Fig. 3.7 with an arbitrary CoM in each element. Also each element has an inertia I_i about its CoM S_i . In general, the angular momentum about the common CoM in S within the xy -plane can be written as

$$\begin{aligned} H_S = (I_1 + I_{12} + I_{13})\dot{\theta}_1 + (I_2 + I_{11} + I_{31})\dot{\theta}_2 + (I_3 + I_{32} + I_{33})\dot{\theta}_3 + \\ m_1(\bar{r}_1 \times \dot{\bar{r}}_1)_z + m_2(\bar{r}_2 \times \dot{\bar{r}}_2)_z + m_3(\bar{r}_3 \times \dot{\bar{r}}_3)_z + \end{aligned} \quad (6.18)$$

$$m_{11}(\bar{r}_{11} \times \dot{\bar{r}}_{11})_z + m_{12}(\bar{r}_{12} \times \dot{\bar{r}}_{12})_z + m_{13}(\bar{r}_{13} \times \dot{\bar{r}}_{13})_z + \\ m_{31}(\bar{r}_{31} \times \dot{\bar{r}}_{31})_z + m_{32}(\bar{r}_{32} \times \dot{\bar{r}}_{32})_z + m_{33}(\bar{r}_{33} \times \dot{\bar{r}}_{33})_z$$

where vectors \bar{r}_i describe the positions of the link CoMs S_i relative to the common CoM in S and can be written with the principal vectors as

$$\begin{aligned}\bar{r}_1 &= a_3 \Pi_3 - a_{21} \Pi_{21} - p_1 \Pi_1 + q_1 \Pi'_1 \\ \bar{r}_2 &= a_1 \Pi_1 + a_3 \Pi_3 + p_2^a \Pi_{21} + q_2^a \Pi'_{21} - p_2^b \Pi_{23} + q_2^b \Pi'_{23} \\ \bar{r}_3 &= a_1 \Pi_1 + a_{23} \Pi_{23} - p_3 \Pi_3 - q_3 \Pi'_3 \\ \bar{r}_{11} &= a_3 \Pi_3 - p_{11} \Pi_{21} - q_{11} \Pi'_{21} \\ \bar{r}_{12} &= a_3 \Pi_3 + p_{12} \Pi_1 - q_{12} \Pi'_1 \\ \bar{r}_{13} &= p_{13} \Pi_1 - q_{13} \Pi'_1 \\ \bar{r}_{31} &= a_1 \Pi_1 + p_{31} \Pi_{23} - q_{31} \Pi'_{23} \\ \bar{r}_{32} &= a_1 \Pi_1 + p_{32} \Pi_3 + q_{32} \Pi'_3 \\ \bar{r}_{33} &= p_{33} \Pi_3 + q_{33} \Pi'_3\end{aligned}\tag{6.19}$$

where

$$\Pi_i = \begin{bmatrix} \cos \theta_i \\ \sin \theta_i \\ 0 \end{bmatrix} \quad \Pi'_i = \begin{bmatrix} -\sin \theta_i \\ \cos \theta_i \\ 0 \end{bmatrix}$$

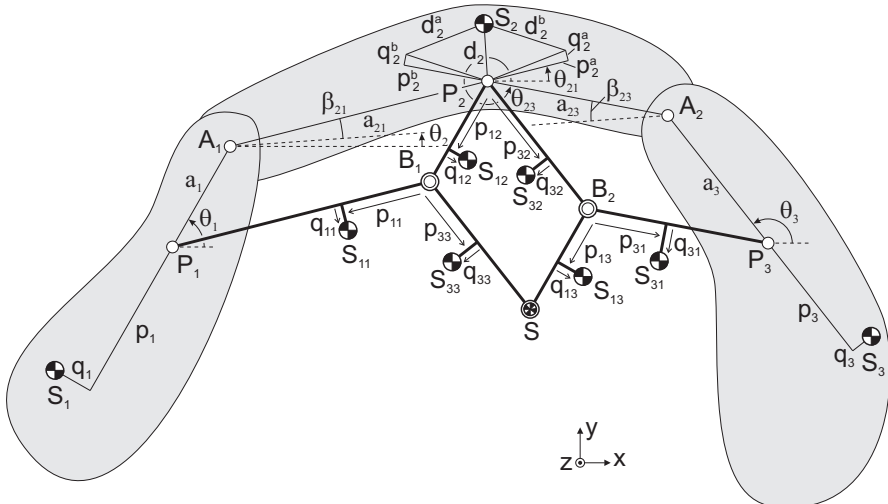


Fig. 6.3 General open-chain 3-DoF principal vector linkage with common CoM in S . Each of the nine elements has an arbitrary mass distribution with link mass m_i and link inertia I_i in and about link CoM S_i .

Here angles $\theta_{21} = \theta_2 + \beta_{21}$ and $\theta_{23} = \theta_2 - \beta_{23}$ divide θ_2 with respect to the principal dimensions a_{21} and a_{23} , respectively, as illustrated in Fig. 6.3. When these vectors and their derivatives are substituted, the angular momentum can be written as

$$\begin{aligned}
H_S = & (I_1 + I_{12} + I_{13} + m_1(p_1^2 + q_1^2) + (m_2 + m_3 + m_{31} + m_{32})a_1^2 + \\
& m_{12}(p_{12}^2 + q_{12}^2) + m_{13}(p_{13}^2 + q_{13}^2))\dot{\theta}_1 + \\
& (I_2 + I_{11} + I_{31})\dot{\theta}_2 + \\
& (m_1a_{21}^2 + m_2((p_2^a)^2 + (q_2^a)^2) + m_{11}(p_{11}^2 + q_{11}^2))\dot{\theta}_{21} + \\
& (m_2((p_2^b)^2 + (q_2^b)^2) + m_3a_{23}^2 + m_{31}(p_{31}^2 + q_{31}^2))\dot{\theta}_{23} + \\
& (I_3 + I_{32} + I_{33} + m_3(p_3^2 + q_3^2) + (m_1 + m_2 + m_{11} + m_{12})a_3^2 + \\
& m_{32}(p_{32}^2 + q_{32}^2) + m_{33}(p_{33}^2 + q_{33}^2))\dot{\theta}_3 + \\
& (m_1a_{21}p_1 + m_2a_1p_2^a)\cos(\theta_1 - \theta_{21})(\dot{\theta}_1 + \dot{\theta}_{21}) + \\
& (-m_2a_1p_2^b + m_3a_1a_{23} + m_{31}a_1p_{31})\cos(\theta_1 - \theta_{23})(\dot{\theta}_1 + \dot{\theta}_{23}) + \\
& (-m_1a_3p_1 + m_2a_1a_3 - m_3a_1p_3 + m_{12}a_3p_{12} + m_{32}a_1p_{32})\cos(\theta_1 - \theta_3)(\dot{\theta}_1 + \dot{\theta}_3) + \\
& (-m_2p_2^ap_2^b + m_2q_2^aq_2^b)\cos(\theta_{21} - \theta_{23})(\dot{\theta}_{21} + \dot{\theta}_{23}) + \\
& (-m_1a_{21}a_3 + m_2a_3p_2^a - m_{11}a_3p_{11})\cos(\theta_{21} - \theta_3)(\dot{\theta}_{21} + \dot{\theta}_3) + \\
& (-m_2a_3p_2^b - m_3a_{23}p_3)\cos(\theta_{23} - \theta_3)(\dot{\theta}_{23} + \dot{\theta}_3) + \\
& (m_1a_{21}q_1 + m_2a_1q_2^a)\sin(\theta_1 - \theta_{21})(\dot{\theta}_1 + \dot{\theta}_{21}) + \\
& (m_2a_1q_2^b - m_{31}a_1q_{31})\sin(\theta_1 - \theta_{23})(\dot{\theta}_1 + \dot{\theta}_{23}) + \\
& (-m_1a_3q_1 - m_3a_1q_3 + m_{12}a_3q_{12} + m_{32}a_1q_{32})\sin(\theta_1 - \theta_3)(\dot{\theta}_1 + \dot{\theta}_3) + \\
& (m_2p_2^aq_2^b + m_2p_2^bq_2^a)\sin(\theta_{21} - \theta_{23})(\dot{\theta}_{21} + \dot{\theta}_{23}) + \\
& (-m_2a_3q_2^a + m_{11}a_3q_{11})\sin(\theta_{21} - \theta_3)(\dot{\theta}_{21} + \dot{\theta}_3) + \\
& (-m_2a_3q_2^b - m_3a_{23}q_3)\sin(\theta_{23} - \theta_3)(\dot{\theta}_{23} + \dot{\theta}_3)
\end{aligned} \tag{6.20}$$

Then when the relations $\theta_{21} = \theta_2 + \beta_{21}$, $\theta_{23} = \theta_2 - \beta_{23}$, and $\dot{\theta}_{21} = \dot{\theta}_{23} = \dot{\theta}_2$ are substituted, the angular momentum equation becomes

$$\begin{aligned}
H_S = & m_{tot}\{\chi_1^2\dot{\theta}_1 + \chi_2^2\dot{\theta}_2 + \chi_3^2\dot{\theta}_3\} + \\
& (m_1a_{21}p_1 + m_2a_1p_2^a)\cos(\theta_1 - \theta_2 - \beta_{21})(\dot{\theta}_1 + \dot{\theta}_2) + \\
& (-m_2a_1p_2^b + m_3a_1a_{23} + m_{31}a_1p_{31})\cos(\theta_1 - \theta_2 + \beta_{23})(\dot{\theta}_1 + \dot{\theta}_2) + \\
& (-m_1a_3p_1 + m_2a_1a_3 - m_3a_1p_3 + m_{12}a_3p_{12} + m_{32}a_1p_{32})\cos(\theta_1 - \theta_3)(\dot{\theta}_1 + \dot{\theta}_3) + \\
& (-m_1a_{21}a_3 + m_2a_3p_2^a - m_{11}a_3p_{11})\cos(\theta_2 - \theta_3 + \beta_{21})(\dot{\theta}_2 + \dot{\theta}_3) + \\
& (-m_2a_3p_2^b - m_3a_{23}p_3)\cos(\theta_2 - \theta_3 - \beta_{23})(\dot{\theta}_2 + \dot{\theta}_3) + \\
& (m_1a_{21}q_1 + m_2a_1q_2^a)\sin(\theta_1 - \theta_2 - \beta_{21})(\dot{\theta}_1 + \dot{\theta}_2) + \\
& (m_2a_1q_2^b - m_{31}a_1q_{31})\sin(\theta_1 - \theta_2 + \beta_{23})(\dot{\theta}_1 + \dot{\theta}_2) + \\
& (-m_1a_3q_1 - m_3a_1q_3 + m_{12}a_3q_{12} + m_{32}a_1q_{32})\sin(\theta_1 - \theta_3)(\dot{\theta}_1 + \dot{\theta}_3) + \\
& (-m_2a_3q_2^a + m_{11}a_3q_{11})\sin(\theta_2 - \theta_3 + \beta_{21})(\dot{\theta}_2 + \dot{\theta}_3) + \\
& (-m_2a_3q_2^b - m_3a_{23}q_3)\sin(\theta_2 - \theta_3 - \beta_{23})(\dot{\theta}_2 + \dot{\theta}_3)
\end{aligned} \tag{6.21}$$

with $m_{tot} = m_1 + m_2 + m_3 + m_{11} + m_{12} + m_{13} + m_{31} + m_{32} + m_{33}$ and with the reduced inertias $m_{tot}\chi_1^2$, $m_{tot}\chi_2^2$, and $m_{tot}\chi_3^2$ written as

$$\begin{aligned} m_{tot}\chi_1^2 &= I_1 + I_{12} + I_{13} + m_1(p_1^2 + q_1^2) + (m_2 + m_3 + m_{31} + m_{32})a_1^2 + \\ &\quad m_{12}(p_{12}^2 + q_{12}^2) + m_{13}(p_{13}^2 + q_{13}^2) \end{aligned} \quad (6.22)$$

$$\begin{aligned} m_{tot}\chi_2^2 &= I_2 + I_{11} + I_{31} + m_1a_{21}^2 + m_2d_2^2 + m_3a_{23}^2 + \\ &\quad m_{11}(p_{11}^2 + q_{11}^2) + m_{31}(p_{31}^2 + q_{31}^2) \end{aligned} \quad (6.23)$$

$$\begin{aligned} m_{tot}\chi_3^2 &= I_3 + I_{32} + I_{33} + m_3(p_3^2 + q_3^2) + (m_1 + m_2 + m_{11} + m_{12})a_3^2 + \\ &\quad m_{32}(p_{32}^2 + q_{32}^2) + m_{33}(p_{33}^2 + q_{33}^2) \end{aligned} \quad (6.24)$$

where $d_2^2 = (p_2^a)^2 + (q_2^a)^2 + (p_2^b)^2 + (q_2^b)^2 + 2(-p_2^ap_2^b + q_2^aq_2^b)\cos(\beta_{21} + \beta_{23}) + 2(p_2^aq_2^b + p_2^bq_2^a)\sin(\beta_{21} + \beta_{23})$, with d_2 the distance P_2S_2 as in Fig. 6.3. These reduced inertia terms can be found also from the ELMSs of the individual motions of the three relative DoFs (Figs. 3.11 and 3.13), which are shown in Fig. 6.4. They are calculated as the inertia of the masses in each ELMS about the principal point together with the link inertias.

Subsequently the force balance conditions (3.22) can be substituted for m_1p_1 , m_1q_1 , $m_2p_2^a$, $m_2q_2^a$, $m_2p_2^b$, $m_2q_2^b$, m_3p_3 , and m_3q_3 with which the angular momentum results in its final form as

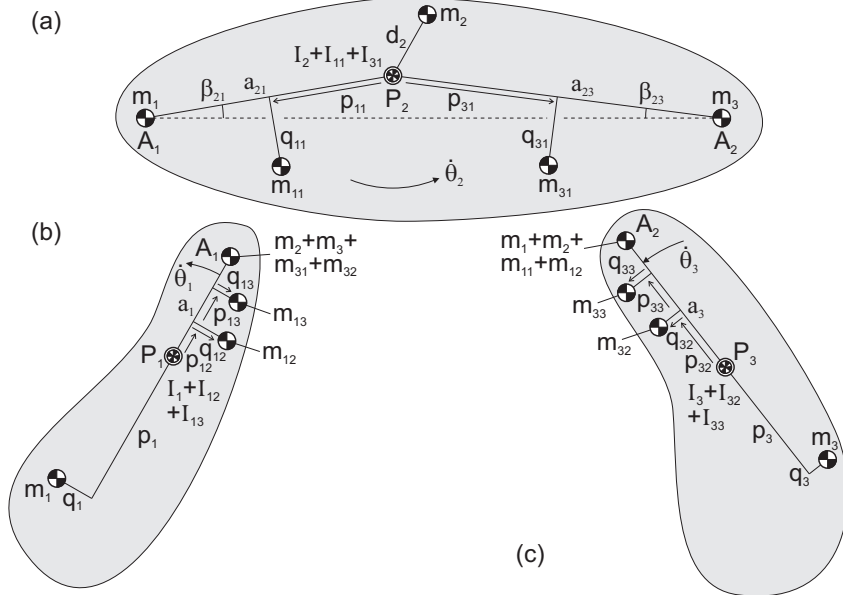


Fig. 6.4 ELMSs of the relative DoFs from which the three reduced inertias are obtained as the inertia of each model about the principal point.

$$\begin{aligned}
H_S = m_{tot} \{ & \chi_1^2 \dot{\theta}_1 + \chi_2^2 \dot{\theta}_2 + \chi_3^2 \dot{\theta}_3 - a_1 a_3 \cos(\theta_1 - \theta_3) (\dot{\theta}_1 + \dot{\theta}_3) + \\
& a_1 a_{21} \cos(\theta_1 - \theta_2 - \beta_{21}) (\dot{\theta}_1 + \dot{\theta}_2) - a_3 a_{23} \cos(\theta_2 - \theta_3 - \beta_{23}) (\dot{\theta}_2 + \dot{\theta}_3) \} - \\
& (m_{33} a_1 a_{21} + m_{11} (a_{21} - p_{11}) a_1 + m_{12} (a_1 - p_{12}) a_{21} + \\
& m_{13} (a_1 - p_{13}) a_{21}) \cos(\theta_1 - \theta_2 - \beta_{21}) (\dot{\theta}_1 + \dot{\theta}_2) + \\
& (m_{33} (a_3 - p_{33}) a_1 + m_{13} (a_1 - p_{13}) a_3) \cos(\theta_1 - \theta_3) (\dot{\theta}_1 + \dot{\theta}_3) + \\
& (m_{13} a_3 a_{23} + m_{31} (a_{23} - p_{31}) a_3 + m_{32} (a_3 - p_{32}) a_{23} + \\
& m_{33} (a_3 - p_{33}) a_{23}) \cos(\theta_2 - \theta_3 - \beta_{23}) (\dot{\theta}_2 + \dot{\theta}_3) - \\
& (m_{11} a_1 q_{11} + m_{12} a_{21} q_{12} + m_{13} a_{21} q_{13}) \sin(\theta_1 - \theta_2 - \beta_{21}) (\dot{\theta}_1 + \dot{\theta}_2) - \\
& (m_{13} a_3 q_{13} + m_{33} a_1 q_{33}) \sin(\theta_1 - \theta_3) (\dot{\theta}_1 + \dot{\theta}_3) - \\
& (m_{31} a_3 q_{31} + m_{32} a_{23} q_{32} + m_{33} a_{23} q_{33}) \sin(\theta_2 - \theta_3 - \beta_{23}) (\dot{\theta}_2 + \dot{\theta}_3)
\end{aligned} \tag{6.25}$$

The first part of the angular momentum is mainly related to the three principal elements with

$$\begin{aligned}
H_{S,P} = m_{tot} (\chi_1^2 \dot{\theta}_1 + \chi_2^2 \dot{\theta}_2 + \chi_3^2 \dot{\theta}_3 - a_1 a_3 \cos(\theta_1 - \theta_3) (\dot{\theta}_1 + \dot{\theta}_3) + \\
a_1 a_{21} \cos(\theta_1 - \theta_2 - \beta_{21}) (\dot{\theta}_1 + \dot{\theta}_2) - a_3 a_{23} \cos(\theta_2 - \theta_3 - \beta_{23}) (\dot{\theta}_2 + \dot{\theta}_3))
\end{aligned} \tag{6.26}$$

From the angular momentum the moment balance condition of the 3-DoF principal vector linkage in Fig. 6.3 is found as:

$$\begin{aligned}
m_{tot} (\chi_1^2 \dot{\theta}_1 + \chi_2^2 \dot{\theta}_2 + \chi_3^2 \dot{\theta}_3) + ((m_{tot} - m_{33}) a_1 a_{21} - m_{11} (a_{21} - p_{11}) a_1 - \\
m_{12} (a_1 - p_{12}) a_{21} - m_{13} (a_1 - p_{13}) a_{21}) \cos(\theta_1 - \theta_2 - \beta_{21}) (\dot{\theta}_1 + \dot{\theta}_2) + \\
(-m_{tot} a_1 a_3 + m_{33} (a_3 - p_{33}) a_1 + m_{13} (a_1 - p_{13}) a_3) \cos(\theta_1 - \theta_3) (\dot{\theta}_1 + \dot{\theta}_3) + \\
(-(m_{tot} - m_{13}) a_3 a_{23} + m_{31} (a_{23} - p_{31}) a_3 + m_{32} (a_3 - p_{32}) a_{23} + \\
m_{33} (a_3 - p_{33}) a_{23}) \cos(\theta_2 - \theta_3 - \beta_{23}) (\dot{\theta}_2 + \dot{\theta}_3) + \\
(m_{11} a_1 q_{11} + m_{12} a_{21} q_{12} + m_{13} a_{21} q_{13}) \sin(\theta_1 - \theta_2 - \beta_{21}) (\dot{\theta}_1 + \dot{\theta}_2) - \\
(m_{13} a_3 q_{13} + m_{33} a_1 q_{33}) \sin(\theta_1 - \theta_3) (\dot{\theta}_1 + \dot{\theta}_3) - \\
(m_{31} a_3 q_{31} + m_{32} a_{23} q_{32} + m_{33} a_{23} q_{33}) \sin(\theta_2 - \theta_3 - \beta_{23}) (\dot{\theta}_2 + \dot{\theta}_3) = \Lambda
\end{aligned} \tag{6.27}$$

with constant $\Lambda \in \Re$.

Moment balance solutions

To have the moment balance condition (6.27) hold, also here the relative motions need to be related linearly or nonlinearly in specific way, for which there are various possibilities. As an example one case is shown where $\Lambda = 0$, $\theta_3 = t_1 - \theta_1$, and $\theta_2 = t_2$, which means that $\dot{\theta}_3 = -\dot{\theta}_1$ and $\dot{\theta}_2 = 0$ and principal element 2 does not rotate while principal elements 1 and 3 rotate with the same angular velocity in opposite direction. The moment balance condition (6.27) then reduces to

$$\begin{aligned}
& m_{tot}(\chi_1^2 - \chi_3^2) + ((m_{tot} - m_{33})a_1a_{21} - m_{11}(a_{21} - p_{11})a_1 - \\
& m_{12}(a_1 - p_{12})a_{21} - m_{13}(a_1 - p_{13})a_{21})\cos(\theta_1 - t_2 - \beta_{21}) + \\
& (-(m_{tot} - m_{13})a_3a_{23} + m_{31}(a_{23} - p_{31})a_3 + m_{32}(a_3 - p_{32})a_{23} + \\
& m_{33}(a_3 - p_{33})a_{23})\cos(\theta_1 - t_1 + t_2 - \beta_{23}) + \\
& (m_{11}a_1q_{11} + m_{12}a_{21}q_{12} + m_{13}a_{21}q_{13})\sin(\theta_1 - t_2 - \beta_{21}) + \\
& (m_{31}a_3q_{31} + m_{32}a_{23}q_{32} + m_{33}a_{23}q_{33})\sin(\theta_1 - t_1 + t_2 - \beta_{23}) = 0
\end{aligned}$$

and a set of moment balance conditions is found as

$$\begin{aligned}
\theta_2 &= t_2 \\
\theta_3 &= t_1 - \theta_1 \\
\chi_1^2 &= \chi_3^2 \\
(m_{tot} - m_{33})a_1a_{21} - m_{11}(a_{21} - p_{11})a_1 - m_{12}(a_1 - p_{12})a_{21} - m_{13}(a_1 - p_{13})a_{21} &= 0 \\
(m_{13} - m_{tot})a_3a_{23} + m_{31}(a_{23} - p_{31})a_3 + m_{32}(a_3 - p_{32})a_{23} + m_{33}(a_3 - p_{33})a_{23} &= 0 \\
m_{11}a_1q_{11} + m_{12}a_{21}q_{12} + m_{13}a_{21}q_{13} &= 0 \\
m_{31}a_3q_{31} + m_{32}a_{23}q_{32} + m_{33}a_{23}q_{33} &= 0
\end{aligned} \tag{6.28}$$

For the symmetric opposite motion of principal elements 1 and 3 with respect to element 2 where $t_1 = \pi + 2t_2$, then when the principal vector linkage is designed with the symmetry $\beta_{21} = \beta_{23}$, the moment balance condition reduces to

$$\begin{aligned}
& m_{tot}(\chi_1^2 - \chi_3^2) + ((m_{tot} - m_{33})a_1a_{21} - m_{11}(a_{21} - p_{11})a_1 - \\
& m_{12}(a_1 - p_{12})a_{21} - m_{13}(a_1 - p_{13})a_{21} + (m_{tot} - m_{13})a_3a_{23} - \\
& m_{31}(a_{23} - p_{31})a_3 - m_{32}(a_3 - p_{32})a_{23} - m_{33}(a_3 - p_{33})a_{23})\cos(\theta_1 - t_2 - \beta_{21}) + \\
& (m_{11}a_1q_{11} + m_{12}a_{21}q_{12} + m_{13}a_{21}q_{13} - \\
& m_{31}a_3q_{31} - m_{32}a_{23}q_{32} - m_{33}a_{23}q_{33})\sin(\theta_1 - t_2 - \beta_{21}) = 0
\end{aligned}$$

and a set of moment balance conditions is found as

$$\begin{aligned}
\theta_2 &= t_2 \\
\theta_3 &= \pi + 2t_2 - \theta_1 \\
\chi_1^2 &= \chi_3^2 \\
(m_{tot} - m_{33})a_1a_{21} - m_{11}(a_{21} - p_{11})a_1 - m_{12}(a_1 - p_{12})a_{21} - m_{13}(a_1 - p_{13})a_{21} + \\
(m_{tot} - m_{13})a_3a_{23} - m_{31}(a_{23} - p_{31})a_3 - m_{32}(a_3 - p_{32})a_{23} - m_{33}(a_3 - p_{33})a_{23} &= 0 \\
m_{11}a_1q_{11} + m_{12}a_{21}q_{12} + m_{13}a_{21}q_{13} - m_{31}a_3q_{31} - m_{32}a_{23}q_{32} - m_{33}a_{23}q_{33} &= 0
\end{aligned} \tag{6.29}$$

For both sets of moment balance solutions the principal vector linkage of three DoFs is reduced to a dynamically balanced mechanism of one DoF.

6.1.3 Moment balance of four principal elements in series

Figure 6.5 shows the planar open-chain 3-DoF principal vector linkage of Fig. 3.23 with a general CoM in each element. Also each element has an inertia I_i about its CoM S_i . In general, the angular momentum about the common CoM in S within the xy -plane can be written as

$$\begin{aligned}
 H_S = & (I_1 + I_{12} + I_{13} + I_{14})\dot{\theta}_1 + (I_2 + I_{11} + I_{21} + I_{22})\dot{\theta}_2 + \\
 & (I_3 + I_{31} + I_{32} + I_{41})\dot{\theta}_3 + (I_4 + I_{42} + I_{43} + I_{44})\dot{\theta}_4 + \\
 & m_1(\bar{r}_1 \times \dot{\bar{r}}_1)_z + m_2(\bar{r}_2 \times \dot{\bar{r}}_2)_z + m_3(\bar{r}_3 \times \dot{\bar{r}}_3)_z + m_4(\bar{r}_4 \times \dot{\bar{r}}_4)_z + \\
 & m_{11}(\bar{r}_{11} \times \dot{\bar{r}}_{11})_z + m_{12}(\bar{r}_{12} \times \dot{\bar{r}}_{12})_z + m_{13}(\bar{r}_{13} \times \dot{\bar{r}}_{13})_z + m_{14}(\bar{r}_{14} \times \dot{\bar{r}}_{14})_z + \\
 & m_{21}(\bar{r}_{21} \times \dot{\bar{r}}_{21})_z + m_{22}(\bar{r}_{22} \times \dot{\bar{r}}_{22})_z + m_{31}(\bar{r}_{31} \times \dot{\bar{r}}_{31})_z + m_{32}(\bar{r}_{32} \times \dot{\bar{r}}_{32})_z + \\
 & m_{41}(\bar{r}_{41} \times \dot{\bar{r}}_{41})_z + m_{42}(\bar{r}_{42} \times \dot{\bar{r}}_{42})_z + m_{43}(\bar{r}_{43} \times \dot{\bar{r}}_{43})_z + m_{44}(\bar{r}_{44} \times \dot{\bar{r}}_{44})_z
 \end{aligned} \tag{6.30}$$

where vectors \bar{r}_i describe the positions of the link CoMs S_i relative to the common CoM in S and can be written with the principal vectors as

$$\begin{aligned}
 \bar{r}_1 &= a_4\Pi_4 - a_{32}\Pi_{32} - a_{21}\Pi_{21} - p_1\Pi_1 + q_1\Pi'_1 \\
 \bar{r}_2 &= a_1\Pi_1 + a_4\Pi_4 - a_{32}\Pi_{32} + p_2^a\Pi_{21} + q_2^a\Pi'_{21} - p_2^b\Pi_{23} + q_2^b\Pi'_{23} \\
 \bar{r}_3 &= a_1\Pi_1 + a_4\Pi_4 + a_{23}\Pi_{23} + p_3^a\Pi_{32} + q_3^a\Pi'_{32} - p_3^b\Pi_{34} + q_3^b\Pi'_{34} \\
 \bar{r}_4 &= a_1\Pi_1 + a_{23}\Pi_{23} + a_{34}\Pi_{34} - p_4\Pi_4 - q_4\Pi'_4 \\
 \bar{r}_{11} &= a_4\Pi_4 - a_{32}\Pi_{32} - p_{11}\Pi_{21} - q_{11}\Pi'_{21}
 \end{aligned}$$

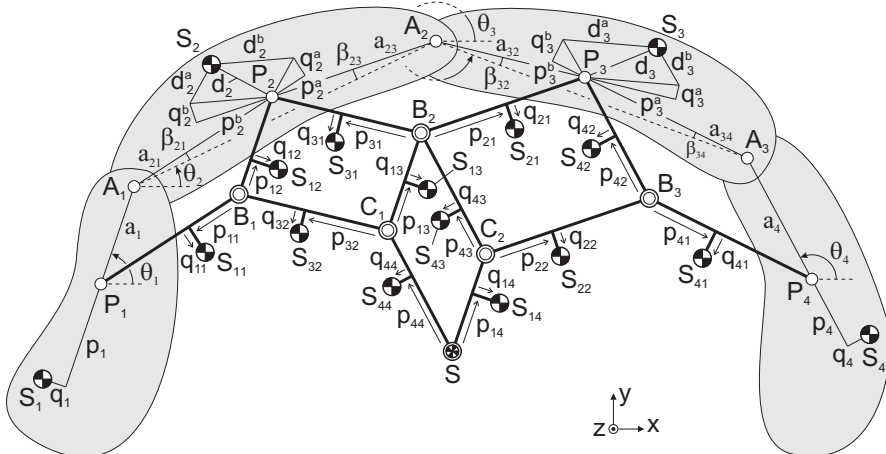


Fig. 6.5 General open-chain 4-DoF principal vector linkage with common CoM in S . Each of the 16 elements has an arbitrary mass distribution with link mass m_i and link inertia I_i in and about link CoM S_i .

$$\begin{aligned}
\bar{r}_{12} &= a_4 \Pi_4 - a_{32} \Pi_{32} + p_{12} \Pi_1 - q_{12} \Pi'_1 & (6.31) \\
\bar{r}_{13} &= a_4 \Pi_4 + p_{13} \Pi_1 - q_{13} \Pi'_1 \\
\bar{r}_{14} &= p_{14} \Pi_1 - q_{14} \Pi'_1 \\
\bar{r}_{21} &= a_1 \Pi_1 + a_4 \Pi_4 + p_{21} \Pi_{23} - q_{21} \Pi'_{23} \\
\bar{r}_{22} &= a_1 \Pi_1 + p_{22} \Pi_{23} - q_{22} \Pi'_{23} \\
\bar{r}_{31} &= a_1 \Pi_1 + a_4 \Pi_4 - p_{31} \Pi_{32} - q_{31} \Pi'_{32} \\
\bar{r}_{32} &= a_1 \Pi_1 - p_{32} \Pi_{32} - q_{32} \Pi'_{32} \\
\bar{r}_{41} &= a_1 \Pi_1 + a_{23} \Pi_{23} + p_{41} \Pi_{34} - q_{41} \Pi'_{34} \\
\bar{r}_{42} &= a_1 \Pi_1 + a_{23} \Pi_{23} + p_{42} \Pi_4 + q_{42} \Pi'_4 \\
\bar{r}_{43} &= a_1 \Pi_1 + p_{43} \Pi_4 + q_{43} \Pi'_4 \\
\bar{r}_{44} &= p_{44} \Pi_4 + q_{44} \Pi'_4
\end{aligned}$$

with

$$\Pi_i = \begin{bmatrix} \cos \theta_i \\ \sin \theta_i \\ 0 \end{bmatrix} \quad \Pi'_i = \begin{bmatrix} -\sin \theta_i \\ \cos \theta_i \\ 0 \end{bmatrix}$$

Here angles $\theta_{21} = \theta_2 + \beta_{21}$ and $\theta_{23} = \theta_2 - \beta_{23}$ divide θ_2 with respect to the principal dimensions a_{21} and a_{23} , respectively, and angles $\theta_{32} = \theta_3 + \beta_{32}$ and $\theta_{34} = \theta_3 - \beta_{34}$ divide θ_3 with respect to the principal dimensions a_{32} and a_{34} , respectively. When these vectors and their derivatives are substituted, the angular momentum can be written as

$$\begin{aligned}
H_S = & \\
& (I_1 + I_{12} + I_{13} + I_{14} + (m_2 + m_3 + m_4 + m_{21} + m_{22} + m_{31} + m_{41} + m_{42} + m_{43})a_1^2 + \\
& m_1(p_1^2 + q_1^2) + m_{12}(p_{12}^2 + q_{12}^2) + m_{13}(p_{13}^2 + q_{13}^2) + m_{14}(p_{14}^2 + q_{14}^2))\dot{\theta}_1 + \\
& (I_2 + I_{11} + I_{21} + I_{22})\dot{\theta}_2 + (I_3 + I_{31} + I_{32} + I_{41})\dot{\theta}_3 + \\
& (m_1 a_{21}^2 + m_2((p_2^a)^2 + (q_2^a)^2) + m_{11}(p_{11}^2 + q_{11}^2))\dot{\theta}_{21} + \\
& ((m_3 + m_4 + m_{41} + m_{42})a_{23}^2 + m_2((p_2^b)^2 + (q_2^b)^2) + \\
& m_{21}(p_{21}^2 + q_{21}^2) + m_{22}(p_{22}^2 + q_{22}^2))\dot{\theta}_{23} + \\
& ((m_1 + m_2 + m_{11} + m_{12})a_{32}^2 + m_3((p_3^a)^2 + (q_3^a)^2) + \\
& m_{31}(p_{31}^2 + q_{31}^2) + m_{32}(p_{32}^2 + q_{32}^2))\dot{\theta}_{32} + \\
& (m_3((p_3^b)^2 + (q_3^b)^2) + m_4 a_{34}^2 + m_{41}(p_{41}^2 + q_{41}^2))\dot{\theta}_{34} + \\
& (I_4 + I_{42} + I_{43} + I_{44} + (m_1 + m_2 + m_3 + m_{11} + m_{12} + m_{13} + m_{21} + m_{31} + m_{32})a_4^2 + \\
& m_4(p_4^2 + q_4^2) + m_{42}(p_{42}^2 + q_{42}^2) + m_{43}(p_{43}^2 + q_{43}^2) + m_{44}(p_{44}^2 + q_{44}^2))\dot{\theta}_4 + \\
& (m_1 a_{21} p_1 + m_2 a_1 p_2^a) \cos(\theta_1 - \theta_{21})(\dot{\theta}_1 + \dot{\theta}_{21}) + \\
& ((m_3 + m_4 + m_{41} + m_{42})a_1 a_{23} - m_2 a_1 p_2^b + m_{21} a_1 p_{21} + \\
& m_{22} a_1 p_{22}) \cos(\theta_1 - \theta_{23})(\dot{\theta}_1 + \dot{\theta}_{23}) + \\
& (m_1 a_{32} p_1 - m_2 a_1 a_{32} + m_3 a_1 p_3^a - m_{12} a_{32} p_{12} -
\end{aligned}$$

$$\begin{aligned}
& m_{31}a_1p_{31})\cos(\theta_1 - \theta_{32})(\dot{\theta}_1 + \dot{\theta}_{32}) + \\
& (-m_3a_1p_3^b + m_4a_1a_{34} + m_4a_1p_{41})\cos(\theta_1 - \theta_{34})(\dot{\theta}_1 + \dot{\theta}_{34}) + \\
& (-m_1a_4p_1 + (m_2 + m_3 + m_{21} + m_{31})a_1a_4 - m_4a_1p_4 + m_{12}a_4p_{12} + \\
& m_{13}a_4p_{13} + m_{42}a_1p_{42} + m_{43}a_1p_{43})\cos(\theta_1 - \theta_4)(\dot{\theta}_1 + \dot{\theta}_4) + \\
& (-m_2p_2^a p_2^b + m_2q_2^a q_2^b)\cos(\theta_{21} - \theta_{23})(\dot{\theta}_{21} + \dot{\theta}_{23}) + \\
& (m_1a_{21}a_{32} - m_2a_{32}p_2^a + m_{11}a_{32}p_{11})\cos(\theta_{21} - \theta_{32})(\dot{\theta}_{21} + \dot{\theta}_{32}) + \\
& (-m_1a_{21}a_4 + m_2a_4p_2^a - m_{11}a_4p_{11})\cos(\theta_{21} - \theta_4)(\dot{\theta}_{21} + \dot{\theta}_4) + \\
& (m_2a_{32}p_2^b + m_3a_{23}p_3^a)\cos(\theta_{23} - \theta_{32})(\dot{\theta}_{23} + \dot{\theta}_{32}) + \\
& (-m_3a_{23}p_3^b + m_4a_{23}a_{34} + m_{41}a_{23}p_{41})\cos(\theta_{23} - \theta_{34})(\dot{\theta}_{23} + \dot{\theta}_{34}) + \\
& (-m_2a_4p_2^b + m_3a_{23}a_4 - m_4a_{23}p_4 + m_{21}a_4p_{21} + \\
& m_{42}a_{23}p_{42})\cos(\theta_{23} - \theta_4)(\dot{\theta}_{23} + \dot{\theta}_4) + \\
& (-m_3p_3^a p_3^b + m_3q_3^a q_3^b)\cos(\theta_{32} - \theta_{34})(\dot{\theta}_{32} + \dot{\theta}_{34}) + \\
& (-m_1a_{32}a_4 - m_2a_{32}a_4 + m_3a_4p_3^a - m_{11}a_{32}a_4 - m_{12}a_{32}a_4 - \\
& m_{31}a_4p_{31} - m_{32}a_4p_{32})\cos(\theta_{32} - \theta_4)(\dot{\theta}_{32} + \dot{\theta}_4) + \\
& (-m_3a_4p_3^b - m_4a_{34}p_4)\cos(\theta_{34} - \theta_4)(\dot{\theta}_{34} + \dot{\theta}_4) + \\
& (m_1a_{21}q_1 + m_2a_1q_2^a)\sin(\theta_1 - \theta_{21})(\dot{\theta}_1 + \dot{\theta}_{21}) + \\
& (m_2a_1q_2^b - m_{21}a_1q_{21} - m_{22}a_1q_{22})\sin(\theta_1 - \theta_{23})(\dot{\theta}_1 + \dot{\theta}_{23}) + \\
& (m_1a_{32}q_1 + m_3a_1q_3^a - m_{12}a_{32}q_{12} - m_{31}a_1q_{31})\sin(\theta_1 - \theta_{32})(\dot{\theta}_1 + \dot{\theta}_{32}) + \\
& (m_3a_1q_3^b - m_{41}a_1q_{41})\sin(\theta_1 - \theta_{34})(\dot{\theta}_1 + \dot{\theta}_{34}) + \\
& (-m_1a_4q_1 - m_4a_1q_4 + m_{12}a_4q_{12} + m_{13}a_4q_{13} + m_{42}a_1q_{42} + \\
& m_{43}a_1q_{43})\sin(\theta_1 - \theta_4)(\dot{\theta}_1 + \dot{\theta}_4) + \\
& (m_2p_2^a q_2^b + m_2p_2^b q_2^a)\sin(\theta_{21} - \theta_{23})(\dot{\theta}_{21} + \dot{\theta}_{23}) + \\
& (m_2a_{32}q_2^a - m_{11}a_{32}q_{11})\sin(\theta_{21} - \theta_{32})(\dot{\theta}_{21} + \dot{\theta}_{32}) + \\
& (-m_2a_4q_2^a + m_{11}a_4q_{11})\sin(\theta_{21} - \theta_4)(\dot{\theta}_{21} + \dot{\theta}_4) + \\
& (m_2a_{32}q_2^b + m_3a_{23}q_3^a)\sin(\theta_{23} - \theta_{32})(\dot{\theta}_{23} + \dot{\theta}_{32}) + \\
& (m_3a_{23}q_3^b - m_{41}a_{23}q_{41})\sin(\theta_{23} - \theta_{34})(\dot{\theta}_{23} + \dot{\theta}_{34}) + \\
& (-m_2a_4q_2^b + m_{21}a_4q_{21} - a_{23}m_4q_4 + a_{23}m_{42}q_{42})\sin(\theta_{23} - \theta_4)(\dot{\theta}_{23} + \dot{\theta}_4) + \\
& (m_3p_3^a q_3^b + m_3p_3^b q_3^a)\sin(\theta_{32} - \theta_{34})(\dot{\theta}_{32} + \dot{\theta}_{34}) + \\
& (-m_3a_4q_3^a + m_{31}a_4q_{31} + m_{32}a_4q_{32})\sin(\theta_{32} - \theta_4)(\dot{\theta}_{32} + \dot{\theta}_4) + \\
& (-m_3a_4q_3^b - m_4a_{34}q_4)\sin(\theta_{34} - \theta_4)(\dot{\theta}_{34} + \dot{\theta}_4)
\end{aligned} \tag{6.32}$$

Then when relations $\theta_{21} = \theta_2 + \beta_{21}$, $\theta_{23} = \theta_2 - \beta_{23}$, $\dot{\theta}_{21} = \dot{\theta}_{23} = \dot{\theta}_2$, $\theta_{32} = \theta_3 + \beta_{32}$, $\theta_{34} = \theta_3 - \beta_{34}$, and $\dot{\theta}_{32} = \dot{\theta}_{34} = \dot{\theta}_3$ are substituted, the angular momentum equation becomes

$$\begin{aligned}
H_S = & \\
& m_{tot}\{\chi_1^2\dot{\theta}_1 + \chi_2^2\dot{\theta}_2 + \chi_3^2\dot{\theta}_3 + \chi_4^2\dot{\theta}_4\} + \\
& (m_1a_{21}p_1 + m_2a_1p_2^a)\cos(\theta_1 - \theta_2 - \beta_{21})(\dot{\theta}_1 + \dot{\theta}_2) +
\end{aligned}$$

$$\begin{aligned}
& ((m_3 + m_4 + m_{41} + m_{42})a_1a_{23} - m_2a_1p_2^b + m_{21}a_1p_{21} + \\
& m_{22}a_1p_{22})\cos(\theta_1 - \theta_2 + \beta_{23})(\dot{\theta}_1 + \dot{\theta}_2) + \\
& (m_1a_{32}p_1 - m_2a_1a_{32} + m_3a_1p_3^a - m_{12}a_{32}p_{12} - \\
& m_{31}a_1p_{31})\cos(\theta_1 - \theta_3 - \beta_{32})(\dot{\theta}_1 + \dot{\theta}_3) + \\
& (-m_3a_1p_3^b + m_4a_1a_{34} + m_{41}a_1p_{41})\cos(\theta_1 - \theta_3 + \beta_{34})(\dot{\theta}_1 + \dot{\theta}_3) + \\
& (-m_1a_4p_1 + (m_2 + m_3 + m_{21} + m_{31})a_1a_4 - m_4a_1p_4 + m_{12}a_4p_{12} + \\
& m_{13}a_4p_{13} + m_{42}a_1p_{42} + m_{43}a_1p_{43})\cos(\theta_1 - \theta_4)(\dot{\theta}_1 + \dot{\theta}_4) + \\
& (m_1a_{21}a_{32} - m_2a_{32}p_2^a + m_{11}a_{32}p_{11})\cos(\theta_2 - \theta_3 + \beta_{21} - \beta_{32})(\dot{\theta}_2 + \dot{\theta}_3) + \\
& (-m_1a_{21}a_4 + m_2a_4p_2^a - m_{11}a_4p_{11})\cos(\theta_2 - \theta_4 + \beta_{21})(\dot{\theta}_2 + \dot{\theta}_4) + \\
& (m_2a_{32}p_2^b + m_3a_{23}p_3^a)\cos(\theta_2 - \theta_3 - \beta_{23} - \beta_{32})(\dot{\theta}_2 + \dot{\theta}_3) + \\
& (-m_3a_{23}p_3^b + m_4a_{23}a_{34} + m_{41}a_{23}p_{41})\cos(\theta_2 - \theta_3 - \beta_{23} + \beta_{34})(\dot{\theta}_2 + \dot{\theta}_3) + \\
& (-m_2a_4p_2^b + m_3a_{23}a_4 - m_4a_{23}p_4 + m_{21}a_4p_{21} + \\
& m_{42}a_{23}p_{42})\cos(\theta_2 - \theta_4 - \beta_{23})(\dot{\theta}_2 + \dot{\theta}_4) + \\
& (-m_1a_{32}a_4 - m_2a_{32}a_4 + m_3a_4p_3^a - m_{11}a_{32}a_4 - m_{12}a_{32}a_4 - \\
& m_{31}a_4p_{31} - m_{32}a_4p_{32})\cos(\theta_3 - \theta_4 + \beta_{32})(\dot{\theta}_3 + \dot{\theta}_4) + \\
& (-m_3a_4p_3^b - m_4a_{34}p_4)\cos(\theta_3 - \theta_4 - \beta_{34})(\dot{\theta}_3 + \dot{\theta}_4) + \\
& (m_1a_{21}q_1 + m_2a_1q_2^a)\sin(\theta_1 - \theta_2 - \beta_{21})(\dot{\theta}_1 + \dot{\theta}_2) + \\
& (m_2a_1q_2^b - m_{21}a_1q_{21} - m_{22}a_1q_{22})\sin(\theta_1 - \theta_2 + \beta_{23})(\dot{\theta}_1 + \dot{\theta}_2) + \\
& (m_1a_{32}q_1 + m_3a_1q_3^a - m_{12}a_{32}q_{12} - m_{31}a_1q_{31})\sin(\theta_1 - \theta_3 - \beta_{32})(\dot{\theta}_1 + \dot{\theta}_3) + \\
& (m_3a_1q_3^b - m_{41}a_1q_{41})\sin(\theta_1 - \theta_3 + \beta_{34})(\dot{\theta}_1 + \dot{\theta}_3) + \\
& (-m_1a_4q_1 - m_4a_1q_4 + m_{12}a_4q_{12} + m_{13}a_4q_{13} + m_{42}a_1q_{42} + \\
& m_{43}a_1q_{43})\sin(\theta_1 - \theta_4)(\dot{\theta}_1 + \dot{\theta}_4) + \\
& (m_2a_{32}q_2^a - m_{11}a_{32}q_{11})\sin(\theta_2 - \theta_3 + \beta_{21} - \beta_{32})(\dot{\theta}_2 + \dot{\theta}_3) + \\
& (-m_2a_4q_2^a + m_{11}a_4q_{11})\sin(\theta_2 - \theta_4 + \beta_{21})(\dot{\theta}_2 + \dot{\theta}_4) + \\
& (m_2a_{32}q_2^b + m_3a_{23}q_3^a)\sin(\theta_2 - \theta_3 - \beta_{23} - \beta_{32})(\dot{\theta}_2 + \dot{\theta}_3) + \\
& (m_3a_{23}q_3^b - m_{41}a_{23}q_{41})\sin(\theta_2 - \theta_3 - \beta_{23} + \beta_{34})(\dot{\theta}_2 + \dot{\theta}_3) + \\
& (-m_2a_4q_2^b + m_{21}a_4q_{21} - a_{23}m_4q_4 + a_{23}m_{42}q_{42})\sin(\theta_2 - \theta_4 - \beta_{23})(\dot{\theta}_2 + \dot{\theta}_4) + \\
& (-m_3a_4q_3^a + m_{31}a_4q_{31} + m_{32}a_4q_{32})\sin(\theta_3 - \theta_4 + \beta_{32})(\dot{\theta}_3 + \dot{\theta}_4) + \\
& (-m_3a_4q_3^b - m_4a_{34}q_4)\sin(\theta_3 - \theta_4 - \beta_{34})(\dot{\theta}_3 + \dot{\theta}_4)
\end{aligned} \tag{6.33}$$

with $m_{tot} = m_1 + m_2 + m_3 + m_4 + m_{11} + m_{12} + m_{13} + m_{14} + m_{21} + m_{22} + m_{31} + m_{32} + m_{41} + m_{42} + m_{43} + m_{44}$ and with the reduced inertias $m_{tot}\chi_1^2$, $m_{tot}\chi_2^2$, $m_{tot}\chi_3^2$, and $m_{tot}\chi_4^2$ written as

$$\begin{aligned}
m_{tot}\chi_1^2 = & I_1 + I_{12} + I_{13} + I_{14} + m_1(p_1^2 + q_1^2) + m_{12}(p_{12}^2 + q_{12}^2) + \\
& m_{13}(p_{13}^2 + q_{13}^2) + m_{14}(p_{14}^2 + q_{14}^2) + \\
& (m_2 + m_3 + m_4 + m_{21} + m_{22} + m_{31} + m_{41} + m_{42} + m_{43})a_1^2
\end{aligned} \tag{6.34}$$

$$\begin{aligned} m_{tot} \chi_2^2 &= I_2 + I_{11} + I_{21} + I_{22} + m_1 a_{21}^2 + m_2 d_2^2 + (m_3 + m_4 + m_{41} + m_{42}) a_{23}^2 + \\ &\quad m_{11}(p_{11}^2 + q_{11}^2) + m_{21}(p_{21}^2 + q_{21}^2) + m_{22}(p_{22}^2 + q_{22}^2) \end{aligned} \quad (6.35)$$

$$\begin{aligned} m_{tot} \chi_3^2 &= I_3 + I_{31} + I_{32} + I_{41} + m_4 a_{34}^2 + m_3 d_3^2 + (m_1 + m_2 + m_{11} + m_{12}) a_{32}^2 + \\ &\quad m_{41}(p_{41}^2 + q_{41}^2) + m_{31}(p_{31}^2 + q_{31}^2) + m_{32}(p_{32}^2 + q_{32}^2) \end{aligned} \quad (6.36)$$

$$\begin{aligned} m_{tot} \chi_4^2 &= I_4 + I_{42} + I_{43} + I_{44} + m_4(p_4^2 + q_4^2) + m_{42}(p_{42}^2 + q_{42}^2) + \\ &\quad m_{43}(p_{43}^2 + q_{43}^2) + m_{44}(p_{44}^2 + q_{44}^2) + \\ &\quad (m_1 + m_2 + m_3 + m_{11} + m_{12} + m_{13} + m_{21} + m_{31} + m_{32}) a_4^2 \end{aligned} \quad (6.37)$$

where

$$\begin{aligned} d_2^2 &= (p_2^a)^2 + (q_2^a)^2 + (p_2^b)^2 + (q_2^b)^2 + 2(-p_2^a p_2^b + q_2^a q_2^b) \cos(\beta_{21} + \beta_{23}) + \\ &\quad 2(p_2^a q_2^b + p_2^b q_2^a) \sin(\beta_{21} + \beta_{23}) \\ d_3^2 &= (p_3^a)^2 + (q_3^a)^2 + (p_3^b)^2 + (q_3^b)^2 + 2(-p_3^a p_3^b + q_3^a q_3^b) \cos(\beta_{32} + \beta_{34}) + \\ &\quad 2(p_3^a q_3^b + p_3^b q_3^a) \sin(\beta_{32} + \beta_{34}) \end{aligned}$$

with d_2 the distance $P_2 S_2$ and d_3 the distance $P_3 S_3$ as illustrated in Fig. 6.5. These reduced inertia terms can be found also from the ELMSSs of the individual motions of the four relative DoFs, of which the ELMSSs of DoF 2 and of DoF 3 are shown in Fig. 3.28. They are calculated as the inertia of the masses in each ELMSS about the principal point together with the link inertias.

The final form of the angular momentum is obtained when the force balance conditions (3.67) are substituted for $m_1 p_1$, $m_1 q_1$, $m_2 p_2^a$, $m_2 q_2^a$, $m_2 p_2^b$, $m_2 q_2^b$, $m_3 p_3^a$, $m_3 q_3^a$, $m_3 p_3^b$, $m_3 q_3^b$, $m_4 p_4$, and $m_4 q_4$ which results in

$$\begin{aligned} H_S = & m_{tot} \{ \chi_1^2 \dot{\theta}_1 + \chi_2^2 \dot{\theta}_2 + \chi_3^2 \dot{\theta}_3 + \chi_4^2 \dot{\theta}_4 + \\ & a_1 a_{21} \cos(\theta_1 - \theta_2 - \beta_{21})(\dot{\theta}_1 + \dot{\theta}_2) + a_1 a_{32} \cos(\theta_1 - \theta_3 - \beta_{32})(\dot{\theta}_1 + \dot{\theta}_3) - \\ & a_1 a_4 \cos(\theta_1 - \theta_4)(\dot{\theta}_1 + \dot{\theta}_4) + a_{23} a_{32} \cos(\theta_2 - \theta_3 - \beta_{23} - \beta_{32})(\dot{\theta}_2 + \dot{\theta}_3) - \\ & a_{23} a_4 \cos(\theta_2 - \theta_4 - \beta_{23})(\dot{\theta}_2 + \dot{\theta}_4) - a_4 a_{34} \cos(\theta_3 - \theta_4 - \beta_{34})(\dot{\theta}_3 + \dot{\theta}_4) \} + \\ & (-(m_{32} + m_{44})a_1 a_{21} - m_{11}(a_{21} - p_{11})a_1 - m_{12}(a_1 - p_{12})a_{21} - \\ & m_{13}(a_1 - p_{13})a_{21} - m_{14}(a_1 - p_{14})a_{21}) \cos(\theta_1 - \theta_2 - \beta_{21})(\dot{\theta}_1 + \dot{\theta}_2) + \\ & (-m_{44}a_1 a_{32} - m_{13}(a_1 - p_{13})a_{32} - m_{14}(a_1 - p_{14})a_{32} - \\ & m_{32}(a_{32} - p_{32})a_1) \cos(\theta_1 - \theta_3 - \beta_{32})(\dot{\theta}_1 + \dot{\theta}_3) + \\ & (m_{14}(a_1 - p_{14})a_4 + m_{44}(a_4 - p_{44})a_1) \cos(\theta_1 - \theta_4)(\dot{\theta}_1 + \dot{\theta}_4) + \\ & (-(m_{13} + m_{14} + m_{43} + m_{44})a_{23}a_{32} - m_{21}(a_{23} - p_{21})a_{32} - m_{22}(a_{23} - p_{22})a_{32} - \\ & m_{31}(a_{32} - p_{31})a_{23} - m_{32}(a_{32} - p_{32})a_{23}) \cos(\theta_2 - \theta_3 - \beta_{23} - \beta_{32})(\dot{\theta}_2 + \dot{\theta}_3) + \\ & (m_{14}a_{23}a_4 + m_{22}(a_{23} - p_{22})a_4 + m_{43}(a_4 - p_{43})a_{23} + \\ & m_{44}(a_4 - p_{44})a_{23}) \cos(\theta_2 - \theta_4 - \beta_{23})(\dot{\theta}_2 + \dot{\theta}_4) + \\ & ((m_{14} + m_{22})a_4 a_{34} + m_{41}(a_{34} - p_{41})a_4 + m_{42}(a_4 - p_{42})a_{34} + \\ & m_{43}(a_4 - p_{43})a_{34} + m_{44}(a_4 - p_{44})a_{34}) \cos(\theta_3 - \theta_4 - \beta_{34})(\dot{\theta}_3 + \dot{\theta}_4) + \end{aligned} \quad (6.38)$$

$$\begin{aligned}
& (m_{11}a_1q_{11} + a_{21}(m_{12}q_{12} + m_{13}q_{13} + m_{14}q_{14})) \sin(\theta_1 - \theta_2 - \beta_{21})(\dot{\theta}_1 + \dot{\theta}_2) + \\
& (m_{13}a_{32}q_{13} + m_{14}a_{32}q_{14} + m_{32}a_1q_{32}) \sin(\theta_1 - \theta_3 - \beta_{32})(\dot{\theta}_1 + \dot{\theta}_3) + \\
& (-m_{14}a_4q_{14} - m_{44}a_1q_{44}) \sin(\theta_1 - \theta_4)(\dot{\theta}_1 + \dot{\theta}_4) + \\
& ((m_{21}q_{21} + m_{22}q_{22})a_{32} + \\
& (m_{31}q_{31} + m_{32}q_{32})a_{23}) \sin(\theta_2 - \theta_3 - \beta_{23} - \beta_{32})(\dot{\theta}_2 + \dot{\theta}_3) + \\
& (m_{22}a_4q_{22} + m_{43}a_{23}q_{43} + m_{44}a_{23}q_{44}) \sin(\theta_2 - \theta_4 - \beta_{23})(\dot{\theta}_2 + \dot{\theta}_4) + \\
& (-a_4m_{41}q_{41} - a_{34}(m_{42}q_{42} + m_{43}q_{43} + m_{44}q_{44})) \sin(\theta_3 - \theta_4 - \beta_{34})(\dot{\theta}_3 + \dot{\theta}_4)
\end{aligned}$$

Also here the first part of the angular momentum is mainly related to the four principal elements with

$$\begin{aligned}
H_{S,P} = m_{tot} & \{ \chi_1^2 \dot{\theta}_1 + \chi_2^2 \dot{\theta}_2 + \chi_3^2 \dot{\theta}_3 + \chi_4^2 \dot{\theta}_4 + \\
& a_1 a_{21} \cos(\theta_1 - \theta_2 - \beta_{21})(\dot{\theta}_1 + \dot{\theta}_2) + a_1 a_{32} \cos(\theta_1 - \theta_3 - \beta_{32})(\dot{\theta}_1 + \dot{\theta}_3) - \\
& a_1 a_4 \cos(\theta_1 - \theta_4)(\dot{\theta}_1 + \dot{\theta}_4) + a_{23} a_{32} \cos(\theta_2 - \theta_3 - \beta_{23} - \beta_{32})(\dot{\theta}_2 + \dot{\theta}_3) - \\
& a_{23} a_4 \cos(\theta_2 - \theta_4 - \beta_{23})(\dot{\theta}_2 + \dot{\theta}_4) - a_4 a_{34} \cos(\theta_3 - \theta_4 - \beta_{34})(\dot{\theta}_3 + \dot{\theta}_4) \}
\end{aligned}$$

From the angular momentum the moment balance condition of the 4-DoF principal vector linkage in Fig. 6.5 is found as:

$$\begin{aligned}
& m_{tot}(\chi_1^2 \dot{\theta}_1 + \chi_2^2 \dot{\theta}_2 + \chi_3^2 \dot{\theta}_3 + \chi_4^2 \dot{\theta}_4) + ((m_{tot} - m_{32} - m_{44})a_1 a_{21} - \\
& m_{11}(a_{21} - p_{11})a_1 - m_{12}(a_1 - p_{12})a_{21} - m_{13}(a_1 - p_{13})a_{21} - \\
& m_{14}(a_1 - p_{14})a_{21}) \cos(\theta_1 - \theta_2 - \beta_{21})(\dot{\theta}_1 + \dot{\theta}_2) + \quad (6.39) \\
& ((m_{tot} - m_{44})a_1 a_{32} - m_{13}(a_1 - p_{13})a_{32} - m_{14}(a_1 - p_{14})a_{32} - \\
& m_{32}(a_{32} - p_{32})a_1) \cos(\theta_1 - \theta_3 - \beta_{32})(\dot{\theta}_1 + \dot{\theta}_3) + \\
& (-m_{tot}a_1 a_4 + m_{14}(a_1 - p_{14})a_4 + m_{44}(a_4 - p_{44})a_1) \cos(\theta_1 - \theta_4)(\dot{\theta}_1 + \dot{\theta}_4) + \\
& ((m_{tot} - m_{13} - m_{14} - m_{43} - m_{44})a_{23}a_{32} - m_{21}(a_{23} - p_{21})a_{32} - m_{22}(a_{23} - p_{22})a_{32} - \\
& m_{31}(a_{32} - p_{31})a_{23} - m_{32}(a_{32} - p_{32})a_{23}) \cos(\theta_2 - \theta_3 - \beta_{23} - \beta_{32})(\dot{\theta}_2 + \dot{\theta}_3) + \\
& (-m_{tot} - m_{14})a_{23}a_4 + m_{22}(a_{23} - p_{22})a_4 + m_{43}(a_4 - p_{43})a_{23} + \\
& m_{44}(a_4 - p_{44})a_{23}) \cos(\theta_2 - \theta_4 - \beta_{23})(\dot{\theta}_2 + \dot{\theta}_4) + \\
& (-m_{tot} - m_{14} - m_{22})a_4 a_{34} + m_{41}(a_{34} - p_{41})a_4 + m_{42}(a_4 - p_{42})a_{34} + \\
& m_{43}(a_4 - p_{43})a_{34} + m_{44}(a_4 - p_{44})a_{34}) \cos(\theta_3 - \theta_4 - \beta_{34})(\dot{\theta}_3 + \dot{\theta}_4) + \\
& (m_{11}a_1q_{11} + a_{21}(m_{12}q_{12} + m_{13}q_{13} + m_{14}q_{14})) \sin(\theta_1 - \theta_2 - \beta_{21})(\dot{\theta}_1 + \dot{\theta}_2) + \\
& (m_{13}a_{32}q_{13} + m_{14}a_{32}q_{14} + m_{32}a_1q_{32}) \sin(\theta_1 - \theta_3 - \beta_{32})(\dot{\theta}_1 + \dot{\theta}_3) + \\
& (-m_{14}a_4q_{14} - m_{44}a_1q_{44}) \sin(\theta_1 - \theta_4)(\dot{\theta}_1 + \dot{\theta}_4) + \\
& (m_{21}a_{32}q_{21} + m_{22}a_{32}q_{22} + m_{31}a_{23}q_{31} + \\
& m_{32}a_{23}q_{32}) \sin(\theta_2 - \theta_3 - \beta_{23} - \beta_{32})(\dot{\theta}_2 + \dot{\theta}_3) + \\
& (m_{22}a_4q_{22} + m_{43}a_{23}q_{43} + m_{44}a_{23}q_{44}) \sin(\theta_2 - \theta_4 - \beta_{23})(\dot{\theta}_2 + \dot{\theta}_4) + \\
& (-a_4m_{41}q_{41} - a_{34}(m_{42}q_{42} + m_{43}q_{43} + m_{44}q_{44})) \sin(\theta_3 - \theta_4 - \beta_{34})(\dot{\theta}_3 + \dot{\theta}_4) = \Lambda
\end{aligned}$$

with constant $\Lambda \in \Re$.

Moment balance solutions

With an increasing number of DoFs, there is an increasing number of possible solutions to have the moment balance condition (6.39) hold. For example for $\Lambda = 0$, when for a symmetric opposite motion of principal elements 1 and 4, and a symmetric opposite motion of principal elements 2 and 3 $\theta_4 = \pi - \theta_1$, and $\theta_3 = \pi - \theta_2$ and $\dot{\theta}_4 = -\dot{\theta}_1$ and $\dot{\theta}_3 = -\dot{\theta}_2$. Then when the design has the specific symmetries $\beta_{32} = \beta_{23}$ and $\beta_{34} = \beta_{21}$, the moment balance condition (6.39) reduces to

$$\begin{aligned}
 & m_{tot}(\chi_1^2 - \chi_4^2)\dot{\theta}_1 + m_{tot}(\chi_2^2 - \chi_3^2)\dot{\theta}_2 + ((m_{tot} - m_{32} - m_{44})a_1a_{21} - \\
 & m_{11}(a_{21} - p_{11})a_1 - m_{12}(a_1 - p_{12})a_{21} - m_{13}(a_1 - p_{13})a_{21} - m_{14}(a_1 - p_{14})a_{21} + \\
 & (m_{tot} - m_{14} - m_{22})a_4a_{34} - m_{41}(a_{34} - p_{41})a_4 - m_{42}(a_4 - p_{42})a_{34} - \\
 & m_{43}(a_4 - p_{43})a_{34} - m_{44}(a_4 - p_{44})a_{34})\cos(\theta_1 - \theta_2 - \beta_{21})(\dot{\theta}_1 + \dot{\theta}_2) - \\
 & ((m_{tot} - m_{44})a_1a_{32} - m_{13}(a_1 - p_{13})a_{32} - m_{14}(a_1 - p_{14})a_{32} - \\
 & m_{32}(a_{32} - p_{32})a_1 - (m_{tot} - m_{14})a_{23}a_4 - m_{22}(a_{23} - p_{22})a_4 - \\
 & m_{43}(a_4 - p_{43})a_{23} - m_{44}(a_4 - p_{44})a_{23})\cos(\theta_1 + \theta_2 - \beta_{23})(\dot{\theta}_1 - \dot{\theta}_2) + \\
 & (m_{11}a_1q_{11} + a_{21}(m_{12}q_{12} + m_{13}q_{13} + m_{14}q_{14}) + \\
 & a_4m_{41}q_{41} + a_{34}(m_{42}q_{42} + m_{43}q_{43} + m_{44}q_{44}))\sin(\theta_1 - \theta_2 - \beta_{21})(\dot{\theta}_1 + \dot{\theta}_2) - \\
 & (m_{13}a_{32}q_{13} + m_{14}a_{32}q_{14} + m_{32}a_1q_{32} - \\
 & m_{22}a_4q_{22} - m_{43}a_{23}q_{43} - m_{44}a_{23}q_{44})\sin(\theta_1 + \theta_2 - \beta_{23})(\dot{\theta}_1 - \dot{\theta}_2) = 0
 \end{aligned} \tag{6.40}$$

A set of moment balance conditions then is obtained as

$$\begin{aligned}
 \theta_4 &= \pi - \theta_1 \\
 \theta_3 &= \pi - \theta_2 \\
 \beta_{32} &= \beta_{23} \\
 \beta_{34} &= \beta_{21} \\
 \chi_1^2 &= \chi_4^2 \\
 \chi_2^2 &= \chi_3^2 \\
 & (m_{tot} - m_{32} - m_{44})a_1a_{21} - m_{11}(a_{21} - p_{11})a_1 - m_{12}(a_1 - p_{12})a_{21} - \\
 & m_{13}(a_1 - p_{13})a_{21} - m_{14}(a_1 - p_{14})a_{21} + (m_{tot} - m_{14} - m_{22})a_4a_{34} - \\
 & m_{41}(a_{34} - p_{41})a_4 - m_{42}(a_4 - p_{42})a_{34} - m_{43}(a_4 - p_{43})a_{34} - \\
 & m_{44}(a_4 - p_{44})a_{34} = 0 \\
 & (m_{tot} - m_{44})a_1a_{32} - m_{13}(a_1 - p_{13})a_{32} - m_{14}(a_1 - p_{14})a_{32} - \\
 & m_{32}(a_{32} - p_{32})a_1 - (m_{tot} - m_{14})a_{23}a_4 - m_{22}(a_{23} - p_{22})a_4 - \\
 & m_{43}(a_4 - p_{43})a_{23} - m_{44}(a_4 - p_{44})a_{23} = 0
 \end{aligned} \tag{6.41}$$

$$\begin{aligned}
& m_{11}a_1q_{11} + a_{21}(m_{12}q_{12} + m_{13}q_{13} + m_{14}q_{14}) + \\
& a_{44}m_{41}q_{41} + a_{34}(m_{42}q_{42} + m_{43}q_{43} + m_{44}q_{44}) = 0 \\
& m_{13}a_{32}q_{13} + m_{14}a_{32}q_{14} + m_{32}a_1q_{32} - m_{22}a_4q_{22} - \\
& m_{43}a_{23}q_{43} - m_{44}a_{23}q_{44} = 0
\end{aligned}$$

With this solution the principal vector linkage with four DoFs has become a dynamically balanced mechanism with two DoFs. An example of such a mechanism is shown in chapter 7.

6.2 Moment balance conditions of closed-chain principal vector linkages

When a closed-chain principal vector linkage is obtained by closing an open-chain principal vector linkage with the open-chain method, then the angular momentum of the linkage is known from the open-chain principal vector linkage. For instance the angular momentum of the linkage in Fig. 4.1 is written with (6.38) and the moment balance conditions follow from (6.39). Therefore the open-chain method can be used to derive a variety of inherently moment-balanced linkages.

Considering the loop closure relations to obtain the angular momentum of inherent closed-chain principal vector linkages, such as in Fig. 4.11, is more challenging. It was shown that to derive the force balance conditions (i.e. to define the principal vector linkage) one element in a closed chain can be modeled with equivalent masses. To find the angular momentum this way, the equivalent model should not only be mass equivalent but also inertia equivalent. In other words, a dynamic equivalent model of one element in a closed chain is needed.

The mass equivalent models in Fig. 4.10b and Fig. 4.10c have a specific inertia about their CoMs, but they are both different and they in general do not equal the real inertia of the element. In case that the real inertia is equal to one of them, would this mean that the angular momentum of the element then is considered with the inertias of the masses that are projected in the mass equivalent principal chain? Although it is technically possible to adapt the virtual equivalent mass and its location in the mass equivalent models to fit the real inertia of the element, for a mass symmetric element where the virtual equivalent mass is zero this is not possible and the inertia of the element then is determined as $m_i^a e_i^2 + m_i^b (l_i - e_i)^2$. Therefore it seems that still something is missing in the development of a general dynamic equivalent model of an element in a closed chain.

It is known from literature that an element can be modeled dynamically equivalent when the inertia of the (real) equivalent masses in the joints equals the real inertia of the element [108]. When this is applied for the closed-chain principal vector linkage in Fig. 4.11, then the dynamic equivalent model of the mass-symmetric element A_0A_3 where $f_4 = 0$ becomes as in Fig. 6.6, which has an inertia $I_4 = m_4^a e_4^2 + m_4^b (l_4 - e_4)^2$. This means that with the two real equivalent masses

in the MEPC in Fig. 4.12a, inertia I_4 is included and the ELMS of each relative DoF becomes as in Fig. 6.7, which are combined from the ELMSSs in Fig. 4.19, Fig. 4.20, and Fig. 6.4. The angular momentum of the MEPC is found with (6.25) with $m_{tot} = m_1 + m_2 + m_3 + m_4 + m_{11} + m_{12} + m_{13} + m_{31} + m_{32} + m_{33}$ and with the reduced inertias $m_{tot}\chi_1^2$, $m_{tot}\chi_2^2$, and $m_{tot}\chi_3^2$ written as

$$\begin{aligned} m_{tot}\chi_1^2 &= I_1 + I_{12} + I_{13} + m_1(p_1^2 + q_1^2) + m_4^b d_1^2 + (m_2 + m_3 + m_4^a + m_{31} + m_{32})a_1^2 \\ &\quad m_{12}(p_{12}^2 + q_{12}^2) + m_{13}(p_{13}^2 + q_{13}^2) \end{aligned} \quad (6.42)$$

$$\begin{aligned} m_{tot}\chi_2^2 &= I_2 + I_{11} + I_{31} + (m_1 + m_4^b)a_{21}^2 + m_2 d_2^2 + (m_3 + m_4^a)a_{23}^2 + \\ &\quad m_{11}(p_{11}^2 + q_{11}^2) + m_{31}(p_{31}^2 + q_{31}^2) \end{aligned} \quad (6.43)$$

$$\begin{aligned} m_{tot}\chi_3^2 &= I_3 + I_{32} + I_{33} + m_3(p_3^2 + q_3^2) + m_4^a d_3^2 + (m_1 + m_2 + m_4^b + m_{11} + m_{12})a_3^2 + \\ &\quad m_{32}(p_{32}^2 + q_{32}^2) + m_{33}(p_{33}^2 + q_{33}^2) \end{aligned} \quad (6.44)$$

These reduced inertias are the inertias of the ELMSSs in Fig. 6.7 about their CoM.

The next question is how to model a mass-symmetric element where $I_4 \neq m_4^q e_4^2 + m_4^b(l_4 - e_4)^2$ such that it can be included in the MEPC. The model with solely two real equivalent masses in the joints then is not applicable. Maybe the real equivalent masses can also be modeled outside the joints in locations based on scaled dimensions to fit the real inertia of the element. Or there could be other (negative) (virtual) equivalent masses to model the inertia with. Subsequently, how can an element with two joints and with an arbitrary CoM where $f_4 \neq 0$ be modeled dynamically equivalent? Do the virtual equivalent masses also have rotational inertia? These are open questions that need further investigation.

As an illustration, the dynamic simulations in Fig. 4.21 and Fig. 5.20 show dynamically balanced motions since the two applied torques are equal and opposite with which the resultant moment in the base is zero.

6.3 Discussion and conclusion

This chapter showed that the angular momentum of principal vector linkages can be written with reduced inertias and principal dimensions from which moment balance conditions can be derived. A pantograph, an open-chain principal vector linkage of three principal elements in series, and an open-chain principal vector linkage of four

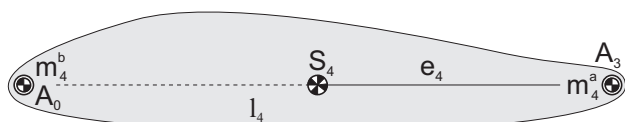


Fig. 6.6 Dynamic equivalent model of a mass symmetric element A_0A_3 where $f_4 = 0$.

principal elements in series were investigated. The same approach can be applied for principal vector linkages with more principal elements, in series or in parallel.

Deriving the angular momentum equation in its final form becomes cumbersome especially when the number of relative DoFs increases. However, for each principal vector linkage it only has to be derived once. For all mechanism solutions that are subsequently synthesized from a principal vector linkage, the angular momentum equation only has to be adapted.

Since in general the angular momentum of a principal vector linkage is not zero, shaking moment balance can only be obtained by reducing the DoFs. It was shown how linear relations among the relative DoFs can be included to derive specific sets of moment balance conditions. Still it remains a challenging puzzle to derive moment balance solutions, especially when nonlinear relations among the relative DoFs have to be considered. For instance, it should be possible to derive the moment balance solutions of the 4R four-bar mechanism as in [85, 78] from a 3-DoF principal vector linkage of which the three DoFs are nonlinearly related. Tools to do this are desired. Because of the specific compact form of the angular momentum equation, this approach has the potential to be simpler than current methods such as in [85, 78] that are complex and hard to apply for synthesis.

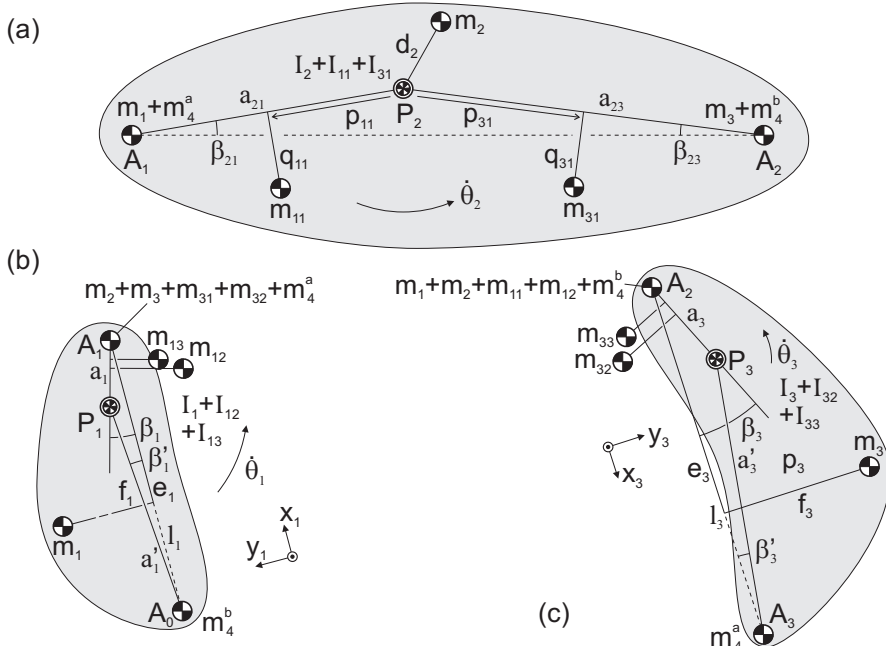


Fig. 6.7 ELMS of each relative DoF of the closed-chain principal vector linkage in Fig. 4.11 with mass-symmetric element A_0A_3 from which the three reduced inertias are found. The mass m_4 and the inertia I_4 of element A_0A_3 are included with the real equivalent masses m_4^a and m_4^b .

Also closed-chain principal vector linkages were considered, where the angular momentum of a mass equivalent principal chain was found only for the specific case that the inertia of the equivalently modeled element equals the inertia of the two real equivalent masses about their CoM. The development of an inertia equivalent model of a general element in a closed chain with which its inertia is included in the mass equivalent principal chain requires further investigation.

Chapter 7

Synthesis of inherently dynamically balanced (IDB) mechanisms

Abstract The *method of principal vector linkages* is presented in this chapter for the kinematic synthesis of inherently dynamically balanced mechanisms from principal vector linkage architectures. For specific tasks and functions, dynamic balance solutions are derived by various methods, including changing the parameters of the elements, eliminating elements, reduction of DoFs, introducing gears and sliders, and by combining them. Examples of dynamically balanced graspers and manipulators are presented together with examples of force-balanced movable structures such as a bridge and a roof.

7.1 Approach for synthesis of IDB mechanisms

Synthesis of inherently balanced mechanisms can be approached in two ways. In chapter 2 it was shown how with the method of linearly independent linear momentum inherent and advantageous force balance solutions can be obtained of initial kinematic architectures. Then for specific kinematic conditions the geometric parameters of the linkage are adapted, i.e. by rearranging the locations of the base pivots and by changing the dimensions of the elements together with the mass parameters.

Another approach for synthesis is to derive balanced mechanisms from principal vector linkage architectures such as those in chapters 3-6, which will be named the *method of principal vector linkages*. Principal vector linkage architectures are force balanced and can be adapted kinematically in various ways, e.g. for path, motion or function generation, while maintaining the essential kinematic relations for balance. For moment balance the relative motions of a principal vector linkage architecture have to be constrained by additional elements.

Principal vector linkage architectures can be adapted by redesigning the principal vector links and their locations such as in Fig. 3.18 and Fig. 3.20. From architectures that are overconstrained such as in Fig. 5.7, balanced mechanism solutions can be derived by eliminating redundant links. Under certain conditions it is also pos-

sible to exchange links with other mechanism elements such as sliders and gears, to replace joints with other types of joints, and to fix or merge links to reduce the relative motions. Balanced mechanism solutions can be obtained also by combining principal vector linkage architectures.

Since dynamic balance is all about similar opposite motion of masses and inertias, this aspect can assist in finding solutions intuitively. From a kinematic point of view elements need to counter-rotate and to counter-translate with respect to one another to obtain balance. In general, the more the motions are similar and opposite, the better the balanced solution can be. The level of similar opposite motions depends on the mass distribution in each element. Moment balance solutions can be obtained by combining force-balanced linkages such that their elements counter-rotate.

The following sections illustrate the synthesis approach from principal vector linkage architectures with engineering examples of inherently balanced mechanisms.

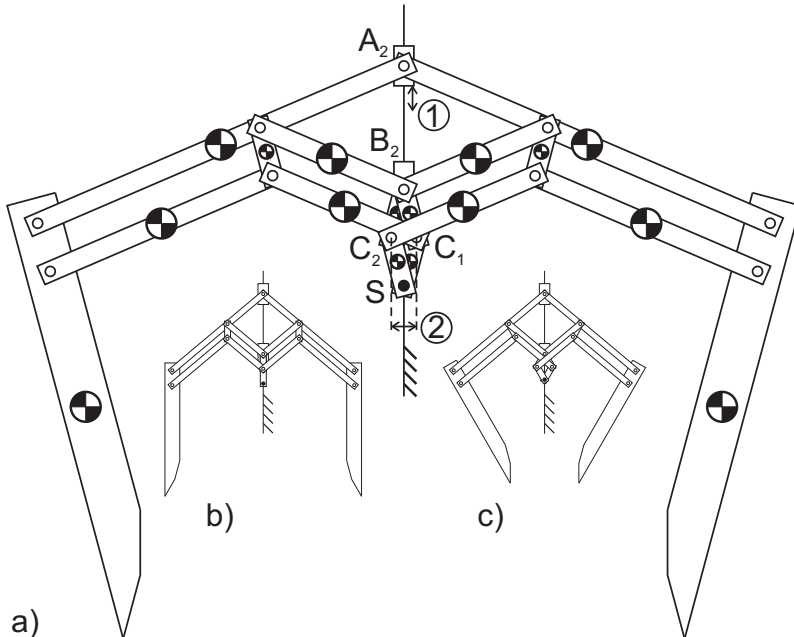


Fig. 7.1 Synthesis of a 2-DoF shaking-force and shaking-moment-balanced grasper mechanism from the 4-DoF principal vector linkage in Fig. 3.23 by including a slider element in A_2 and B_2 .

7.2 Synthesis of an IDB 2-DoF grasper

A common end-effector of pick and place machines and manipulators is a grasper or gripper. When a grasper is not dynamically balanced, because of the accelerations of the manipulator the motion of backdrivable and underactuated fingers is perturbed and grasping difficulties can be experienced such as losing grip, losing control, and damaging the grasped object.

When a grasper is dynamically balanced, the motions of the manipulator do not affect the relative (internal) motions of the grasper and the fingers. The grasper then is dynamically decoupled from the manipulator: instead of dangling like multisegmented pendula, the fingers move along with the manipulator as a rigid body. This means that the actuators of the grasper mechanism are not perturbed by the manipulator motion and the control of the grasping motion is simpler. With force balance actuators also do not need to compensate for gravity. Therefore, when dynamically

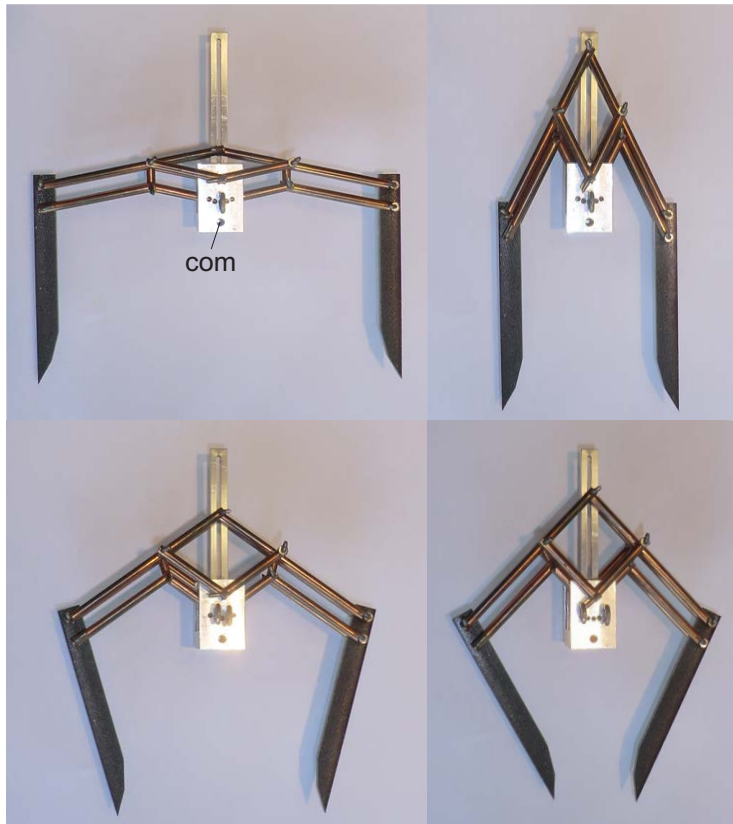


Fig. 7.2 Prototype of an 1-DoF inherently dynamically balanced grasper mechanism where the orientation of the fingers can be adapted manually by relocating joints C_1 and C_2 within the base.

balanced, underactuated or backdrivable graspers can perform pick and place tasks faster and with increased accuracy.

For an end-effector for high-speed manipulation a low mass is of particular importance. A low inertia of the grasping motion is only of importance if this motion is at high speed too. In practice however grasping motions have relatively low speeds.

An inherently dynamically balanced 2-DoF grasper can be synthesized from the 4-DoF principal vector linkage in Fig. 3.23 and Fig. 6.5. Figure 7.1 shows the conceptual design of a possible result. With slider elements in A_2 and B_2 the motion of the 4-DoF principal vector linkage is reduced such that the left side and the right side of the mechanism move similarly and oppositely. The path of the sliders is a line through S , which is the CoM of all elements for the force balance conditions (3.67) where the mass of the sliders can be included in their connecting links. For the moment balance conditions (6.41) the grasper mechanism is dynamically balanced for both relative motions.

The motion of the slider in B_2 relative to S determines the rotational motion of the fingers, while the relative motion between the sliders in A_2 and B_2 determines the translational motion of the fingers. With these motions, illustrated in Fig. 7.1a-b-c, various large grasps and precision grasps are possible. To move the slider in A_2 an actuator 1 can be included to act in between A_2 and S , while an actuator 2 could be implemented to act in between C_1 and C_2 such that these points can cross-over without kinematic problems.

The design can be developed further for instance by integrating links SC_1 , C_1B_2 , B_2C_2 , and C_2S with actuator 2 to reduce the complexity in this area. If the rotational motion of the fingers is not needed, these links can be merged with the base. This was accomplished in the prototype grasper in Fig. 7.2. It has 1-DoF dynamically balanced motion and the orientation of the fingers can be adapted manually by relocating the joints C_1 and C_2 . Various other changes are possible to optimize the design. Elements can be designed asymmetrically, for instance to adapt to specific product shapes, compactness can be improved, or additional components such as electric cables or sensors on the moving elements can be included in the balance.

The grasper mechanism can also be transformed into a compliant dynamically balanced grasper mechanism where the revolute pairs are designed as flexible joints. Another application for grasping is, for example, in suction naps where the grasper mechanism (or a principal vector linkage in general) may be integrated as reinforcement of the flexible material to impose the suction nap to move in a balanced way.

7.3 Synthesis of multi-DoF IDB manipulators

The transfer of components from one part of the machine to another or the pick and place in assembly processes are frequent industrial tasks, for instance in printed circuit board assembly. To keep the costs per product low, low cycle times are required. A manipulator then has to act at high speeds with short settling times while accuracy and precision have to be maintained.

With a high-speed dynamically balanced manipulator base vibrations remain low and do not perturb metrology tools and other parts of the system (and other systems) that are mounted on the same base, with which settling times can be reduced. In this application low inertia solutions are important for low actuator torques. A low mass is not of specific importance since the total mass of the balanced manipulator is stationary in the base and the base is stationary too.

An inherently dynamically balanced planar 4-RRR parallel manipulator can be synthesized by combining two balanced pantographs as shown in Fig. 7.3. Each pantograph in Fig. 7.3a is force balanced for the conditions (3.2) where each pantograph can include part of the mass of the platform. Subsequently each pantograph can be divided in two parts which are placed at a certain offset as shown in Fig. 7.3b with the platform connecting them together. As long as the relative motions of the elements are not changed, which is for all translational motion of the platform, force balance is maintained. The moment balance conditions can be obtained from the sum of the angular momentum of each pantograph (6.8) and the angular momentum of the platform. Then it is obtained that when all links have equal lengths, links A_iB_i have equal inertia, and links B_iC_i have equal inertia, the manipulator in Fig. 7.3b is shaking moment balanced for motion along the orthogonal axes with non-rotated platform.

This configuration can also be synthesized from the configuration in Fig. 2.29a with the force balance conditions (2.51) by relocating the pivots in the base. For rotational motion of the platform the links do not remain parallel and exact force balance is not obtained. Also for rotational motion of the platform and for motion off the orthogonal axes exact moment balance is not obtained. Since for these motions the links remain close to parallel and move around the orthogonal axes, it can be expected that the obtained force and moment balance still is significant. In fact, motion with non-rotated platform along the diagonal axes in Fig. 7.3b is near to exact dynamic balance since the links counter-rotate almost linearly with one another. Regarding dynamic balance, this manipulator is most suitable for tasks where perfect translational motion of the platform is required and is obtained by accurate

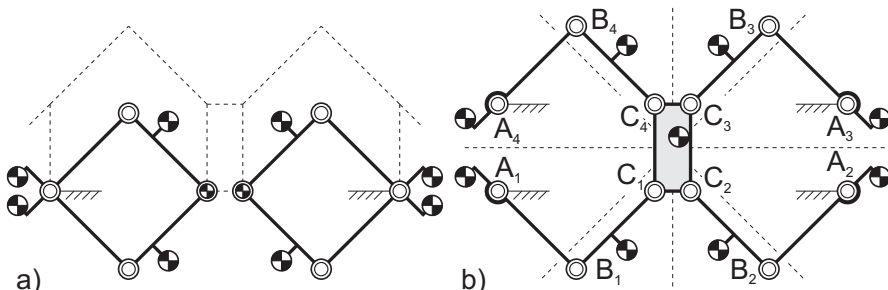


Fig. 7.3 a) By combining two balanced pantographs that are placed oppositely of one another an b) inherently dynamically balanced 4-RRR parallel manipulator can be synthesized where each pantograph is divided in two with the platform connecting the parts together.

control of the rotational motion of the platform to compensate for issues such as production inaccuracies and clearance.

Figure 7.4 shows a prototype of the inherently dynamically balanced planar 4-RRR manipulator that was developed and built. For optimal force transmission to the platform and for compactness, the platform was reduced kinematically to a link with two double revolute pairs on each side (C_1 and C_2 coincide with C_3 and C_4 , respectively). This configuration will be named the *DUAL-V manipulator*. With an actuator in each of the four pivots with the base, the manipulator has one degree of actuation redundancy. This is advantageous since manipulators with actuation redundancy have an increased acceleration capability and have more homogeneous dynamic characteristics (e.g. force transmission to the platform) throughout the workspace [35].

About each pivot with the base a counter-mass is applied to tune the mass distribution of the links connecting the base such that a low inertia of the manipulator is obtained. This means that their mass should be as high as possible since then their CoMs are located the closest to their center of rotation (i.e. closest to the pivot). This results into a large design of the counter-masses. An evaluation of the DUAL-V manipulator is presented in the next chapter.

Solutions of inherently balanced manipulators can also be derived from the principal vector linkage architecture in Fig. 5.7. Figure 7.5a shows for instance a 3-DoF mechanism solution without elements A_0A_3 , D_8E_8 , and D_9E_9 , and Fig. 7.5b shows a 2-DoF mechanism solution without the principal vector links and where the func-

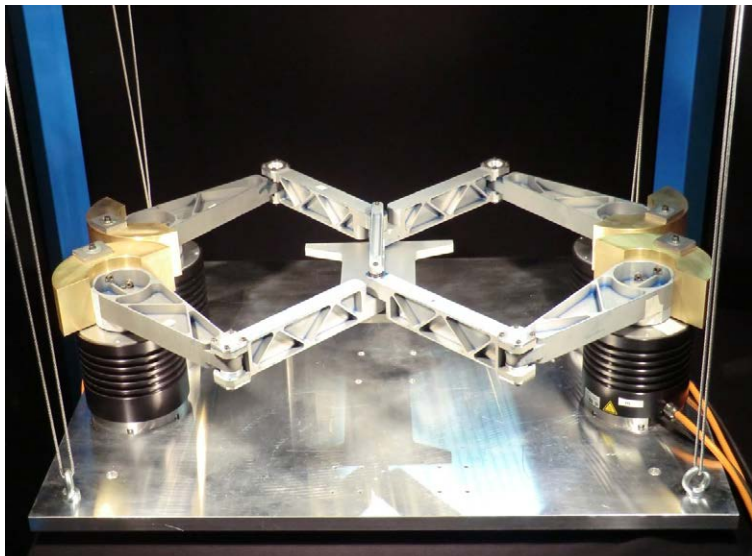


Fig. 7.4 Prototype of the balanced planar 4-RRR manipulator *DUAL-V*, redundantly actuated with four actuators, with counter-masses about the fixed pivots and with the platform reduced to a link with two double revolute pairs on each side.

tion of element D_9E_9 is maintained by a combination of three gears. The mass of the gears can be included in the element to which they are pivoted and their inertia can be included in the elements that determine their rotational motion.

Another inherently balanced mechanism solution that can be derived from the principal vector linkage architecture in Fig. 5.7 is shown in Fig. 7.6. Here elements P_2B_2 , P_3B_2 , SB_2 , A_6A_7 , D_8E_8 , and D_9E_9 were eliminated, link P_1B_1 shortened, link P_2B_1 shifted to the left, and element A_5A_6 was extended to the left.

New principal vector linkage architectures can be created by combining principal vector linkages. Figure 7.7 shows an architecture that can be obtained when two 3-DoF principal vector linkages in Fig. 4.6 are combined by connecting them in their similarity points A_0 , A_3 , and S and merging their outer elements 1 and 3. The illustrated triangle of the similarity points remains similar for all motion of the mechanism. Links B_1S and B'_1S , and B_2S and B'_2S can also be merged, respectively, since their motions are equal.

From the principal vector linkage architecture in Fig. 7.7 various inherently balanced solutions can be derived, for instance the solution shown in Fig. 7.8a. Here elements A_2A_3 , P_2B_2 , B_2P_3 , $B_2SB'_2$, $P'_2B'_2$, and $B'_2P'_3$ were eliminated. The obtained

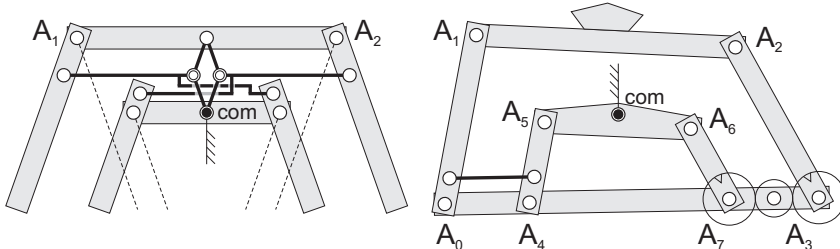


Fig. 7.5 Synthesis examples from the principal vector linkage architecture in Fig. 5.7 (a) without elements A_0A_3 , D_9E_8 , and D_9E_9 and (b) without the principal vector links and element D_9E_9 replaced with three gears.

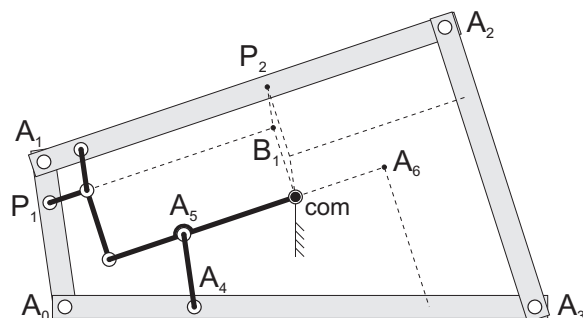


Fig. 7.6 Synthesis example from the principal vector linkage architecture in Fig. 5.7 without elements P_2B_2 , P_3B_2 , SB_2 , A_6A_7 , D_8E_8 , and D_9E_9 , and with link P_1B_1 shortened, link P_2B_1 shifted to the left, and element A_5A_6 extended to the left.

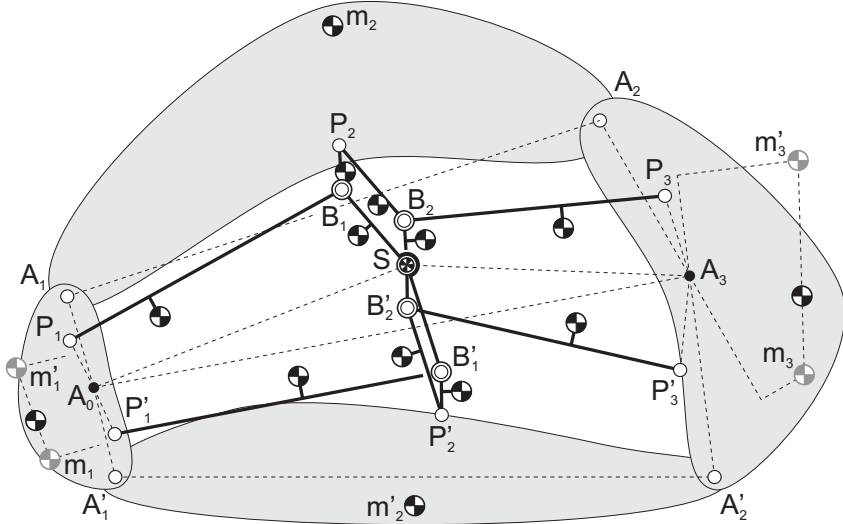


Fig. 7.7 Principal vector linkage architecture obtained by combining two 3-DoF principal vector linkages in Fig. 4.6 by connecting their similarity points A_0 , A_3 , and S and merging their outer elements 1 and 3. This results in a focal mechanism with the common CoM in focal point S .

solution can also be regarded a combination of two pantographs as in Fig. 3.6c where one principal element is shared, with the difference that here the common CoM is in an invariant point in a single link instead of in a third pantograph. Therefore this solution has 2-DoF motion, which is one less than in Fig. 3.6c.

Figure 7.8b shows a 2-DoF mechanism solution that is derived from Fig. 7.7 by eliminating elements P_1B_1 , P_2B_1 , $P'_2B'_2$, and $P'_3B'_2$. This solution can be regarded a combination of two pantographs opposite of one-another, connected in the middle with a dyad of which the middle joint is the common CoM.

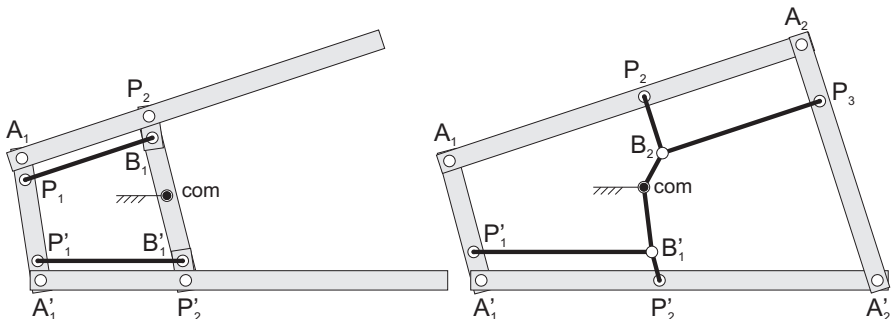


Fig. 7.8 Synthesis examples from the principal vector linkage architecture in Fig. 7.7 without elements (a) A_2A_3 , P_2B_2 , B_2P_3 , $B_2SB'_2$, $P'_2B'_2$, and $B'_2P'_3$ and (b) P_1B_1 , P_2B_1 , $P'_2B'_2$, and $P'_3B'_2$.

The architecture in Fig. 7.7 can be considered a new type of focal mechanism, which is an overconstrained but movable linkage [40]. Characteristic of this focal mechanism is that the focal point coincides with the common CoM, which are both in joint S . Another balanced focal mechanism is obtained when two of the balanced pantographs in Fig. 4.7 are combined by connecting them in their similarity points. This results in a balanced version of Burmester's focal mechanism where the common CoM is in the focal point. Also from this architecture inherently balanced mechanism solutions can be derived.

7.4 Synthesis of large-size balanced devices

For the motion of large-size mechanisms such as movable bridges and movable roofs, force balance is important to reduce actuation power and to increase safety. No actuation power is needed to keep a force-balanced mechanism in position and with failure of the drive system it will not start to move on its own (i.e. not fall down). In force balance solutions for large-size mechanisms a low mass is preferred.

The design of the counter-masses in movable bascule bridges is often challenging. When they are mounted about the horizontal axis of rotation of the deck, they need significant space within the ground. A common solution is to apply them on a mechanism above the ground as shown in the bascule bridge in Fig. 1.11. There are various designs of counter-masses in movable bascule bridges and vertical lift bridges [63, 62, 68]. An advanced design is for instance the "Heel Trunnion Bascule" where the balancing is based on a pantograph linkage with counter-mass such that the bridge remains compact when opened [68].

An example of balanced movable bridges without a counter-mass are Swing-bridges that rotate horizontally about a vertical axis in the center of mass [63]. The only bascule bridge that was found balanced without a counter-mass is the Milwaukee bascule bridge shown in 7.9, which was built in the 1890s in Milwaukee, Wisconsin, US, and removed in 1929 [68]. This bridge opens by sliding the rear

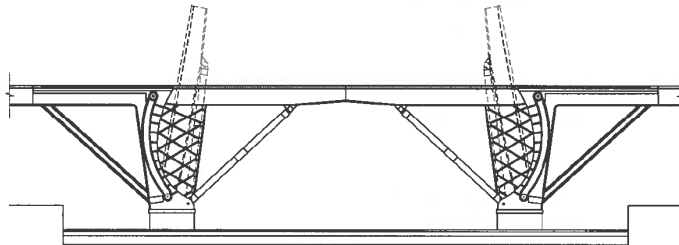


Fig. 7.9 The Milwaukee bascule bridge (built in the 1890s, removed in 1929) which was balanced without counter-mass [68].

end of the bridge down along a curved path for which the overall mass of the bridge remains at about the same height.

For the synthesis of force-balanced bascule bridges without counter-mass, new solutions can be derived from the balanced pantograph linkage in Fig. 3.2. For instance in Fig. 7.10 a solution is shown which is obtained when the pantograph mechanism is divided in two parts that are placed apart, similarly to the DUAL-V in Fig. 7.3. Both parts are connected on top by the base and below with a slider element. The mechanism opens and closes by moving the slider hence an forth the straight path.

The mechanism in Fig. 7.10 will be named a *Double Wing-type bascule bridge*, referring to each side as a wing. A Double Wing-type bridge can span two separate waterways while it can be driven with a single actuator. The Double Wing-type bridge can be both force and moment balanced by which it also does not exert static horizontal forces and static moments to the base. Therefore it can be placed on a single pillar that mainly has to resist the weight of the bridge.

Figure 7.11a shows how the Double Wing-type bascule bridge can also be designed for slopes with a straight vertical sliding path. In Fig. 7.11b a single Wing-type mechanism is shown which, contrary to the double Wing-type mechanism, exerts a static moment to the base. Figure 7.11c shows how another point in the wing element can be used as a slider where the curvature of the slider path is obtained by tracing the selected point while sliding along the straight path. When compared to the bascule bridge in Fig. 7.9, this solution has a shorter strut supporting the deck which is located above the deck and loaded in tension, whereas in Fig. 7.9 the strut reaches towards the end of the deck from underneath, obstructing traffic to pass underneath, and is loaded in compression. Figure 7.11d shows a balanced Wing-type mechanism solution where both elements share part of the deck.

To investigate the applicability of the Wing-type bascule bridge, together with Hollandia, a Dutch corporate in bridge engineering, a conceptual design of the Wing-type bascule bridge in Fig. 7.12 was developed. The configuration in Fig. 7.11b was taken as a starting point. In finding the best compromise between force balance and wind loads acting on the opened bridge, the resulting design has not become

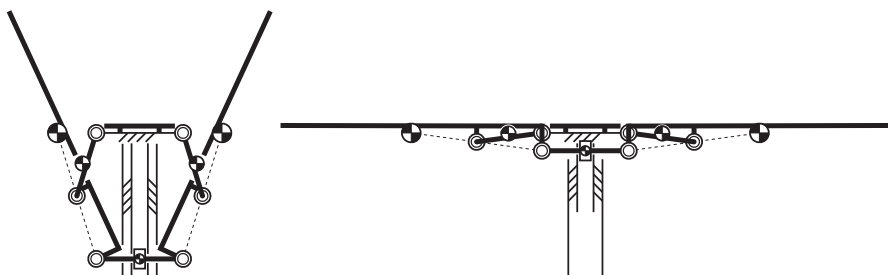


Fig. 7.10 Double Wing-type bascule bridge synthesized from the 2-DoF principal vector linkage in Fig. 3.2, spanning two sides and located on a single pillar.

exactly force balanced. While the driving force is increased due to unbalance, the surface the wind acts upon is reduced since the deck moves down further. To limit the axial forces within the struts, they were designed longer and are pivoted at a specific height for which the angle between the struts and the deck remains sufficiently large.

Other advantages of the Wing-type bascule bridge were found in energy saving since linear guides such as rack and pinions are energy friendly gears as compared to hydraulic drives, and the simplicity of the design which makes it a low cost solution. The space required for the deck to move down is relatively small but deep. A higher road level therefore is advantageous.

In architecture force-balanced mechanisms can be applied to obtain movable buildings. For instance in Fig. 7.13 the conceptual design of the *Inside-out house* is presented, a building where inside and outside become one. Both the left side and the right side of the house act as a force-balanced pantograph mechanism where part of the roof and the side-wall balance one another. The pantographs are connected in the top of the roof. Because of force balance the top of the roof can be moved down with minimal effort by which the walls move up and the building opens itself.

In Fig. 7.14 dynamic balance solutions are shown where principal vector linkages are combined spatially. Figure 7.14a shows how 5 pantographs-halves can be connected along the central axis to obtain a 1-DoF balanced mechanism. When the top is moved, the common CoM is stationary in the connecting point with the shaft. Similarly 5 halves of a 3-DoF principal vector linkage can be combined as shown in Fig. 7.14b, and 5 halves of a 4-DoF principal vector linkage can be combined as

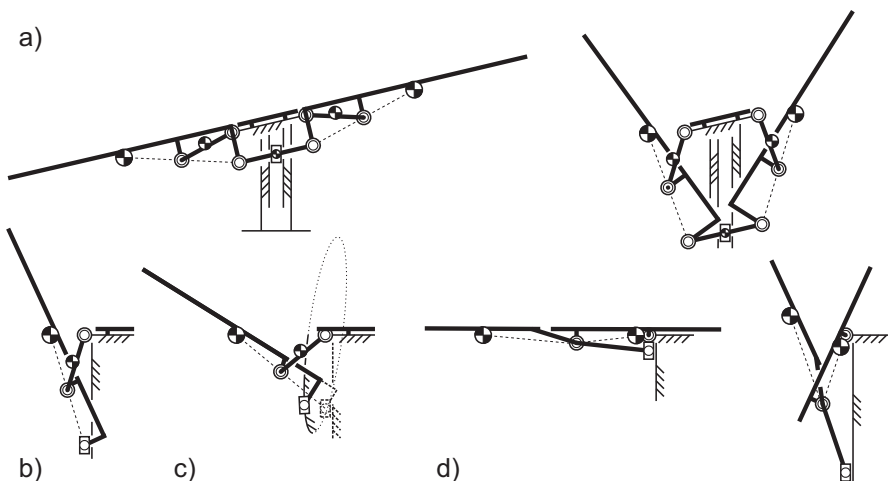


Fig. 7.11 a) Double Wing-type bascule bridge for slopes; b) Single Wing-type bascule solution; c) The slider trajectory can be straight or curved; d) Wing-type bascule solution where both elements share part of the deck.

shown in Fig. 7.14c and 7.14d. These foldable devices can have 2-DoF and 3-DoF dynamically balanced motions, respectively.

7.5 Discussion and conclusion

In this chapter the synthesis of inherently dynamically balanced (IDB) mechanisms from principal vector linkage architectures was investigated. A conceptual design of an IDB 2-DoF grasper mechanism was derived from a 4-DoF principal vector linkage by introducing slider elements (Fig. 7.1). A 3-DoF IDB parallel manipulator was synthesized by combining two divided 2-DoF principal vector linkages (Fig. 7.3). Some other manipulator solutions were obtained from a principal vector linkage architecture by eliminating links (Fig. 7.5a), exchanging a link with gears (Fig. 7.5b), and by redesigning links to relocate joints (Fig. 7.6). These results are the first step in the kinematic synthesis of IDB mechanisms. Subsequently the designs can be optimized for detailed kinematic requirements.

It was shown that principal vector linkages can be combined in various ways. Where in Fig. 7.13 two 2-DoF principal vector linkages were simply connected, in Fig. 7.3 and Fig. 7.10 two 2-DoF principal vector linkages were connected and divided, in Fig. 7.7 two 3-DoF principal vector linkages were combined and partly merged by application of the similarity points, and in Fig. 7.14 parts of principal vector linkages were combined. Other strategies for combining principal vector linkages may exist, leading to a variety of IDB mechanism solutions that can be synthesized.

The DUAL-V manipulator was designed for a low inertia which was achieved with counter-masses about the fixed pivots. The manipulator solutions in Fig. 7.5, Fig. 7.6, and Fig. 7.8 are typically low mass solutions instead of low inertia solutions since they consist of relatively long elements located relatively far from the common CoM of which the mass can be low. These mechanisms have a single pivot with the base about which a counter-mass could be applied advantageously, however the effect of this is limited. When the element in which common CoM is located is fixed with the base more fixed pivots are obtained and more counter-masses can be included advantageously to lower the inertia. Since then the motion of the mechanism is reduced, this solution is interesting for synthesis with higher DoF principal vector linkage architectures. Multiple fixed pivots are obtained naturally by combining principal vector linkages as was shown for the DUAL-V.

The mechanism solutions in Fig. 7.10 and Fig. 7.11 were considered in the context of bascule bridges, but they can also have other applications such as foldable devices or as real wings in flying devices. They can be fully dynamically balanced. The solutions in Fig. 7.14 can be developed also for example as dynamically balanced graspers or as dynamically balanced floating devices.



Fig. 7.12 Conceptual design of the Wing-type bascule bridge (Conceptual design together with Gerard Bouwman & Martijn van Dijk, Hollandia, 2012)

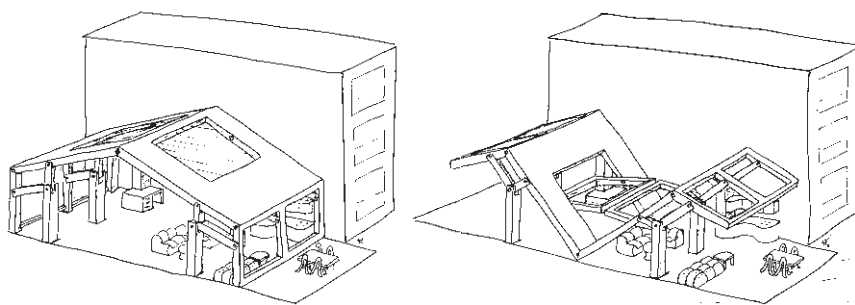


Fig. 7.13 Conceptual design of the *Inside-out house* where the walls and the roof are movable and balanced, synthesized from two 2-DoF balanced pantographs. (see: www.kineticart.nl)

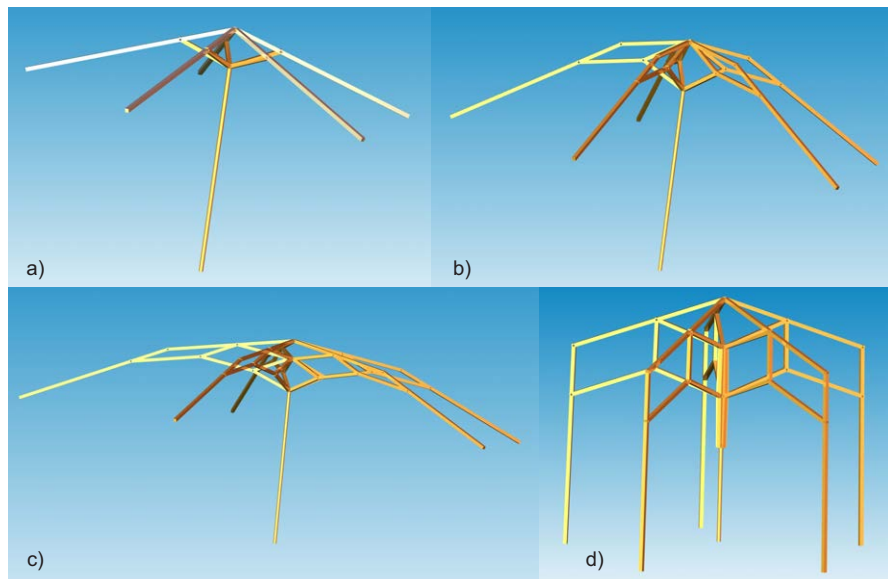


Fig. 7.14 Dynamically balanced foldable devices synthesized from (a) the 2-DoF pantograph; (b) the 3-DoF principal vector linkage; (c-d) the 4-DoF principal vector linkage (shown in two poses).

Chapter 8

Experimental evaluation of a dynamically balanced redundant planar 4-RRR parallel manipulator

Abstract In this chapter an approach for the evaluation of high-speed dynamically balanced parallel manipulators is presented and applied to a comparative experimental investigation of a balanced and unbalanced *DUAL-V* planar 4-RRR parallel manipulator. For precise simulation of the manipulator motion, the inverse dynamic model of the manipulator is derived and validated. Experiments show that the balanced manipulator has up to 97% lower shaking forces and up to a 96% lower shaking moment. For small inaccuracies of the counter-masses or for a small unbalanced payload on the platform, base vibrations may be considerable for high-speed manipulation, however their values remain significantly low as compared to the unbalanced manipulator. For the balanced manipulator the actuator torques are about 1.6 times higher and the bearing forces are about 71% lower as compared to the unbalanced manipulator.

8.1 Introduction

Most literature on dynamic balancing, both for mechanisms and for manipulators, is theoretical, there are relatively few experimental results. Regarding serial manipulators, the experiments on the PUMA-760 showed that shaking force balancing reduced the actuator torques significantly since actuators do not have to compensate gravity forces [30]. The inertia increased with balancing, but it was found that the actuator torques due to coulomb friction dominated, for which the inertia increase was found acceptable. Because of lower actuator torques, it was experimentally shown that shaking force balancing is advantageous for the accuracy of the dynamic identification of the unbalanced robot [72]. The balanced PUMA-760 also had a nine times higher payload capacity, or the ability to move at double acceleration and at about three times higher velocities [73].

Regarding parallel manipulators, in Ref. [5] a shaking-force-balanced parallel mechanism based on the principal vector linkage of Fischer [53] was presented and tested. Although presented as a balanced serial chain, it can be regarded as a

force-balanced parallel manipulator. The center-of-mass (CoM) of the linkage is an invariant point in one of the joints, which was verified by moving the mechanism in a statically balanced way while measuring the joint angles.

In Ref. [58] a dynamically balanced 3-DoF planar parallel manipulator was presented and tested. The manipulator was composed of two independently force-balanced parallelograms pivoted to the base and coupled with an end-effector link. Shaking moment balance was achieved with separate counter-rotating inertias (inertia-wheels). The manipulator was suspended by vertical cables which allowed it to float within the horizontal plane and it was actuated at a low speed corresponding to the eigenmotion of this suspension. The motion of a point in the base of the manipulator was measured to verify the balance performance.

The goal of this chapter is to present an approach for the evaluation of high-speed dynamically-balanced parallel manipulators, and to apply this approach for a comparative experimental investigation of the balanced and the unbalanced DUAL-V planar 4-RRR parallel manipulator.

In addition to the balance performance, other important aspects such as the influence of the balance elements on the actuator torques and on the bearing forces are investigated. Also the sensitivity of the balance parameters and the influence of payload are evaluated.

First the evaluation approach is presented followed by the detailed design of the balanced DUAL-V manipulator. For this manipulator the exact inverse dynamic model is derived and validated and used for precise simulations without the need of a controller. The experimental setup and the experiments are described and the experimental results are presented and discussed.

8.2 Approach to the evaluation and comparison of a balanced manipulator

This section presents and discusses the approach to the evaluation and comparison of high-speed balanced parallel manipulators which are applied for investigation of the planar 4-RRR parallel manipulator.

To verify if theoretical results are correct, the first step of the evaluation of the balanced manipulator is to measure the balance performance. The shaking forces and shaking moments can be obtained from a multi-body simulation with an accurate model of the prototype manipulator or from measurements in an experimental setup. From the fabrication process of the prototype manipulator and from the obtained balance precision, the costs of the balance solution in terms of structural design and production effort can be derived together with the sensitivity to balance inaccuracies. For the potential of the manipulator it is important to also investigate and measure the required driving power (actuator torques) and the bearing forces, which determine the structural demand on the design, e.g. the size of the actuators and the stiffness of the system.

For both the evaluation and the comparative investigation, it is important to exclude the influence of the controller and the control design. Although a controller is required to move the manipulator and in practice it will never move the manipulator exactly as desired, the shaking forces and shaking moments do not depend on the controller directly. They depend solely on the actual motion of the manipulator. This means that even with a bad controller the balance performance can be evaluated well when the real motion of the manipulator is considered and measured and also is used as input in the simulations.

To validate the measured results, the measured manipulator motion can be simulated precisely with a multi-body dynamic model when the exact inverse dynamics are known. Then the design of a controller for the simulation is omitted since open-loop control can be applied, calculating the required actuator torques at each time step.

Also the bearing forces do not depend on the controller directly but they depend on the real motion of the manipulator. In practice it is challenging to measure the bearing forces in an experimental setup but they can be estimated from a precise simulation of the measured manipulator motion.

8.3 Design of the DUAL-V manipulator

The prototype of the DUAL-V manipulator in Fig. 7.4 was designed and fabricated with the parameters in Table 8.1. These parameters and the kinematic variables of the manipulator are illustrated in Fig. 8.1a and Fig. 8.2, of which the latter shows the top-view of the computer-aided design (CAD) of the prototype manipulator. All arm links $i1$ and $i2$ have equal lengths l_{i1} and l_{i2} , respectively, the fixed pivots are located at distances $a = l_{i1}\sqrt{2}$ and b with respect to the center, and the platform link 5 has a length $l_5 = 2b$. With these parameters the pairs of arms are parallelograms for motion along the orthogonal axes with non-rotated platform. The theoretical

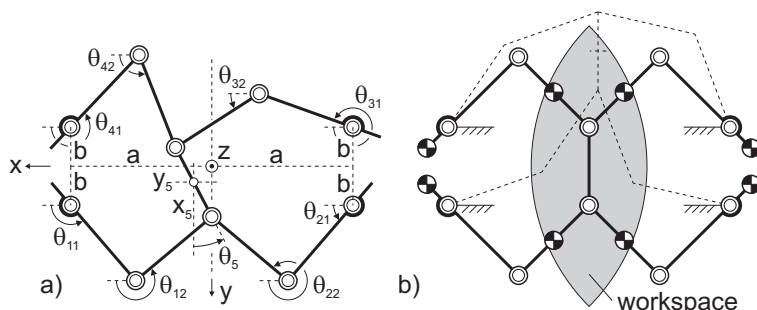


Fig. 8.1 a) Definition of the kinematic variables and the parameters of the base; b) Workspace of the DUAL-V manipulator.

workspace of the manipulator for the given dimensions is shown in Fig. 8.1b and consists of the intersection of two circles with radii $l_{i1} + l_{i2} = 0.56$ m of which the maximal width along x is $2(l_{i1} + l_{i2} - a) = 0.328$ m and the maximal width along y is $2\sqrt{(l_{i1} + l_{i2})^2 - a^2} = 2a = 0.792$ m. Due to collisions, the motion of the prototype along x is limited to a workspace width of 0.288 m.

The links of the manipulator are made of aluminium and were designed and produced before the counter-masses. Together with all bolts, nuts, bearings, etc., they were measured with a 0.01 mm accurate digital caliper and weighted with a 0.01 g accurate balance. Together with the CAD model in SolidWorks the parameters of the link CoMs p_{i1} and p_{i2} , the masses of the links m_{i1} , m_{i2} , and m_5 , and their inertia about their CoM I_{i1} , I_{i2} , and I_5 were determined.

Subsequently the counter-masses were designed of circular segments made of brass. Their required mass $m_{cm,i}$ and CoM location at distance $p_{cm,i}$ relative to A_i were calculated with the force balance conditions which can be derived from (2.51) as

$$\begin{aligned} m_{11}p_{11} + m_{12}l_{11}(1 - \frac{p_{12}}{l_{12}}) + m_{42}p_{42} + m_{32}l_{42}\frac{p_{32}}{l_{32}} + m_5\frac{l_{42}}{2} &= m_{cm,1}p_{cm,1} \\ m_{21}p_{21} + m_{22}l_{21} + m_{12}l_{21}\frac{p_{12}}{l_{12}} + \frac{m_5}{2}l_{21} &= m_{cm,2}p_{cm,2} \\ m_{31}p_{31} + m_{32}l_{31}(1 - \frac{p_{32}}{l_{32}}) + m_{22}p_{22} + m_{12}l_{22}\frac{p_{12}}{l_{12}} + m_5\frac{l_{22}}{2} &= m_{cm,3}p_{cm,3} \\ m_{41}p_{41} + m_{42}l_{41} + m_{32}l_{41}\frac{p_{32}}{l_{32}} + \frac{m_5}{2}l_{41} &= m_{cm,4}p_{cm,4} \end{aligned} \quad (8.1)$$

and from (3.2) as

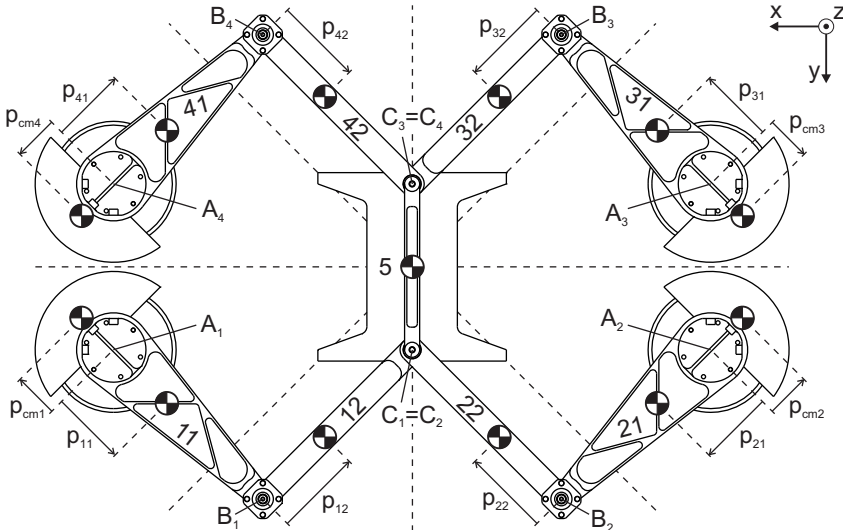


Fig. 8.2 Computer-aided design of the DUAL-V manipulator prototype with parameter definitions. (patented [103])

$$\begin{aligned}
 m_{11}p_{11} + m_{12}l_{11} + m_{42}p_{42} + m_5 \frac{l_{11}}{2} &= m_{cm,1}p_{cm,1} \\
 m_{21}p_{21} + m_{22}l_{21} + m_{32}p_{32} + m_5 \frac{l_{21}}{2} &= m_{cm,2}p_{cm,2} \\
 m_{31}p_{31} + m_{32}l_{31} + m_{22}p_{22} + m_5 \frac{l_{31}}{2} &= m_{cm,3}p_{cm,3} \\
 m_{41}p_{41} + m_{42}l_{41} + m_{12}p_{12} + m_5 \frac{l_{41}}{2} &= m_{cm,4}p_{cm,4}
 \end{aligned} \tag{8.2}$$

which both give equal results.

The main aim of the design of the counter-masses was to have the reduced inertia $I_{cm,i} + m_{cm,i}p_{cm,i}^2$ of each counter-mass relative to A_i be as low as possible since this is advantageous for low actuator torques [93]. Therefore a high mass of each counter-mass with its CoM as close to A_i as possible is needed. A counter-mass material with high density such as brass and a design which can be large in the out-of-plane direction (thick counter-masses) therefore are advantageous. The design of the counter-masses was verified with the mass properties function in SolidWorks, with which it was also verified that the common CoM of the complete manipulator is at the same location for any position in the workspace with non-rotated platform.

Each counter-mass was designed such that part of its mass $m_{tun,i} = 0.188$ kg is a separate element made of lead, placed at a distance $p_{tun,i} = 0.080$ m from A_i on top of the brass segments. This was done to fine-tune the counter-masses, compensating for production inaccuracies and to be able to remove a small mass for experiments investigating the balance performance with non-perfect counter-masses. The mass and inertia of these tuning masses are included in the parameters $m_{cm,i}$ and $I_{cm,i}$ in Table 8.1.

8.4 Inverse dynamic model and validation with simulation model

In this section the inverse dynamic model of the DUAL-V is derived and validated with a multi-body simulation.

8.4.1 Inverse dynamic model to derive the actuator torques

The motion of the platform of the DUAL-V can be prescribed with $\bar{u} = [x_5(t), y_5(t), \theta_5(t)]^T$ with the position of the center of the platform (x_5, y_5) and

Table 8.1 DUAL-V parameters

[m]	[kg]	[kgm ²]	[m]
$l_{i1} = 0.2800$	$m_{i1} = 1.169$	$I_{i1} = 0.012967$	$p_{i1} = 0.0737$
$l_{i2} = 0.2800$	$m_{i2} = 0.606$	$I_{i2} = 0.006417$	$p_{i2} = 0.1279$
$l_5 = 0.2200$	$m_5 = 0.899$	$I_5 = 0.008168$	$p_{cm,i} = 0.0575$
$a = 0.3960$	$m_{cm,i} = 7.983$	$I_{cm,i} = 0.026845$	$p_{tun,i} = 0.080$
$b = 0.1100$	$m_{tun,i} = 0.188$	$I_{act,i} = 0.004100$	

the orientation of the platform θ_5 relative to the xy -reference frame at a time t , as illustrated in Fig. 8.1a. The actuator torques $\bar{\tau}$ required at a time t for a prescribed motion \bar{u} can be calculated as a combination of three individual parts as

$$\bar{\tau} = \bar{\tau}_I + \bar{\tau}_{II} + \bar{\tau}_{III} \quad (8.3)$$

Here $\bar{\tau}_I$ is the required actuator torque to move the platform and part of the mass of links $i2$, $\bar{\tau}_{II}$ is the required actuator torque to move links $i1$ and part of the mass of links $i2$, and $\bar{\tau}_{III}$ is the required actuator torque of part of the rotational motion of links $i2$. This approach follows from Ref. [35] and is extended to being exact by not simplifying the dynamics of the links $i2$. Similar to Ref. [35], the mass of links $i2$ is distributed equivalently to joints B_i and C_i and is included in both $\bar{\tau}_I$ and $\bar{\tau}_{II}$. However the rotational inertia of links $i2$ then is not completely considered. $\bar{\tau}_{III}$ therefore is the torque required to include the rotational inertia of links $i2$ exactly, as will become clear later on.

8.4.1.1 Actuator torques $\bar{\tau}_I$ for the motion of the platform

The actuator torques $\bar{\tau}_I$ for the motion of the platform can be calculated from the equations of the power of the actuator torques $\bar{\tau}_I$ that has to be equal to the power of the motion of the platform, which is written as

$$\dot{\bar{q}}^T \bar{\tau}_I = \dot{\bar{u}}^T \bar{F}_p \quad (8.4)$$

where $\dot{\bar{q}} = [\dot{\theta}_{11}, \dot{\theta}_{21}, \dot{\theta}_{31}, \dot{\theta}_{41}]^T$ is the vector of the angular velocities of the driven links $i1$, $\dot{\bar{u}} = [\dot{x}_5, \dot{y}_5, \dot{\theta}_5]^T$ is the vector of the velocities of the platform motion, and \bar{F}_p is the vector of the resultant forces and the resultant moment that act on the platform. For a prescribed motion of the platform, $\dot{\bar{q}}$ can be derived from the velocity vectors of joints B_i and C_i along the line B_iC_i which, for a rigid link, are equal. These vectors are shown in Fig. 8.3a and are written and calculated as

$$v_{n,i}^B = v_{n,i}^C \quad \rightarrow \quad \bar{X}_n \dot{\bar{q}} = \bar{Y}_n \dot{\bar{u}} \quad (8.5)$$

with

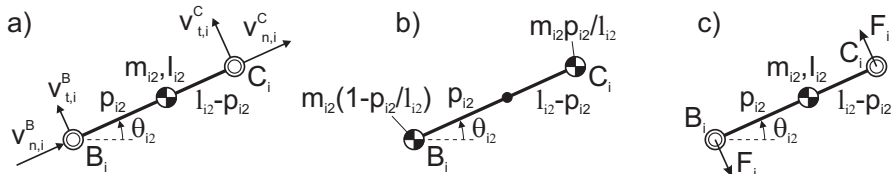


Fig. 8.3 a) Velocity vectors of joints B_i and C_i of links $i2$; b) Equivalent mass model of links $i2$; c) Forces F_i in joints B_i and C_i for rotational acceleration of links $i2$.

$$\bar{X}_n = \begin{bmatrix} -l_{11}s(\theta_{11} - \theta_{12}) & 0 & 0 & 0 \\ 0 & -l_{21}s(\theta_{21} - \theta_{22}) & 0 & 0 \\ 0 & 0 & -l_{31}s(\theta_{31} - \theta_{32}) & 0 \\ 0 & 0 & 0 & -l_{41}s(\theta_{41} - \theta_{42}) \end{bmatrix} \quad (8.6)$$

$$\bar{Y}_n = \begin{bmatrix} c(\theta_{12}) & s(\theta_{12}) & -c(\theta_{12} - \theta_5)b \\ c(\theta_{22}) & s(\theta_{22}) & -c(\theta_{22} - \theta_5)b \\ c(\theta_{32}) & s(\theta_{32}) & c(\theta_{32} - \theta_5)b \\ c(\theta_{42}) & s(\theta_{42}) & c(\theta_{42} - \theta_5)b \end{bmatrix} \quad (8.7)$$

Here $s()$ and $c()$ are used as shorthand notation for $\sin()$ and $\cos()$, respectively, and b is the parameter in Table 8.1. From (8.5) $\dot{\bar{q}}$ then is derived as

$$\dot{\bar{q}} = \bar{X}_n^{-1} \bar{Y}_n \dot{\bar{u}} = \bar{J} \dot{\bar{u}} \quad (8.8)$$

in which \bar{J} is the jacobian matrix

$$\bar{J} = \begin{bmatrix} \frac{-c(\theta_{12})}{l_{11}s(\theta_{11}-\theta_{12})} & \frac{-s(\theta_{12})}{l_{11}s(\theta_{11}-\theta_{12})} & \frac{c(\theta_{12}-\theta_5)}{l_{11}s(\theta_{11}-\theta_{12})}b \\ \frac{-c(\theta_{22})}{l_{21}s(\theta_{21}-\theta_{22})} & \frac{-s(\theta_{22})}{l_{21}s(\theta_{21}-\theta_{22})} & \frac{c(\theta_{22}-\theta_5)}{l_{21}s(\theta_{21}-\theta_{22})}b \\ \frac{-c(\theta_{32})}{l_{31}s(\theta_{31}-\theta_{32})} & \frac{-s(\theta_{32})}{l_{31}s(\theta_{31}-\theta_{32})} & \frac{c(\theta_{32}-\theta_5)}{l_{31}s(\theta_{31}-\theta_{32})}b \\ \frac{-c(\theta_{42})}{l_{41}s(\theta_{41}-\theta_{42})} & \frac{-s(\theta_{42})}{l_{41}s(\theta_{41}-\theta_{42})} & \frac{c(\theta_{42}-\theta_5)}{l_{41}s(\theta_{41}-\theta_{42})}b \end{bmatrix} \quad (8.9)$$

The resultant forces and the resultant moment on the platform can be calculated as $\bar{F}_p = \bar{M}_I \ddot{\bar{u}}$, where $\ddot{\bar{u}} = [\ddot{x}_5, \ddot{y}_5, \ddot{\theta}_5]^T$ are the accelerations of the platform motion and \bar{M}_I is the mass matrix

$$\bar{M}_I = \begin{bmatrix} m_5 + \sum_{i=1}^4 m_{eq,i2} & 0 & 0 \\ 0 & m_5 + \sum_{i=1}^4 m_{eq,i2} & 0 \\ 0 & 0 & I_5 + (\sum_{i=1}^4 m_{eq,i2})b^2 \end{bmatrix} \quad (8.10)$$

with the equivalent masses $m_{eq,i2} = m_{i2} p_{i2} / l_{i2}$ of links $i2$ that are modeled in joints C_i as illustrated in Fig. 8.3b. From (8.4) $\bar{\tau}_I$ then is obtained as

$$(\bar{J} \dot{\bar{u}})^T \bar{\tau}_I = \dot{\bar{u}}^T \bar{M}_I \ddot{\bar{u}} \quad \Rightarrow \quad \bar{\tau}_I = \bar{J}^{T*} \bar{M}_I \ddot{\bar{u}} \quad (8.11)$$

with the pseudo-inverse jacobian \bar{J}^* .

8.4.1.2 Actuator torques $\bar{\tau}_{II}$ for the motion of links $i1$

The actuator torques $\bar{\tau}_{II}$ for the motion of links $i1$ can be calculated with

$$\bar{\tau}_{II} = \bar{M}_{II} \ddot{\bar{q}} \quad (8.12)$$

with $\ddot{\vec{q}} = [\ddot{\theta}_{11}, \ddot{\theta}_{21}, \ddot{\theta}_{31}, \ddot{\theta}_{41}]^T$ the vector of the angular accelerations of the driven links $i1$ and with mass matrix \bar{M}_{II} written as

$$\bar{M}_{II} = \begin{bmatrix} I_{11} + m_{11}p_{11}^2 + I_{cm,1} + m_{cm,1}p_{cm,1}^2 + I_{act,1} + m_{eq,11}l_{11}^2 & 0 & 0 & 0 \\ 0 & I_{21} + m_{21}p_{21}^2 + I_{cm,2} + m_{cm,2}p_{cm,2}^2 + I_{act,2} + m_{eq,21}l_{21}^2 & 0 & 0 \\ 0 & 0 & I_{31} + m_{31}p_{31}^2 + I_{cm,3} + m_{cm,3}p_{cm,3}^2 + I_{act,3} + m_{eq,31}l_{31}^2 & 0 \\ 0 & 0 & 0 & I_{41} + m_{41}p_{41}^2 + I_{cm,4} + m_{cm,4}p_{cm,4}^2 + I_{act,4} + m_{eq,41}l_{41}^2 \end{bmatrix} \quad (8.13)$$

which includes the inertias $I_{ii} + m_{ii}p_{ii}^2$ of links $i1$ about joints A_i , the inertias $I_{cm,i} + m_{cm,i}p_{cm,i}^2$ of counter-masses i about joints A_i , the inertias $I_{act,i}$ of actuators i , and the inertias of the equivalent masses $m_{eq,ii} = m_{i2}(1 - p_{i2}/l_{i2})$ of links $i2$ that are modeled in joints B_i as shown in Fig. 8.3b. From (8.5) $\ddot{\vec{q}}$ can be derived as

$$\begin{aligned} \frac{d}{dt}(\bar{X}_n \dot{\vec{q}}) &= \frac{d}{dt}(\bar{Y}_n \dot{\vec{u}}) \\ \frac{d\bar{X}_n}{dt} \dot{\vec{q}} + \bar{X}_n \ddot{\vec{q}} &= \frac{d\bar{Y}_n}{dt} \dot{\vec{u}} + \bar{Y}_n \ddot{\vec{u}} \\ \ddot{\vec{q}} &= (\bar{X}_n)^{-1} \left(\frac{d\bar{Y}_n}{dt} \dot{\vec{u}} + \bar{Y}_n \ddot{\vec{u}} - \frac{d\bar{X}_n}{dt} \dot{\vec{q}} \right) \end{aligned} \quad (8.14)$$

with

$$\frac{d\bar{X}_n}{dt} = \begin{bmatrix} -l_{11}c(\theta_{11} - \theta_{12})(\dot{\theta}_{11} - \dot{\theta}_{12}) & 0 & 0 & 0 \\ 0 & -l_{21}c(\theta_{21} - \theta_{22})(\dot{\theta}_{21} - \dot{\theta}_{22}) & 0 & 0 \\ 0 & 0 & -l_{31}c(\theta_{31} - \theta_{32})(\dot{\theta}_{31} - \dot{\theta}_{32}) & 0 \\ 0 & 0 & 0 & -l_{41}c(\theta_{41} - \theta_{42})(\dot{\theta}_{41} - \dot{\theta}_{42}) \end{bmatrix} \quad (8.15)$$

$$\frac{d\bar{Y}_n}{dt} = \begin{bmatrix} -s(\theta_{12})\dot{\theta}_{12} c(\theta_{12})\dot{\theta}_{12} & s(\theta_{12} - \theta_5)(\dot{\theta}_{12} - \dot{\theta}_5)b \\ -s(\theta_{22})\dot{\theta}_{22} c(\theta_{22})\dot{\theta}_{22} & s(\theta_{22} - \theta_5)(\dot{\theta}_{22} - \dot{\theta}_5)b \\ -s(\theta_{32})\dot{\theta}_{32} c(\theta_{32})\dot{\theta}_{32} & -s(\theta_{32} - \theta_5)(\dot{\theta}_{32} - \dot{\theta}_5)b \\ -s(\theta_{42})\dot{\theta}_{42} c(\theta_{42})\dot{\theta}_{42} & -s(\theta_{42} - \theta_5)(\dot{\theta}_{42} - \dot{\theta}_5)b \end{bmatrix} \quad (8.16)$$

The angular velocities $\dot{\vec{q}}_2 = [\dot{\theta}_{12}, \dot{\theta}_{22}, \dot{\theta}_{32}, \dot{\theta}_{42}]^T$ of links $i2$ can be obtained from $l_{i2}\dot{\theta}_{i2} = -v_{t,i}^B + v_{t,i}^C$ with the velocity vectors $v_{t,i}^B$ and $v_{t,i}^C$ of joints B_i and C_i normal to line B_iC_i , respectively, as illustrated in Fig. 8.3a. In matrix notation this is written as

$$\bar{l}_2 \dot{\vec{q}}_2 = -\bar{X}_t \dot{\vec{q}} + \bar{Y}_t \dot{\vec{u}} \quad \Rightarrow \quad \dot{\vec{q}}_2 = (\bar{l}_2)^{-1}(-\bar{X}_t \dot{\vec{q}} + \bar{Y}_t \dot{\vec{u}}) \quad (8.17)$$

with

$$\bar{l}_2 = \begin{bmatrix} l_{12} & 0 & 0 & 0 \\ 0 & l_{22} & 0 & 0 \\ 0 & 0 & l_{32} & 0 \\ 0 & 0 & 0 & l_{42} \end{bmatrix} \quad \bar{X}_t = \begin{bmatrix} l_{11}c(\theta_{11} - \theta_{12}) & 0 & 0 & 0 \\ 0 & l_{21}c(\theta_{21} - \theta_{22}) & 0 & 0 \\ 0 & 0 & l_{31}c(\theta_{31} - \theta_{32}) & 0 \\ 0 & 0 & 0 & l_{41}c(\theta_{41} - \theta_{42}) \end{bmatrix} \quad (8.18)$$

and

$$\bar{Y}_t = \begin{bmatrix} -s(\theta_{12}) & c(\theta_{12}) & s(\theta_{12} - \theta_5)b \\ -s(\theta_{22}) & c(\theta_{22}) & s(\theta_{22} - \theta_5)b \\ -s(\theta_{32}) & c(\theta_{32}) & -s(\theta_{32} - \theta_5)b \\ -s(\theta_{42}) & c(\theta_{42}) & -s(\theta_{42} - \theta_5)b \end{bmatrix} \quad (8.19)$$

The actuator torques $\bar{\tau}_{II}$ then are written as

$$\bar{\tau}_{II} = \bar{M}_{II}(\bar{X}_n)^{-1}\left(\frac{d\bar{Y}_n}{dt}\dot{u} + \bar{Y}_n\ddot{u} - \frac{d\bar{X}_n}{dt}\dot{\bar{q}}\right) \quad (8.20)$$

8.4.1.3 Actuator torques $\bar{\tau}_{III}$ for the rotational motion of links $i2$

The actuator torques for motion of the mass of links $i2$ is included in $\bar{\tau}_I$ and $\bar{\tau}_{II}$ with the equivalent masses in Fig. 8.3b. Then also a specific inertia of links $i2$ is included, which is the inertia of the equivalent model about its CoM calculated as $m_{eq,i1}p_{i2}^2 + m_{eq,i2}(l_{i2} - p_{i2})^2$. In general the real inertia of links $i2$ will not be equal to this value. This means that actuator torques $\bar{\tau}_{III}$ are required for the difference in the real inertia and the modeled inertia of links $i2$, which can be written in the mass matrix \bar{M}_{III} as

$$\bar{M}_{III} = \begin{bmatrix} I_{12} - m_{eq,11}p_{12}^2 - m_{eq,12}(l_{12} - p_{12})^2 & 0 & 0 & 0 \\ 0 & I_{22} - m_{eq,21}p_{22}^2 - m_{eq,22}(l_{22} - p_{22})^2 & 0 & 0 \\ 0 & 0 & I_{32} - m_{eq,31}p_{32}^2 - m_{eq,32}(l_{32} - p_{32})^2 & 0 \\ 0 & 0 & 0 & I_{42} - m_{eq,41}p_{42}^2 - m_{eq,42}(l_{42} - p_{42})^2 \end{bmatrix} \quad (8.21)$$

The torques $\bar{\Gamma} = [\Gamma_1, \Gamma_2, \Gamma_3, \Gamma_4]^T$ that act on links $i2$ for rotational motion of this difference can be written as

$$\bar{\Gamma} = \bar{M}_{III}\ddot{\bar{q}}_2 \quad (8.22)$$

with angular accelerations $\ddot{\bar{q}}_2 = [\ddot{\theta}_{12}, \ddot{\theta}_{22}, \ddot{\theta}_{32}, \ddot{\theta}_{42}]^T$ of links $i2$ which can be derived from (8.17) as

$$\frac{d}{dt}(\bar{l}_2\dot{\bar{q}}_2) = \frac{d}{dt}(-\bar{X}_t\dot{\bar{q}} + \bar{Y}_t\dot{u}) \Rightarrow \ddot{\bar{q}}_2 = (\bar{l}_2)^{-1}\left(-\frac{d\bar{X}_t}{dt}\dot{\bar{q}} - \bar{X}_t\ddot{\bar{q}} + \frac{d\bar{Y}_t}{dt}\dot{u} + \bar{Y}_t\ddot{u}\right) \quad (8.23)$$

with

$$\frac{d\bar{X}_t}{dt} = \begin{bmatrix} -l_{11}s(\theta_{11} - \theta_{12})(\dot{\theta}_{11} - \dot{\theta}_{12}) & 0 & 0 & 0 \\ 0 & -l_{21}s(\theta_{21} - \theta_{22})(\dot{\theta}_{21} - \dot{\theta}_{22}) & 0 & 0 \\ 0 & 0 & -l_{31}s(\theta_{31} - \theta_{32})(\dot{\theta}_{31} - \dot{\theta}_{32}) & 0 \\ 0 & 0 & 0 & -l_{41}s(\theta_{41} - \theta_{42})(\dot{\theta}_{41} - \dot{\theta}_{42}) \end{bmatrix} \quad (8.24)$$

and

$$\frac{d\bar{Y}_t}{dt} = \begin{bmatrix} -c(\theta_{12})(\dot{\theta}_{12}) & -s(\theta_{12})(\dot{\theta}_{12}) & c(\theta_{12} - \theta_5)(\dot{\theta}_{12} - \dot{\theta}_5)b \\ -c(\theta_{22})(\dot{\theta}_{22}) & -s(\theta_{22})(\dot{\theta}_{22}) & c(\theta_{22} - \theta_5)(\dot{\theta}_{22} - \dot{\theta}_5)b \\ -c(\theta_{32})(\dot{\theta}_{32}) & -s(\theta_{32})(\dot{\theta}_{32}) & -c(\theta_{32} - \theta_5)(\dot{\theta}_{32} - \dot{\theta}_5)b \\ -c(\theta_{42})(\dot{\theta}_{42}) & -s(\theta_{42})(\dot{\theta}_{42}) & -c(\theta_{42} - \theta_5)(\dot{\theta}_{42} - \dot{\theta}_5)b \end{bmatrix} \quad (8.25)$$

The torque T_i on each link l_{i2} can be modeled with forces F_i in both B_i and C_i normal to line B_iC_i as illustrated in Fig. 8.3c. These forces are calculated with

$$\bar{F}_{III} = (\bar{l}_2)^{-1}\bar{T} \quad (8.26)$$

with $\bar{F}_{III} = [F_1, F_2, F_3, F_4]^T$. These forces determine the required actuator torques $\bar{\tau}_{III}$ and can be calculated in two parts. The forces F_i in B_i cause a direct torque onto the actuators which is written as

$$\bar{\tau}_{III}^a = -\bar{X}_t \bar{F}_{III} \quad (8.27)$$

The forces F_i in C_i act on the platform and therefore they can be distributed among the actuators with \bar{J}^{T*} in a similar way as $\bar{\tau}_I$ was calculated, which results in

$$\bar{\tau}_{III}^b = \bar{J}^{T*} \bar{Y}_t \bar{F}_{III} \quad (8.28)$$

Altogether, the actuator torques $\bar{\tau}_{III}$ are calculated with

$$\bar{\tau}_{III} = \bar{\tau}_{III}^a + \bar{\tau}_{III}^b = (-\bar{X}_t + \bar{J}^{T*} \bar{Y}_t) \bar{F}_{III} \quad (8.29)$$

8.4.2 Simulation and validation of the inverse dynamic model

The DUAL-V manipulator was modeled with the multi-body simulation software package Spacar¹ and the simulation model is shown in Fig. 8.4. Since all mass and inertia data were modeled in the nodes, the shapes of the elements have no meaning.

Figure 8.5 shows the simulated motion for validation of the inverse dynamic model and the validation results. At each time step the actuator torques were calculated for a given platform motion and the dynamics were solved with solver ODE45 (Dormand-Prince), with maximal step size of 0.0001 s, and with a relative tolerance of $1e^{-12}$ m. The results show the accuracy of the output platform motion with respect to the input platform motion, which is in the order of the relative tolerance of the solver. The platform motion consisted of accelerations up to 118 m/s^2 in x-direction, up to 202 m/s^2 in y-direction and up to 1612 rad/s^2 rotationally.

¹ <http://www.spacar.nl/>

8.5 Experimental setup

The experimental setup of the prototype manipulator is shown in Fig.8.6a. The manipulator of aluminium links and brass counter-masses was mounted on four *ETEL RTMB0140-100* direct drive actuators, which could deliver maximal torques of 127 Nm. The actuators were mounted on an aluminum base plate of 1.0×0.8 m with a thickness of 25 mm. The unbalanced manipulator for comparison was the same manipulator but without the counter-masses and for evaluation of the sensitivity of the counter-masses on the shaking forces and the shaking moment, the tuning masses of lead were removed from the brass elements.

To measure the shaking forces and the shaking moment of the manipulator in the horizontal plane, an *ATI mini 45* six-axes force/torque sensor was positioned and centered between the base plate and the fixed frame as shown in Fig. 8.6b. This sensor could measure a maximum of 500 N shaking force in both x - and y - direction and 20 Nm shaking moment with a measurement noise that was estimated to be about 3 N and 0.02 Nm. To unload the sensor from the gravity force, to align it horizontally, and to prevent damage during assembly, the base plate was suspended by four cables to float just above the sensor. Four pins fixed the sensor with respect to the base plate for in-plane motion while translation in vertical direction was not restricted.

The control of the manipulator was based on a PID-controller at a frequency of 10 kHz. The actuator torques and the actuator orientations were recorded with the same frequency, while the measurement frequency of the force/torque sensor was 1 kHz. With the information of the actuator encoders and the direct kinematic model, the real manipulator motion was determined.

Since at high speeds the PID-controller allowed significant trajectory deviations, to avoid damaging the prototype, the experiments were limited to motion

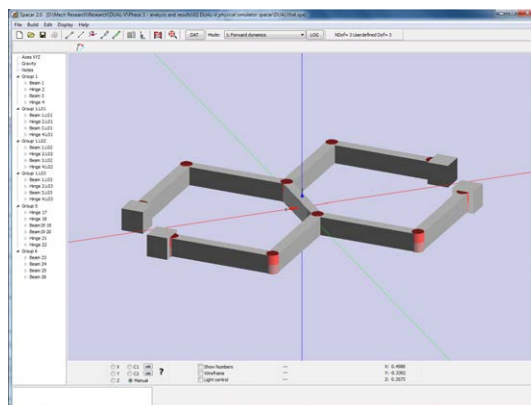


Fig. 8.4 Spacar model of the balanced DUAL-V manipulator with mass and inertia modeled in the nodes.

within a centered circular workspace with a diameter of 0.2 m. From Fig. 8.7, which shows the condition number $\text{cond}(\bar{J}_h)$ of the harmonized jacobian matrix $\bar{J}_h = \bar{J}[1, 0, 0; 0, 1, 0; 0, 0, 1/b]$ for three platform orientations, it can be observed that within this area the force transmission to the platform is optimal.

8.6 Experiments and experimental results

In this section the experiments are described and the results are presented. First various results of the shaking forces and the shaking moment are shown, followed by the results of the actuation torques and the results of the bearing forces. Discussion of the results is in section 8.7.

For motion of the center of the platform along the orthogonal axes and without platform rotation, the unbalanced manipulator is expected to exhibit shaking forces and a zero shaking moment, of which the latter is because of the symmetric design. The balanced manipulator is expected to have zero shaking forces and a zero shaking moment.

Columns 3 and 5 in Fig. 8.8 show the measured shaking forces and shaking moment of the unbalanced and the balanced manipulator, respectively, for the motion shown in column 1². This motion has a maximal acceleration of 51 m/s^2 in both directions and 43 rad/s^2 rotationally, which therefore is not perfect balanced motion along the orthogonal axes. For validation, the shaking forces and the shaking moment of the unbalanced and the balanced manipulator from simulation of the measured motion are shown in column 2 and 4, respectively.

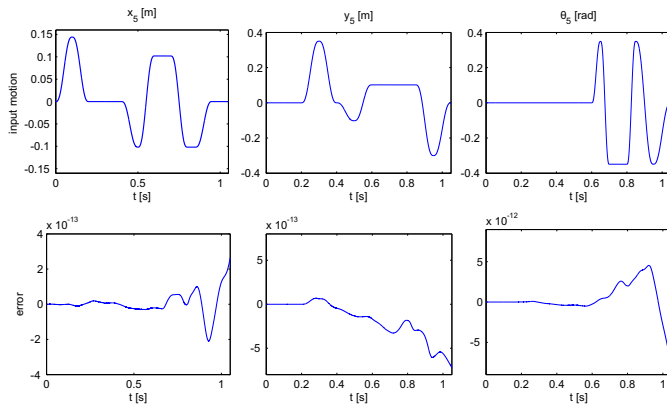


Fig. 8.5 Validation of the inverse dynamic model for a motion throughout the workspace of the balanced manipulator. The error between the input platform motion and the output platform motion is in the order of the relative tolerance of the solver.

² See video at: http://www.ijrr.org/ijrr_2013/484183.htm

For motion with a non-rotated platform the unbalanced manipulator can be considered as a reduced mass m_{red} moving with the platform with which the expected shaking forces can be calculated. This reduced mass can be derived from the force balance conditions in (8.1) or (8.2). For the unbalanced manipulator the product $m_{cm,i}p_{cm,i}$ is zero, which can also be interpreted as that factor $m_3l_{i1}/2$ is increased with $m_{cm,i}p_{cm,i}$. Then the reduced mass representing the unbalanced manipulator can be obtained from $m_{red}l_{i1}/2 = m_{cm,i}p_{cm,i}$ as $m_{red} = 2m_{cm,i}p_{cm,i}/l_{i1} = 3.279$ kg. The shaking forces of the unbalanced manipulator in Fig. 8.8 then are expected to be $51 \cdot 3.279 = 167$ N.

A typical motion for pick-and-place tasks including referencing is motion along a triangular trajectory. Column 1 in Fig. 8.9 shows the measured motion of the manipulator when moved along a triangular trajectory with equal sides of 0.173 m and with maximal accelerations of 66 m/s^2 along x , 63 m/s^2 along y , and 129 rad/s^2 rotationally. For the unbalanced and the balanced manipulator, the shaking forces and the shaking moment from simulation of the measured motion are shown in columns 2 and 4, respectively, and the measured results are shown in columns 3 and 5, respectively. When the platform rotation is zero, the unbalanced manipulator is expected to have shaking forces of $66 \cdot 3.279 = 216$ N along x and $63 \cdot 3.279 = 207$ N along y and the balanced manipulator is expected to exhibit only a shaking moment, while shaking forces are zero.

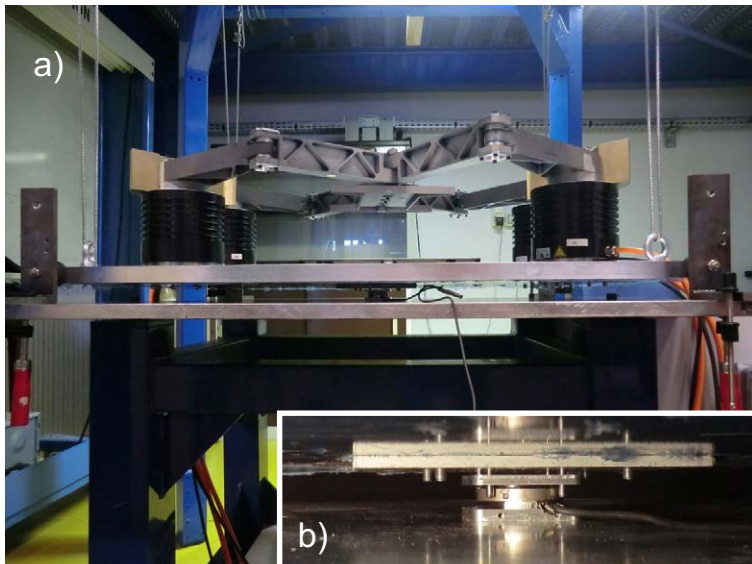


Fig. 8.6 a) Experimental setup of the balanced DUAL-V manipulator prototype suspended by cables and mounted on a six-axes force/torque sensor for measurement of the in-plane shaking forces and shaking moment; b) close-up of sensor mount.

To evaluate the sensitivity of the balance masses, the tuning-masses were removed from each counter-mass for which each product $m_{cm,i}p_{cm,i}$ is 96.72% of the value for perfect balance, or has a 3.28% balance inaccuracy. Fig. 8.10 shows the experimental results of this 96.72% balanced manipulator and of the fully balanced manipulator for the motion in column 1 which has maximal accelerations of 186 m/s^2 along x , 3 m/s^2 along y , and 50 rad/s^2 rotationally.

The results in Fig. 8.10 also represent the influence of payload on the platform. An equal 3.28% balance inaccuracy is also obtained by placing 0.107 kg in the center of the platform, instead of leaving the tuning masses out. This is calculated similarly as for the reduced mass of the unbalanced manipulator as $2m_{tun,i}p_{tun,i}/l_{i1} = 2 \cdot 0.188 \cdot 0.080/0.280 = 0.107 \text{ kg}$. By moving this mass with 186 m/s^2 along x , a shaking force of $186 \cdot 0.107 = 20 \text{ N}$ is expected.

For comparison, Fig. 8.11 shows the theoretical simulation results of the inverse dynamic model for the smooth motion along the triangular trajectory of column 1 with maximal accelerations of 82.6 m/s^2 and 71.6 m/s^2 in the x - and y -directions, respectively. The shaking forces and the shaking moment of the unbalanced manipulator, of the 96.72% balanced manipulator, and of the fully balanced manipulator are shown in columns 2, 3, and 4, respectively. Here the shaking forces of the unbalanced manipulator are expected to be $82.6 \cdot 3.279 = 271 \text{ N}$ and $71.6 \cdot 3.279 = 235 \text{ N}$ in the x - and y -directions, respectively, while for the 96.72% balanced manipulator they are expected to be $82.6 \cdot 0.107 = 8.9 \text{ N}$ and $71.6 \cdot 0.107 = 7.7 \text{ N}$ in the x - and y -directions, respectively.

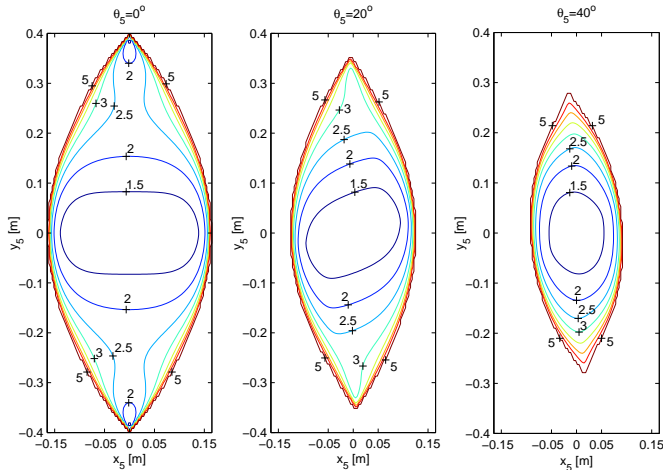


Fig. 8.7 The condition number throughout the workspace for three platform orientations shows that the optimal dynamic performance is found in the center and along the y -axis.

Since the balance masses add inertia to the manipulator, the balanced manipulator is expected to require higher actuator torques. For the motion in Fig. 8.9, the measured actuator torques of the unbalanced manipulator and the balanced manipulator are shown in columns 1 and 2 in Fig. 8.12, respectively. Column 3 shows the actuator torques of both manipulators calculated from the inverse dynamic model for equal input motion. The smaller curves represent the unbalanced manipulator.

The improved mass distribution due to the counter-masses is expected to have an advantageous influence on the bearing forces of the balanced manipulator. For simulations of the measured motion in Fig. 8.9, columns 1 and 2 in Fig. 8.13 show the bearing forces of the unbalanced and the balanced manipulator, respectively. For validation, columns 3 and 4 show the bearing forces from the simulations for smooth motion along the triangular trajectory with equal maximal accelerations.

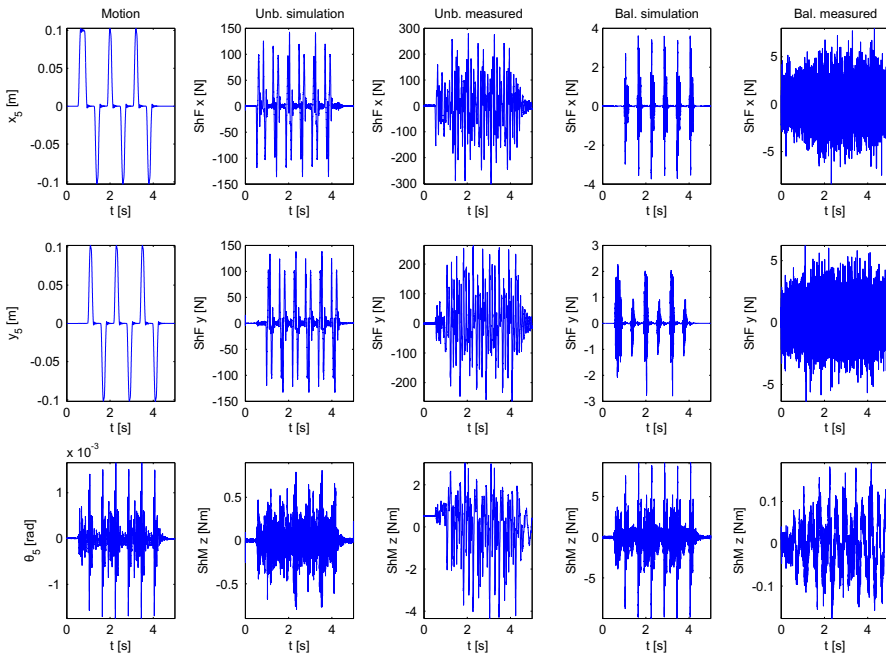


Fig. 8.8 Results from simulation and experiments of the unbalanced and the balanced manipulator for the measured motion in column one, which is motion along the orthogonal axes with maximal accelerations of 51 m/s^2 and 43 rad/s^2 rotationally. It shows that the measured shaking forces of the balanced manipulator are 97% and 98% lower in x - and y -direction, respectively, and the measured shaking moment is 96% lower as compared to the unbalanced manipulator.

8.7 Discussion

In this section the experimental results are discussed. First the shaking forces and the shaking moment are considered and subsequently the sensitivity to unbalance, the actuator torques, and the bearing forces are treated. Also the evaluation method and the experimental setup are discussed.

8.7.1 Shaking forces and shaking moments

The measurements in Fig. 8.8 show a significant reduction of the shaking forces of the balanced manipulator. While for the unbalanced manipulator the maximal measured shaking forces are 302 N along x and 263 N along y , the balanced manipulator has maximal shaking forces of 8.4 N along x and 6.4 N along y , being close to the noise level of the sensor. This means a reduction of 97% and 98% of shaking forces along x and y , respectively. The shaking forces of the balanced manipulator are non-zero mainly due to the rotational motion of the platform.

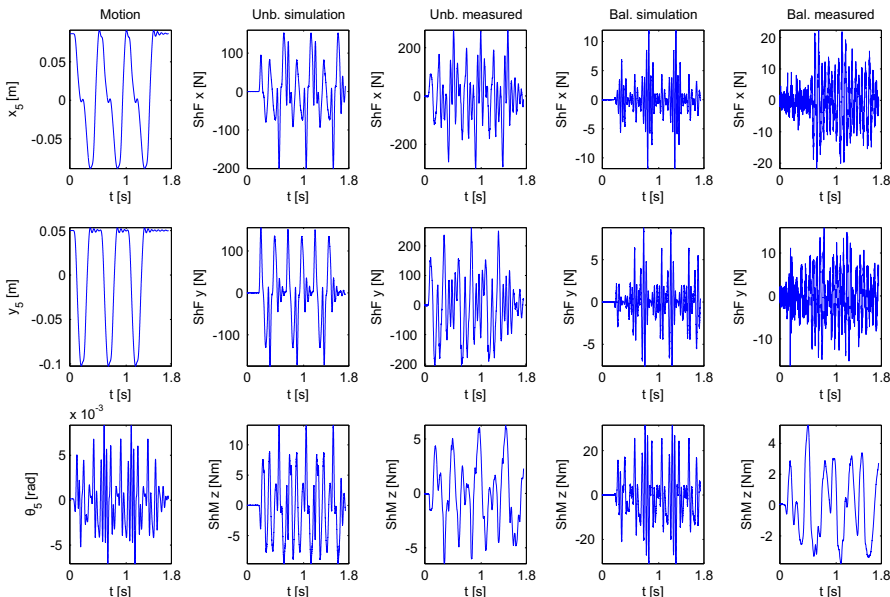


Fig. 8.9 For the measured motion with maximal accelerations of 66 m/s^2 along x , 63 m/s^2 along y , and 129 rad/s^2 rotationally along a triangular trajectory with equal sides of 0.173 m in column 1, columns 2 and 4 show the simulation results and columns 3 and 5 show the experimental results for the unbalanced and the balanced manipulator, respectively. For the balanced manipulator the measured shaking forces are 93% and 94% lower in x - and y -direction, respectively, and the measured shaking moment is 16% lower as compared to the unbalanced manipulator.

From simulation of the measured motion, the maximal shaking forces of the unbalanced manipulator are about 142 N along x and 138 N along y (column 3) while for the balanced manipulator they are about 3.7 N along x and 2.8N along y (column 4). Also for these values the reduction of shaking forces is 97% and 98% along x and y , respectively, however the values differ significantly from the measured maximal values. Also both values of the unbalanced manipulator differ from the expected 167 N shaking forces. Most likely this is caused by the calculations of the derivative (velocity) and the second derivative (acceleration) of the measured motion, which are needed for the inverse dynamic model. Since the derivatives of the measured position information result in unrealistically high values, the values were filtered with a first order low pass filter. However the simulation results show that this is not sufficient. In addition, the mentioned maximal accelerations were obtained from these derivatives, which explains why the expected shaking forces are closer to the results of the simulation of the measured motion.

The measured shaking moment of the unbalanced manipulator has a maximal value of 4.3 Nm, while for the balanced manipulator it is at most 0.19 Nm, which is 96% lower. It is likely that the measurements of the unbalanced manipulator are affected significantly by frame vibrations. In the experimental setup the relatively large inertia of the manipulator with the base plate in combination with the stiffness of the force/torque sensor caused the base plate to rotate in the lowest eigenmode

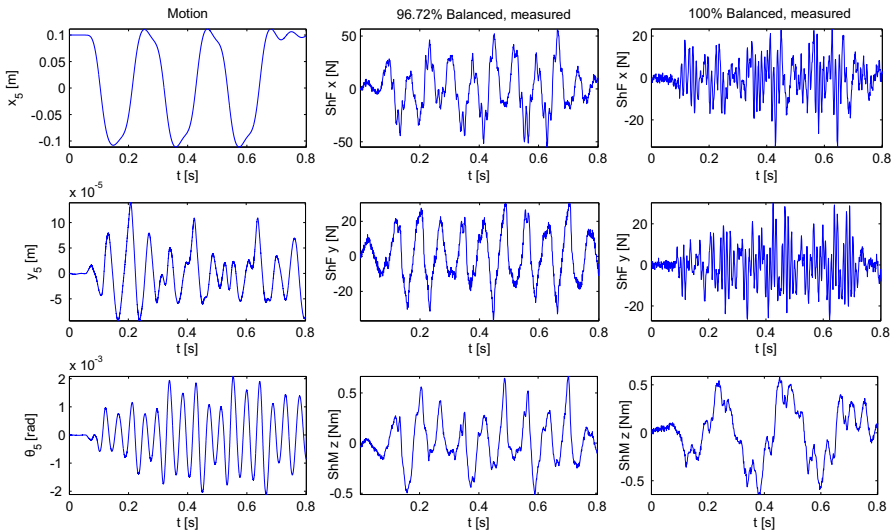


Fig. 8.10 Experimental results of the 96.72% balanced manipulator and of the fully balanced manipulator for the motion in column 1 with maximal accelerations of 186 m/s^2 along x , 3 m/s^2 along y , and 50 rad/s^2 rotationally. The maximal shaking forces of the 96.72% balanced manipulator are increased with 73% along x and 23% along y , while maximal shaking moment is reduced with 13%.

with measured eigenfrequency of about 3.4 Hz. This may have caused interference of the relatively high shaking forces with the measured shaking moment.

The simulation results of the shaking moment (columns 2 and 4) are dramatically affected by the mentioned differentiation problem. Although the values of the unbalanced manipulator could be realistic, the values of the balanced manipulator are, with a maximal value of 10 Nm, significantly higher as compared to the measured values. The shaking moment is obtained from the simulation as the sum of the actuator torques together with the moments created by the individual reaction forces in A_i with respect to the center. Due to the differentiation problem, all individual reaction forces are affected for which the resulting shaking moments become useless.

For motion along the triangular trajectory, Fig. 8.9 shows that the measured shaking forces of the balanced manipulator have maximal values of 22 N along x and 16 N along y , which are non-zero because of rotational motion of the platform. Compared with the unbalanced manipulator showing maximal measured shaking forces of 300N along x and 262 N along y , the balanced manipulator has 93% and 94% reduced shaking forces, respectively. The maximal measured shaking moment of the unbalanced manipulator is 6.5 Nm while of the balanced manipulator it is 5.2 Nm, which is 16% lower.

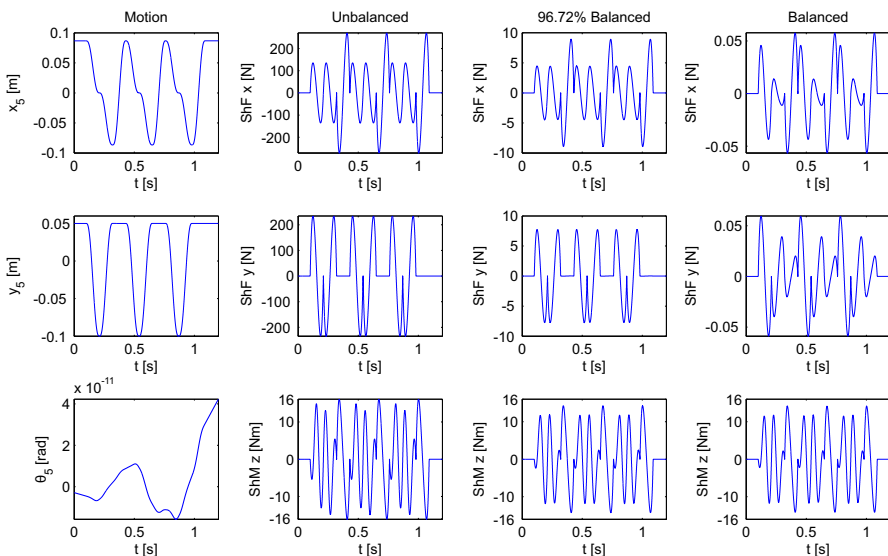


Fig. 8.11 Theoretical simulation results of the inverse dynamic model of the unbalanced, the 96.72% balanced, and the fully balanced manipulator for the motion in column 1 with maximal accelerations of 82.6 m/s^2 and 71.6 m/s^2 in x - and y -directions, respectively. 96.72% balance represents 0.107 kg of unbalanced mass on the platform for which the shaking forces increase considerably. The shaking moment of the balanced manipulator is 12% lower as compared to the unbalanced manipulator.

From the simulations in columns 2 and 4, the unbalanced manipulator has maximal shaking forces of 200 N along x and 175 N along y , while for the balanced manipulator the maximal shaking forces are 12 N along x and 8.8 N along y . This results in 94% and 95% reduced shaking forces along x and y , respectively, for which they differ 1% from the results from the measurements. Regarding the simulated results, the same remarks apply as for Fig. 8.8, for which the simulated shaking moments cannot be interpreted.

From the theoretical simulation of motion along the triangular trajectory in Fig. 8.11, the unbalanced manipulator has maximal shaking forces of 271 N along x and 235 N along y , as expected, while the balanced manipulator has minimal shaking forces. The maximal shaking moment of the unbalanced manipulator is 16.1 Nm while the maximal shaking moment of the balanced manipulator is 14.1 Nm which is 12% lower. This is less than the measured difference in maximal shaking moment of 16% in Fig. 8.9.

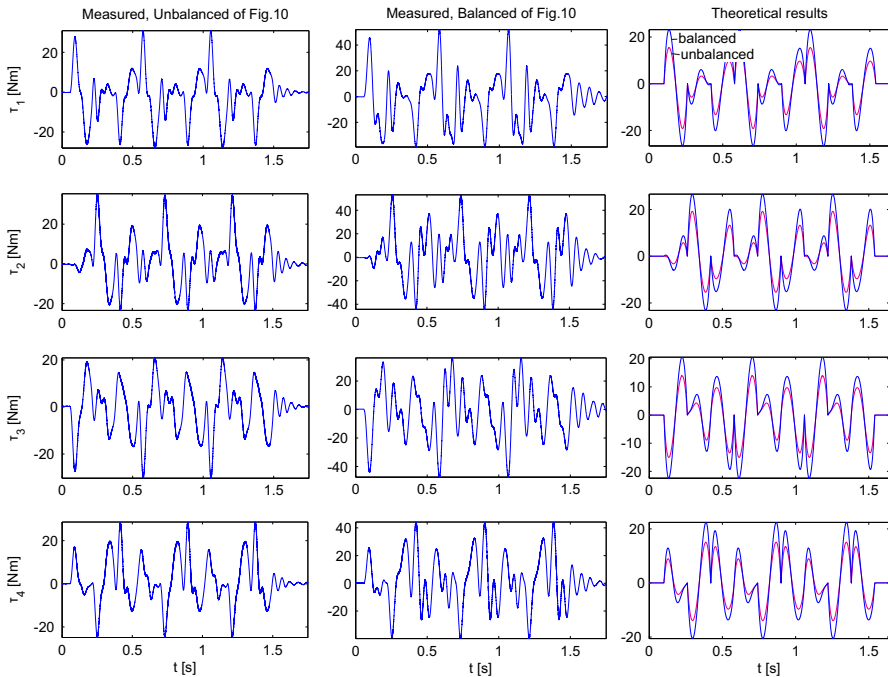


Fig. 8.12 For the motion in Fig. 8.9 the measured actuator torques of the unbalanced and the balanced manipulator are shown in columns 1 and 2, respectively. Column 3 shows the actuator torques of both manipulators from the inverse dynamic model for equal input motion. The smaller curves represent the unbalanced manipulator. From experiments, the actuator torques of the balanced manipulator are about $1.6 \times$ higher while theoretically they are about $1.4 \times$ higher than the actuator torques of the unbalanced manipulator.

8.7.2 Sensitivity to balance inaccuracy and payload

The sensitivity of the dynamic balance was investigated for a balance inaccuracy of 3.28%, representing the effect of inaccurate counter-masses that are 0.188 kg too lightweight or of a payload of 0.107 kg on the platform. The results in Fig. 8.10 show that for 3.28% balance inaccuracy, the shaking forces increase from maximal values of 33 N along x and 30 N along y (column 3) to maximal values of 57 N along x and 37 N along y (column 2). This means an increase of shaking forces of 73% along x and 23% along y . The difference in shaking force along x is $57 - 33 = 24$ N and close to the expected 20 N shaking force for the 3.28% balance inaccuracy. The maximal shaking moment shows to be reduced from 0.64 Nm (column 3) to 0.56 Nm (column 2) which is a reduction of 13%.

The theoretical simulation of motion along the triangular trajectory in Fig. 8.11 shows that the 96.72% balanced manipulator has maximal shaking forces of 8.9 N along x and 7.7 N along y , as expected from the calculations from the force balance conditions. This means that the expected shaking forces of the manipulator for

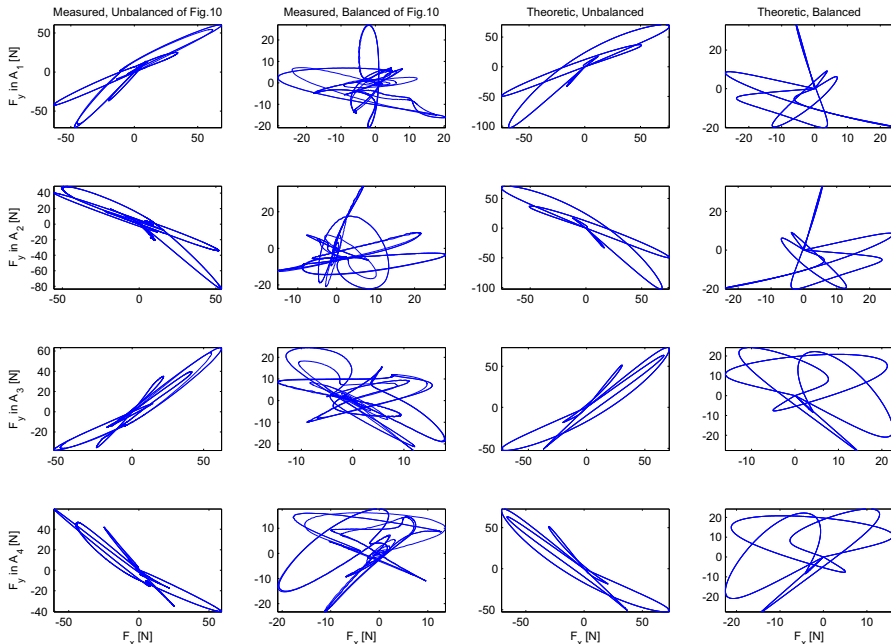


Fig. 8.13 For the motion in Fig. 8.9, the bearing forces from simulation of the measured motion of the unbalanced and the balanced manipulator are shown in columns 1 and 2, respectively. Columns 3 and 4 show the results from simulation of smooth motion along the triangular trajectory with equal maximal accelerations. It was found that the maximal bearing forces of the balanced manipulator were 73% lower in joints A_1 and A_2 and were 69% lower in joints A_3 and A_4 as compared to the unbalanced manipulator.

motion without rotation of the platform can be described as

$$\begin{bmatrix} ShF_x \\ ShF_y \end{bmatrix} = \frac{2(m_{cm,i}p_{cm,i})^{dif}}{l_{i1}} \begin{bmatrix} \ddot{x}_5 \\ \ddot{y}_5 \end{bmatrix} = m_{payload} \begin{bmatrix} \ddot{x}_5 \\ \ddot{y}_5 \end{bmatrix} \quad (8.30)$$

showing a linear relation between the shaking forces ShF_x and ShF_y and the balance inaccuracy or difference from perfect balance $(m_{cm,i}p_{cm,i})^{dif}$ and the payload $m_{payload}$ on the platform. The maximal shaking moment of the 96.72% balanced manipulator in Fig. 8.11 is 14.2 Nm, which is, contrary to the measured results, about 1% higher than of the fully balanced manipulator.

Due to the PID-controller that allowed the manipulator to move not perfectly along the desired trajectories, from the results in Figs. 8.8, 8.9, and 8.10 the sensitivity to motion inaccuracy is also shown. For imperfect motion along the orthogonal axes, Fig. 8.8 shows that shaking moments exist, however they remain small as compared to the motion in Fig. 8.9. The sensitivity to rotation of the platform is shown too. Small rotations of the platform can already contribute significantly to the shaking forces since the measured shaking forces of the balanced manipulator in Figs. 8.8, 8.9, and 8.10 are not zero as expected.

Altogether it can be concluded that small inaccuracies of the counter-masses, of unbalanced payload on the platform, and of platform rotations can already lead to considerable vibration for high-speed manipulations although they remain significantly low as compared to the unbalanced manipulator. Therefore high accuracy in the design, production, and control of a balanced manipulator is important for optimal dynamic balance.

8.7.3 Actuator torques

The measured actuator torques in Fig. 8.12 show that the torques required to move the balanced manipulator are higher than the torques of the unbalanced manipulator. The maximal values of the torques τ_1 , τ_2 , τ_3 , and τ_4 of the unbalanced manipulator are 31 Nm, 35 Nm, 30 Nm, and 29 Nm, respectively, and of the balanced manipulator they are 52 Nm, 53 Nm, 47 Nm, and 44 Nm, respectively. This means that for the balanced manipulator they are 1.68, 1.51, 1.57, and 1.52 times the torques of the unbalanced manipulator, respectively, which is on average $1.6\times$ higher.

From the theoretical results in column 3 in Fig. 8.12, the maximal torques τ_1 and τ_2 are both 1.42 times higher being 27 Nm and maximal torques τ_3 and τ_4 are both 1.47 times higher being 22 Nm, which is on average $1.4\times$ higher for the balanced manipulator. The actuator torques from the theoretical results are lower than the measured torques which may be caused by the high torques that the PID-controller calculates to correct the output motion and by friction which was not included in the calculations with the inverse dynamic model.

8.7.4 Bearing forces

The bearing forces shown in column 1 and 2 in Fig. 8.13 were derived from the simulation of the real motion in Fig. 8.9. Since the values of the shaking forces from these simulations have been considered to be inaccurate due to the differentiation problem, the values of the individual bearing forces are also inaccurate. However the results from the simulation in Figs. 8.8 and 8.9 have shown to be suitable for comparing the unbalanced and the balanced manipulator.

For simulation of precise motion along the triangular trajectory with equal accelerations, columns 3 and 4 of Fig. 8.13 show the bearing forces of which the shapes and size are comparable with columns 1 and 2. From both simulations it is found that the maximal bearing forces in A_1 and A_2 are 73% lower and in A_3 and A_4 are 69% lower for the balanced manipulator. The maximal forces were calculated as $\max(\sqrt{F_x^2 + F_y^2})$ in each bearing. The lower bearing forces imply that the balanced manipulator has increased stiffness characteristics.

8.7.5 Evaluation method and experimental setup

The approaches to the design of balanced manipulators have resulted in a new manipulator which has been shown to be both feasible for high-speed tasks and to have low vibration of its base. The aim was to have a perfectly dynamically balanced manipulator along the orthogonal axes. Since all motion of the manipulator remains in the vicinity of perfect balance, the manipulator has proved to have significant balance performance throughout the workspace.

The evaluation method of considering the measured motion of the manipulator and using this motion as input for the simulations has shown to be partly successful. Since only position data of the manipulator motion were recorded, these data had to be differentiated twice to obtain the velocity data and the acceleration data at each time step. Because of this, the obtained values for the shaking forces and shaking moment were not equal to the measured values. However, the resulting shaking forces from simulations were shown to be applicable for the relative comparison of the balanced and the unbalanced manipulator. This was not true for the shaking moments. Therefore, for a better application of this evaluation method, it is required to have accurate velocity and acceleration data, for example by measuring as well the position, the velocity, and the acceleration of the manipulator motion during experiments with additional sensors.

For the measurements of the shaking forces the force/torque sensor mounted in the center of the base plate was shown sufficient. However due to the low rotational stiffness of the experimental setup, measurement of the shaking moment was shown problematic. A solution to this is to measure the shaking forces with solely force sensors at the corners of the base plate such that the base plate is fully constrained

for in-plane translational and rotational motion. From the measured forces then the shaking moment can be derived.

8.8 Conclusion

A prototype of a dynamically balanced redundant planar 4-RRR parallel manipulator in an experimental setup was presented for evaluation and comparison with the unbalanced manipulator. A method was proposed for a fair evaluation and comparison in which the measured motion from the experiments was used as input for the simulation. For precise simulation of the manipulator motion, the inverse dynamic model of the manipulator was derived and validated.

The prototype manipulator successfully performed high-speed motion with low base vibration. Experiments showed that the balanced manipulator has about 97% lower shaking forces and a 96% lower shaking moment for motion along the orthogonal axes. For motion throughout the workspace, the balanced manipulator showed about 93% lower shaking forces and 16% lower shaking moment. Since the PID-controller allowed small rotational motion of the platform, causing shaking forces, it is expected that these values will reduce further when the control of the rotation of the platform is improved.

A relatively small balance inaccuracy of 3.28%, representing too light counter-masses or an unbalanced payload on the platform, was shown to increase the shaking forces considerably, while they still remain significantly low as compared to the unbalanced manipulator. For a manipulator with optimal dynamic balance, accurate design and production therefore are important. The actuator torques of the balanced manipulator were shown to be about $1.6 \times$ higher than for the unbalanced manipulator and the bearing forces of the balanced manipulator were shown to be about 71% lower than for the unbalanced manipulator.

It was found that shaking forces and shaking moments obtained from precise simulation of the measured manipulator motion with the inverse dynamic model are affected by the differentiation of the measured position data to obtain velocities and accelerations. The obtained values were shown to be useful for the relative comparison of the shaking forces of the balanced and the unbalanced manipulator, but their values were not equal to the measured values.

Chapter 9

Reflection on the design of inherently balanced mechanisms

For the synthesis of inherently dynamically balanced mechanisms two methods have been proposed. In chapter 2 the method of linearly independent linear momentum was introduced as an intuitive and straightforward method to derive planar inherently force-balanced mechanisms from given kinematic architectures by adapting the geometric and mass parameters. Closed kinematic chains were investigated by substituting the derivatives of the loop equations in the linear momentum equations. It was shown how the linear momentum equations of a mechanism with multiple closed loops include not only the general force balance conditions, but also a variety of general and specific configurations of force-balanced mechanisms as subsets.

Since for this method an initial kinematic architecture is required, it can be advantageous in situations where the designer already has some ideas of the kinematic solution that is desired. Advantageous force balance solutions then are obtained which determine the exact geometry and kinematics of the mechanism. Although force balance then is considered prior to the kinematic synthesis, the obtained solutions depend significantly on the initial choice of the kinematic architecture.

Application of the method of linearly independent linear momentum to spatial mechanisms is challenging because of the $\sin()$ and $\cos()$ products that appear which prevents writing the linear momentum in linearly independent terms. This problem also exists when the angular momentum of a kinematic architecture is written, for which it is challenging to investigate the moment balance. A possibility for analysis of the moment balance is to apply the method of principal vectors as it was proposed by Fischer as solely a method for analysis, and subsequently to continue as in chapter 6 by writing the angular momentum similarly as for the principal vector linkages from which the moment balance conditions can be derived. Then the angular momentum equation depends only on principal elements.

In chapter 7 the method of principal vector linkages was presented where inherently dynamically balanced mechanisms are derived from principal vector linkage architectures. In other words, mechanism solutions are synthesized with dynamic balance as a design principle. Because principal vector linkage architectures are based on the essential kinematic conditions for dynamic balance solely, dynamic balance is considered prior to the kinematic synthesis. This method gives liberty to

the designer to find a multitude of new kinematic solutions of dynamically balanced mechanisms.

In section 3.5 it was shown that principal vector linkages can also move spatially, but that it is challenging to build them in real because of the joints that cannot constrain the element to move as spatial parallelograms. It was not investigated how the angular momentum and the moment balance conditions of spatial principal vector linkages can be derived. Since Fischer showed that the principal vector method is applicable for analysis of spatial mechanisms, it is likely that principal vectors can be used also for analysis of the dynamic balance of spatial kinematic architectures. Then similar to the method of linearly independent linear momentum, inherently dynamically balanced solutions may be synthesized by adapting the geometric and mass parameters of a given spatial mechanism.

In chapter 7 it was shown that inherently balanced mechanism solutions for desired tasks and functions can be synthesized from principal vector linkage architectures by various methods. The obtained solutions are among the easiest to derive from the principal vector linkage architectures by changing the parameters of the elements, eliminating elements, and by combining them. Alternative designs of the principal vector links such as in Fig. 3.18 and Fig. 3.20 and the exchange of links with other mechanism elements such as sliders and gears have to be developed further to achieve advanced solutions. It is also possible to find new principal vector linkage architectures, for instance by developing the graphical solutions related to the principal vector method in [53, 79, 104, 87] into mechanisms where each element has mass and inertia, similarly as shown in this work, or by application of mass equivalent linkages of which the theory was not included [101].

To obtain inherent moment balance, the degrees-of-freedom of a principal vector linkage architecture are reduced such that the moment balance conditions hold, for instance by introducing slider elements as was shown for the grasper mechanism in Fig. 7.1. It still is challenging to obtain moment balance conditions for non-linear relations among the relative motions, for which a systematic approach is needed. Since the parallelogram can be considered fundamental in the analysis and synthesis of dynamic balance - principal vector linkages are based on parallelograms - the parallelogram may be fundamental in such an approach too.

The kinematic solutions in chapter 7 are a glimpse of the potential of the method of principal vector linkages. The kinematic solutions such as the grasper mechanism in Fig. 7.1, the DUAL-V in Fig. 7.4, and the mechanisms in Fig. 7.6 and Fig. 7.8b are new and would not have been found if dynamic balance would not have been considered prior to the kinematic synthesis. The complexity of the grasper mechanism in Fig. 7.1 is not more than other grasper mechanisms with the same functionality and with its actuators on the base. Since the mechanism does not need counter-masses it is a low mass solution. The complexity of the DUAL-V manipulator in Fig. 7.4 is significantly less than known manipulators that are balanced with additional elements [106, 107, 9]. Since it has only counter-masses about the fixed pivots it is a low inertia solution.

It was shown that inherently balanced mechanisms can be obtained by combining principal vector linkage architectures. For example in Fig. 7.3 the DUAL-V manipu-

lator was synthesized by combining two pantographs. This can be regarded a kind of leg-by-leg approach, comparable with the approach in chapter 2 where in this case the DUAL-V is considered with two 3-DoF legs. The difference of combining principal vector linkages as legs is that a leg is not selected to be balanced afterwards with additional elements. By summing the angular momentum of each leg, moment balance is investigated of all legs together.

An inherently dynamically balanced mechanism was defined in chapter 1 as a mechanism where all elements contribute to the motion and to the dynamic balance. The balanced linkage architectures such as in Fig. 5.7 however are overconstrained and have more elements than required for its motion. Technically, these architectures then are not inherently balanced. However when for synthesis elements are eliminated, inherently balanced mechanisms are derived that are normally constrained. Since the DUAL-V manipulator has 3-DoF motion of the platform and it has four legs, its inherent balance can be questioned. With the condition number in chapter 8, however, it was shown that the fourth leg is not only advantageous for dynamic balance, but also for the motion of the manipulator because of its influence on the workspace. The DUAL-V manipulator therefore can be considered inherently balanced.

With a prototype of a planar 3-DoF inherently dynamically balanced parallel manipulator in chapter 8, for the first time a high-speed dynamically balanced multi-degree-of-freedom parallel manipulator was designed, built, and tested. It successfully performed motions up to 180 m/s^2 . By evaluation and comparison with the unbalanced 3-DoF parallel manipulator, experiments and simulations showed that the balanced manipulator has up to 97% lower shaking forces, up to a 96% lower shaking moment, and about 71% lower bearing forces. The actuator torques of the balanced manipulator however were about 1.6 times higher. To determine if incorporating a dynamically balanced manipulator in a machine system is beneficial, also the circumstances such as its influence on the costs and performance of other equipment are important. To know if the costs per product can be reduced with dynamic balance, it is required to develop and investigate a conceptual design of the complete machine together with a corresponding business plan.

With the DUAL-V it was shown that with dynamic balance the performance of a manipulator can be improved. Similar results are likely for other balanced mechanisms with counter-masses solely about fixed pivots, since this leads to low bearing forces and to low inertia addition. For instance when the elements of the delta robot in Fig. 2.10 would all be parallel, which is when all links of the arms have equal length and the size of the platform is equal to the base, then it can be force balanced with solely counter-masses about the pivots with the base. The result can be regarded a spatial version of one side of the DUAL-V. Since for the DUAL-V both sides are needed for moment balance, a copy of this delta robot can be placed oppositely to obtain moment balance. In practice however, this solution will prevent the delta robot to do its common tasks. It is also possible to moment balance a force-balanced delta robot with three additional counter-inertias on the base that are driven with three additional actuators [99, 95]. Then the shaking moments of all elements are balanced together actively, which is a low inertia solution. How the

results of dynamic balance apply to parallel manipulators with prismatic joints was not investigated.

In chapter 4 a method was found where a mass equivalent model of an element in planar motion is obtained with one virtual and two real equivalent masses. With these equivalent masses it was shown that closed kinematic chains can be modeled and analyzed for force balance as open kinematic chains. This model was not found applicable for analysis of the moment balance of closed kinematic chains. Therefore a new inertia equivalent model needs to be found.

A set of one virtual and two real equivalent masses showed to represent planar rotational motion of an element. Since a single equivalent mass - which equals the total mass of an element - can represent the translational motion of an element, no other equivalent masses are needed to model this motion. This holds also for spatial translational motion where a single equivalent mass is sufficient. How a mass equivalent model of an element for spatial rotational motion can be designed was not investigated. Because of the three rotational motions it can be hypothesized that such a model requires three virtual equivalent masses together with the two real equivalent masses in the joints of the considered loop.

It will be interesting to investigate the application of the mass equivalent model not only for the purpose of dynamic balance but also for multi-body dynamics in general, which may lead to new insights in dynamic modeling. Also the principal vector method may be considered again for dynamic analysis. It was shown in this work how the principal vectors can be applied to describe the linear and angular momentum of the motion of masses and inertias relatively to their common CoM. Fischer has shown how with the principal vector method the lagrange equations of motion can be derived [53]. His objective was to derive the acting forces and moments on and in a multi-body system that cause its motion. Maybe with principal vectors efficient algorithms can be designed to monitor the internal forces and moment in elements, or to detect and locate clearance and wear in a system. These are topics that need further investigation.

The main goal of this work was to show how to design dynamically balanced mechanisms that encourage them to be applied. Although in general the focus in machine design is on the reduction of mass, it was shown that for dynamic balance a focus on the location of mass is also important. In fact, machine design involves the reduction of mass where it is disadvantageous and the *addition* of mass where it is advantageous. When this is achieved *in a well-balanced way*, new opportunities are ahead. Figure 9.1 shows the prospect of the *vertical factory*. Since dynamically balanced devices do not interact with the environment, no vibrations are exerted to e.g. the floor and the wall, they can be placed easily at any location in any orientation in buildings with multiple levels. Since for end-effectors of cable-driven manipulators dynamic balance is of particular importance, it is also shown how a dynamically balanced manipulator can be applied as a cable-driven manipulator end-effector for a large workspace throughout the factory.

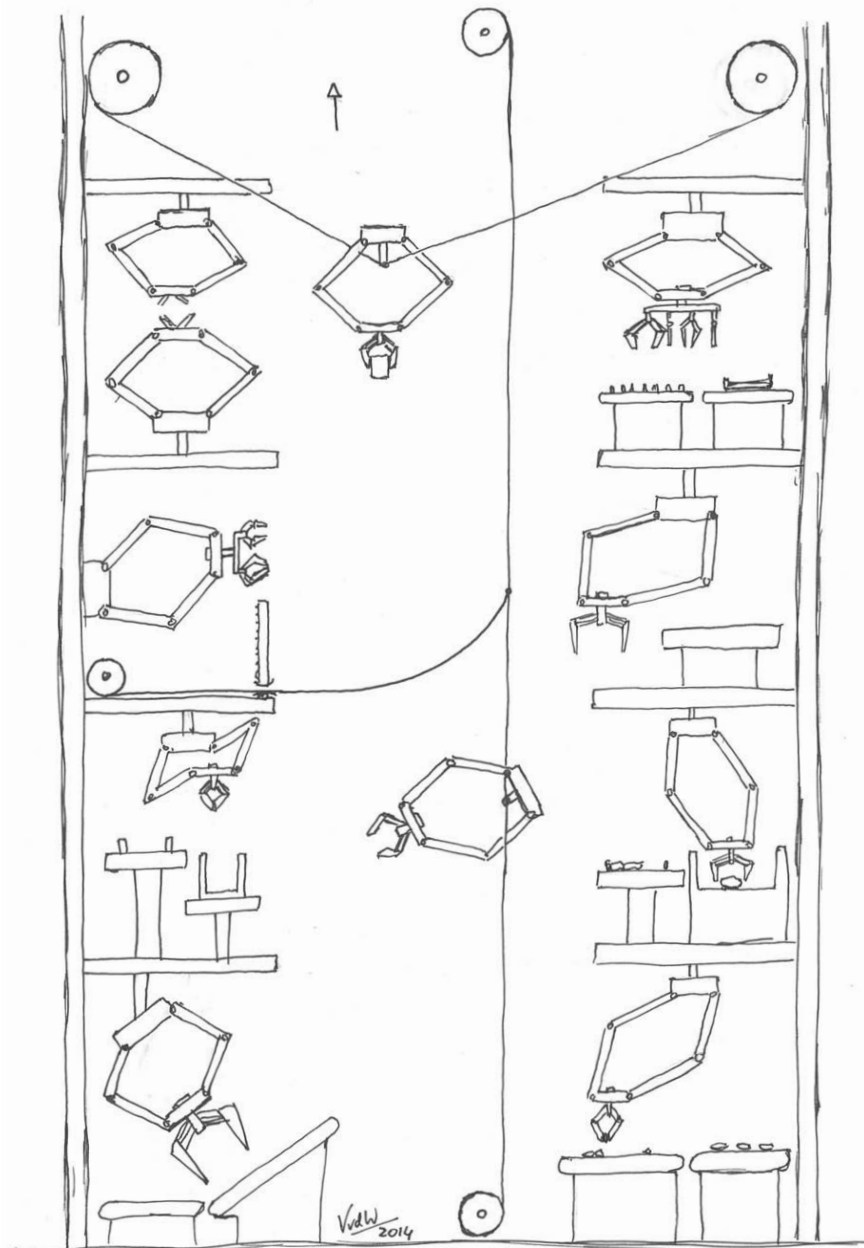


Fig. 9.1 Prospect of the *vertical factory* where dynamically balanced devices such as manipulators can be placed at any location in any orientation in buildings with multiple levels and can be applied as end-effector in cable-driven manipulators for a large workspace throughout the factory.

Chapter 10

Conclusion

Two methods for the synthesis of inherently dynamically balanced mechanisms have been proposed which consider dynamic balance prior to the kinematic synthesis. Instead of adding mass and inertia to a given mechanism with additional elements as with common dynamic balancing methods, with these methods the mechanism elements are considered for both the motion and the dynamic balance. With the method of linearly independent linear momentum inherently force-balanced mechanisms are derived from given kinematic architectures by adapting the geometric and mass parameters. With the method of principal vector linkages inherently dynamically balanced mechanisms are derived from principal vector linkage architectures that have solely the essential geometric conditions for force balance.

It was shown that inherently balanced mechanism solutions for desired tasks and functions can be synthesized from principal vector linkage architectures by various methods, including changing the parameters of the elements, eliminating elements, reduction of degrees-of-freedom, introducing gears and sliders, and by combining them. To obtain inherent moment balance, the degrees-of-freedom of a principal vector linkage architecture are reduced such that the moment balance conditions hold, for instance by introducing slider elements.

New multi-degree-of-freedom kinematic solutions have been found that would not have been obtained if dynamic balance would have been considered after the kinematic synthesis. A planar 2-DoF inherently dynamically balanced grasper mechanism was synthesized from a 4-DoF principal vector linkage consisting of 6 parallelograms and 2 slider elements and a planar 3-DoF inherently dynamically balanced parallel manipulator was synthesized from two 2-DoF principal vector linkages consisting of parallel links of equal lengths and counter-masses solely about pivots with the base. Also the potential for large moving structures was investigated by synthesis of a dynamically balanced movable bridge and of a force-balanced movable building from 2-DoF principal vector linkages.

A prototype of a planar 3-DoF inherently dynamically balanced parallel manipulator in an experimental setup was presented for evaluation and comparison with the unbalanced 3-DoF parallel manipulator. The prototype manipulator successfully performed high-speed motion up to 180 m/s^2 and showed that with dynamic balance

the performance of the manipulator can be improved. Experiments and simulations showed that the balanced manipulator has up to 97% lower shaking forces, up to a 96% lower shaking moment, and about 71% lower bearing forces as compared to the unbalanced manipulator at the price of about 1.6 times higher actuator torques.

A method was found by which the loop closure relations of general planar closed kinematic chains can be considered implicitly. Therefore the mass of an element with general CoM is modeled with one virtual equivalent mass and two real equivalent masses. A closed kinematic chain then is analyzed by including these equivalent masses in the analysis of the open kinematic chain without the modeled element. This method was applied for analysis and for deriving the force balance conditions of closed principal vector linkage architectures with 1 and with 3 closed loops.

Appendix A

The work of Otto Fischer and the historical development of his method of principal vectors for mechanism and machine science

Abstract This article gives an overview of the distinctive work of Otto Fischer (1861-1916) on the motion of the human musculoskeletal system. In order to derive the individual muscle forces for human in motion, he invented the *method of principal vectors* to describe the motion of the centers-of-mass and the inertias of body segments. This method has proven to be successful, not only for the studies on biomechanics but in particular also for mechanism and machine science. A historical development of the application of the method is presented for today's potential.

A.1 Introduction

With time the amount of knowledge increases at a rapid pace. For research it is a challenge to both remain up-to-date and to not forget the past. Particularly this is a challenge when old research results and ideas lose interest for a certain time, for decades or for ages. To retrieve the results, and more importantly to retrieve the philosophy with which they were obtained, often investigation of the original sources is needed. Citations of old literature in current articles often tend to become rather 'automatic' or indirect, e.g. because of language differences or unavailability, and therefore do not reveal the essence and the potential of the original sources. This however is necessary to discover the value old methods may have for contemporary research goals.

With this perspective, the work of the physiologist, physicist, and medical doctor (Physiologe, Physiker, Arzt) Otto Fischer¹ is summarized and the philosophy and application of his *method of principal vectors* is investigated. In addition to his still relevant results on the mechanical properties of the human musculoskeletal system and of his investigation of the human gait, this method has been essential for studying the individual muscle forces for human motion in the pre-computer era. Although invented for biomechanics, Fischer emphasized the potential of his method

¹ *26-04-1861 Altenburg (Thüringen), Germany †16-12-1916 Leipzig, Germany

for mechanism and machine science, which was taken over by various researchers. This article includes a historical development of his method in mechanism and machine science to illustrate its current potential.

A.2 Otto Fischer and his works

[2][3][1] Otto Fischer studied mathematics and physics at the German universities of Jena, München, and Leipzig and obtained his PhD-degree (Dr. phil.) in mathematics from the University of Leipzig in 1885, supervised by Prof. Felix Klein. In 1887 he became teacher of mathematics and physics at the business school (Handelslehranstalt) of Leipzig. He continued as a teacher at the Petri-Realgymnasium in Leipzig in 1895, where he would teach until the end of his life, from 1912 onward at the position of rector.

At the same time Fischer worked on medical and biological research together with the anatomist Prof. Christian Wilhelm Braune at the Anatomic institute of the University of Leipzig. In 1893 he obtained his habilitation on physiological physics (Physiologische Physik) at the University of Leipzig and became teacher at this topic at the Faculty of Philosophy. In 1896 he became Professor extraordinarius on medical physics (Medizinische Physik) at the Medical Faculty of the University of Leipzig where he remained until his early death in 1916.

Together with Braune, Fischer was pioneering the research on biomechanics of the human musculoskeletal system in motion. While anatomists at that time investigated the mechanics of the human body empirically, he understood the necessity of theoretical investigation. He stated that only with an accurate kinematic model of the human skeletal system the functioning of human motion and of the muscles could be investigated to achieve full understanding. Being a mathematician, he stressed in probably his first publication in 1885 that a mathematical method was needed to gain exact and reliable results in human kinematics [16].

The investigation in [16] consists of three-dimensional measurements of the motion of the forearm. At three non-collinear points at the bone wooden needles were attached. The motions of the tips of the needles were recorded by drawing their projections on millimeter-paper and by recording the distance from the needle to the plane of the paper. With these measurements he became the first to make three-dimensional motion analysis of human. A mathematical description of the measured motions was derived by screw motion, for which he determined the screw-axes of each body segment. Based on the motion of the screw-axes the real motion could be interpreted accurately.

His results led to important corrections on the results from purely two-dimensional empirical analysis by others. For example in 1887 he reexamined the motion of the elbow and the hand with a 'rigorous mathematical analysis' gaining new insight at a topic that had been considered known [18].

In [17] Fischer considered the importance of measurements on the living hand as compared to a cadaver hand, because of the significant influence muscles have

on the real motion capabilities in addition to the joint geometry. To measure the motions, he placed metal tubes around the finger to which the wooden needles and steel wires for measuring were attached. In 1888 he started analyzing the combined motion of multiple body segments by considering the shoulder with the humerus [19] and in 1889 the functioning of the flexor muscles of the elbow was investigated [20].

For the first time in 1889, Fischer considered the motion of the center of mass (CoM) of the complete human body [21]. As compared to statics and mechanics of the human body at a certain pose, which can be analyzed from individual body segments, he stated that for deriving the muscle forces for certain human motion knowledge is needed about the motion of the body CoM. One argument was that while each body segment has various possible motions, the body CoM always moves in a very specific manner. Fischer and Braune determined the positions of the CoM of human bodies and of parts of human bodies by using rigidly frozen cadavers. They verified their results with the results of anatomists for individual body segments and presented them as ratios or coefficients in order to account for differences of individuals. Their results remained important well into the computer era [111, 86].

In 1891 advanced kinematic measurements and analysis of the knee joint were published [22] followed in 1892 by measurements of the inertia values of body segments [23].

One year after the death of Braune, Fischer published in 1893 his habilitation work on determining the muscle forces for human motion [42]. He noted that the human body had become a mechanically known object. At anatomic level the properties of each body segment were well known and at kinematic level the relative motion of the body segments had become well known too. With the rich knowledge on the functioning of individual muscles at an anatomic level, the next new step had to be the investigation of the combined muscle forces that cause human motion. He distinguished human motion by the absolute motion of the body CoM and by the relative motion of the body segments with respect to the body CoM. For the analysis of the relative motions and to derive muscle forces he invented 'The method to derive kinetic energy' ('Die Methode der Ableitung der lebendigen Kraft'), of which a part would be named later 'The method of principal vectors' [74]. With this method, Fischer investigated the muscle forces of the lower arm in 1895 [43] and he made other contributions to the statics and dynamics of muscles in 1896 [44] and 1897 [45].

From 1895 to 1904 Fischer published a series of six works on human gait (*Der Gang des Menschen*). The first part consists of the measurements of the motion of unloaded and loaded humans within a spatial co-ordinate system with high accuracy [24]. The results of these measurements were used for analysis in the following five parts for which Otto Fischer is said to be the first to conduct three-dimensional gait analysis [12]. In part two in 1899 the precise motion of the body CoM based on the CoM of individual body segments is investigated in relation with the external forces that apply [46]. In part three in 1900 the lower extremities are investigated [47], while part four in 1901 treats the forces and moments in the foot [48]. In both part five in 1903 [50] and part six in 1904 [51] the motion of the upper-leg is treated

with which he became the first to give the exact proof that for walking the upper-leg does not solely swing forward as a passive pendulum.

In 1902 Fischer studied the influence of muscles on one another to stress, again, the importance of considering the motion of the complete human musculoskeletal system in order to investigate the functioning of the individual muscles [49]. In 1905 he extended his method of principal vectors to derive the spatial equations of motion of spatial chains [52].

In 1906 Fischer published his book 'Theoretical fundamentals for mechanics of moving bodies' ('Theoretische Grundlagen für eine Mechanik der lebenden Körper') [53]. In the first part of what would become a classical work [2] all of his achievements on the method of principal vectors are presented and developed from the very beginning. The second part summarizes his investigations on human motion to which the method had been applied. The book ends by illustrating the potentials of his method for mechanism and machine science.

Fischer published also a book on descriptions of human joints from a rather kinematical point of view instead of from the common anatomical point of view in 1907 [54]. In 1909 he published a work on spherical kinematics of Listing's law (das Listinsche Gesetz) [56] and of the humeroradial joint [55].

Most of the cited publications of Otto Fischer were published in the proceedings of the Mathematisch-Physikalischen Classe der Königlich-Sächsischen Gesellschaft der Wissenschaften in Leipzig of which he was extraordinary member since 1893 and ordinary member as of 1905. All cited literature is freely accessible on the internet in the DMG-library² or in the SLUB-library of Dresden³.

A.3 The method of principal vectors

To derive individual muscle forces for a human in motion, the motion of all body segments needs to be considered. For instance the motion of the elbow affects the forces at the shoulder or motion of the arm may affect to forces in the leg. However, calculations with the inverse dynamic model of the human at each instant are cumbersome to do by hand. Therefore Fischer developed a method that is capable of reducing the mechanics of the human mechanism to solely the element of interest, e.g. the elbow, knee, or foot. From the resulting reduced mass and inertia model the equations for the kinetic energy and the equations of motion could be derived.

The essential choice Fischer made was to investigate the motion of the body CoM independently from the relative motions of the body segments with respect to the body CoM. Since the motion of the body CoM is determined by external forces while the relative motion of body segments is determined by internal (muscle) forces, then also these can be investigated independently. The relative motion of the body segments about the body CoM is determined from the kinematics for which the

² <http://dmglib.org/dmglib/handler?biogr=34004> (April 2014)

³ www.digital.slub-dresden.de/en/digital-collections (April 2014)

dynamic model can be reduced. It is exactly this reduction step which is named *the method of principal vectors*, which is part of Fischer's complete 'method to derive kinetic energy' [42].

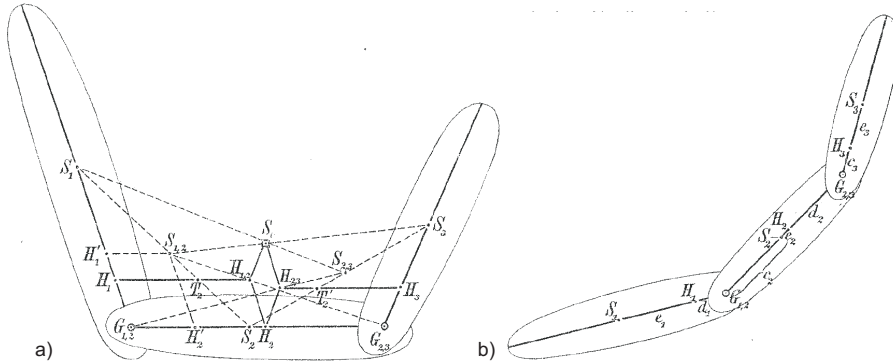


Fig. A.1 Derivation of the principal points H_i that define the principal dimensions of a linkage of three elements with their CoM at S_i . The linkage Com S_0 then is found geometrically [53].

Fischer explained his method for the linkage of three elements shown in Fig. A.1. The elements are linked with revolute pairs at $G_{1,2}$ and $G_{2,3}$ and each element has a mass m_i centered at position S_i . It is possible to define *principal points* H_i at each element. At element 1 principal point H_1 is defined as being the CoM of mass m_1 at S_1 and mass $m_2 + m_3$ at joint $G_{1,2}$. This is a projection of the mass of elements 2 and 3 at element 1. Equivalently, at element 3 principal point H_3 is defined as being the CoM of mass m_3 at S_3 and mass $m_1 + m_2$ at joint $G_{2,3}$. At element 2 principal point H_2 is defined as being the CoM of m_2 at S_2 , m_1 at $G_{1,2}$, and m_3 at $G_{2,3}$.

With the principal points, lengths $H_1G_{1,2} = d_1$, $H_2G_{2,3} = d_2$, $G_{1,2}H_2 = c_2$, and $H_3G_{2,3} = c_3$, are determined which are the principal dimensions of the linkage. With these lengths the CoM of all three links S_0 can be geometrically found by parallelograms as indicated in Fig. A.1a. Since the principal dimensions are independent of the motion of the linkage, these parallelograms trace the linkage CoM for all motion of the links. With respect to a fixed reference frame, the vectors describing the principal dimensions are named the principal vectors.

The geometric result of Fig. A.1 can be seen as a linkage as shown in Fig. A.2. Assuming the linkage CoM S_0 to be stationary, the position of the linkage is completely defined with the rotation of each element φ_i and its motion by their derivatives. Then for $\dot{\varphi}_2 = \dot{\varphi}_3 = 0$ element 1 rotates about H_1 while elements 2 and 3 solely translate. The inertia of this motion is the reduced inertia of the mechanism with respect to element 1. For each of the three elements this can be done with which the motion of the linkage consists of three reduced subsystems. For $\dot{\varphi}_1 = \dot{\varphi}_2 = 0$ element 3 rotates about H_3 while elements 1 and 2 solely translate and for $\dot{\varphi}_1 = \dot{\varphi}_3 = 0$ element 2 rotates about H_2 while elements 1 and 3 solely translate.

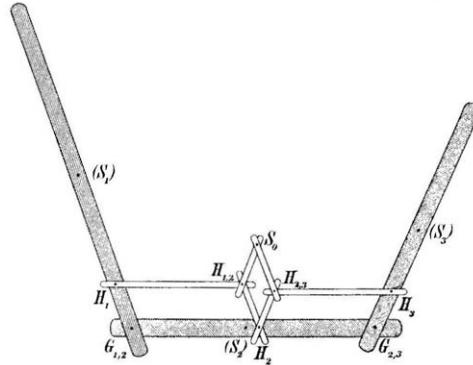


Fig. A.2 Mechanism by Fischer to trace the CoM of three links at S_0 by additional links [53].

Based on these subsystems Fischer was able to formulate the kinetic energy equation of the motion of the complete linkage to depend solely on the total mass $m_0 = m_1 + m_2 + m_3$, the three reduced inertias k_i , and the principal lengths. The kinetic energy of the linkage relative to the linkage CoM then is written as

$$T_r = \frac{m_0}{2} (k_1^2 \dot{\phi}_1^2 + k_2^2 \dot{\phi}_2^2 + k_3^2 \dot{\phi}_3^2) + m_0 d_1 c_2 \cos(\varphi_1 - \varphi_2) \dot{\phi}_1 \dot{\phi}_2 + m_0 d_1 c_3 \cos(\varphi_1 - \varphi_3) \dot{\phi}_1 \dot{\phi}_3 + m_0 d_2 c_3 \cos(\varphi_2 - \varphi_3) \dot{\phi}_2 \dot{\phi}_3 \quad (\text{A.1})$$

Including also the kinetic energy of the motion of the linkage CoM, which depends on m_0 and on the velocity of the CoM \dot{x}_0 and \dot{y}_0 , results in the equation of the kinetic energy for both relative and absolute motion of the linkage

$$T = \frac{m_0}{2} (\dot{x}_0^2 + \dot{y}_0^2 + k_1^2 \dot{\phi}_1^2 + k_2^2 \dot{\phi}_2^2 + k_3^2 \dot{\phi}_3^2) + m_0 d_1 c_2 \cos(\varphi_1 - \varphi_2) \dot{\phi}_1 \dot{\phi}_2 + m_0 d_1 c_3 \cos(\varphi_1 - \varphi_3) \dot{\phi}_1 \dot{\phi}_3 + m_0 d_2 c_3 \cos(\varphi_2 - \varphi_3) \dot{\phi}_2 \dot{\phi}_3 \quad (\text{A.2})$$

Deriving the equations of motion with Lagrange then results in five differential equations, two for the motion of the linkage CoM and three for the motion of the links with respect to the linkage CoM. The force components of the first two equations correspond with the external forces applied to the linkage CoM. The force components of the latter three equations correspond to the resultant moment on each link about the principal point H_i . These components are the resultants of all internal and external forces applied at the linkage that apply to an individual element from which the muscle forces can be derived at anatomic level.

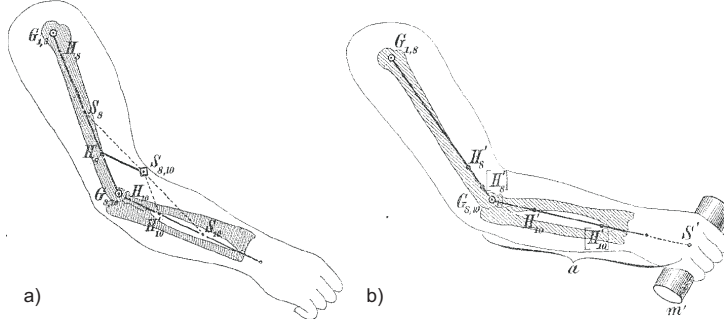


Fig. A.3 Fischer's method applied to (a) the right arm, (b) the right arm holding a mass [53].

A.4 Applications by Otto Fischer

Fischer applied his method to investigate the muscle activity of various parts of the human body. Figure A.3 shows the method applied to the right arm. In this case the forces in the shoulder and elbow were considered with the trunk being stationary and the hand being rigidly attached to the lower arm. In Fig. A.3a the position of the CoM of the arm with hand is $S_{8,10}$. Figure A.3b shows the same arm but with the hand holding a mass for which the principal points are located closer to the hand.

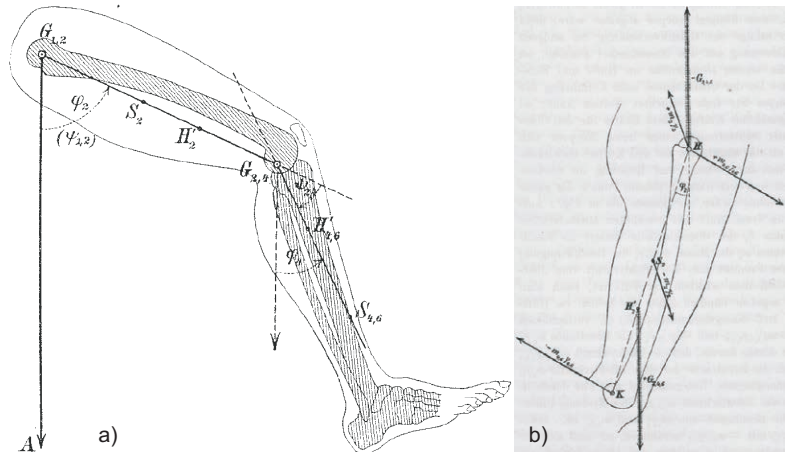


Fig. A.4 Investigation of (a) forces in the leg [53] and (b) the swing phase of the leg [50, 51].

Equivalently, Fig. A.4a shows the method applied to a leg, assuming the trunk to be stationary and the foot to be rigidly attached to the lower leg. Figure A.4b shows the upper leg for the investigation of the forward swing of a leg during walking.

Here the motion of the complete human was considered as being reduced to the motion of the leg. The reduced system was regarded as a linkage of three elements with the lower leg with rigidly attached foot being element 1, the upper leg being element 2, and the upper body being element 3 as compared to Fig. A.1.

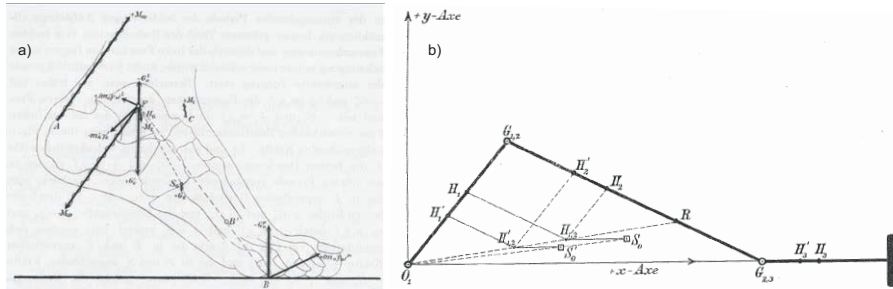


Fig. A.5 Investigation of (a) the foot [48] and (b) the shaking force balancing of a crank-slider mechanism [53].

Fischer also studied the forces and moments in the foot during walking. Figure A.5a shows the foot in contact with the ground just before making a step [48]. In [53] Fischer illustrates the potential use of his method for machines and mechanisms by applying it to a crank-slider mechanism as shown in Fig A.5b. He investigated the shaking forces, i.e. the resulting dynamic forces at the base, and derived the conditions for which they become zero and the mechanism is shaking force balanced. In [53] he also shows the benefit of his method for deriving the equations of motion with a pendulum used as example. From the reduced system the equations of motions are readily obtained, 'without the need of taking the indirect route by the kinetic energy and the general Lagrange differential equations of motion', with which he concludes his book.

Fischer developed his method in [52] for more complex linkages such as a linkage with six elements in series and a linkage with twenty elements. Also he showed that his method applies to spatial mechanisms for which he investigated a linkage of two elements with spatial motion. It is likely that Fischer planned to apply his method for the investigation of spatial joints. Therefore he investigated the spherical kinematics of Listing's law [56] and of the humeroradial joint [55] of which Fig. A.6 shows a mechanism model and an illustration.

A.5 Development and application by other researchers

The method of principal vectors is described and applied by various authors. Nerreter in 1912 used the method for an extensive investigation of the shaking forces of a four-cylinder motor [79]. Wittenbauer in 1923 developed the method for inves-

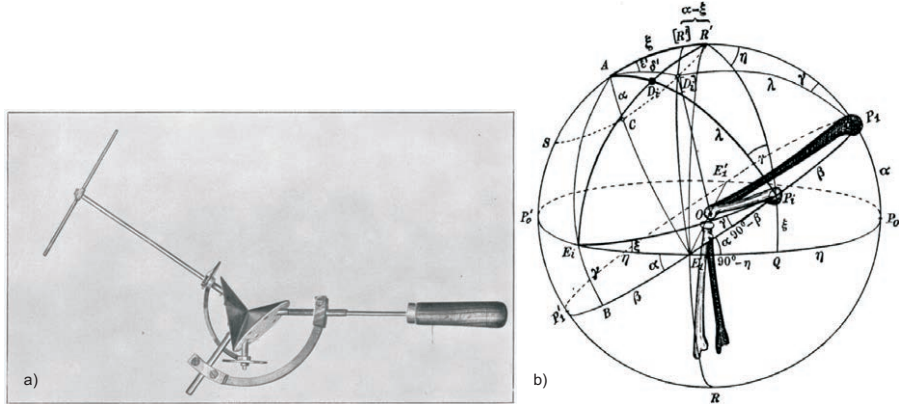


Fig. A.6 (a) Spherical mechanism model of the kinematics of Listing's Law [56], (b) Study of the relative motion of the radius at the humeroradial joint [55].

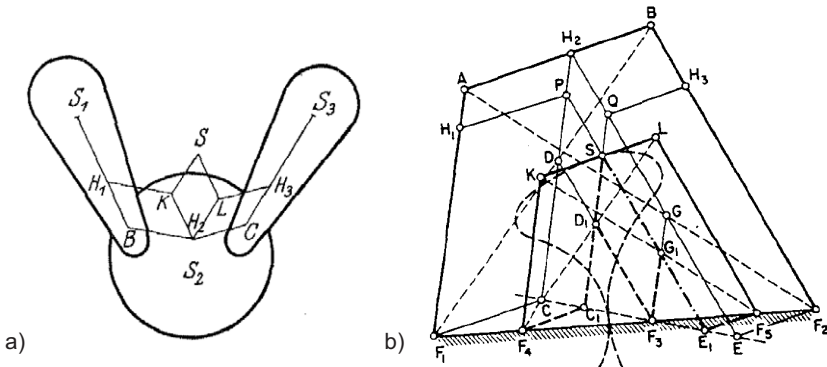


Fig. A.7 (a) Application of the method by Wittenbauer for an arbitrary mass distribution of each of the three links [104]. (b) Illustration by Kreutzinger to show that the trajectory of the CoM of a 4R four-bar linkage is similar to a coupler curve of this linkage [69].

tigating the motion of the linkage CoM and applied it to more complex mechanisms among which a parallel linkage [104]. He also applied the method to the linkage with three elements of Fig. A.2, but with each element having an arbitrary CoM location as shown in Fig. A.7a. Summaries of the method have been presented by, among others, Beyer in 1931 and 1960 [14, 15], Federhofer in 1932 [41], and Rao and Dukkipati in 1989 [84]. Among others, Wittenburg identified the concept of principal vectors in multi-body dynamic equations by applying concepts of graph theory, referring to the principal point as a Barycenter [105].

Kreutzinger in 1942 applied the method of principal vectors to show that the trajectory of the CoM of a 4R four-bar linkage is a curve similar to a coupler curve of this linkage [69]. His solution is illustrated in Fig. A.7b.

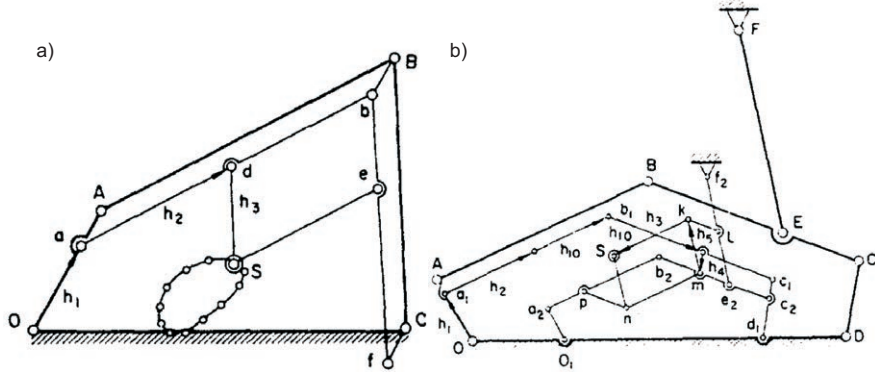


Fig. A.8 Alternative geometric solutions by principal vectors to trace the CoM (a) by Artobolevskii and (b) by the *double contour transformation* on a six-bar linkage by Shchepetil'nikov [87].

For the purpose of dynamic balancing, Shchepetil'nikov in 1957 extended the method of principal vectors to the method of *double contour transformation* [87]. He based his research on the findings of Artobolevskii in 1951 [10] who had proposed an alternative geometric solution to trace the CoM with principal dimensions, shown in Fig. A.8a. Since for mechanisms with multiple closed chains the geometric solution by parallelograms quickly leads to excessive bulkiness, Shchepetil'nikov showed how the CoM can be traced by similar auxiliary linkages being jointed to the original linkage. One example of the application to a six-bar linkage is shown in Fig. A.8b. His approach towards balancing was to have the linkage CoM move along a circular trajectory with a rotation synchronous to the driving crank. Then with a single counter-mass moving along with the driving crank the mechanism could be force balanced. By placing the counter-mass at an additional link elsewhere at the base, also the first harmonic of the shaking moment could be balanced. Having applied his method solely to linkages with mass symmetric links, he extended his method in 1975 to linkages with general mass distributions [88].

Hilpert in 1965 considered the balancing of a 4R four-bar linkage for which he used Fischer's geometrical solution together with a pantograph with counter-mass to bring the linkage CoM at a stationary position with respect to the base as shown in Fig. A.9a [61].

When the geometric solution to trace the CoM becomes a real linkage as in Fig. A.9a, the masses of the auxiliary links have to be considered too. Agrawal et al. in 2001 showed by experiments that the mass of the auxiliary links of Fischer's original linkage of Fig. A.2 can be included for which this linkage traces the CoM of all links together [5]. Then by having the CoM be stationary with the base results in a balanced manipulator as shown in Fig. A.10a. In 2004 Agrawal and Fattah showed that also for a spatial manipulator the mass of all links can be included, of which a prototype is shown in Fig. A.10b [4]. In this case the linkage CoM was statically balanced by a spring.

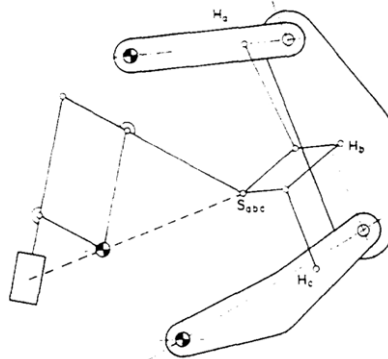


Fig. A.9 (a) Hilpert's solution to balance the CoM of a 4R four-bar linkage by a pantograph with counter-mass [61].

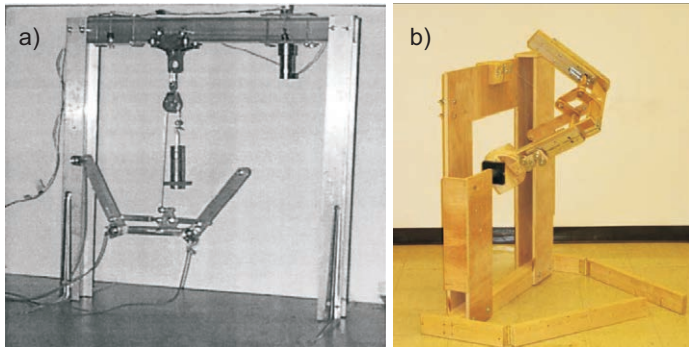


Fig. A.10 Applications by (a) Agrawal et al. to include the mass of all links and [5] (b) by Agrawal and Fattah to derive a statically balanced spatial manipulator [4].

A.6 Conclusion

An overview of the work of Otto Fischer was presented showing his contributions to three-dimensional human gait analysis and in particular the investigation of muscle forces for human motion. His method of principal vectors was summarized and a selection of Fischer's applications of the method were shown. The historical development of the method for mechanism and machine science was investigated, showing a clear focus on the motion of the center of mass of mechanisms for the purpose of static and dynamic balancing.

References

1. Biographisches Lexikon hervorragender Ärzte des neunzehnten Jahrhunderts pp. 513, Berlin, Wien (1901)
2. Neue Deutsche Biographie 5, 202, Berlin (1961)
3. http://histv.uni-leipzig.de/dozenten/fischer_o.html (Dec. 2011)
4. Agrawal, S.K., Fattah, A.: Gravity-balancing of spatial robotic manipulators. *Mechanism and Machine Theory* **39**, 1331–1344 (2004)
5. Agrawal, S.K., Gardner, G., Pledgie, S.: Design and fabrication of an active gravity balanced planar mechanism using auxiliary parallelograms. *Mechanical Design* **123**, 525–528 (2001)
6. Angeles, J., Nahon, M.A., Thümmel, T.: Active control for the complete dynamic balancing of linkages. *Flexible Mechanisms, Dynamics, and Analysis* **47**, 305–310 (1992)
7. Arakelian, V.G., Smith, M.R.: Shaking force and shaking moment balancing of mechanisms: A historical review with new examples. *Mechanical Design* **127**, 334–339 (2005)
8. Arakelian, V.H., Smith, M.R.: Erratum: Shaking force and shaking moment balancing of mechanisms: A historical review with new examples. *Mechanical Design* **127**, 1035 (2005)
9. Arakelian, V.H., Smith, M.R.: Design of planar 3-dof 3-RRR reactionless parallel manipulators. *Mechatronics* **18**, 601–606 (2008)
10. Artobolevskii, I.I.: Theory of Mechanisms and Machines, Chap. XXV. Gos. Izdat. Tekh.-Teoret. Lit., Moscow (1951)
11. Artobolevskii, I.I.: Mechanisms for the Generation of Plane Curves. Pergamon Press (1964)
12. Baker, R.: The history of gait analysis before the advent of modern computers. *Gait & Posture* **26**, 331–342 (2007)
13. Berkof, R.S., Lowen, G.G.: A new method for completely force balancing simple linkages. *Engineering for Industry* pp. 21–26 (1969)
14. Beyer, R.: Technische Kinematik. Johann Ambrosius Barth, Leipzig (1931)
15. Beyer, R.: Kinematisch-getriebedynamisches Praktikum. Springer-Verlag, Berlin/Göttingen/Heidelberg (1960)
16. Braune, W., Fischer, O.: Die bei der Untersuchung von Gelenkbewegungen anzuwendende Methode, erläutert am Gelenkmechanismus des Vorderarms beim Menschen. Hirzel, Leipzig (1885)
17. Braune, W., Fischer, O.: Das Gesetz der Bewegungen in den Gelenken an der Basis der mittleren Finger und im Handgelenk des Menschen. Hirzel, Leipzig (1887)
18. Braune, W., Fischer, O.: Untersuchungen über die Gelenke des menschlichen Armes. Hirzel, Leipzig (1887)
19. Braune, W., Fischer, O.: Über den Anteil den die einzelnen Gelenke des Schultergürtels an der Beweglichkeit des menschlichen Humerus haben. Hirzel, Leipzig (1888)
20. Braune, W., Fischer, O.: Die Rotationsmomente der Beugemuskeln am Ellenbogengelenk des Menschen. Hirzel, Leipzig (1889)

21. Braune, W., Fischer, O.: Über den Schwerpunkt des menschlichen Körpers mit Rücksicht auf die Ausrüstung des deutschen Infanteristen. Hirzel, Leipzig (1889)
22. Braune, W., Fischer, O.: Die Bewegungen des Kniegelenks, nach einer neuen Methode am lebenden Menschen gemessen. Hirzel, Leipzig (1891)
23. Braune, W., Fischer, O.: Bestimmung der Trägheitsmomente des menschlichen Körpers und seiner Glieder. Hirzel, Leipzig (1892)
24. Braune, W., Fischer, O.: Der Gang des Menschen. I. Theil: Versuche am unbelasteten und belasteten Menschen. Hirzel, Leipzig (1895)
25. Briot, S., Arakelian, V.H., Guégan, S.: PAMINSA: A new family of partially decoupled parallel manipulators. *Mechanism and Machine Theory* **44**, 425–444 (2009)
26. Briot, S., Bonev, I.A., Gosselin, C.M., Arakelian, V.: Complete shaking force and shaking moment balancing of planar parallel manipulators with prismatic pairs. *Multi-body Dynamics* **223**(K), 43–52 (2009)
27. Brown, G.W.: Suspension system for supporting and conveying equipment, such as a camera, patent US-4710819 (1987)
28. Chao, P.C.P., Chiu, C.W., Shih, K.T.: A novel low-torque ball re-positioning scheme based on a sliding-mode ball observer for an automatic balancer system. *Shock and Vibration* **15**, 101–126 (2008)
29. Chaudhary, H., Saha, S.K.: Balancing of shaking forces and shaking moments for planar mechanisms using the equimomental systems. *Mechanism and Machine Theory* **43**, 310–334 (2008)
30. Chung, W.K., Cho, H.S.: On the dynamic characteristics of a balanced PUMA-760 robot. *Industrial Electronics* **35**(2), 222–230 (1988)
31. Chung, W.K., Cho, H.S., Lee, C.W., Warnecke, H.J.: Performance of robotic manipulators with an automatic balancing mechanism. *Computer-Integrated Manufacturing and Robotics, ASME PED* **13**, 111–121 (1984)
32. Clavel, R.: Device for displacing and positioning an element in space, patent WO8703528A1 (1987)
33. Clavel, R.: Conception d'un Robot Parallel Rapide à 4 Degrés de Liberté - PhD. thesis. Lausanne EPFL (1991)
34. Collard, J.F., Gosselin, C.: Optimal synthesis of a planar reactionless three-degree-of-freedom parallel mechanism. *Mechanisms and Robotics* **3**(041009), 1–9 (2011)
35. Corbel, D., Gouttefarde, M., Company, O., Pierrot, F.: Towards 100G with PKM. Is actuation redundancy a good solution for pick-and-place? Proc. of the IEEE International Conference on Robotics and Automation, Anchorage, USA (2010)
36. Cox, H.H.M., Van Balleijoj, R.N.J., Vosters, P.M.H., Hol, S.A.J., Cornelissen, S.M.J.: Lithographic apparatus and device manufacturing method, patent US 6906786 B2 (2005)
37. Demeulenaere, B.: Dynamic Balancing of Reciprocating Machinery With Application to Weaving Machines - PhD. thesis. KU Leuven (2004)
38. Demeulenaere, B., Berkof, R.S.: Improving machine drive dynamics: A structured design approach toward balancing. *Mechanical Design* **130**(082302) (2008)
39. Demeulenaere, B., Spaepen, P., Masselis, S., Cornelissen, P., Pinte, G., Hemelsoen, J., Boone, R., Roelstraete, K., Desmet, W., Swevers, J., De Schutter, J.: Experimental validation of input torque balancing applied to weaving machinery. *Mechanical Design* **130**(2), 022,307 (2008)
40. Dijksman, E.A.: Motion Geometry of Mechanisms. Cambridge University Press (1979)
41. Federhofer, K.: Graphische Kinematik und Kinetostatik. Springer, Berlin (1932)
42. Fischer, O.: Die Arbeit der Muskeln und die lebendige Kraft des menschlichen Körpers. Hirzel, Leipzig (1893)
43. Fischer, O.: Beiträge zu einer Muskeldynamik. Erste Abhandlung: Über die Wirkungsweise eingelenkiger Muskeln. Hirzel, Leipzig (1895)
44. Fischer, O.: Beiträge zur Muskelstatik. Erste Abhandlung: Ueber das Gleichgewicht zwischen Schwere und Muskeln am zweigliedrige System. Hirzel, Leipzig (1896)
45. Fischer, O.: Beiträge zu einer Muskeldynamik. Zweite Abhandlung: Ueber die Wirkung der Schwere und beliebiger Muskeln auf das zweigliedrige System. Hirzel, Leipzig (1897)

46. Fischer, O.: *Der Gang des Menschen. II. Theil: Die Bewegung des Gesamtschwerpunktes und die äusseren Kräfte.* Teubner, Leipzig (1899)
47. Fischer, O.: *Der Gang des Menschen. III. Theil: Betrachtungen über die weiteren Ziele der Untersuchung und Überblick über die Bewegungen der unteren Extremitäten.* Teubner, Leipzig (1900)
48. Fischer, O.: *Der Gang des Menschen. IV. Theil: Über die Bewegung des Fusses und die auf denselben einwirkenden Kräfte.* Teubner, Leipzig (1901)
49. Fischer, O.: *Das statische und das kinetische Maass für die Wirkung eines Muskels, erläutert an ein- und zweigelenkigen Muskeln des Oberschenkels.* Teubner, Leipzig (1902)
50. Fischer, O.: *Der Gang des Menschen. V. Theil: Die Kinematik des Beinschwingens.* Teubner, Leipzig (1903)
51. Fischer, O.: *Der Gang des Menschen. VI. Theil: Über den Einfluss der Schwere und der Muskeln auf die Schwingungsbewegung des Beins.* Teubner, Leipzig (1904)
52. Fischer, O.: *Über die Bewegungsgleichungen räumlicher Gelenksysteme.* Teubner, Leipzig (1905)
53. Fischer, O.: *Theoretische Grundlagen für eine Mechanik der lebenden Körper.* Teubner, Leipzig (1906)
54. Fischer, O.: *Kinematik organischer Gelenke.* Vieweg, Braunschweig (1907)
55. Fischer, O.: *Zur Kinematik der Gelenke vom Typus des Humero-Radialgelenks.* Teubner, Leipzig (1909)
56. Fischer, O.: *Zur Kinematik des Listingschen Gesetzes.* Teubner, Leipzig (1909)
57. Foucault, S., Gosselin, C.M.: On the development of a planar 3-dof reactionless parallel mechanism. *Proceedings of DETC 2002, ASME* (2002)
58. Foucault, S., Gosselin, C.M.: Synthesis, design, and prototyping of a planar three degree-of-freedom reactionless parallel mechanism. *Mechanical Design* **126**, 992–999 (2004)
59. Gosselin, C.M., Vollmer, F., Côté, G., Wu, Y.: Synthesis and design of reactionless three-degree-of-freedom parallel mechanisms. *IEEE Transactions on Robotics and Automation* **20**(2), 191–199 (2004)
60. Herder, J.L.: Energy-free Systems - PhD. thesis. TU-Delft (2001)
61. Hilpert, H.: Weight balancing of precision mechanical instruments. *Mechanisms* **3**, 289–302 (1968)
62. Hool, G.A., Kinne, W.S.: Movable and long-span steel bridges. McGraw-Hill Book Company (1943)
63. Hovey, O.E.: Movable bridges, Vol. I Superstructure. John Wiley & Sons (1926)
64. Ishida, K., Matsuda, T.: Performance characteristics and working comfortableness of forest workers of a new non-vibrating chain saw utilizing perfectly balanced rotation-reciprocation device. *Proceedings of the Fifth World Congress of Theory of Machines and Mechanisms, ASME* pp. 951–954 (1979)
65. Jean, M., Gosselin, C.M.: Static balancing of planar parallel manipulators. *Proc. of Int. Conference on Robotics and Automation* pp. 3732–3737 (1996)
66. Kochev, I.S.: Full shaking moment balancing of planar linkages by a prescribed input speed fluctuation. *Mechanism and Machine Theory* **25**(4), 459–466 (1990)
67. Kochev, I.S.: General theory of complete shaking moment balancing of planar linkages: A critical review. *Mechanism and Machine Theory* **35**, 1501–1514 (2000)
68. Koglin, T.L.: Movable bridge engineering. Wiley (2003)
69. Kreutzinger, R.: Über die Bewegung des Schwerpunktes beim Kurbelgetriebe. *Getriebetechnik* **10**(9), 397–398 (1942)
70. Kwan, Y.B.P., Van de Wiel, W.J.T.P.: Balanced positioning system for use in lithographic apparatus, patent US 6525803 B2 (2003)
71. Lecours, A., Gosselin, C.: Reactionless two-degree-of-freedom planar parallel mechanism with variable payload. *Proc. of ASME-DETC (DETC2009-86700)* (2009)
72. Lim, T.G., Cho, H.S., Chung, W.K.: A parameter identification method for robot dynamic models using a balancing mechanism. *Robotica* **7**, 327–337 (1989)
73. Lim, T.G., Cho, H.S., Chung, W.K.: Payload capacity of balanced robotic manipulators. *Robotica* **8**, 117–123 (1990)

74. Lowen, G.G., Berkof, R.S.: Survey of investigations into the balancing of linkages. *Mechanisms* **3**, 221–231 (1968)
75. Menschaar, H.F., Ariens, A.B., Herder, J.L., Bakker, B.M.: Five-bar mechanism with dynamic balancing means and method for dynamically balancing a five-bar mechanism, patent WO 2006/080846 (2006)
76. Moore, B.: Dynamic balancing of linkages by algebraic methods (PhD-thesis). Johannes Kepler University Linz, Austria (2009)
77. Moore, B., Schicho, J.: Two methods for force balancing of bennett linkages. In: Kecskeméthy and Müller, Computational Kinematics, Proc. of the 5th Int. Workshop on Computational Kinematics pp. 241–248 (2009). Springer, ISBN 978-3-642-01946-3
78. Moore, B., Schicho, J., Gosselin, C.M.: Determination of the complete set of shaking force and shaking moment balanced planar four-bar linkages. *Mechanism and Machine Theory* **44**, 1338–1347 (2009)
79. Nerreter, A.: Graphodynamische Untersuchung einer vierzylindrischen Fahrzeugmaschine mit veränderlichen Hub, Dissertation T.H. München. M. Krayn, Berlin (1912)
80. Papadopoulos, E., Abu-Abed, A.: Design and motion planning for a zero-reaction manipulator. *Proc. of IEEE Int. Conf. on Robotics and Automation* pp. 1554–1559 (1994)
81. Pierrot, F., Nabat, V., Company, O., Krut, S., Poignet, P.: Optimal design of a 4-dof parallel manipulator: From academia to industry. *IEEE Transactions on Robotics* **25**(2), 213–224 (2009)
82. Plug, R.T., Den Boef, A.J., Van der Mast, K.D.: Metrology tool, system comprising a lithographic apparatus and a metrology tool, and a method for determining a parameter of a substrate, patent US 7502103 B2 (2009)
83. Raaijmakers, R.: Besi zoekt snelheidslimiet pakken en plaatsen op (Besi investigates the speedlimit for pick and place motion). *Mechatronica nieuws* (Dutch magazine) pp. 26–31 (2007)
84. Rao, J.S., Dukkipati, R.V.: Mechanism and Machine Theory. John Wiley & Sons (1989)
85. Ricard, R., Gosselin, C.M.: On the development of reactionless parallel manipulators. *Proc. of ASME-DETC (DETC2000/MECH-14098)* (2000)
86. Rohlmann, A., Graichen, F., Bergmann, G.: Influence of load carrying on loads in internal spinal fixators. *Biomechanics* **33**, 1099–1104 (2000)
87. Shchepetil'nikov, V.A.: The determination of the mass centers of mechanisms in connection with the problem of mechanism balancing. *Mechanisms* **3**, 367–389 (1968)
88. Shchepetil'nikov, V.A.: The balancing of bar mechanisms with unsymmetrical links. *Mechanism and Machine Theory* **10**, 461–466 (1975)
89. Thuemmel, T.: Dynamic balancing of linkages by active control with redundant drives. *Proc. 9th World Congress of the Theory of Machines and Mechanisms* pp. 970–974 (1995)
90. VDI2149: Blatt 1: Getriebedynamik-starrkörper mechanismen (dynamics of mechanisms-rigid body mechanisms). Verein Deutscher Ingenieure - Richtlinien (1999)
91. Verschueren, M., Demeulenaere, B., Swevers, J., De Schutter, J.: Counterweight balancing for vibration reduction of elastically mounted machine frames: a second-order cone programming approach. *Mechanical Design* **130**(022302), 1–11 (2008)
92. Van der Wijk, V.: Towards low mass and low inertia dynamic balancing of mechanisms - MSc. thesis. TU Delft (2008)
93. Van der Wijk, V., Demeulenaere, B., Gosselin, C., Herder, J.L.: Comparative analysis for low-mass and low-inertia dynamic balancing of mechanisms. *Mechanisms and Robotics* **4**(3, 031008) (2012)
94. Van der Wijk, V., Herder, J.L.: Dynamic balancing of mechanisms by using an actively driven counter-rotary counter-mass for low mass and low inertia. *Proc. of the Second Int. Workshop on Fundamental Issues and Future Research Directions for Parallel Mechanisms and Manipulators, Montpellier* pp. 241–251 (2008)
95. Van der Wijk, V., Herder, J.L.: Dynamic balancing of Clavel's delta robot. In: Kecskeméthy and Müller, Computational Kinematics, Proc. of the 5th Int. Workshop on Computational Kinematics pp. 315–322 (2009). Springer, ISBN 978-3-642-01946-3

96. Van der Wijk, V., Herder, J.L.: Force balancing of variable payload by active force-balanced reconfiguration of the mechanism. In: ASME/IFTOMM Int. Conf. on Reconfigurable Mechanisms and Robots pp. 323–330 (2009). KC Edizioni, ISBN 978-88-89007-37-2
97. Van der Wijk, V., Herder, J.L.: Guidelines for low mass and low inertia dynamic balancing of mechanisms and robotics. In: Kröger and Wahl, Advances in Robotics Research, Proc. of the German Workshop on Robotics pp. 21–30 (2009). Springer, ISBN 978-3-642-01212-9
98. Van der Wijk, V., Herder, J.L.: Synthesis of dynamically balanced mechanisms by using counter-rotary counter-mass balanced double pendula. *Mechanical Design* **131**(11, 11003) (2009)
99. Van der Wijk, V., Herder, J.L.: Active dynamic balancing unit for controlled shaking force and shaking moment balancing. *Proceedings of ASME IDETC 2010*, Montreal, CA p. DETC2010 28423 (2010)
100. Van de Wijk, V., Herder, J.L.: Delta robot. patent WO2010/128849A1 (2010)
101. Van der Wijk, V., Herder, J.L.: On the addition of degrees of freedom to force-balanced linkages. *Proceedings of the 19th CISM-IFTOMM Symposium on Robot Design, Dynamics, and Control* pp. 2012–025 (2012)
102. Van der Wijk, V., Herder, J.L., Demeulenaere, B.: Comparison of various dynamic balancing principles regarding additional mass and additional inertia. *Mechanisms and Robotics* **1**(4), 04 1006 (2009)
103. Van der Wijk, V., Krut, S., Pierrot, F., Herder, J.L.: Manipulator comprising a fixed base and a movable platform, with four motor-driven chains of articulated links. patent WO2012/173471A1 (2012)
104. Wittenbauer, F.: Graphische Dynamik. Julius Springer, Berlin (1923)
105. Wittenburg, J.: Dynamics of Systems of Rigid bodies. B.G. Teubner Stuttgart (1977)
106. Wu, Y., Gosselin, C.M.: On the synthesis of reactionless spatial 3-dof mechanisms using planar four-bar linkages. *Proc. of ASME DETC, Montreal, CA.* (2002). DETC2002/MECH-34311
107. Wu, Y., Gosselin, C.M.: Design of reactionless 3-dof and 6-dof parallel manipulators using parallelepiped mechanisms. *IEEE Transactions on Robotics* **21**(5), 821–833 (2005)
108. Wu, Y., Gosselin, C.M.: On the dynamic balancing of multi-dof parallel mechanisms with multiple legs. *Mechanical Design* **129**, 234–238 (2007)
109. Wunderlich, W.: Concerning the trajectory of the center of mass of the four-bar linkage and the slider-crank mechanism. *Mechanisms* **3**, 391–396 (1968)
110. Yu, Y.Q., Jiang, B.: Analytical and experimental study on the dynamic balancing of flexible mechanisms. *Mechanism and Machine Theory* **42**, 626–635 (2007)
111. Zarrugh, M.Y., Radcliffe, C.W.: Computer generation of human gait kinematics. *Biomechanics* **12**, 99–111 (1979)
112. Zhou, S., Shi, J.: Active balancing and vibration control of rotating machinery: a survey. *The Shock and Vibration Digest* **33**(4), 361–371 (2001)

Summary

Methodology for analysis and synthesis of inherently force and moment-balanced mechanisms

When mechanisms or machines move at high speeds, the dynamic reaction forces and moments that are produced at the base are a significant cause of undesired vibrations which impairs the behavior, including the accuracy and cycle time of the machine. When a mechanism is designed dynamically balanced, then the total of the dynamic reaction forces (the shaking forces) and the total of the dynamic reaction moments (the shaking moments) on the base are zero for all motion. As a result, the cause of the vibrations is eliminated and the base remains still. This is also advantageous for robotic end-effectors which for all dynamically balanced end-effector motion do not perturb their manipulator. A mechanism that is shaking force balanced is also statically balanced. This means that its motion is not affected by gravity. Then it remains stationary in any position which is advantageous for realizing safe and energy efficient large motion of objects such as in movable architecture.

The design of dynamically balanced mechanisms, in particular dynamically balanced multi-degree-of-freedom mechanisms, however is a challenge since common methods for balancing hardly result in advantageous solutions due to excessive mass, inertia, and complexity addition. One of the reasons for this is that dynamic balancing is considered after the kinematic synthesis of a mechanism. Then it is likely that an element that is added for balancing does not improve but worsen the performance of a mechanism. Another reason is that current balancing methods do not consider the loop closure relations of closed-chain mechanisms which limits the solutions that can be found. Therefore the aim of this work has been to develop a methodology that considers dynamic balance as a design principle in the synthesis of multi-degree-of-freedom mechanisms and to find mechanisms where all elements contribute to the motion as well as to the dynamic balance. Such a mechanism was named an *inherently dynamically balanced mechanism*. This work was aimed also at showing the application potential of the results.

Two methods for the synthesis of inherently dynamically balanced mechanisms were proposed which consider dynamic balance prior to the kinematic synthesis. With the method of linearly independent linear momentum inherently force-balanced mechanisms are derived from given kinematic architectures by adapting the geometric and mass parameters in the linear momentum equations. After substituting the derivative of the loop equations in the linear momentum equations, the linear momentum equations can be written in linearly independent terms from which mechanism configurations can be derived with advantageous balance solutions.

Based on a theory of over 120 years old, general mechanism architectures were developed that are inherently force balanced with solely the essential kinematic conditions for balance. These were named *principal vector linkages*. By combining and generalizing multiple related theories from literature, extended principal vector linkage architectures were developed. It was shown that from these architectures

inherently dynamically balanced mechanism solutions for desired tasks and functions can be synthesized by various methods, including changing the parameters of elements, eliminating elements, reduction of degrees-of-freedom, introducing gears and sliders, and by combining them. It was also shown that to obtain inherent moment balance, the degrees-of-freedom of a principal vector linkage architecture can be reduced such that the moment balance conditions hold, for instance by introducing slider elements.

New multi-degree-of-freedom balanced kinematic mechanism solutions were found that would not have been obtained if dynamic balance would have been considered after the kinematic synthesis. A planar 2-DoF inherently dynamically balanced grasper mechanism was synthesized from a 4-DoF principal vector linkage and a planar 3-DoF inherently dynamically balanced parallel manipulator was synthesized from two 2-DoF principal vector linkages. Examples of balanced movable architecture were shown by the design of a new balanced bascule bridge and a building that can open and close by moving its roof and walls.

A prototype of a planar 3-DoF inherently dynamically balanced parallel manipulator in an experimental setup was presented for evaluation and comparison with the unbalanced 3-DoF parallel manipulator. The prototype manipulator performed successfully high-speed motion up to accelerations of 180 m/s^2 and showed that with dynamic balance the performance of the manipulator can be improved. Experiments and simulations showed that the balanced manipulator has up to 97% lower shaking forces, up to a 96% lower shaking moment, and about 71% lower bearing forces as compared to the unbalanced manipulator at the price of about 1.6 times higher actuator torques.

A method was found by which the loop closure relations of general planar closed kinematic chains can be considered implicitly. Therefore the mass of an element with general center-of-mass is modeled with one virtual equivalent mass and two real equivalent masses. A closed kinematic chain then is analyzed by including these equivalent masses in the analysis of the open kinematic chain without the modeled element. This method was applied for analysis and for deriving the force balance conditions of closed principal vector linkage architectures with 1 and with 3 closed loops.

Samenvatting

Methodologie voor analyse en synthese van inherente kracht- en momentgebalanceerde mechanismen

Wanneer mechanismen of machines snel bewegen, dan zijn de dynamische reactiekrachten en -momenten op de basis van de machine een significante bron van ongewenste trillingen die onder andere de nauwkeurigheid en de omlooptijd van een machine benadelen. Als een mechanisme dynamisch gebalanceerd is ontworpen, dan is de som van de reactiekrachten (de schudkrachten) en de som van de reactiemomenten (de schudmomenten) op de basis voor alle bewegingen gelijk aan nul, waardoor de bron van de trillingen is weggenomen en de basis stil blijft. Dit is ook voordelig voor eindpunteffectoren zoals grijppers die, indien dynamisch gebalanceerd, voor willekeurige bewegingen hun manipulator niet verstören. Een dynamisch krachtgebalanceerd mechanisme is ook statisch gebalanceerd. Dit betekent dat de beweging ervan niet beïnvloed wordt door de gravitatiekracht. Het mechanisme blijft dan bijvoorbeeld in iedere positie vanzelf stilstaan. Dit is gunstig voor het realiseren van veilige en energievriendelijke grote bewegingen van objecten zoals in de bewegende architectuur.

Het ontwerpen van dynamisch gebalanceerde mechanismen, in het bijzonder van dynamisch gebalanceerde mechanismen met meerdere vrijheidsgraden, is een uitdaging omdat met bestaande methoden voor balanceren vrijwel geen gunstige oplossingen worden gevonden doordat te veel massa, traagheid en complexiteit moet worden toegevoegd. Eén van de oorzaken is dat dynamische balans pas na de kinematische synthese van het mechanisme wordt beschouwd. Dan is het voor de hand liggend dat een toegevoegd element voor balans het mechanisme niet verbetert maar juist verslechters. Een andere oorzaak is dat bestaande methoden geen gebruik maken van het verband van een gesloten keten, waardoor het vinden van oplossingen beperkt wordt. Daarom is het doel van dit werk geweest een methodologie te ontwikkelen waarbij dynamische balans een ontwerprinciple is in de synthese van mechanismen met meerdere vrijheidsgraden en waarin alle elementen bijdragen aan zowel de beweging als aan de dynamische balans. Zo'n mechanisme wordt in dit werk een *inherent dynamisch gebalanceerd mechanisme* genoemd. Dit werk heeft ook als doel gehad de potentie te tonen van toepassing van dynamische balans in de praktijk.

Twee methoden voor de synthese van inherent dynamisch gebalanceerde mechanismen zijn voorgesteld waarbij dynamische balans wordt beschouwd vóór de kinematische synthese. Met de methode van lineair onafhankelijke impuls worden krachtgebalanceerde mechanismen afgeleid van een gegeven kinematische architectuur door het aanpassen van de geometrische en massa parameters in de impulsvergelijkingen. Na substitutie van de afgeleide van de vergelijkingen van een gesloten keten kunnen de impulsvergelijkingen in lineair onafhankelijke termen worden geschreven waaruit configuraties van mechanismen met gunstige balans-eigenschappen kunnen worden gevonden.

Op basis van een meer dan 120 jaar oude theorie zijn algemene mechanisme-architecturen ontwikkeld die inherent krachtgebalanceerd zijn met slechts de essentiële kinematische voorwaarden voor balans. Deze hebben de naam *hoofdvectormechanismen* gekregen. Door verschillende theoriën uit de literatuur te combineren en te generaliseren zijn uitgebreide hoofdvectormechanisme-architecturen ontwikkeld. Vanuit deze architecturen kunnen op verschillende manieren inherent dynamisch gebalanceerde mechanismen voor gewenste taken en functies worden ontworpen waaronder het aanpassen van de parameters van elementen, weglaten van elementen, reduceren van vrijheidsgraden, invoeren van tandwieloverbrengingen en schuifverbindingen, en door ze te combineren. Voor inherente momentbalans kunnen de vrijheidsgraden van een hoofdvectormechanisme-architectuur worden gereduceerd zodanig dat aan de voorwaarden voor momentbalans wordt voldaan, bijvoorbeeld door het invoeren van schuifverbindingen.

Nieuwe kinematische oplossingen van gebalanceerde mechanismen met meerder vrijheidsgraden zijn gevonden die niet zouden zijn gevonden als dynamische balans pas na de kinematische synthese zou zijn onderzocht. Een vlak inherent dynamisch gebalanceerd mechanisme met twee vrijheidsgraden was afgeleid van een hoofdvectormechanisme met vier vrijheidsgraden en een vlak inherent dynamisch gebalanceerde parallelle manipulator met drie vrijheidsgraden was ontworpen door het combineren van twee hoofdvectormechanismen met elk twee vrijheidsgraden. Voorbeelden van gebalanceerde bewegende architectuur zijn getoond waaronder een nieuw ontwerp van een gebalanceerde bascule brug en een gebouw die kan worden geopend door het dak en de muren op een neer te bewegen.

Een prototype van een vlak inherent dynamisch gebalanceerde parallelle manipulator met drie vrijheidsgraden in een experimentele opstelling was gemaakt voor een evaluatie en een vergelijking met de ongebalanceerde parallelle manipulator. Dit prototype heeft met succes op hoge snelheid met versnellingen tot 180 m/s^2 bewogen en heeft aangetoond dat met dynamische balans de prestatie van een manipulator kan worden verbeterd. Uit experimenten en simulaties is gebleken dat de gebalanceerde manipulator tot 97% lagere schudkrachten, tot 96% lagere schudmomenten, en ongeveer 71% lagere lagerkrachten heeft in vergelijking met de ongebalanceerde manipulator waarbij de aandrijfmomenten 1.6 maal hoger zijn.

Een methode was voorgesteld waarin de vergelijkingen van een vlakke gesloten keten impliciet kunnen worden meegenomen in de analyse. Hierbij wordt de massa van een element met een generieke massaverdeling gemodelleerd met één virtuele equivalente massa en twee werkelijke equivalente massa's. De analyse van een gesloten keten bestaat dan uit de analyse van de open keten zonder het gemodelleerde element waarin deze equivalente massa's worden meegenomen. Met deze methode waren de voorwaarden voor krachtbalans van gesloten hoofdvectormechanisme-architecturen met één en met drie gesloten ketens afgeleid.

About the author



The Delta Rodeo (photo made by Just Herder, 2010).

Volkert van der Wijk is a researcher in design of mechanisms and robotics at the University of Twente and in addition he is a kinetic sculptor. In 2000-2002 he studied Aerospace Engineering, for which he obtained a propaedeutic degree, and in 2002-2008 he studied Mechanical Engineering at the Delft University of Technology. In 2002-2004 he also studied Art History at the University of Leiden. In 2008 he obtained a master's degree (with honors) in Mechanical Engineering from the Department of Biomechanical Engineering of the Delft University of Technology with the thesis *Towards low-mass and low-inertia dynamic balancing of mechanisms*. This work received in 2008 the *Win van der Hoek Constructor Award* for excellence in mechanical design engineering. In 2004 he was winner of the mechanical engineering design contest of the Delft University of Technology for designing the fastest and most durable non-rolling human powered vehicle and in 2010 he received the best student paper award at the European Conference on Mechanism Science EUCOMES. He has published 22 scientific articles, 3 patents, and 4 articles in industrial magazines, and he has initiated multiple cooperative projects with industrial partners. In 2006-2007 he received an Erasmus grant for a 2 months stay at the Institut für Getriebetechnik und Maschinendynamik of the RWTH-Aachen in Germany and for a 3 months stay at the Mechanical Engineering department of the KU-Leuven in Belgium. In 2010 he stayed at LIRRM in France for 4 months and again in 2011 for 1 month. Since 2008 Volkert van der Wijk is a member of the ASME, since 2010 a member of the IFToMM technical committee for robotics and mechatronics, and since 2011 a member of the IFToMM technical committee for computational kinematics.



ISBN 978-90-365-3630-1